Explorations of the Quark Substructure of the Nucleon in Lattice QCD

by

Jonathan D. Bratt

Submitted to the Department of Physics
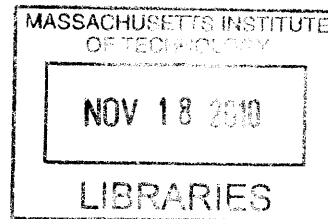in partial fulfillment of the requirements for the degree of

Doctor of Philosophy

at the

MASSACHUSETTS INSTITUTE OF TECHNOLOGY

September 2009

Author . . . .
Department of Physics
July 30, 2009

Certified by . . . .
John W. Negele
William A. Coolidge Professor of Physics
Thesis Supervisor

Accepted by . . . .
Thomas J. Greytak
Associate Department Head for Education

Explorations of the Quark Substructure of the Nucleon in Lattice QCD

by

Jonathan D. Bratt

Abstract

Lattice gauge theory is a valuable tool for understanding how properties of the nucleon arise from the fundamental interactions of QCD. Numerical computations on the lattice can be used not only for first principles calculations of experimentally accessible quantities, but also for calculations of quantities that are not (yet) known from experiment.

This thesis presents two lattice studies of the quark substructure of nucleons. The first study used overlaps calculated on the lattice to evaluate the goodness of trial nucleon sources. A variational study was performed to find the trial source that best approximated the true nucleon ground state. In this exploratory work with relatively simple trial sources on quenched lattices, we obtained overlaps as high as 80%.

The second study was performed using domain wall valence fermions on Asqtad improved staggered lattices provided by the MILC collaboration, with pion masses as low as 290 MeV. We compute nucleon matrix elements of local quark operators: $\langle P', S' | \bar{\psi}(0) \, \Gamma^{\{\mu_1} \overleftrightarrow{D}^{\mu_2} \cdots i \overleftrightarrow{D}^{\mu_n\}} \psi(0) | P, S \rangle$, where $\Gamma^\mu \in \{\gamma^\mu, \gamma^\mu \gamma_5, -i\sigma^{\mu\alpha}\}$. These operators are parameterized by generalized form factors, which in the infinite momentum frame can be unambiguously interpreted in terms of Fourier transforms of the transverse spatial distributions of quarks in a nucleon. By calculating the local operators at many different values of nucleon momentum, we extract a complete set of generalized form factors for the lowest two moments of the vector, axial and tensor operators. From the form factors, we compute a variety of quantities characterizing the internal structure of the nucleon. Finally, we explore chiral extrapolations of the lattice results to the physical pion mass.

Acknowledgments

I owe an enormous debt of gratitude to many people—far too many to name here. Certain names, though, must be mentioned. I would like to thank the following people:

- John Negele, my thesis adviser, for applying pressure when and where it was needed

- Philipp Hägler, for patiently answering my questions as I tracked down all my mistakes

- Massimiliano Procura, for helping me make some sense of chiral perturbation theory

- Michael Engelhardt, for overseeing most of the production on the unchopped lattices

- Andrew Pochinsky and Sergey Syritsyn, for developing the AFF data storage format

Thanks!

Many other people contributed to my time at MIT in non-academic ways. I will especially miss all my dear friends from GCF, both past and present. Thank you for helping me survive the past six years.

Libby, my wife, deserves particular mention. Her patience and unwavering support kept me going through the many trials of grad school. Especially during the last year with all its hardships, she showed amazing endurance. Libby, thank you.

Psalm 127:1-2

Ebenezer

Contents

List of Figures

10

11

List of Tables

Chapter 1

Introduction

Protons and neutrons were once thought to be elementary particles. We now know, however, that they are in fact composite particles, with a rich internal structure. Experiments such as deep inelastic scattering have revealed many features of proton structure (for example, the distribution of the light-cone momentum of the constituents). Meanwhile, there has been great progress in understanding the fundamental interactions that govern the quarks and gluons that make up protons and neutrons. The goal of this work is to better understand how these fundamental interactions give rise to nucleons, and to calculate experimentally observed properties of nucleons from first principles.

The Lagrangian governing these interactions is extremely simple, but the resulting systems can be quite complex. Fortunately, there are some approximations we can make to simplify matters. The first approximation we make is to ignore the electromagnetic interaction. Although the quarks within the proton do carry an electric charge, it is the strong "color force" which dominates their interactions. Therefore, we will restrict our attention in this study to quantum chromodynamics (Eq. 2.2). Furthermore, we will ignore the mass difference between the up and down quarks. Since most of the mass of the proton comes from its binding energy, this is a reasonable approximation to make. Under these two approximations, neutrons and protons behave identically (isospin SU(2) becomes an exact symmetry), and so we typically refer only to a generic "nucleon."

Calculations in QCD are difficult. At present, the only way to obtain quantitative results for QCD at low energies is to numerically compute the theory on a discrete spacetime lattice. In recent years, the combination of developments in lattice field theory, algorithms and computer hardware have reached the point that calculations from lattice QCD are becoming comparable to experimental results. For example, the statistical errors in our lattice calculations of $\Delta\Sigma^{(u+d)}$ are in some cases smaller than the errors on the experimental number (see Chapter 6). Numerical calculations which reproduce experimental values are an important test of the validity of lattice QCD, but they do not necessarily provide much insight into how a particular value arises. So, we would like to use lattice calculations not only to reproduce experimental numbers, but also as a "tool" to explore the quark and gluon structure of the nucleon.

This thesis is organized as follows. In Chapter 2, we will briefly review some fundamental aspects of lattice gauge theory, with particular focus on quantities calculated in this work. Chapter 3 presents the results of an exploratory variational calculation using lattice QCD (this chapter is fairly self-contained and can be considered apart from the rest of the thesis). Chapter 4 contains an introduction to generalized parton distributions and related topics, and provides the background for the work presented in the rest of the thesis. Chapters 5 and 6 present results and analysis for an extensive set of lattice calculations of nucleon generalized form factors, and the final chapter summarizes our findings.

Chapter 2

Nucleon Structure and Lattice QCD

The nucleon is essentially a collection of quarks and gluons held together by the strong force. A theoretical study of nucleon structure must therefore begin with QCD, the quantum theory of the strong interactions. Our goal, then, is to understand the properties of multi-quark systems, and how they arise from the QCD Lagrangian.

In a meaningful physical theory, one must have a way of calculating numbers which correspond to physically observable quantities. As we will demonstrate, many quantities of interest can be expressed in terms of n-point correlation functions[1] of quark fields in Euclidean space-time. So, our first task is to calculate quark correlation functions using lattice QCD.

2.1   The Path Integral Formalism

Path integrals provide a nonperturbative way to calculate correlation functions in any theory defined by a Lagrangian. This is particularly useful when dealing with QCD, for which perturbative expansions in the coupling constant are inapplicable at low energies. In the path integral formalism, a quark correlation function can be

---

[1]A *correlation function* can be thought of as the amplitude for some set of particles to propagate from initial spacetime points $\{x_i\}$ to final points $\{x_f\}$.

written[5]:[2]

$$\langle\Omega|\, \mathcal{T}\, \hat{\psi}(x_1)\cdots\hat{\psi}(x_n)\,\hat{\bar{\psi}}(x_{n+1})\cdots\hat{\bar{\psi}}(x_{2n})\,|\Omega\rangle$$

$$= \frac{\int D\psi\, D\bar{\psi}\, D\mathcal{U}\, e^{-S[\psi,\bar{\psi},\mathcal{U}]}\,\psi(x_1)\cdots\psi(x_n)\,\bar{\psi}(x_{n+1})\cdots\bar{\psi}(x_{2n})}{\int D\psi\, D\bar{\psi}\, D\mathcal{U}\, e^{-S[\psi,\bar{\psi},\mathcal{U}]}} \qquad (2.1)$$

where ψ, $\bar{\psi}$ are fermion (quark) fields, and $\mathcal{U}$ represents the gauge (gluon) field. Quantities with hats $(\hat{\psi},\hat{\bar{\psi}})$ represent creation and annihilation operators acting on the vacuum state $|\Omega\rangle$, and $\mathcal{T}$ denotes time-ordering. The field variables are functionally integrated over all field configurations consistent with the (implicit) boundary conditions at spacetime points $x_1,\cdots x_{2n}$. The action is given by the integral of the Lagrangian:

$$S[\psi,\bar{\psi},\mathcal{U}] = \int d^4x\,\mathcal{L}$$

which in this case is simply the QCD Lagrangian:

$$\mathcal{L}_{QCD} = \frac{1}{4}G^a_{\mu\nu}G^{a\,\mu\nu} + \bar{\psi}(\slashed{D}+m)\psi. \qquad (2.2)$$

The covariant derivative is defined as $D_\mu = \partial_\mu - igA_\mu$, where in terms of the generators of $SU(3)$ the gauge field is: $A_\mu = A^a_\mu \tau^a$. The field strength tensor is: $G^a_{\mu\nu} = D_\mu A^a_\nu - D_\nu A^a_\mu$. Equations 2.1 and 2.2 completely specify the quark correlation function.

2.2 QCD on the Lattice

The functional integral in Eq. 2.1 is formally very elegant, but actually using it in a calculation is not necessarily simple. In practice, we discretize the theory—write down the QCD Lagrangian for a discrete, four-dimensional Euclidean lattice—and evaluate the path integral numerically.

---

[2]Here I write the path integral directly in Euclidean space. For a more general treatment, see [6].

2.2.1 Path Integrals on the Lattice

Here we give a very brief outline of the evaluation of the path integral. Details can be found in [5, 7].

The Lagrangian in Eq. 2.2 can be separated into a quark term and a pure gauge term. These two pieces can be considered (almost) independently in the path integral. Let us write the action as $S = S_G + S_q$, where S_G depends only on the gluon field, and where S_q can depend on both the quark and gluon fields. On a discrete spacetime lattice we have:

$$S_q = \bar{\psi}_m M_{mn} \psi_n,$$
(2.3)

where the indices m, n represent lattice site, as well as dirac and color indices (M is typically a very large matrix!). The integral over fermion field configurations can be performed analytically, giving:

$$\int D\bar{\psi}\, D\psi\, e^{-S_q} = \det M$$
(2.4)

$$\int D\bar{\psi}\, D\psi\, e^{-S_q} \psi_m \bar{\psi}_n = \det M\, [M^{-1}]_{mn}$$
(2.5)

$$\int D\bar{\psi}\, D\psi\, e^{-S_q} \psi_m \bar{\psi}_n \psi_l \bar{\psi}_k = \det M\, \big([M^{-1}]_{mn}\, [M^{-1}]_{lk}$$
$$- [M^{-1}]_{ln}\, [M^{-1}]_{mk}\big)$$
(2.6)

etc.

Note that any arbitrary n-point correlation function of quark fields can be expressed as a series of products of quark two-point functions, or *propagators*, M^{-1}. Including the integral over gauge field configurations (recall that M depends on the gauge field), we obtain path integrals of the form $\int D\mathcal{U}\, e^{-S_G} \det M\, F(\mathcal{U})$, where F is some function

that may depend on the gauge field. We can write the integral as a discrete sum:

$$\langle F \rangle = Z^{-1} \sum_{\mathcal{U}} e^{-S_G} \det M \, F(\mathcal{U}) \equiv \sum_{\mathcal{U}} W_{\mathcal{U}} \, F(\mathcal{U}), \qquad (2.7)$$

where $Z \equiv \sum_{\mathcal{U}} e^{-S_G} \det M$, and where the sum runs over all configurations of the gauge field $\mathcal{U}$. In practice, we perform the sum numerically, using Monte Carlo techniques to sample the space of all gauge configurations. An essential part of a program of lattice calculations is thus the generation of an *ensemble* of sample gauge configurations. It is natural to absorb the factor $W_{\mathcal{U}} \equiv Z^{-1}(e^{-S_G} \det M)$ into the definition of the ensemble as a "weighting factor." Then instead of Eq. 2.7 we have:

$$\langle F \rangle = \frac{1}{N} \sum_{\mathcal{U} \in \{\mathcal{U}_W\}} F(\mathcal{U}), \qquad (2.8)$$

where N is the number of configurations in the ensemble $\{\mathcal{U}_W\}$, and where the probability of finding configuration $\mathcal{U}$ in the ensemble is proportional to $W_{\mathcal{U}}$. The path integral has now been reduced to a simple average (of whatever quark correlation function we are interested in, calculated on each individual configuration) over an ensemble of gauge configurations.

Generating the ensembles of gauge field configurations is one of the most computationally expensive parts of a lattice calculation, and evaluating the determinant of M is one of the most demanding parts of ensemble generation. For this reason, it has been common[3] to set $\det M = 1$, effectively ignoring the fermion "sea." Such lattices are called *quenched* lattices. Chapter 3 of this thesis presents a calculation using quenched lattices.

Once an ensemble of configurations is available, calculating the quark propagator M^{-1} on each configuration is usually[4] the most computationally intensive task remaining. In fact, it is generally impractical to calculate the entire inverse of the matrix M, and only the product $[M^{-1}] \cdot S$ is calculated, for a particular quark source

---

[3]In times past. The steady rise of computational power and efficiency has made these quenched calculations all but obsolete.

[4]But not always [8].

field S.

2.2.2   Aspects of Lattice Gauge Theory

In the discussion so far, we have not needed to know any details about the discrete lattice action (S_G and S_q), nor have we considered any of the potential issues arising from the process of discretization. While a complete description of the discretized theory is beyond the scope of this thesis, it is appropriate here to review some practical aspects of lattice QCD.

Lattice action

The first step in putting QCD on a lattice is to discretize the Lagrangian (Eq. 2.2). There is clearly more than one right way to do this—any expression with the correct continuum limit could in principle be used. But there are some pitfalls to avoid. A naïve discretization of the fermion action results in the infamous fermion doubling problem. The fermion doublers can be avoided by Wilson's projection operator technique [5], but this introduces a term that breaks chiral symmetry at any finite lattice spacing. To preserve chiral symmetry at finite lattice spacing, we resort to more expensive actions, such as the five-dimensional *domain wall* fermion action [9, 10].

The choice of lattice action is a non-trivial matter. We will not pursue the subject further, however, but refer the reader to the works cited in the text.

Systematics

Any actual calculation must be performed in a finite volume with non-zero lattice spacing. Each of these approximations introduces systematic effects, which must be controlled. Ideally, one would repeat a lattice calculation at several different lattice spacings, as well as at several different lattice volumes, and extrapolate the results to the continuum limit. Realistically, finite computing resources constrain the available number of lattices. The calculations presented in Chapter 5 were performed at two different lattice volumes; however, only one lattice spacing was available.

In QCD, the (bare) quark masses enter as input parameters. To accurately simulate the world we live in, we of course ought to perform our calculations using the correct values for the quark masses. However, the computational cost of lattice calculations increases dramatically with decreasing quark mass, and only in recent months has it become possible for some groups [11] to perform calculations near the physical pion[5] mass. In most cases, it is necessary to do calculations at heavy pion masses, and perform an extrapolation to the physical point. This topic will be explored in more detail in Chapter 6.

2.2.3 Nucleon Two-Point Function

We want to use lattice QCD to study the nucleon, so an important object to calculate is the nucleon two-point correlation function. Since a nucleon is composed of three valence quarks (along with an unknown number of sea quark-antiquark pairs), this is equivalent to calculating a *six*-point quark correlation function. A proton can be written in terms of quark operators acting on the vacuum:[6]

$$|N_\alpha(x)\rangle \equiv \hat{\bar{N}}_\alpha(x)\,|\Omega\rangle = \bar{f}_{\delta\gamma\beta\alpha}\,\epsilon^{dcb}\,\hat{\bar{U}}^b_\beta(x)\,\hat{\bar{U}}^c_\gamma(x)\,\hat{\bar{D}}^d_\delta(x)\,|\Omega\rangle, \tag{2.9}$$

where $\hat{\bar{U}}$, $\hat{\bar{D}}$ represent quark creation operators for u and d flavor quarks, respectively. The factor $\bar{f}_{\delta\gamma\beta\alpha}$ depends on the particular nucleon source chosen[12], but it is important that the chosen operator $\hat{\bar{N}}$ have the quantum numbers of a nucleon (see Chapter 3 for more detailed discussion of the sources used in this thesis). The proton two-point function is then:

$$\langle\, N_{\alpha'}(x')\,|\,N_\alpha(x)\,\rangle = f_{\alpha'\beta'\gamma'\delta'}\,\bar{f}_{\delta\gamma\beta\alpha}\,\epsilon^{b'c'd'}\,\epsilon^{dcb}$$
$$\times\,\langle\Omega|\,\hat{D}^{d'}_{\delta'}(x')\,\hat{U}^{c'}_{\gamma'}(x')\,\hat{U}^{b'}_{\beta'}(x')\,\hat{\bar{U}}^b_\beta(x)\,\hat{\bar{U}}^c_\gamma(x)\,\hat{\bar{D}}^d_\delta(x)\,|\Omega\rangle. \tag{2.10}$$

---

[5]Since it is extremely cumbersome to calculate quark masses on the lattice and the phenomenological values are not precisely known, rather than tuning bare quark masses in lattice field theory to reproduce a suitably defined quark mass, it is preferable to tune them to reproduce the pion mass.

[6]Note that $|N_\alpha(x)\rangle$ is *not* a pure proton state. It is rather our best *approximation* of a proton, and generally has significant contamination from other (higher energy) states. See Chapters 3 and 6.

It is straightforward to write this in terms of quark propagators after the pattern of Eqs. 2.4 - 2.6 (in practice, one just applies Wick's theorem—see Fig. 2-1).
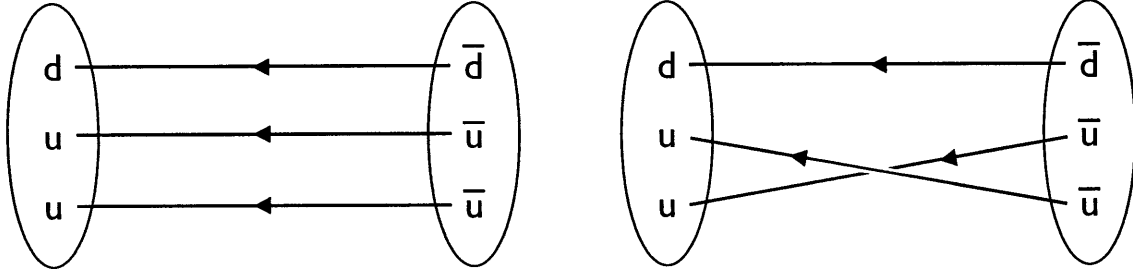
Figure 2-1: Schematic diagrams of the quark propagator contractions that contribute to the nucleon two-point function.

2.2.4 Nucleon Three-Point Function

Another thing we will want to do is calculate matrix elements of quark operators between nucleon states (after working so hard to construct a nucleon on the lattice, we want to be able to look inside and see what the quarks are doing). This is usually (misleadingly) referred to as a "nucleon three-point function"; in fact it is more properly thought of as a quark *eight*-point function.[7] Graphically, some contributions to the three point functions of interest in this work are represented in Fig. 2-2. The inserted operators take the form:

$$\mathcal{O}_{\Gamma}^{(n)}(y) = \bar{\psi}_{\alpha}^{a}(y)\,\Gamma_{\alpha\beta}\,\overleftrightarrow{D}^{\mu_1} \cdots \overleftrightarrow{D}^{\mu_{n-1}}\,\psi_{\beta}^{a}(y), \qquad (2.11)$$

where Γ is some 4×4 dirac matrix, and $\overleftrightarrow{D}^{\mu}$ represents a symmetric covariant lattice derivative: $\overleftrightarrow{D} = 1/2(\overrightarrow{D} - \overleftarrow{D})$.[8] The fermion operator ψ represents either $\hat{U}$ or $\hat{D}$. Written completely in terms of quark operators, the nucleon three-point function is

---

[7]Through force of history and habit, we will continue to refer to such objects as "three-point functions."

[8]Don't confuse this $\overleftrightarrow{D}$ with the quark operator $\hat{D}$.

25

thus:

$$\langle\, N_{\alpha'}(x')\,|\,\mathcal{O}_\Gamma^{(n)}(y)\,|\,N_\alpha(x)\,\rangle = f_{\alpha'\beta'\gamma'\delta'}\,\bar{f}_{\delta\gamma\beta\alpha}\,\epsilon^{b'c'd'}\,\epsilon^{dcb}$$

$$\times\,\langle\Omega|\,\hat{D}_{\delta'}^{d'}(x')\,\hat{U}_{\gamma'}^{c'}(x')\,\hat{U}_{\beta'}^{b'}(x')\,\bar{\psi}_\lambda^a(y)\,\Gamma_{\lambda\rho}\,\overrightarrow{D}^{\mu_1}\cdots\overleftarrow{D}^{\mu_{n-1}}\,\psi_\rho^a(y)\,\hat{U}_\beta^b(x)\,\hat{U}_\gamma^c(x)\,\hat{D}_\delta^d(x)\,|\Omega\rangle.$$

$$(2.12)$$

where the nucleon states are given by Eq. 2.9. If we wish (and we typically do), we can project the inserted operator onto a definite momentum. For a more thorough discussion of the calculation of lattice three-point functions, see [12].

One of the possible contractions of the quark operators in Eq. 2.12 is of ψ with $\bar{\psi}$. This corresponds to the product of a nucleon two-point function with a quark loop (with the operator insertion in the quark loop), and is represented graphically by the right-hand side of Fig. 2-2. Such contributions are known as "disconnected diagrams."[9] To calculate the disconnected quark loop, one would need the quark propagator *from* every lattice site *to* every lattice site—that is, one would need the full inverse matrix M^{-1}. (This is somewhat of an oversimplification: see [13].) For this reason, it is common to ignore the disconnected contributions, which are expected to be small (but not, in general, negligible: [14, 15]). In such cases, special emphasis is placed on the quark flavor combination $u - d$ (the isovector combination), for which the disconnected piece cancels out (since the disconnected contributions for operator insertions on the u quarks and d quarks are identical).

The calculations performed in this thesis do not include contributions from disconnected diagrams.

---

[9]Of course, the pieces of the diagram are actually connected by gluon lines, which are not drawn in Fig. 2-2.
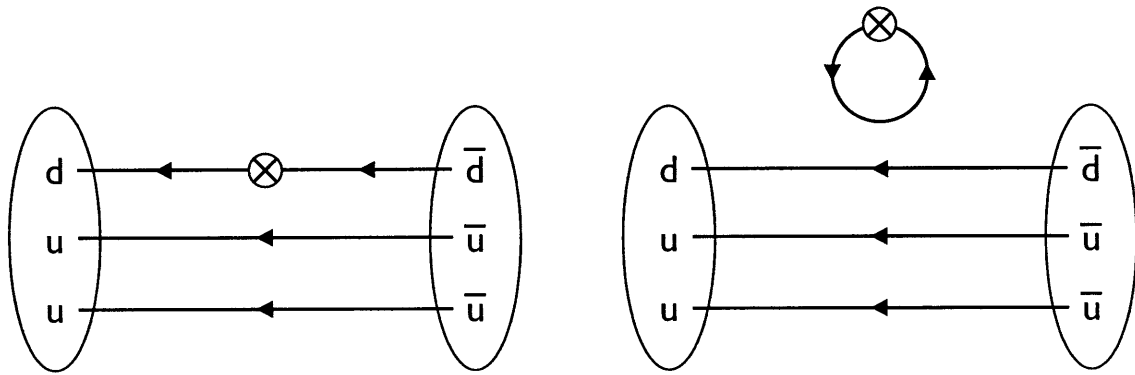
Figure 2-2: Schematic diagrams of some quark propagator contractions that contribute to the nucleon three-point function. The operator insertion is represented by $\otimes$.

Chapter 3

A Variational Study of the Nucleon

As we said in the introduction, we would like to use lattice calculations as a tool to explore the quark and gluon structure of the nucleon. One such tool is the calculation of overlaps. For a given trial nucleon state $|N_{trial}\rangle$, it is a straightforward matter (Section 3.1) to calculate the normalized quantum mechanical overlap with the "actual" nucleon state $|N_{QCD}\rangle$. The overlap $|\langle N_{QCD}|N_{trial}\rangle|^2$ is a direct measure of how closely the trial state approximates the actual nucleon. By systematically varying the trial state, we can obtain insight into key features of the nucleon wavefunction.

The only practical way to calculate nucleon correlation functions on a lattice is to express them in terms of valence quark correlation functions (Section 3.2), so our trial states can be varied by choosing the position and spatial extent of each quark source. We also explore the smoothing of gluon fluctuations achieved by smearing the gauge links included in the quark source, and the inclusion of only upper or of both upper and lower spinor components (in the dirac basis).

Given recent resurgence of interest[16, 17, 18] in diquarks [19], it is of interest to look for evidence of diquark substructure variationally. We could, in principle, study two possible diquark configurations in a nucleon[20, 21]: the scalar channel $(u\,C\gamma_5\,d)$, and the vector channel $(u\,C\gamma_\mu\,d)$. However, at the one gluon exchange level, quarks in the scalar configuration have lower energy than quarks in the vector configuration [17], which are thus called "good" and "bad" diquarks respectively, and we will focus our attention only on the good diquarks and consider sources of the form $(u\,C\gamma_5\,d)\,u$.

Furthermore, in the limit where two quarks are bound into a point-like diquark, one could also develop a "dog bone" model of baryons with a diquark and quark connected by a flux tube.[1] This model is phenomenologically successful [18, 19]. We can explore this picture in our trial function by allowing for a diquark to have a different degree of spatial localization and to be separated from the remaining quark.

3.1   Variational Method

In this study, a simple variational approach was used to study the ground state of the nucleon. For a trial source operator $\bar{N}(x)$, the overlap with the ground state is calculated from a fit to the nucleon two-point correlation function [22]. Starting with the correlation function in position space:

$$C_N(\mathbf{x}, t) = \langle N(\mathbf{x}, t) \,|\, N(\mathbf{0}, 0) \rangle$$

where $|N(\mathbf{0}, 0)\rangle \equiv \hat{\bar{N}}(\mathbf{0}, 0)|\Omega\rangle$, we project onto zero momentum[2] and insert a complete set of states in the usual way to obtain:

$$C_N(t) \equiv \sum_{\mathbf{x}} C_N(\mathbf{x}, t) = \sum_n e^{-E_n t} |\langle N(\mathbf{0}, 0)|n\rangle|^2 \equiv \sum_n A_{N,n} e^{-E_n t}.$$

The energies E_n and coefficients $A_{N,n}$ are extracted by fitting $C(t)$ with a sum of exponentials, which at sufficiently large t (in practice, $t \geq 1$ is generally big enough) can be truncated at two exponentials. The normalized overlap of our trial source with the nucleon ground state is then given by:

$$\frac{|\langle N(0)|0\rangle|^2}{\sum_n |\langle N(0)|n\rangle|^2} = \frac{A_{N,0}}{C_N(0)} \equiv \bar{A}_{N,0} \tag{3.1}$$

Figure 3-1 shows some typical nucleon two-point functions with fits.

The overlap $\bar{A}_{N,0}$ is a measure of how closely the initial state (created by trial

---

[1]This simple baryon model is analogous to the simple picture of a meson comprised of an antiquark and quark connected by a flux tube, which leads naturally to Regge trajectories.

[2]on the lattice, this simply means summing over all lattice sites on each timeslice

30

source $\hat{\tilde{N}}$) approximates the true nucleon ground state. By calculating the overlap for many different trial sources, we can determine which is the "best" nucleon source. This is interesting for both computational and physical reasons.

Computationally, it is desirable to find an optimal nucleon source for use in other lattice calculations (e.g. calculating generalized form factors). Although it is true that regardless of our initial state, it will eventually (if we "wait" long enough in imaginary time) become dominated by the ground state, there are practical limits on the quality of data at large source-sink separations. Especially for gauge configurations at light quark masses, signal-to-noise ratios decrease dramatically as the time separation increases. By starting with an optimized nucleon source, one can perform lattice calculations closer to the source, and thus obtain less noisy data than would otherwise be obtained with the same computing resources.

Physically, a variational study can provide insight into the nucleon wavefunction. In the following, we emphasize this aspect of the study.

Note that this variational study with individual trial sources differs from the variational approach used extensively in spectroscopy[23], which considers a superposition of distinct sources with arbitrary coefficients and determines the optimal coefficients by minimizing the energy, rather than maximizing the overlap.

3.2   The Nucleon Two-Point Function

Let us briefly review how the two-point correlation function for the nucleon is constructed. A nucleon is created by the source operator $\hat{\tilde{N}}_\alpha(x_i)$ and annihilated by the sink operator $\hat{N}_{\alpha'}(x_f)$.[3] Following the notation of [12], we can write a general nucleon operator in terms of quark operators as:

$$\hat{N}_\alpha(x) = f_{\alpha\beta\gamma\delta}\, \epsilon^{bcd}\, \hat{U}^b_\beta(x)\, \hat{U}^c_\gamma(x)\, \hat{D}^d_\delta(x). \tag{3.2}$$

---

[3]In this section, operators will be consistently denoted with "hats" (e.g. $\hat{\mathcal{O}}$) to distinguish them from the corresponding classical fields.

The nucleon two-point function on a single gauge field configuration $\mathcal{U}$ is then:

$$\begin{aligned}
C_{N,\mathcal{U}}(x) &= T_{\alpha\alpha'} \langle\Omega|\hat{N}_{\alpha'}(x)\,\hat{\bar{N}}_\alpha(0)|\Omega\rangle_{\mathcal{U}} \\
&= T_{\alpha\alpha'}\, f_{\alpha'\beta'\gamma'\delta'}\, \bar{f}_{\delta\gamma\beta\alpha}\, \epsilon^{b'c'd'}\, \epsilon^{dcb} \times \\
&\quad \langle\Omega|\,\hat{D}_{\delta'}^{d'}(x)\,\hat{U}_{\gamma'}^{c}(x)\,\hat{U}_{\beta'}^{b'}(x)\,\hat{\bar{U}}_\beta^b(0)\,\hat{\bar{U}}_\gamma^c(0)\,\hat{\bar{D}}_\delta^d(0)\,|\Omega\rangle_{\mathcal{U}}
\end{aligned} \tag{3.3}$$

where we take the spin projection matrix $T_{\alpha\alpha'} = \delta_{\alpha 0}\delta_{\alpha'0}$ in the dirac basis. Using Wick's theorem, the quark six-point function in Eq. (3.3) can be written in terms of quark propagators:

$$S_{\alpha\beta}^{ab}(x;0)_{\mathcal{U}} \equiv \langle\Omega|\,\hat{q}_\alpha^a(x)\hat{\bar{q}}_\beta^b(0)\,|\Omega\rangle_{\mathcal{U}}. \tag{3.4}$$

On the lattice, quark propagators are calculated using the path integral method [5] to evaluate correlation functions of quark fields.

3.2.1 Quark Propagators at t=0

We emphasize that Eqs. (3.3) and (3.4) are written in terms of quark *operators*. To evaluate the quark propagators using (for example) path integrals, we need an unambiguous way of associating operator expressions with the corresponding classical quark *field* expressions.[4] In general, a time-ordered correlation function of classical field variables (calculated using the path integral formulation) is equal to the corresponding operator correlation function, when the equal-time operators are normal-ordered using an appropriate prescription:

$$\langle\mathcal{T}\{\mathcal{O}\}\rangle \equiv \langle\mathcal{T}\{N[\hat{\mathcal{O}}]\}\rangle \tag{3.5}$$

where $\mathcal{O}$ is a function of the quark fields $(q, \bar{q})$, and similarly for the corresponding operators. Equation (3.5) can be thought of as *defining* the equal-time normal-ordering prescription N. It has been shown [24] that for the Wilson action, the correct normal-

---

[4]The potential for ambiguity arises because of the differing anticommutation relations for operators and the corresponding classical fields. The fermionic field variables in the path integral anticommute: $\{\psi^\dagger, \psi\} = 0$. On the other hand, for the field creation and annihilation operators we have $\{\hat{\psi}_a^\dagger, \hat{\psi}_b\} \propto \delta_{ab}$.

ordering prescription in a basis where $\gamma_0 = \text{diag}(1, 1, -1, -1)$ is:

$$N[\hat{q}_\alpha \hat{\bar{q}}_\beta] = \begin{cases} \hat{q}_\alpha \hat{\bar{q}}_\beta & \text{if } \alpha, \beta = 1, 2 \\ -\hat{\bar{q}}_\beta \hat{q}_\alpha & \text{if } \alpha, \beta = 3, 4 \,. \end{cases} \tag{3.6}$$

Furthermore, the quark operators obey the (non-canonical) anticommutation relation [24] :

$$\{\hat{q}_\alpha^a(\mathbf{x}), \hat{\bar{q}}_\beta^b(\mathbf{y})\} = [B^{-1}]_{\alpha\beta}^{ab} \gamma_0 \tag{3.7}$$

where

$$B_{\alpha\beta}^{ab}(\mathbf{x}, \mathbf{y}) = \delta_{\alpha\beta} \left(\delta^{ab} \delta(\mathbf{x}, \mathbf{y}) - \kappa \sum_{j=1}^{3} [\mathcal{U}_j^{\dagger\,ab}(\mathbf{y})\delta(\mathbf{x} - \mathbf{y} - \hat{j}) + \mathcal{U}_j^{ab}(\mathbf{x})\delta(\mathbf{x} - \mathbf{y} + \hat{j})] \right) . \tag{3.8}$$

We emphasize again that the preceding discussion applies specifically for the *Wilson* fermion action.

Equation (3.4) is the quark propagator needed in the calculation of the nucleon two-point function. Rewriting it so that the operators are normal-ordered according to (3.6), we find:

$$\langle\, \hat{q}_\alpha^a(x)\, \hat{\bar{q}}_\beta^b(0)\, \rangle \;=\; \langle\, N[\hat{q}_\alpha^a(x)\, \hat{\bar{q}}_\beta^b(0)]\, \rangle - \delta_{t0} \left(\frac{1 - \gamma_0}{2} \right)_{\alpha\alpha'} [B^{-1}]_{\alpha'\beta}^{ab}(\mathbf{x}, \mathbf{0}). \tag{3.9}$$

Note that $\langle\, N[\hat{q}_\alpha^a(x)\, \hat{\bar{q}}_\beta^b(0)]\, \rangle = \langle\, q_\alpha^a(x)\, \bar{q}_\beta^b(0)\, \rangle$ is the naïve quark propagator typically calculated on the lattice. Equation (3.9) makes it clear that the naïve propagator is incorrect at $t = 0$. To obtain the correct propagator, it is necessary to include the B^{-1} term. In practice, inclusion of this term made a difference of about 2% in our calculated values of $C_N(t = 0)$.

3.3   Calculation

We performed our exploratory calculation on $16^3 \times 32$ quenched Wilson lattices with $\beta = 6.0$ and $\kappa = 0.1530$ ($a \approx 0.09$ fm, $m_\pi \approx 900$ MeV) for ensemble sizes of 100 - 200
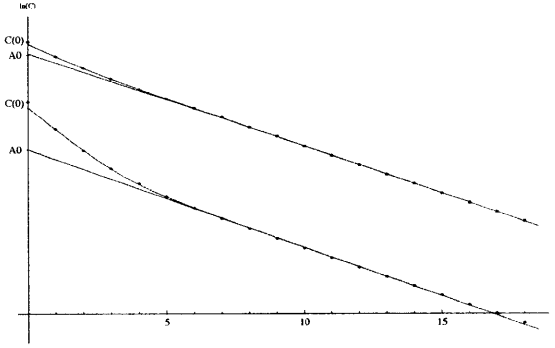
Figure 3-1: Log plots of some typical two-point correlation functions fit with the sum of two exponentials (blue lines are extrapolated ground state terms). Top curve shows a source with a large ground state overlap.
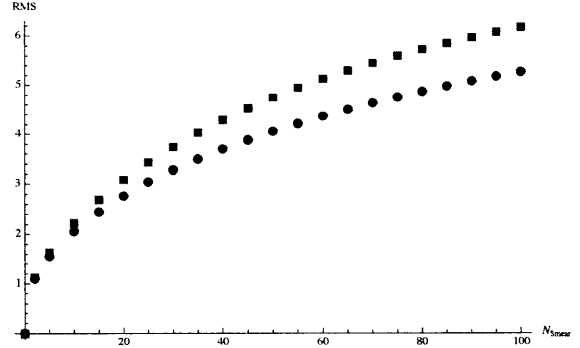
Figure 3-2: RMS radius of quark source field vs. number of smearing steps. Blue circles are with no link smearing; red squares are with APE-smeared links.

configurations. The trial sources were of the form

$$N_\alpha = \left(U_\beta \left[C \, \gamma_5 \right]_{\beta\gamma} D_\gamma \right) U_\alpha \tag{3.10}$$

where $C = i\gamma^2\gamma^0$ is the charge conjugation matrix.

We varied the number of gauge-invariant smearing steps for the quark sources, controlling their RMS radius [22], the number of dirac spinor components (four, or two in the non-relativistic limit), the gauge field smearing in the source links, the relative size of the quark and diquark radius, and the relative position of the quark and diquark.

3.3.1 Quark Radius

A delta function (or "point source") is the simplest gauge-invariant expression that we could imagine using for the quark fields in Eq. 3.10. However, the quarks in a nucleon certainly have wavefunctions with finite spatial extent. To model this, we "smear" the quark source fields over many different lattice sites. We use Wuppertal smearing to produce gauge-invariant smeared sources [22]:

34
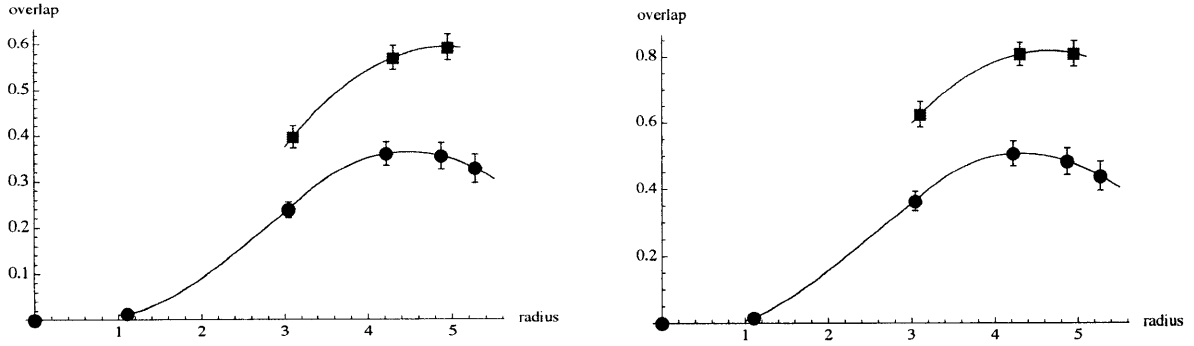
Figure 3-3: Overlap vs. quark RMS radius (in lattice units). Blue circles are results for sources with no link smearing; red squares are with APE-smeared links. Interpolating curves are shown to guide the eye. Results are shown for four-component spinors (left) and for non-relativistic two-component spinors (right). (Note difference in vertical scales.)

$$Q^{(i)}(x) = Q^{(i-1)}(x) + \alpha \sum_{\mu=1}^{3} \left(\mathcal{U}_{\mu}^{\dagger}(x - \hat{\mu}) Q^{(i-1)}(x - \hat{\mu}) + \mathcal{U}_{\mu}(x) Q^{(i-1)}(x + \hat{\mu}) \right)$$

$$Q_{sm}(x) = Q^{(N_{smear})}(x) \tag{3.11}$$

where we take $\alpha = 3$ and $Q_a^{(0)}(x) = \delta_{x\,x_0} \delta_{a\,a_0}$. [5] The RMS radius of the quark source is controlled by varying the number of smearing iterations (see Fig 3-2).

As a first step, we smear all three quark fields in Eq. 3.10 to the same RMS radius and locate them at the same spatial position. Results for the variation of the quark radius are shown in Fig 3-3 . The overlap behaves as in previous studies, starting at the order of 10^{-5} for a small quark radius, increasing to a maximum at some finite radius, and falling off at larger radii. This reflects the finite spatial extent of the quark wavefunction within a nucleon. The peak occurs around 4.5 lattice units (≈ 0.4 fm), consistent with [22].

3.3.2   Number of Spinor Components

The quark fields in Eq. 3.10 are, in general, four-component spinor fields. However, one could also construct a nucleon source using non-relativistic quark fields. In the

---

[5]Here, a represents both color and dirac indices.

35
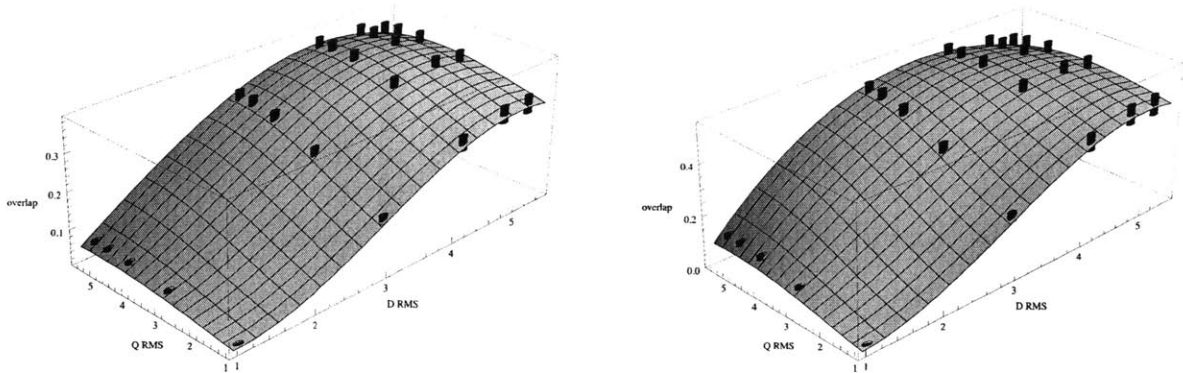
Figure 3-4: Overlap vs. diquark, quark RMS radius (in lattice units). Blue cylinders represent points with error bars; interpolating surface is shown to guide the eye (left: four-component spinors; right: two-component spinors). Numerical values for overlaps plotted here are given in Tables A.1 and A.2.

dirac basis, this corresponds to taking the upper two components of the quark spinors, so we have:

$$N^{NR} = \left(U^{NR} \, C \, \gamma_5 \, D^{NR} \right) U^{NR} \tag{3.12}$$

Where $Q^{NR} \equiv \frac{1}{2}(1 + \gamma_0)Q$.

For every trial source of the form given in Eq. 3.10, we get the corresponding two-component source (Eq. 3.12) "for free." The right-hand side of Fig 3-3 shows results for trial sources with two components. We find that the two-component sources have significantly greater ground-state overlaps than the full four-component sources. This is consistent with the expectation from the dirac equation that the lower components for a single quark in a central mean field be in a p-wave type state, which has very poor overlap with the approximately gaussian wavefunction used as a trial source (also see discussion in [25]).

3.3.3 Link Smearing

Another variation tested was the smearing of the gauge fields used to construct trial sources. For this purpose, we used 25 iterations of APE smearing with $\epsilon = 0.35$ in the notation of [26]. Each iteration of APE smearing adds to each link the sum of its
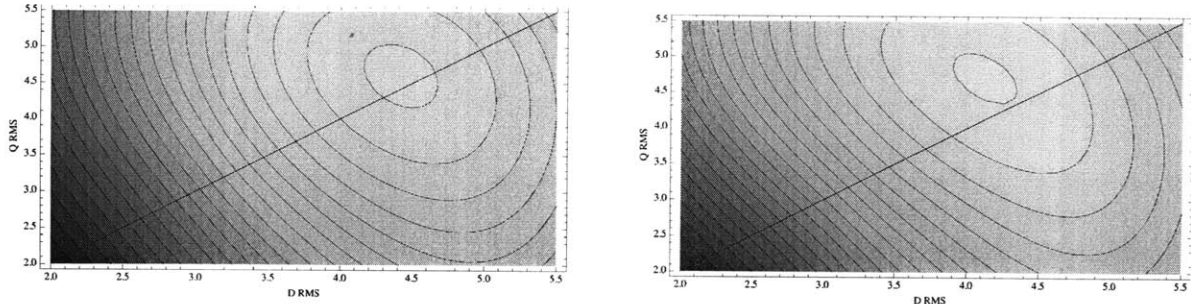
Figure 3-5: Contour plots for the surfaces shown in Fig 3-4. Diagonal line at $R_{quark} = R_{diquark}$ shown for reference. Contour spacing is 0.0125 for the left-hand plot (four-component spinors) and 0.167 for the right-hand plot (two-component spinors).

neighboring "staples" (with some coefficient), and projects the resulting matrix back onto SU(3). Link smearing has the effect of smoothing out short-range fluctuations in the gauge field, so fewer steps of quark smearing are required to reach a given RMS radius (see Fig 3-2). As shown in Fig 3-3, the inclusion of APE smearing resulted in a significant increase in overlaps.

The observant reader will note that the largest overlap obtained with smeared links lies at the edge of our explored parameter space. So, we cannot claim to have found even a local maximum. We believe, however, that we are close to the local maximum, based on the corresponding results for unsmeared links. The fact that the overlap peaks at different values of the RMS radius in the two cases reflects the fact that a single parameter (the RMS quark radius) is not sufficient to completely specify the quark distribution.

3.3.4 Relative Size of Quark, Diquark

If we take the diquark picture seriously, we might expect the quarks to have different wavefunctions depending on whether or not they are "in" the diquark. To check this, we considered sources in which the "diquark quarks" were smeared to a different radius than the "lone quark":

$$J = \left(U^{(r1)} \, C \, \gamma_5 \, D^{(r1)} \right) U^{(r2)} \tag{3.13}$$

where $r1$ and $r2$ represent the RMS radii of the diquark and lone quark, respectively. Results for the variation of these two parameters are shown in Figs 3-4 and 3-5. A clear off-diagonal peak in Fig 3-5 would suggest diquark substructure. In our results, the peak overlap is very nearly centered along the $r1 = r2$ diagonal, showing little evidence for diquark substructure. However, though there is no statistically significant asymmetry, the slight asymmetry that is observed tends towards "smaller" diquarks and "bigger" quarks, which is consistent with the expectation that diquarks exist as a more tightly bound state.

3.3.5   Relative Position of Quark, Diquark

Motivated by the flux tube model, we constructed trial sources with the diquark and lone quark spatially displaced. For these sources, we symmetrized the sink by summing over displacement directions:

$$C_{disp}(t) = \sum_{\mathbf{r}, \hat{j}} \left\langle U(\mathbf{r}, t) \, C\gamma_5 \, D(\mathbf{r}, t) \, U(\mathbf{r} + \ell\hat{j}, t) \; \bar{U}(\mathbf{0}, 0) \, C\gamma_5 \, \bar{D}(\mathbf{0}, 0) \, \bar{U}(\ell\hat{x}, 0) \right\rangle. \quad (3.14)$$

Results for a variety of displacements ℓ and smearing combinations are shown in Fig 3-6. The maximum overlap is observed for zero displacement, suggesting no flux tube substructure. It may be noted, though, that for some values of quark/diquark smearing, displacing the quark does marginally increase the calculated overlap. Intuitively, this can be understood by imagining that we take our trial state and set the quark (or diquark) to be smaller than it "wants" to be. In this case, a displacement of the quark from the diquark may work to restore the quark to its "ideal" mean distance to the center of the nucleon. Such a displaced trial source may then have a greater overlap than its non-displaced counterpart.
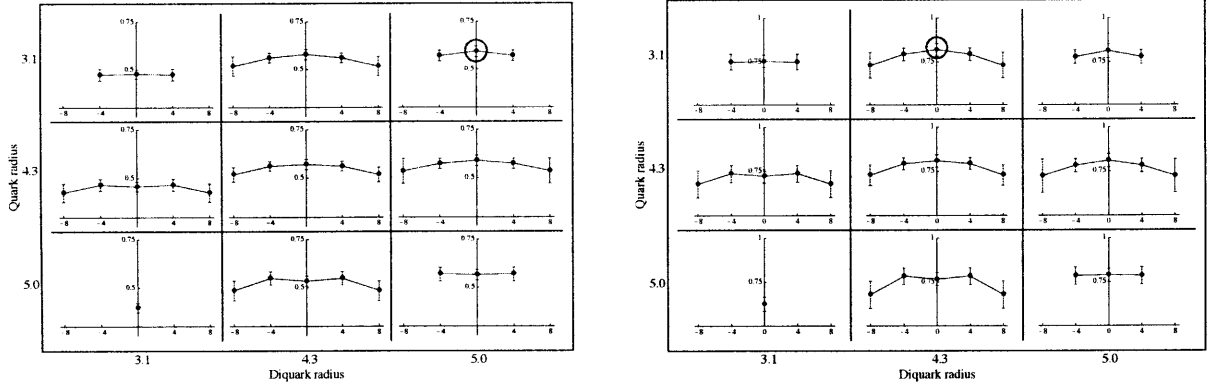
Figure 3-6: Array of plots showing overlap as a function of quark displacement (in lattice units). Positive and negative displacements are identical, but are plotted for clarity. Maximum achieved overlaps are circled. (Left panel: four-component spinors; right panel: two-component spinors.) Numerical values for overlaps plotted here are given in Tables A.3 and A.4.

3.4 Conclusions From the Variational Study

In summary, we observe dramatic changes in the overlap between a trial state and the nucleon as we vary accessible features of the trial state. Smearing the quark source fields from a point to an optimal RMS radius increases the overlap for a four-component trial function from a fraction of a percent to about 35%. Removing the unphysical S-wave lower components increases the overlap from 35% to 50%. Smearing the gauge field further improves the overlap from 50% to more than 80%. Attempts to increase the overlap by including diquark correlations associated with the relative size and position of the quarks and diquarks yielded no significant improvement, suggesting that such substructures do not play a major role in the nucleon ground state.

From the perspective of lattice calculation technology, these results are extremely useful in generating sources that involve minimal contaminants from excited states. From a physics perspective, they give useful insight into what the quark and gluon degrees of freedom are doing. It would be valuable to extend these calculations to

39

lighter quark masses, but for our work using light domain wall quarks, we would need to find an alternative to the transfer matrix construction required for the calculation of unambiguous overlaps.

Chapter 4

Parton Distributions

In the rest of this thesis we will focus on another way to explore nucleon structure with lattice calculations. Generalized parton distributions (see [27] for a review) contain much information about the spatial and spin structure of the nucleon. In this chapter, we will provide a brief introduction to GPDs and review their connection to lattice calculations.

A few words regarding partons are in order. For our purposes, a "parton" may be defined as an elementary (point-like) constituent of a nucleon, i.e. a quark or gluon. In this study we focus almost exclusively on quarks, so when we refer to "parton distributions," we generally have in mind *quark* distributions. The interaction between partons is complicated—hence our need to resort to numerical calculations. We note, however, that a parton's transverse position and longitudinal momentum are well-defined quantities[28]. In addition, we interpret our results using an intuitive (though somewhat simplistic) picture of the nucleon. Imagine the nucleon as composed of a cloud of point-like partons. In the infinite momentum frame (see next section), Lorentz contraction flattens this cloud into a pancake in the transverse plane. We will study the distribution of partons—more specifically, of parton charge and energy—in this pancake.

The phrase "parton distribution" typically refers to the distribution of the parton *plus-momentum*, expressed as a fraction of nucleon plus-momentum. On the lattice, we can only access Mellin moments of such plus-momentum distributions. As dis-

cussed in this chapter, however, we *can* calculate the transverse spatial distributions of quarks in a nucleon, and we often refer to these as *transverse* parton distributions.

4.1   The Infinite Momentum Frame

Strictly speaking, parton distributions are only well-defined in the infinite momentum frame (IMF): a reference frame moving with speed $u \approx c$ in the $-\hat{z}$-direction.[1] In principle, one could ask what the distribution of, say, quark energy is in any particular reference frame (such as the lab frame). However, such a question is most easily posed—and answered—in the IMF. The reasons for this range from the simple (experimental studies of nucleon structure typically involve high-energy probes, which "see" the nucleon in a fast-moving frame) to the subtle (see the discussion of spin states in Appendix C). We will be content to note that the IMF provides an unambiguous frame in which to define and calculate parton distributions, and refer the interested reader to [29] and [30] for more detailed treatments.

In general, the dynamical details of a physical system are not frame-independent. A familiar example of this can be found in classical electromagnetism, where a magnetic field in one frame develops an electric component in another frame. The resulting kinematics should be the same in all frames (appropriately transformed, of course), but the physical picture we use for the calculation might change. In the same way, the internal dynamics of a proton in the IMF may look very different from the rest-frame dynamics, but the answer to a kinematical question should be the same no matter what frame we choose to compute it in.[2]

---

[1] more precisely, the IMF corresponds to the $u \to c$ limit of such a reference frame.

[2] Assuming, of course, that the *particles* about which we are asking the kinematical questions have a frame-independent existence.

4.1.1 Light-Cone Coordinates

It is impossible to discuss the IMF without mentioning light-cone coordinates. Consider the change of variables:

$$v^{\pm} = \frac{1}{\sqrt{2}}(v^0 \pm v^3) \tag{4.1}$$

for some four-vector[3] v^{μ}. Then the coordinates (x^+, x^1, x^2, x^-) are known as light-cone coordinates. The significance of light-cone coordinates can be appreciated by considering the Lorentz transformation relating the "lab frame" coordinates (x^0, x^1, x^2, x^3) to the coordinates in the IMF $(x^0_{IMF}, x^1_{IMF}, x^2_{IMF}, x^3_{IMF})$:

$$x^0_{IMF} = \gamma(x^0 + \beta x^3)$$
$$x^1_{IMF} = x^1$$
$$x^2_{IMF} = x^2$$
$$x^3_{IMF} = \gamma(x^3 + \beta x^0),$$

where we take the limit $\beta \to 1$. We see that the IMF time coordinate x^0_{IMF} is proportional to the light-cone coordinate x^+ (expressed in the *lab* frame).[4] In the same way, the energy of a particle in the IMF is proportional to its lab frame *plus-momentum*: $p^0_{IMF} \propto p^+$. Choosing to use the light-cone coordinate system is therefore equivalent to choosing the IMF as a reference frame [30].

We will use light-cone coordinates frequently in this thesis, and adopt the convention that roman indices refer to transverse vector components: $v^i = \{v^1, v^2\}$. Also, we commonly (though not exclusively) use boldface type to denote a transverse vector.

---

[3]we use the same notation for the dirac marices γ^{μ}

[4]On the other hand, x^3_{IMF} *isn't* proportional to x^-, but we can ignore x^3_{IMF} since it's not a independent coordinate anyway.

43

4.2 Nucleon Matrix Elements

Let us begin by writing down some matrix elements of quark operators between nucleon states:

$$F_{(f)} \equiv \int \frac{dz^-}{4\pi} e^{ix\bar{P}^+ z^-} \left\langle P', S' \middle| \bar{\psi}\left(-\frac{z}{2}\right) \gamma^+ \mathcal{W} \psi\left(\frac{z}{2}\right) \middle| P, S \right\rangle \bigg|_{z^i = z^+ = 0} \tag{4.2}$$

$$\tilde{F}_{(f)} \equiv \int \frac{dz^-}{4\pi} e^{ix\bar{P}^+ z^-} \left\langle P', S' \middle| \bar{\psi}\left(-\frac{z}{2}\right) \gamma^+ \gamma_5 \mathcal{W} \psi\left(\frac{z}{2}\right) \middle| P, S \right\rangle \bigg|_{z^i = z^+ = 0} \tag{4.3}$$

$$F^j_{T,(f)} \equiv -i \int \frac{dz^-}{4\pi} e^{ix\bar{P}^+ z^-} \left\langle P', S' \middle| \bar{\psi}\left(-\frac{z}{2}\right) \sigma^{+j} \gamma_5 \mathcal{W} \psi\left(\frac{z}{2}\right) \middle| P, S \right\rangle \bigg|_{z^i = z^+ = 0}, \tag{4.4}$$

where $\bar{P} \equiv \frac{1}{2}(P' + P)$. $|P, S\rangle$ denotes a nucleon state with four-momentum P and spin S, and quark creation and annihilation operators are represented by $\bar{\psi}$ and ψ. Here we explicitly include the quark flavor label (f) on the left hand side, but suppress the label on the quark operators.[5] The Wilson line $\mathcal{W} \equiv \mathcal{P} e^{-ig \int_{-.5z^-}^{.5z^-} dz' A^+(z')}$ connecting the quark operators is needed for gauge invariance, but reduces to unity in light-cone gauge ($A^+ = 0$). (Note that by restricting ourselves to the plus-component of the quark bilinear operators, we project out the twist-two distributions[29].)

We will refer to the operators in Eqs. 4.2, 4.3 and 4.4 as vector, axial and tensor operators, respectively.

4.2.1 Forward Matrix Elements

Consider the case where the initial and final nucleon states are the same: $P = P'$, $S = S'$. Then, for $x > 0$, Eq. 4.2 is simply the quark *distribution function* $q_{(f)}(x)$, which represents the probability of finding a quark (flavor f) with plus-momentum $p^+ = xP^+$

---

[5]Note that the matrix elements are also functions of x, P, P', S and S'.

in the nucleon[6]:

$$F_{(f)}(x)|_{P=P',S=S'} = q_{(f)}(x).$$

Equation 4.2 can also be given an interpretation for $x < 0$, in terms of the antiquark distribution $q_{(\bar{f})}(-x)$. To see this, let us examine the behavior of the quark operators in Eq. 4.2 under charge conjugation. This operation interchanges quarks and antiquarks, so the charge conjugated operator now measures the *antiquark* density. We pick up a minus sign from the behavior of the fermion bilinear $\bar{q}\gamma^{\mu}q$ under charge conjugation, and the complex conjugate changes the sign of i (or, equivalently, the sign of x). Keeping track of all the sign changes, we find:

$$F_{(f)}(x)|_{P=P',S=S'} = -q_{(\bar{f})}(-x) \qquad \text{for } x < 0.$$

For future reference, we note here that while F_T^j also changes sign under charge conjugation, $\tilde{F}$ does *not*.

Quark Spin States

Specific quark spin states can be selected with the projectors:

$$P_z^{\pm} = \frac{1 \pm \gamma_5}{2} \tag{4.5}$$

$$P_x^{\pm} = \frac{1 \pm \gamma^x \gamma_5}{2}, \tag{4.6}$$

where we consider the transverse $\hat{x}$-direction for notational simplicity. Equation 4.5 can be thought of as projecting out quarks with definite *light-cone helicity* [30, 31]. To see this, consider a quark spin state written as an arbitrary linear combination of

---

[6]This can be seen by recognizing that Eq. 4.2 is essentially a nucleon matrix element of the quark number operator $\bar{\psi}\gamma^0\psi$ in the infinite momentum frame, projected onto a definite plus-momentum.

positive and negative light cone helicity states:

$$u_q = C_+ \, u_+^{LC} + C_- \, u_-^{LC}.$$

(Light cone helicity states $u_\pm^{LC}$ are defined in Appendix C.) Then it can be shown (see Appendix) that:

$$\bar{u}_q \, \gamma^+ \, P_z^\pm \, u_q = |C_\pm|^2 \, \bar{u}_\pm^{LC} \, \gamma^+ \, u_\pm^{LC} \tag{4.7}$$

Similarly, Eq. 4.6 projects out quarks with definite "transversity" along the $\hat{x}$-direction. If we write:

$$u_q = C_\perp \, u_\perp^{LC} + C_\top \, u_\top^{LC},$$

where $u_{\perp[\top]}^{LC} \equiv \frac{1}{\sqrt{2}} \left(u_+^{LC} \pm u_-^{LC} \right)$, then we find:

$$\bar{u}_q \, \gamma^+ \, P_x^+ \, u_q = |C_\perp|^2 \, \bar{u}_\perp^{LC} \, \gamma^+ \, u_\perp^{LC}. \tag{4.8}$$

A word of caution is in order. The states we are considering are not at rest in the lab frame, and so cannot be eigenstates of the spin operator in an arbitrary direction. Indeed, $u_\perp^{LC}$ is not an eigenstate of the transverse spin operator $\hat{S}_\perp$. However, the spin state defined by $u_\perp^{LC}$ can be given a useful interpretation as the state obtained by boosting a transversely polarized state from rest to a large longitudinal momentum (see discussion in Appendix C). For ease of language, we will often refer to $u_\perp^{LC}$ as a "transversely polarized" spin state; more precisely, it is a state of definite *transversity* [4, 32].

By taking appropriate linear combinations of Eqs. 4.2, 4.3 and 4.4, it is possible to write down the distribution function for any quark spin state. For example, the distribution of quarks with positive helicity in a longitudinally polarized nucleon is given by

$$q_\uparrow^\uparrow(x) = \frac{1}{2}(F + \tilde{F})\big|_{P=P', S=S'=\uparrow},$$

while the distribution of quarks with spin in a transverse direction in a transversely polarized nucleon is given by:

$$q_{\perp}^{\perp}(x) = \frac{1}{2}(F + F_T^{\perp})\big|_{P=P',S=S'=\perp}.$$

Proton Spin States

In the preceding discussion, the dependence of the distribution functions on proton spin was implicit. In this work, we use light cone helicity states for the proton spin as well, by explicitly writing the proton spinors in terms of the light cone spinors defined above (see Appendix H).

Some Notation

Let us take this opportunity to collect equations and establish some notation. A parton distribution will be written as $q_s^S(x)$, where the *superscript* S indicates the *proton* polarization, and the *subscript* s gives the *quark* polarization. Furthermore, the arrows $\uparrow$, $\downarrow$ will be used to indicate polarization in the plus or minus $\hat{z}$-direction, respectively, while $\perp$, $\top$ indicate polarization parallel or antiparallel to a transverse axis. (For simplicity, we will often take the transverse polarization axis to be the $\hat{x}$-axis, though by rotational symmetry the results can be applied to any transverse axis). A missing index indicates a sum (or average, as appropriate) over the corresponding spin states. For example, we can write distribution functions for quarks of flavor f:

$$q_{(f)}(x) = q_{(f)}^S(x) = F_{(f)}(x)\big|_{P=P',S=S'}$$

$$q_{\uparrow,(f)}^{\uparrow}(x) = \frac{1}{2}(F_{(f)}(x) + \tilde{F}_{(f)}(x))\big|_{P=P',S=S'=\uparrow} \tag{4.9}$$

$$q_{\perp,(f)}^{\perp}(x) = \frac{1}{2}(F_{(f)}(x) + F_{T,(f)}^{\perp}(x))\big|_{P=P',S=S'=\perp}$$

47

defined for $x \geq 0$. Similarly, the *anti*quark (flavor $\bar{f}$) distribution functions are:

$$q_{(\bar{f})}(x) = q_{(\bar{f})}^S(x) = - F_{(f)}(-x)\big|_{P=P',S=S'}$$

$$q_{\uparrow,(\bar{f})}^\uparrow(x) = \frac{1}{2}(-F_{(f)}(-x) + \tilde{F}_{(f)}(-x))\big|_{P=P',S=S'=\uparrow} \tag{4.10}$$

$$q_{\perp,(\bar{f})}^\perp(x) = \frac{1}{2}(-F_{(f)}(-x) - F_{T,(f)}^\perp(-x))\big|_{P=P',S=S'=\perp}$$

also for $x \geq 0$.

Note that we will often use the shorthand notation $Q_{(f\pm f')} \equiv Q_{(f)} \pm Q_{(f')}$, for some quantity Q.

4.2.2 GPDs

The matrix elements in Eqs. 4.2, 4.3 and 4.4 can be expressed in terms of generalized parton distributions (GPDs) by writing out all possible independent terms consistent with lorentz invariance. The parameterization is not unique; in this work, we primarily use the conventions found in [33, 34].[7] Writing the average proton momentum $\bar{P} \equiv \frac{1}{2}(P + P')$, the change in momentum $\Delta \equiv P' - P$, $t \equiv \Delta^2$ and the "skewness"

---

[7]This is the parameterization used in our calculations. Following [4], it will be convenient in the analysis to rearrange some of the terms in Eq. 4.13. In particular, we will use the combination $2\tilde{H}_T + E_T \equiv \bar{E}_T$.

48

$\xi \equiv \frac{\Delta^+}{2\bar{P}^+}$, we have:

$$F_{(f)} = \frac{1}{2\bar{P}^+} \left[H_{(f)}(x,\xi,t)\, \bar{u}\, \gamma^+ u + E_{(f)}(x,\xi,t)\, \bar{u}\, \frac{i\sigma^{+\alpha}\Delta_\alpha}{2m} u \right] \tag{4.11}$$

$$\tilde{F}_{(f)} = \frac{1}{2\bar{P}^+} \left[\tilde{H}_{(f)}(x,\xi,t)\, \bar{u}\, \gamma^+ \gamma_5 u + \tilde{E}_{(f)}(x,\xi,t)\, \bar{u}\, \frac{\gamma_5 \Delta^+}{2m} u \right] \tag{4.12}$$

$$F^j_{T,(f)} = \frac{-i}{2\bar{P}^+} \left[H_{T,(f)}(x,\xi,t)\, \bar{u}\, \sigma^{+j}\gamma_5 u + \tilde{H}_{T,(f)}(x,\xi,t)\, \bar{u}\, \frac{\epsilon^{+j\alpha\beta}\Delta_\alpha \bar{P}_\beta}{m^2} u \right.$$
$$\left. + E_{T,(f)}(x,\xi,t)\, \bar{u}\, \frac{\epsilon^{+j\alpha\beta}\Delta_\alpha \gamma_\beta}{2m} u + \tilde{E}_{T,(f)}(x,\xi,t)\, \bar{u}\, \frac{\epsilon^{+j\alpha\beta}\bar{P}_\alpha \gamma_\beta}{m} u \right]. \tag{4.13}$$

Note that the spinors $\bar{u}, u$ in the above are the *proton* spinors, and depend implicitly on P, P', S and S'. The eight GPDs (H, E, $\tilde{H}$, $\tilde{E}$, H_T, $\tilde{H}_T$, E_T and $\tilde{E}_T$) are functions only of x, ξ and t. Time reversal symmetry further constrains $\tilde{E}_T$ to be an odd function of ξ [27].

The quark distribution functions can now be expressed in terms of GPDs:

$$q^S_{(f)}(x) = q_{(f)}(x) = H_{(f)}(x,0,0)$$

$$q^\uparrow_{\uparrow,(f)}(x) = q^\downarrow_{\downarrow,(f)}(x) = \frac{1}{2}\left(H_{(f)}(x,0,0) + \tilde{H}_{(f)}(x,0,0) \right)$$

$$q^\uparrow_{\downarrow,(f)}(x) = q^\downarrow_{\uparrow,(f)}(x) = \frac{1}{2}\left(H_{(f)}(x,0,0) - \tilde{H}_{(f)}(x,0,0) \right)$$

$$\tag{4.14}$$

$$q^\perp_{\perp,(f)}(x) = \frac{1}{2}\left(H_{(f)}(x,0,0) + H_{T,(f)}(x,0,0) \right)$$

$$q^\perp_{\top,(f)}(x) = \frac{1}{2}\left(H_{(f)}(x,0,0) - H_{T,(f)}(x,0,0) \right).$$

For completeness, we also give the antiquark distributions:

$$q^S_{(\bar{f})}(x) = q_{(\bar{f})}(x) = -H_{(f)}(-x, 0, 0)$$

$$q^\uparrow_{\uparrow,(\bar{f})}(x) = q^\downarrow_{\downarrow,(\bar{f})}(x) = \frac{1}{2}\left(-H_{(f)}(-x, 0, 0) + \tilde{H}_{(f)}(-x, 0, 0)\right)$$

$$q^\uparrow_{\downarrow,(\bar{f})}(x) = q^\downarrow_{\uparrow,(\bar{f})}(x) = \frac{1}{2}\left(-H_{(f)}(-x, 0, 0) - \tilde{H}_{(f)}(-x, 0, 0)\right)$$

(4.15)

$$q^\downarrow_{\perp,(\bar{f})}(x) = \frac{1}{2}\left(-H_{(f)}(-x, 0, 0) - H_{T,(f)}(-x, 0, 0)\right)$$

$$q^\downarrow_{\top,(\bar{f})}(x) = \frac{1}{2}\left(-H_{(f)}(-x, 0, 0) + H_{T,(f)}(-x, 0, 0)\right).$$

Since $q^S_{s,(f)}(x)$ and $q^S_{s,(\bar{f})}(x)$ can be interpreted as probability distributions, they must necessarily be positive functions. This positivity can be used to put constraints on the GPDs. For example, we see immediately from Eq. 4.14 that $H_{(f)}(x, 0, 0) \geq \tilde{H}_{(f)}(x, 0, 0)$. Tighter constraints can be obtained from more comprehensive analysis of the distributions for arbitrary spin states[4].

4.2.3 Off-Forward Matrix Elements

The distribution functions in Eq. 4.14 only depend on the forward ($t = 0$) parts of the GPDs. As we saw in the preceding sections, the GPDs in this limit can be interpreted as probability densities. However, when $t \neq 0$, the initial and final proton states in Eqs. 4.2, 4.3 and 4.4 are different, so we cannot attach to them a simple probabilistic interpretation as we did in the forward case. How then can we interpret the off-forward GPDs?

In this thesis, we focus on the case $\xi = 0$. This corresponds to the situation where the momentum transfer is entirely in the transverse directions ($\Delta^+ = 0$), so the initial and final proton states differ only in their transverse momenta. One might

imagine that if we could somehow integrate out the matrix elements' dependence on the transverse momentum, we could obtain again a result with a probabilistic interpretation.

This is indeed the case, as can be seen by taking the (transverse) Fourier transform of Eq. 4.2. Setting $P^+ = P'^+, S = S'$ and suppressing the spin label and Wilson line (we follow closely the notation in [4, 35]), we find:

$$\mathcal{F} \equiv \int \frac{d^2\boldsymbol{\Delta}}{(2\pi)^2} e^{-i\mathbf{b}\cdot\boldsymbol{\Delta}} \, F\big|_{P^+=P'^+}$$

$$= \int \frac{d^2\boldsymbol{\Delta}}{(2\pi)^2} e^{-i\mathbf{b}\cdot\boldsymbol{\Delta}} \int \frac{dz^-}{4\pi} e^{ix\bar{P}^+z^-} \big\langle \mathbf{P}', P^+ \big| \bar{\psi}(z_1)\,\gamma^+\,\psi(z_2) \big| \mathbf{P}, P^+ \big\rangle$$

$$= N^{-1} \int \frac{d^2\bar{\mathbf{P}}}{(2\pi)^2} \frac{d^2\boldsymbol{\Delta}}{(2\pi)^2} e^{-i\mathbf{b}\cdot\boldsymbol{\Delta}} \int \frac{dz^-}{4\pi} e^{ix\bar{P}^+z^-} \big\langle \mathbf{P}', P^+ \big| \bar{\psi}(z_1)\,\gamma^+\,\psi(z_2) \big| \mathbf{P}, P^+ \big\rangle,$$

where $N \equiv \int \frac{d^2\mathbf{P}}{(2\pi)^2}$, and $z_2^- = -z_1^- = \frac{1}{2}z^-$ (all other components zero).[8] Note that the last step is valid because the integrand is independent of $\bar{\mathbf{P}}$. We can change the integration variables:

$$\mathcal{F} = N^{-1} \int \frac{d^2\mathbf{P}}{(2\pi)^2} \frac{d^2\mathbf{P}'}{(2\pi)^2} e^{-i\mathbf{b}\cdot(\mathbf{P}'-\mathbf{P})} \int \frac{dz^-}{4\pi} e^{ix\bar{P}^+z^-} \big\langle \mathbf{P}', P^+ \big| \bar{\psi}(z_1)\,\gamma^+\,\psi(z_2) \big| \mathbf{P}, P^+ \big\rangle$$

$$= N^{-1} \int \frac{dz^-}{4\pi} e^{ix\bar{P}^+z^-} \big\langle -\mathbf{b};\, P^+ \big| \bar{\psi}(z_1)\,\gamma^+\,\psi(z_2) \big| {-}\mathbf{b};\, P^+ \big\rangle, \tag{4.16}$$

where now the nucleon states are localized in transverse position space:

$$\big| \mathbf{b};\, P^+ \big\rangle \equiv \int \frac{d^2\mathbf{P}}{(2\pi)^2} e^{-i\mathbf{b}\cdot\mathbf{P}} \big| \mathbf{P}, P^+ \big\rangle. \tag{4.17}$$

In the above, $\mathbf{b}$ gives the transverse position of the center of momentum of *all* the partons (both quarks and gluons) in the nucleon, defined as [28, 35] $\mathbf{b}_{cm} = \sum_i x_i \, \mathbf{b}_i$. If we shift our coordinate system so that the nucleon center of momentum is at the

---

[8] N here is divergent. This can be avoided by taking wavepackets spread out over position space.

origin, Eq. 4.16 becomes:

$$\mathcal{F} = N^{-1} \int \frac{dz^-}{4\pi} e^{ix\bar{P}^+ z^-} \langle \mathbf{0}; \, P^+ | \bar{\psi}(z_1) \, \gamma^+ \, \psi(z_2) | \mathbf{0}; \, P^+ \rangle, \qquad (4.18)$$

where now $\mathbf{z_2} = \mathbf{z_1} = \mathbf{b}$. (The fields in the Wilson line—which we suppress in Eq. 4.16—are also shifted to transverse position $\mathbf{b}$.) Equation 4.18 is again a diagonal matrix element of the quark current operator between nucleon states, but now it is a function of transverse position as well as plus-momentum. We interpret this as the *impact parameter-dependent* quark distribution function (or transverse distribution function, for short) $q(x, \mathbf{b})$: the probability to find a quark with momentum fraction x, at transverse position $\mathbf{b}$ relative to the nucleon center of momentum. In the same way, the polarized transverse position dependent quark distribution functions are:

$$q_\uparrow^\uparrow(x, \mathbf{b}) = \frac{1}{2}(\mathcal{F} + \tilde{\mathcal{F}})|_{P=P', S=S'=\uparrow}$$
$$q_\perp^\perp(x, \mathbf{b}) = \frac{1}{2}(\mathcal{F} + \mathcal{F}_T^\perp)|_{P=P', S=S'=\perp}$$

and so on, where $\tilde{\mathcal{F}}$ and $\mathcal{F}_T^i$ are defined analogously to $\mathcal{F}$. In terms of (Fourier transforms of) GPDs, we have (see Appendix H):

$$q(x, \mathbf{b}) = q^\uparrow(x, \mathbf{b}) = \mathcal{H} \qquad (4.19)$$

$$q^\perp(x, \mathbf{b}) = \left(\mathcal{H} - b^y \frac{1}{m} \frac{\partial}{\partial b^2} \mathcal{E} \right) \qquad (4.20)$$

$$q_\uparrow^\uparrow(x, \mathbf{b}) = \frac{1}{2} \left(\mathcal{H} + \tilde{\mathcal{H}} \right) \qquad (4.21)$$

$$q_\downarrow^\uparrow(x, \mathbf{b}) = \frac{1}{2} \left(\mathcal{H} - \tilde{\mathcal{H}} \right) \qquad (4.22)$$

$$q_\perp^\perp(x, \mathbf{b}) = \frac{1}{2}\left(\mathcal{H} - b^y\frac{1}{m}\frac{\partial}{\partial b^2}\mathcal{E} - b^y\frac{1}{m}\frac{\partial}{\partial b^2}(\mathcal{E}_T + 2\tilde{\mathcal{H}}_T)\right) \tag{4.23}$$

$$+ \left(\mathcal{H}_T - \frac{1}{4m^2}\frac{\partial}{\partial b^i}\frac{\partial}{\partial b^i}\tilde{\mathcal{H}}_T\right) + ((b^x)^2 - (b^y)^2)\frac{1}{m^2}\left(\frac{\partial}{\partial b^2}\right)^2\tilde{\mathcal{H}}_T\Bigg)$$

$$q_\top^\perp(x, \mathbf{b}) = \frac{1}{2}\left(\mathcal{H} - b^y\frac{1}{m}\frac{\partial}{\partial b^2}\mathcal{E} + b^y\frac{1}{m}\frac{\partial}{\partial b^2}(\mathcal{E}_T + 2\tilde{\mathcal{H}}_T)\right) \tag{4.24}$$

$$- \left(\mathcal{H}_T - \frac{1}{4m^2}\frac{\partial}{\partial b^i}\frac{\partial}{\partial b^i}\tilde{\mathcal{H}}_T\right) - ((b^x)^2 - (b^y)^2)\frac{1}{m^2}\left(\frac{\partial}{\partial b^2}\right)^2\tilde{\mathcal{H}}_T\Bigg),$$

where $\mathcal{H}(x, \mathbf{b})$ is the Fourier transform of the GPD $H(x, 0, -\boldsymbol{\Delta}^2)$, $\mathcal{E}(x, \mathbf{b})$ is the Fourier transform of $E(x, 0, -\boldsymbol{\Delta}^2)$, etc. Here we take $\perp$ to indicate polarization along $\hat{x}$-axis (more general forms of these equations can be found in [4]).

In order to make contact with notation existing in the literature, we note that the distribution we have called $q^\perp(x, \mathbf{b})$ is the same as the distribution Burkardt calls $q_X(x, \mathbf{b}_\perp)$ in [36], and $\Delta q(x, \mathbf{b}_\perp)$ in [36] is equal to our $q_\top^\uparrow(x, \mathbf{b}) - q_\downarrow^\uparrow(x, \mathbf{b})$.

$\xi \neq 0$ corresponds to the situation where the momentum transfer is in an arbitrary direction. In this case, Eq. 4.2 cannot be given a simple probabilistic interpretation. We do not consider the $\xi \neq 0$ case in this thesis, but refer the reader to the studies in [37, 38].

4.3 On the Lattice: GFFs and Mellin moments

The quark operators in Eqs. 4.2, 4.3 and 4.4 are non-local—the ψ and $\bar{\psi}$ are separated by a light-like displacement (which is integrated over). Such operators are impossible to compute directly on a finite Euclidean lattice. Rather, the operators which are accessible on the lattice are *Mellin moments* of the bi-local operators. The nth Mellin moment of a function $f(x)$ is defined as $\int_{-1}^{1} dx\, x^{n-1} f(x)$. In Appendix G, we show explicitly how the Mellin moments of Eq. 4.2 and following lead to matrix elements of the local operators $\mathcal{O}_\Gamma$:

$$\mathcal{O}_\Gamma^{\{\mu_1\cdots\mu_n\}} = \bar{\psi}(0)\Gamma^{\{\mu_1}i\overleftrightarrow{D}^{\mu_2}\cdots i\overleftrightarrow{D}^{\mu_n\}}\psi(0), \tag{4.25}$$

53

where $\{\cdots\}$ indicates symmetrization of indices, and Γ represents the gamma matrix insertion: $\Gamma^\mu \in \{\gamma^\mu, \gamma^\mu\gamma_5, -i\sigma^{\mu\alpha}\gamma_5\}$[9].

It should be noted that taking Mellin moments of the bilocal operators is equivalent to performing an operator product expansion (OPE). We will not pursue the connection in this thesis, but refer the reader to the discussions of the OPE in [29].

These lattice operators are parametrized in terms of generalized form factors (GFFs),[10] which are (related to) moments of GPDs. Using the conventions in [33, 34], the GFFs for the lowest-moment operators are:

$$\langle P'| \, \bar\psi(0) \, \gamma^\mu \, \psi(0) \, |P\rangle = A_{10}(t) \, \bar u \, \gamma^\mu \, u + \frac{i}{2m} \, B_{10}(t) \, \Delta_\alpha \, \bar u \, \sigma^{\mu\alpha} \, u \tag{4.26}$$

$$\langle P'| \, \bar\psi(0) \, \gamma^\mu\gamma_5 \, \psi(0) \, |P\rangle = \tilde A_{10}(t) \, \bar u \, \gamma^\mu\gamma_5 \, u + \frac{1}{2m} \, \tilde B_{10}(t) \, \Delta^\mu \, \bar u \, \gamma_5 \, u \tag{4.27}$$

$$\langle P'| \, \bar\psi(0) \, i\sigma^{\mu\alpha} \, \psi(0) \, |P\rangle = A_{T10}(t) \, \bar u \, i\sigma^{\mu\alpha} \, u + \frac{1}{m^2} \, \tilde A_{T10}(t) \, \left(\bar P^\mu \Delta^\alpha - \bar P^\alpha \Delta^\mu\right) \, \bar u \, u$$
$$+ \frac{1}{2m} \, B_{T10}(t) \, \bar u \, \left(\gamma^\mu \Delta^\alpha - \gamma^\alpha \Delta^\mu\right) \, u. \tag{4.28}$$

(A complete listing of all GFFs considered in this thesis is given in Appendix G.) Note that the tensor operator in Eq. 4.28 can be written with or without the γ_5 by virtue of the identity [31]:

$$\sigma^{\mu\nu}\gamma_5 = -\frac{i}{2}\epsilon^{\mu\nu\alpha\beta} \, \sigma_{\alpha\beta}.$$

Also, we will generally use the GFF $\bar B_{Tn0} \equiv 2\tilde A_{Tn0} + B_{Tn0}$ in preference to B_{Tn0}. The form factors tend to appear in this combination in the physical observables we consider, so we regard $\bar B_{Tn0}$ as the more fundamental quantity. In addition, the combination $2\tilde A_{Tn0} + B_{Tn0}$ is much more well determined in our actual lattice calculations than either $\tilde A_{Tn0}$ or B_{Tn0} individually.

---

[9]Note that $\sigma^{\mu\alpha}$ is written here with only one "active" index.

[10]in exactly the same way as the *bilocal* operators were parameterized by GPDs

We can write the GFFs in terms of moments of GPDs:

$$A_{10}(t) = \int_{-1}^{1} dx\, H(x,\xi,t)$$

$$B_{10}(t) = \int_{-1}^{1} dx\, E(x,\xi,t)$$

$$\tilde{A}_{10}(t) = \int_{-1}^{1} dx\, \tilde{H}(x,\xi,t)$$

$$\tilde{B}_{10}(t) = \int_{-1}^{1} dx\, \tilde{E}(x,\xi,t) \tag{4.29}$$

$$A_{T10}(t) = \int_{-1}^{1} dx\, H_T(x,\xi,t)$$

$$\tilde{A}_{T10}(t) = \int_{-1}^{1} dx\, \tilde{H}_T(x,\xi,t)$$

$$B_{T10}(t) = \int_{-1}^{1} dx\, E_T(x,\xi,t).$$

Similar identities hold for higher moments (see Appendix G). We also note that the Fourier transforms of the GFFs can be expressed in terms of moments of Fourier transforms of GPDs:

$$\mathcal{A}_{10}(b^2) \equiv \int \frac{d^2\mathbf{\Delta}}{(2\pi)^2} e^{-i\mathbf{b}\cdot\mathbf{\Delta}} A_{10}(-\mathbf{\Delta}^2) = \int_{-1}^{1} dx\, \mathcal{H}(x,\mathbf{b}), \tag{4.30}$$

and so on.

The proliferation of functions, symbols, and subscripts may threaten to overwhelm readers unfamiliar with the territory. To prevent confusion, let us pause to emphasize that GFFs and GPDs can be thought of as two different "languages" for describing the same physics. The primary difference between the two is that while GPDs contain the full x-dependence of the matrix elements in Eq. 4.2 and following, GFFs have the x-dependence integrated out (giving the Mellin moments described above).[11] If we had the complete (infinite!) set of GFFs, we could reconstruct the GPDs. The reason for using GFFs at all is that they are the quantities we can access in lattice calculations. In this thesis, we will often begin a discussion using the language of

---

[11] There is thus an *infinite* number of GFFs corresponding to each GPD.

GPDs, and then translate the conclusions into the language of GFFs in order to make contact with calculations.

4.3.1 More on Moments

Note that the integration interval in the definition of Mellin moments extends from -1 to 1. As discussed in Section 4.2.1, values of x in the range $-1 < x < 0$ lead to *antiquark* distribution functions. So, when we take Mellin moments of GPDs, what we actually calculate are sums (or differences, depending on the moment) of quark and antiquark observables. This is an unavoidable feature of our lattice calculations. In the next section, we will keep careful track of the antiquark terms; in future chapters, we will generally leave these terms implicit.

4.4 Nucleon Structure from Parton Distributions

It is clear that GPDs and GFFs encode a huge amount of information about nucleon structure. It may not be as clear how to understand that information. In this thesis, we will focus on quantities that have a simple physical interpretation in terms of the parton distributions discussed above. It turns out that quite a few physical observables can be extracted from the GFFs within the parton framework.

As we begin this partonic exploration of nucleon structure, it will be helpful to review our primary tools—the transverse position-dependent parton distribution functions in Eqs. 4.19 - 4.23. These distributions will be treated as probability densities, giving the probability of finding a parton (in this case, a quark) with a particular transverse position and longitudinal momentum inside a nucleon.[12] The polarizations of both the quark and the nucleon can be specified.

It is important to emphasize that these distributions, as interpreted above, strictly apply only to a nucleon in the infinite momentum limit. In the lab frame, one could imagine that they correspond to distributions of the plus-component of quark current,

---

[12]As already discussed, lattice calculations do not provide access to the full x-dependence of these distributions, but only to *moments* in x. However, it will be convenient to start with the language of x-dependent GPDs.

and can be more appropriately interpreted as the quark number density *plus* the quark current in the $\hat{z}$-direction. We will occasionally take this point of view, to demonstrate that the results are independent of frame (Section 4.4.4). Also, the spin states used in Eqs. 4.19 - 4.23 are *light cone helicity* states, which are not the same as ordinary helicity or spin states in the lab frame (see Appendix C).

It will be useful to keep in mind the particular roles played by the vector, axial and tensor lattice operators: the vector operators are insensitive to quark polarization (they *sum* over quark spin states), the axial operators involve quark spins along the longitudinal axis, and the tensor operators involve quark spins along a transverse axis.

With these guidelines in mind, let us consider some specific aspects of nucleon structure that can be studied in our calculations. Note that some of the quantities discussed below are not (yet) experimentally accessible. Such quantities still provide valuable insight into what is going on inside a proton, and may be thought of as complementing the available experimental data.[13]

4.4.1 Charges

One of the simplest things we can do with parton distributions is to count.[14] By integrating over all the distribution variables, we can count the number of quarks in a particular state. For example, the total number of quarks of flavor f is given by (using Eqs. 4.14 and 4.15):

$$N_{(f)} = \int_0^1 dx \, q_{(f)}(x) = \int_0^1 dx \, H_{(f)}(x, 0, 0). \qquad (4.31)$$

Note that the range of integration over x is from 0 to 1. As discussed above, lattice calculations only have access to integrals over x from -1 to 1, corresponding in this

---

[13]Of course, such insight from the lattice is only valuable because there *do* exist other quantities which *can* be compared with experiment.

[14]This section will act as a warm-up for the sections to come, so we take extra time to familiarize the reader with our methods and notation.

case to the number of quarks *minus* the number of antiquarks:

$$N_{(f-\bar{f})} = N_{(f)} - N_{(\bar{f})} = \int_{-1}^{1} dx\, H_{(f)}(x, 0, 0) \equiv A_{10}^{(f)}(0). \tag{4.32}$$

This quantity (the *vector* charge) simply counts the number of valence quarks in the nucleon. Since we already know what this number *should* be (we used it to build a nucleon on the lattice in the first place), we use the measured value as a normalization.

Axial charge

If we try to count the number of quarks with spin parallel to the proton spin along the $\hat{z}$-axis, we find that the accessible quantity is the difference:

$$N_{\uparrow,(f)}^{\uparrow} - N_{\downarrow,(\bar{f})}^{\uparrow} = \int_{0}^{1} dx\, \left(q_{\uparrow,(f)}^{\uparrow}(x) - q_{\downarrow,(\bar{f})}^{\uparrow}(x) \right)$$

$$= \int_{0}^{1} dx\, \frac{1}{2} \left(H_{(f)}(x, 0, 0) + \tilde{H}_{(f)}(x, 0, 0) + H_{(f)}(-x, 0, 0) + \tilde{H}_{(f)}(-x, 0, 0) \right)$$

$$= \int_{-1}^{1} dx\, \frac{1}{2} \left(H_{(f)}(x, 0, 0) + \tilde{H}_{(f)}(x, 0, 0) \right)$$

$$\equiv \frac{1}{2} \left(A_{10}^{(f)}(0) + \tilde{A}_{10}^{(f)}(0) \right). \tag{4.33}$$

Similarly:

$$N_{\downarrow,(f)}^{\uparrow} - N_{\uparrow,(\bar{f})}^{\uparrow} = \frac{1}{2} \left(A_{10}^{(f)}(0) - \tilde{A}_{10}^{(f)}(0) \right). \tag{4.34}$$

If we take the difference of the two, we have the *axial* charge:[15]

$$\tilde{A}_{10}^{(f)}(0) = N_{\uparrow,(f+\bar{f})}^{\uparrow} - N_{\downarrow,(f+\bar{f})}^{\uparrow}.$$

---

[15]Usually, the "axial charge" is taken to be specifically the isovector flavor combination: $u - d$. In this section, we use the term more generally, without regard to flavor.

Note that the axial charge (for each flavor) is proportional to the quark spin contribution to the nucleon angular momentum. This fact will be used in our discussion of angular momentum in Section 4.4.5.

Tensor charge

If we take the polarization axis to be in a transverse direction, we get:

$$N_{\perp,f}^{\perp} - N_{\perp,\bar{f}}^{\perp} = \frac{1}{2}\left(A_{10}^{(f)}(0) + A_{T10}^{(f)}(0)\right) \tag{4.35}$$

$$N_{\top,f}^{\perp} - N_{\top,\bar{f}}^{\perp} = \frac{1}{2}\left(A_{10}^{(f)}(0) - A_{T10}^{(f)}(0)\right) \tag{4.36}$$

with the corresponding *tensor* charge:

$$A_{T10}^{(f)}(0) = N_{\perp,(f-\bar{f})}^{\perp} - N_{\top,(f-\bar{f})}^{\perp}.$$

Note that in contrast to the axial charge, which gave the *sum* of the quarks and antiquarks aligned with the nucleon spin (minus those anti-aligned), the tensor charge gives the *difference*. This fact will be discussed later in Section 6.4.

4.4.2 Momentum Fractions

Given the quark distribution functions $q(x)$, the second moment $\int_{-1}^{1} dx\, x\, q(x)$ simply gives the average quark momentum fraction $\langle x \rangle$. This is the fraction of the nucleon plus-momentum (or, in the IMF, the fraction of the total nucleon energy) that is carried by the quarks (plus or minus antiquarks). If we ignore quark polarization, we have the sum:

$$\langle x \rangle_{(f)} + \langle x \rangle_{(\bar{f})} = \int_{-1}^{1} dx\, x\, H_{(f)}(x,0,0) \equiv A_{20}^{(f)}(0). \tag{4.37}$$

59

The contributions to the momentum fraction from polarized quarks are:

$$\langle x \rangle^{\uparrow}_{\uparrow,(f)} + \langle x \rangle^{\uparrow}_{\downarrow,(\bar{f})} = \frac{1}{2} \left(A^{(f)}_{20}(0) + \tilde{A}^{(f)}_{20}(0) \right)$$

$$\langle x \rangle^{\uparrow}_{\downarrow,(f)} + \langle x \rangle^{\uparrow}_{\uparrow,(\bar{f})} = \frac{1}{2} \left(A^{(f)}_{20}(0) - \tilde{A}^{(f)}_{20}(0) \right)$$

$$\langle x \rangle^{\perp}_{\perp,(f)} + \langle x \rangle^{\perp}_{\perp,(\bar{f})} = \frac{1}{2} \left(A^{(f)}_{20}(0) + A^{(f)}_{T20}(0) \right)$$ (4.38)

$$\langle x \rangle^{\perp}_{\top,(f)} + \langle x \rangle^{\perp}_{\top,(\bar{f})} = \frac{1}{2} \left(A^{(f)}_{20}(0) - A^{(f)}_{T20}(0) \right) .$$

It is common to quote the differences:

$$\left(\langle x \rangle^{\uparrow}_{\uparrow,(f-\bar{f})} - \langle x \rangle^{\uparrow}_{\downarrow,(f-\bar{f})} \right) \equiv \langle x \rangle_{\Delta f} = \tilde{A}^{(f)}_{20}(0)$$ (4.39)

$$\left(\langle x \rangle^{\perp}_{\perp,(f+\bar{f})} - \langle x \rangle^{\perp}_{\top,(f+\bar{f})} \right) \equiv \langle x \rangle_{\delta f} = A^{(f)}_{T20}(0).$$ (4.40)

Note that, apart from relativistic effects due to the the choice of a special longitudinal direction, the difference between longitudinal and transverse quark polarizations is again the sign of the antiquark contribution. (It is a straightforward generalization of the above discussion to write down the higher moments $\langle x^2 \rangle$, $\langle x^3 \rangle$. In this thesis, however, we will focus on the lowest two x-moments.)

4.4.3 Charge Radius

In the above calculations of charges and momentum fractions, we used only the "ordinary" parton distributions $q(x)$. What additional information can we extract from the distributions in transverse position space, $q(x, \mathbf{b})$?

One quantity of interest is the mean squared charge radius $\langle b_e^2 \rangle$,[16] which is a

---

[16]here we write the subscript e to indicate that we are considering distributions of electric charge

measure of the transverse distribution of charge in the proton.[17] In terms of GFFs, for unpolarized quarks we find:

$$\langle b_e^2 \rangle_{(f)} + \langle b_e^2 \rangle_{(\bar{f})} = e_{(f)} \int_0^1 dx \int d^2\mathbf{b}\, b^2 \left(q_{(f)}(x,\mathbf{b}) - q_{(\bar{f})}(x,\mathbf{b}) \right)$$

$$= e_{(f)} \int_{-1}^1 dx \int d^2\mathbf{b}\, b^2\, \mathcal{H}_{(f)}(x,\mathbf{b}) \tag{4.41}$$

$$= 4e_{(f)} \frac{\partial}{\partial t} A_{10}^{(f)}(t)\big|_{t=0},$$

where we denote the charge of the quarks by $e_{(f)}$. In this case we have the *sum* of quark, antiquark contributions because $e_{(\bar{f})} = -e_{(f)}$. (Note, however, that $\langle b_e^2 \rangle$ is *negative* for distributions of negative charge.) If we *assume* that the charge distribution in the rest frame of the proton is spherically symmetric, we can define the three-dimensional radius:

$$\langle r^2 \rangle = \frac{3}{2} \langle b^2 \rangle.$$

(In the lab frame, there is no rigorous relation of form factor slope to spatial radius. However, because there *is* a correspondence in the non-relativistic limit, it is common to define the dirac radius $\langle r_1^2 \rangle \equiv 6\frac{\partial}{\partial t} A_{10}^{(f)}(t)\big|_{t=0}$, and to loosely think of it—as we do above—as the radius of a spherically symmetric distribution in three dimensions.[18])

One could also define the mean squared radius of the "spin densities":

$$\langle b^2 \rangle_{\uparrow,(f+\bar{f})}^{\uparrow} - \langle b^2 \rangle_{\downarrow,(f+\bar{f})}^{\uparrow} = 4 \frac{\partial}{\partial t} \tilde{A}_{10}^{(f)}(t)\big|_{t=0} \tag{4.42}$$

$$\langle b^2 \rangle_{\perp,(f-\bar{f})}^{\perp} - \langle b^2 \rangle_{\top,(f-\bar{f})}^{\perp} = 4 \frac{\partial}{\partial t} A_{T10}^{(f)}(t)\big|_{t=0}. \tag{4.43}$$

---

[17]This is the natural quantity to measure in the IMF, where the proton appears flattened due to lorentz contraction. It is analogous to measuring $\langle r_\perp^2 \rangle$, where $r_\perp$ is the distance to the longitudinal axis.

[18]see [39] for some relevant discussion

(Note that here we do *not* include the electric charge $e_{(f)}$ in the definition of $\langle b^2 \rangle$, and the sign of the antiquark contribution is set accordingly.)

4.4.4 Magnetic Moments

The magnetic moment of the proton provides an especially interesting context in which to explore the application of transverse parton distributions. To see this, let us start with the expression for the magnetic moment of a classical current density $\mathbf{j}(\mathbf{r})$ [40, 15]:

$$\mu = \frac{1}{2} \int d^3\mathbf{r} \; \mathbf{r} \times \mathbf{j}(\mathbf{r}). \tag{4.44}$$

If we consider the case where the magnetic moment is in the $\hat{x}$-direction, and furthermore assume that the current density $\mathbf{j}$ is symmetric under rotations about the x-axis, we have:

$$\mu_x = \frac{1}{2} \int d^3\mathbf{r} \; \left(r^y j^z(\mathbf{r}) - r^z j^y(\mathbf{r}) \right)$$

$$= \int d^3\mathbf{r} \, r^y \, j^z(\mathbf{r}). \tag{4.45}$$

If the coordinate origin is taken to be the (lab frame) center of mass of the distribution, we can add $\int d^3\mathbf{r} \, r^y \, j^0(\mathbf{r}) = 0$ to the above equation, where j^0 is the charge distribution. We obtain:

$$\mu_x = \int d^3\mathbf{r} \, r^y \, \left(j^z(\mathbf{r}) + j^0(\mathbf{r}) \right)$$

$$= N \int d^3\mathbf{r} \, r^y \, j^+(\mathbf{r}), \tag{4.46}$$

where the normalization N is chosen such that $N \int d^3\mathbf{r} \, j^+(\mathbf{r})$ gives the total charge. Let us now apply Eq. 4.46 to a proton polarized in the $\hat{x}$-direction, assuming that the

current density is completely due to the constituent partons. As discussed previously, we can take the distribution $e_{(f)} q^\perp(x, \mathbf{b})$ to be the density of the lab frame plus-current j^+ of flavor f quarks in a transversely polarized[19] proton. From Eq. 4.20, we have (for $\perp$ in the $\hat{x}$-direction):

$$q^\perp(x, \mathbf{b}) = \mathcal{H}(x, b^2) - b^y \frac{1}{m} \frac{\partial}{\partial b^2} \mathcal{E}(x, b^2)$$

$$= \mathcal{H}(x, b^2) - \frac{1}{2m} \frac{\partial}{\partial b^y} \mathcal{E}(x, b^2). \tag{4.47}$$

Remembering to include the "Melosh shift" (see Appendix C), we have the flavor f contribution to the magnetic moment of the proton:

$$\mu_{(f+\bar{f})} = e_{(f)} \int_{-1}^{1} dx \int d^2\mathbf{b} \left(b^y + \frac{1}{2m} \right) \left(\mathcal{H}_{(f)}(x, b^2) - \frac{1}{2m} \frac{\partial}{\partial b^y} \mathcal{E}_{(f)}(x, b^2) \right)$$

$$= e_{(f)} \int_{-1}^{1} dx \frac{1}{2m} \left(H_{(f)}(x, 0, 0) + E_{(f)}(x, 0, 0) \right)$$

$$= \frac{e_{(f)}}{2m} \left(A_{10}^{(f)}(0) + B_{10}^{(f)}(0) \right) \tag{4.48}$$

where $e_{(f)}$ is the electric charge for quark flavor f. (Note that we again have the *sum* of quark and antiquark contributions, due to the factor of electric charge.) Referring back to Eq. 4.26, we see that this is the familiar result for the magnetic moment of a spin-$\frac{1}{2}$ particle (see [6], for example). It is interesting to consider how we arrived at Eq. 4.48. Starting with a classical expression (Eq. 4.44) and applying it to a parton model, we obtain the correct field-theoretic result. Moreover, the Melosh shift was key to obtaining the full expression—if we had not included the shift, we would only have gotten the *anomalous* magnetic moment $\kappa = B_{10}(0)$.

In the above calculation, we interpreted the parton distribution $q^\perp(x, \mathbf{b})$ as the lab frame density of the plus-current. However, we would have obtained exactly the

---

[19]in light cone helicity states!

63

same result if we had stayed in the IMF. In that case, we would interpret $e_{(f)} q^{\perp}(x, \mathbf{b})$ as an *electric charge* density, and Eq. 4.48 would be interpreted as an *electric dipole* moment, measured with respect to the lab frame center of mass. This is simply another way of viewing the magnetic moment—a magnetic dipole boosted to a moving frame does indeed develop an electric dipole moment (as a simple consequence of the Lorentz transform). We emphasize that the above manipulations should not be regarded as a derivation, but rather as a suggestive mnemonic, illustrating the extent to which our simplistic model of the nucleon as a cloud of partons gives the correct (previously known) result.

We can also calculate the contribution to the magnetic moment from quarks polarized [anti]parallel to the proton—we simply use the distribution function $q_{\perp}^{\parallel}(x, \mathbf{b})$ [$q_{\perp}^{\nparallel}(x, \mathbf{b})$] (Eq. 4.23) as our current density. The result is:

$$\mu_{(f+\bar{f})}^{\parallel} = \frac{e_{(f)}}{4m} \left(A_{10}^{(f)}(0) + B_{10}^{(f)}(0) + A_{T10}^{(f)}(0) + \bar{B}_{T10}^{(f)}(0) \right) \tag{4.49}$$

$$\mu_{(f+\bar{f})}^{\nparallel} = \frac{e_{(f)}}{4m} \left(A_{10}^{(f)}(0) + B_{10}^{(f)}(0) - A_{T10}^{(f)}(0) - \bar{B}_{T10}^{(f)}(0) \right), \tag{4.50}$$

where $\parallel$ ($\nparallel$) indicates the quark spin (anti)parallel to the proton spin. (This notation denotes basically the same thing as $\mu_{\perp}^{\parallel}$, with μ understood to be measured along the direction of the proton spin.) The difference, $\frac{e_{(f)}}{2m} \left(A_{T10}^{(f)}(0) + \bar{B}_{T10}^{(f)}(0) \right)$, measures how much *more* of the magnetic moment is due to quarks aligned with the proton than to quarks antialigned.

4.4.5 Angular Momentum

The quark contribution to the nucleon spin is in many ways analogous to the quark contribution to the nucleon magnetic moment. One might speculate that the integral:

$$m \int dx \int d^2\mathbf{b}\, b^y\, x\, q^{\perp}(x, \mathbf{b}) \tag{4.51}$$

has something to do with quark orbital angular momentum, since in the rest frame of the proton (where $P^+ \propto m$) it resembles the expectation value of $\mathbf{r} \times \mathbf{p}$, where p is the parton four-momentum:

$$\int dx \int d^2\mathbf{b}\, b^y\, p^+\, q^\perp(x, \mathbf{b}) \;\propto\; \int dx \int d^2\mathbf{b}\, b^y\, (p^z + p^0)\, q^\perp(x, \mathbf{b}).$$

In fact, Burkardt showed [41] that (4.51)—once the Melosh shift is taken into account— actually gives the *total* (orbital plus spin) quark contribution to the proton spin. Using Eq. 4.20, we find that the total angular momentum in the $\hat{x}$-direction for quarks of flavor f inside a proton polarized in the $\hat{x}$-direction is:[20]

$$J_{x,(f+\bar{f})} = \frac{1}{2}\left(A_{20}^{(f)}(0) + B_{20}^{(f)}(0)\right). \tag{4.52}$$

This well-known result was first calculated by Ji in [42].[21] One could further divide this into contributions from quarks polarized parallel or antiparallel to the proton:

$$J_{(f+\bar{f})}^{\|} = \frac{1}{2}\left(A_{20}^{(f)}(0) + B_{20}^{(f)}(0) + A_{T20}^{(f)}(0) + \bar{B}_{T20}^{(f)}(0)\right) \tag{4.53}$$

$$J_{(f+\bar{f})}^{\nparallel} = \frac{1}{2}\left(A_{20}^{(f)}(0) + B_{20}^{(f)}(0) - A_{T20}^{(f)}(0) - \bar{B}_{T20}^{(f)}(0)\right), \tag{4.54}$$

where we use the notation defined previously.

As mentioned earlier, the axial form factor $\tilde{A}_{10}^{(f)}$ gives the total quark *spin* contribution to angular momentum. Subtracting this from Eq. 4.52, we obtain the total quark *orbital* angular momentum:

$$L_{(f+\bar{f})} = \frac{1}{2}\left(A_{20}^{(f)}(0) + B_{20}^{(f)}(0) - \tilde{A}_{10}^{(f)}(b)\right). \tag{4.55}$$

---

[20]The Melosh shift is essential to obtaining the A_{20} term in this result.

[21]It is intriguing to observe that in this formulation, an expression that resembles the classical *orbital* angular momentum density turns out to give the *total* quark angular momentum. Similarly, in the previous section, the total quark contribution to the magnetic moment was calculated using the expression for a classical current density. This suggests that, on some level, all angular momentum can be viewed as a sort of "orbital" angular momentum [43], and all magnetic dipoles can be viewed as current loops.

4.4.6 Quark Center of Charge, Momentum

We have seen that the GFFs B_{n0} appear in the expressions for magnetic moment and angular momentum. These form factors can also be understood in terms of the quark center of charge, or dipole moment (B_{10}), and center of light-cone momentum (B_{20}), measured in a transversely polarized nucleon. This follows directly from the distribution in Eq. 4.20:

$$\langle\, b^y\,\rangle^{\perp} \equiv \int dx \int d^2\mathbf{b}\, b^y\, q^{\perp}(x, \mathbf{b}) = \frac{1}{2m} B_{10} \qquad (4.56)$$

$$\langle\, x\, b^y\,\rangle^{\perp} \equiv \int dx\, x \int d^2\mathbf{b}\, b^y\, q^{\perp}(x, \mathbf{b}) = \frac{1}{2m} B_{20}, \qquad (4.57)$$

where locations are measured relative to the center of (light-cone) momentum of *all* the partons in the nucleon. Similar relations hold for the tensor form factors $\bar{B}_{Tn0}$.

Equation 4.57 implies that $\frac{1}{m} B_{20}^{(u+d)}$ equals the distance between the quark center of momentum and the gluon center of momentum. If this distance is zero (as lattice calculations suggest—see Fig. 5-5), then the total fractional quark contribution to the nucleon *angular* momentum (Eq. 4.52) would be equal to the total fractional quark contribution to the nucleon *plus*-momentum (Eq. 4.37).

4.4.7 Other "Radii"

We have given many examples of quantities that can be expressed in terms of GFFs/GPDs. It should be clear from these examples that parton distribution functions (in particular, transverse position-dependent distribution functions) provide a framework for interpreting many of the GPDs. As a final example, consider the Pauli radius r_2^2, defined in terms of the slope of the GFF B_{10} (for ease of notation we suppress the

quark flavor label):

$$r_2^2 \equiv 6\frac{\partial}{\partial t}B_{10}(t)\big|_{t=0}$$

$$= \frac{3}{2}\int_{-1}^{1}dx\int d^2\mathbf{b}\, b^2\,\mathcal{E}(x,\mathbf{b}). \tag{4.58}$$

One might be inclined to stop at this point and interpret r_2^2 as the mean square radius of the (anomalous) magnetic moment density, motivated by the fact that the integral $\int_{-1}^{1}dx\int d^2\mathbf{b}\,\mathcal{E}(x,\mathbf{b})$ gives the anomalous magnetic moment. Indeed, it is tempting to treat $\mathcal{E}(x,\mathbf{b})$ as the transverse density of the anomalous magnetic moment. However, more careful consideration suggests that $-b^y\frac{\partial}{\partial b^y}\mathcal{E}(x,\mathbf{b})$ more properly deserves that identification (see Eq. 4.48).[22] So let us press on:

$$r_2^2 = -\frac{3}{2}\int_{-1}^{1}dx\int d^2\mathbf{b}\left((b^x)^2 b^y + \frac{1}{3}(b^y)^3\right)\frac{\partial}{\partial b^y}\mathcal{E}(x,\mathbf{b})$$

$$= 3m\int_{-1}^{1}dx\int d^2\mathbf{b}\left((b^x)^2 b^y + \frac{1}{3}(b^y)^3\right)\left(\mathcal{H}(x,b^2) - \frac{1}{2m}\frac{\partial}{\partial b^y}\mathcal{E}(x,\mathbf{b})\right)$$

$$= 3m\int_{-1}^{1}dx\int d^2\mathbf{b}\left(b^2 - \frac{2}{3}(b^y)^2\right)b^y\, q^{\perp}(x,\mathbf{b}). \tag{4.59}$$

We now have an expression for r_2^2 as the expectation value of $(b^2 - \frac{2}{3}(b^y)^2)b^y$ in the distribution $q^{\perp}(x,\mathbf{b})$. This is indeed related to (but not identical to) the mean square radius of the "magnetic moment density" encountered in Eq. 4.48. More generally, r_2^2 can be thought of as one measure of the spatial distribution of quark current in the proton.[23] This interpretation can be extended to the derivative of the tensor GFF $\bar{B}_{T10}$ as well, which contains the corresponding information about the distribution of *polarized* quark current.

Observe what is going on here. The generalized form factors (through their Fourier

---

[22]The integral is the same: $\int d^2\mathbf{b}\,(-b^y)\frac{\partial}{\partial b^y}\mathcal{E}(x,\mathbf{b}) = \int d^2\mathbf{b}\,\mathcal{E}(x,\mathbf{b})$.

[23]Note that the distribution $-b^y\frac{\partial}{\partial b^y}\mathcal{E}(x,\mathbf{b})$ is manifestly *not* rotationally symmetric.

67

transforms) parameterize the transverse spatial distribution of quarks in the nucleon. Any physical quantity that can be computed from charge or current[24] distributions can be expressed in terms of GFFs. Conversely, any moment or derivative of a GFF from the set $\{A_{n0}, B_{n0}, \tilde{A}_{n0}, A_{Tn0}, \tilde{A}_{Tn0}, \bar{B}_{Tn0}\}$ can be interpreted as some aspect of a quark charge or current distribution.

---

[24]charge/current here could also be energy/momentum

Chapter 5

Lattice Calculation

This chapter describes the lattice calculations performed and presents the primary results of these calculations.

5.1   Calculation Parameters

The calculations were performed on gauge configurations produced by the MILC collaboration [44]. These configurations were generated using Asqtad improved staggered fermions [45, 46],[1] with two degenerate flavors of "light" fermions (representing up and down quarks) and one flavor of "heavy" fermion (representing the strange quark). The lattice spacing for these configurations was determined by heavy quark spectroscopy[47] to be $a = 0.124$ fm $= 1.59$ GeV^{-1}. We used HYP smearing[48] to smooth the gauge field sufficiently that dislocations did not induce a large domain wall residual mass. This smearing only induces higher dimension operators, and so does not change the continuum limit of the lattice action.

For the valence quarks, we chose to use the domain wall action[9, 10].[2] Domain wall fermions are significantly more expensive than staggered fermions, but have the advantage of preserving an explicit chiral symmetry at finite lattice spacing. We set the extent of the fifth dimension to $L_5 = 16$, and the domain wall mass to $M_5 = 1.7$

---

[1]This is the action used when calculating det M in Eq. 2.4 and following.

[2]This corresponds to the action used when calculating M^{-1} in Eq. 2.5.

(see [33] for more details on the selection process). The valence quark masses were tuned so that the domain wall pion mass matched the corresponding staggered pion mass on each ensemble. Table 5.1 summarizes the parameters for the ensembles used.

The calculations fall into two categories. The older set of calculations (datasets 1-6 in Table 5.1) was run on configurations that were cut in half in the time direction; we refer to these as the *chopped* calculations. Each chopped configuration was used for only one nucleon measurement (source/sink combination), with ten lattice spacings between source and sink. Some results for these calculations were previously published in [33].

For the newer set of calculations (datasets 7-11 in Table 5.1) we used the full time extent of each configuration; we refer to these as the *unchopped* lattices. For the unchopped calculations, we put four nucleon/antinucleon sources (for an effective total of eight nucleon measurements) on each lattice, with a source-sink separation of nine lattice spacings. We used the so-called "coherent sink" technique [2, 49] to reduce computation time.

Calculations were performed at six different pion masses. Unchopped calculations were done for the lightest four of these (with two volumes in one case, for a total of five unchopped data points), while chopped calculations were done at the five heaviest masses (for a total of six chopped data points). There are thus four ensembles that were used in both chopped and unchopped calculations. In these cases, results were consistent within statistical error. Since the chopped and unchopped calculations in such cases were performed on the same lattices and are therefore not statistically independent, we use only the higher-statistics results from the unchopped calculations in our final analysis (we report the numerical results from all calculations in Appendix A).

The Chroma software suite was used for these runs [50, 51].

5.1.1 Extracting the GFFs

Here we give a summary of the procedure used to extract generalized form factors from actual lattice calculations.

data set	# config	volume	$m_{q,l}^{\text{staggered}}$	m_q^{DWF}	m_π^{DWF}	m_N^{DWF}	m_π^{DWF} [MeV]	Z_A^{nonpert}
1	423	$20^3 \times 32$	0.050	0.0810	0.4771(15)	0.986	759	1.129
2	348		0.040	0.0644	0.4326(18)	0.945	688	1.119
3	557		0.030	0.0478	0.3742(3)	0.877	595	1.109
4	472		0.020	0.0313	0.3108(3)	0.810	494	1.099
5	652		0.010	0.0138	0.2226(3)	0.728	354	1.085
6	270	$28^3 \times 32$	0.010	0.0138	0.2226(3)	0.728	354	1.085
7	563($\times$8)	$20^3 \times 64$	0.030	0.0478	0.3742(3)	0.877	595	1.109
8	484($\times$8)		0.020	0.0313	0.3108(3)	0.810	494	1.099
9	628($\times$8)		0.010	0.0138	0.2226(3)	0.728	354	1.085
10	461($\times$8)		0.007	0.0081	0.1822(8)	0.691	290	1.084
11	273($\times$8)	$28^3 \times 64$	0.010	0.0138	0.2226(3)	0.728	354	1.085

Table 5.1: Data sets used for the calculations in this section. All quantities are given in lattice units unless otherwise indicated. Heavy sea quark mass $m_{q,h}^{\text{staggered}} = 0.05$ for all ensembles. Nucleon masses taken from [1].

Consider a nucleon three-point function of the sort described by Eq. 2.12. This *almost* corresponds to the evaluation of a nucleon matrix element of a local lattice operator (Eq. 4.25). However, the situation is complicated by the fact that the state $\hat{N} |\Omega\rangle$ is not a nucleon state—it contains contamination from excited states. Also, the normalization of the states is unknown (and imaginary time-dependent!), and we must account for that. To see how this is done, consider a nucleon two point function, projected onto momentum P. It can be written as a sum over a complete set of states (generalizing the notation in Chapter 3) [52]:

$$C^{2pt}(P,t) = \sum_n e^{-E_n(P)(t-t_{src})} \, \Gamma_{\alpha\alpha'}^{\text{unpol}} \, \langle N_{\alpha'}(P,t_{src})|n\rangle\langle n|N_\alpha(P,t_{src})\rangle \tag{5.1}$$

$$= e^{-E_0(P)(t-t_{src})} \frac{(Z(P)\bar{Z}(P))^{1/2}}{E_0(P)} \times \text{Trace}\left[\Gamma^{\text{unpol}} U(P)\bar{U}(P)\right]$$

$$+ \text{[contributions from excited states]}, \tag{5.2}$$

where $U_\alpha(P) = Z(P)^{-1/2} E_0(P)^{1/2}\langle N_\alpha(P)|0\rangle$ (note that we use $|0\rangle$ as a shorthand for

the nucleon state with implied momentum P) is a spinor with the usual normalization. Similarly, the three point function for operator $\mathcal{O}$ can be written:

$$C_{\mathcal{O}}^{3pt}(P, P', t) = \sum_{n,k} e^{-E_n(P)(t-t_{src})} e^{-E_k(P')(t_{snk}-t)} \tag{5.3}$$

$$\times \Gamma_{\alpha\alpha'}^{pol} \langle N_{\alpha'}(P', t)|k\rangle\langle k|\mathcal{O}(t)|n\rangle\langle n|N_{\alpha}(P, t)\rangle$$

$$= e^{-E_0(P)(t-t_{src})} e^{-E_0(P')(t_{snk}-t)} \frac{(Z(P)\bar{Z}(P'))^{1/2}}{E_0(P)E_0(P')} \tag{5.4}$$

$$\times \text{Trace}\left[\Gamma^{pol} U(P)\bar{U}(P)\right] \times \langle 0|\mathcal{O}(t)|0\rangle + [\text{excited states}],$$

where the nucleon is created on timeslice t_{src}, the operator is inserted at t, and the nucleon sink is located at t_{snk}.[3] Explicit expressions for our choices of Γ^{pol} and Γ^{unpol} are given in Appendix G. For t sufficiently far from both the source and the sink, the excited states can be ignored. It is important to confirm that this is indeed the case in our calculations; Appendix F summarizes our studies of the excited state contamination. When excited states are negligible (as they are in this work), the three point function is indeed proportional to the desired matrix element $\langle 0|\mathcal{O}(t)|0\rangle$. The exponentials and factors of Z cancel out if we construct the ratio:

$$R_{\mathcal{O}}(P, P', t) \equiv \frac{C_{\mathcal{O}}^{3pt}(P, P', t)}{C^{2pt}(P', t_{snk})} \left(\frac{C^{2pt}(P, t_{snk} - t + t_{src})C^{2pt}(P', t_{snk})C^{2pt}(P', t_{snk})}{C^{2pt}(P', t_{snk} - t + t_{src})C^{2pt}(P, t_{snk})C^{2pt}(P, t_{snk})}\right)^{1/2}.$$
$$\tag{5.5}$$

(Here we use the historically common way of writing the ratio $R_{\mathcal{O}}$. For a more enlightening way of organizing this expression, see [3].) Because of statistical fluctuations in the lattice data, a two-point function in the above ratio may happen to have a negative value. Such cases are excluded from our analysis.

A lattice measurement of $R_{\mathcal{O}}(P, P', t)$ gives a plateau with excited state "tails" in imaginary time (see Appendix F). Near the center of the plateau, $R_{\mathcal{O}}$ approaches the

---

[3]We use t here to indicate time; elsewhere we use it to denote momentum transfer Δ^2. The context should make it clear which meaning is intended.

72

desired lattice operator, and can be written explicitly in terms of GFFs (Appendix G). In practice, we average the R-values over several values of t near the plateau midpoint. For source-sink separations of nine (ten) lattice steps, we take the average of the central two (three) points.

The operators we calculate are renormalization scale dependent. Lattice operators are effectively regularized using a momentum cutoff of $1/a$, and must be converted to the $\overline{\text{MS}}$ scheme at some renormalization scale μ^2. The conversion takes the form [33, 53]:

$$\mathcal{O}_i^{\overline{\text{MS}}}(\mu^2) = Z_{ij}^{\mathcal{O}} \, \mathcal{O}_j^{lattice}, \tag{5.6}$$

where the off-diagonal components of $Z^{\mathcal{O}}$ are operator mixing coefficients, which are negligible in this calculation [33]. Perturbative renormalization factors $Z^{\mathcal{O},\text{pert}}$ were calculated at the one-loop level in [53]. The relevant factors for this work, transformed to an $\overline{\text{MS}}$ scale of $\mu^2 = 4\text{GeV}^2$, are given in Table 5.2.

One factor in the calculation of the perturbative $Z^{\mathcal{O},\text{pert}}$ is common to all operators. The axial current renormalization factor Z_A, which arises from the renormalization of the wave function, is a non-trivial part of the perturbative renormalization factors. Since this factor can also be calculated non-perturbatively (see [33]), we improve the renormalization factors by using $Z^{\mathcal{O}} = \frac{Z_A^{\text{nonpert}}}{Z_A^{\text{pert}}} Z^{\mathcal{O},\text{pert}}$. From [53], we have $Z^{\mathcal{O},\text{pert}} = 0.964$. (The values of Z_A^{nonpert} are listed in Table 5.1.)

operator	$H(4)$ rep	$Z^{\mathcal{O},\text{pert}}(\mu^2 = 4\text{GeV}^2)$
$\bar{\psi}[\gamma_5]\gamma^{\{\mu}D^{\nu\}}\psi$	$\tau_1^{(3)}$	0.9394
$\bar{\psi}[\gamma_5]\gamma^{\{\mu}D^{\nu\}}\psi$	$\tau_1^{(6)}$	0.9453
$\bar{\psi}[\gamma_5]\sigma^{\rho\{\mu}D^{\nu\}}\psi$	$\tau_1^{(8)}, \tau_2^{(8)}$	0.9652

Table 5.2: Perturbative renormalization factors at an $\overline{\text{MS}}$ scale of $\mu^2 = 4\text{GeV}^2$. The $Z^{\mathcal{O},\text{pert}}$ are calculated in the limit of zero quark mass, where the renormalization factors are the same with or without the inclusion of γ_5.

Once we have our renormalized lattice operators, calculated for many values of the

momenta P, P', we have all the ingredients we need to solve for the generalized form factors. As described in Appendix G, each value of $R_{\mathcal{O}}(P, P')$ which is calculated on the lattice can be written as a linear combination of generalized form factors with known coefficients:

$$R_{\mathcal{O}}(P, P') = c_1^{\mathcal{O}}(P, P') \, FF_1(t) + c_2^{\mathcal{O}}(P, P') \, FF_2(t) + c_3^{\mathcal{O}}(P, P') \, FF_3(t) + \cdots . \quad (5.7)$$

The FF_i represent the form factors appropriate for the operator $\mathcal{O}$ under consideration. The coefficients $c_i^{\mathcal{O}}$ are known functions of P, P' and nucleon mass, and are calculated by evaluating the dirac traces in Eq. G.1 (transformed to Euclidean space). Note that the form factors depend only on the magnitude of the momentum transfer $t = \Delta^2$. Since we typically have access to many different P, P' corresponding to each value of t (see Table 5.3), as well as several index combinations for each lattice operator (see Appendix G), Eq. 5.7 represents an overdetermined[4] system of equations, where the unknown quantities are the GFFs $FF_i(t)$. We use an SVD analysis [54] to solve the system of equations and extract the form factors.

Solving the overdetermined system of equations is equivalent to performing a least squares fit to the lattice data. When performing such a fit, we have the option of taking correlations among the data points into account by using the full covariance matrix in the definition of χ^2. Also, many of the index and momentum combinations for a given lattice operator lead to the $R_{\mathcal{O}}(P, P')$ being set equal to zero (that is, all the $c_i^{\mathcal{O}} = 0$). If we are using a correlated χ^2, we have the option of including these "measurements of zero" in the fit.[5] In the data analysis for this thesis, we chose to extract the form factors using an uncorrelated fit (this is the method used in [52]). For studies using the more sophisticated correlated analysis, see [2, 3].

---

[4]for most values of t

[5]For an *uncorrelated* fit, these zero cases necessarily drop out of the analysis.

5.2 GFFs

Here we present the primary results of the lattice calculations described above, and discuss the fits we performed to the form factor data. Full results for all the form factors calculated in this thesis are given numerically in Appendix A. Generalized form factors for the $m_q = 0.01$, $20^3 \times 64$ unchopped MILC ensemble[6] (with fits, as described in the next section) are plotted in Fig. 5-1 and Figs. 5-3 through 5-7. In these plots (and in the fits to all ensembles), we include only a subset of the calculated momenta. The included momenta are indicated with a checkmark in Tab. 5.3. Points at the excluded momenta are generally much noisier than the rest of the data,[7] and tend to be highly correlated with each other[49], so leaving them out of the analysis has a minimal effect numerically. For comparison, Fig. 5-2 shows examples of form factor plots with all the momenta included.

source **k**:	sink **k**′:	included?
$\begin{pmatrix} 0\,0\,0 \\ \text{-}1\,0\,0 \end{pmatrix}$	$\begin{pmatrix} 0\,0\,0 \\ \text{-}1\,0\,0 \end{pmatrix}$	✓
$\begin{pmatrix} \{1\,0\,0\} \\ 0\,0\,0 \end{pmatrix}$	$\begin{pmatrix} 0\,0\,0 \\ \text{-}1\,0\,0 \end{pmatrix}$	✓
-1 {1 0}	-1 0 0	✓
{1 1 0}	0 0 0	✓
-1 {1 1}	-1 0 0	✓
0 {1 0}	-1 0 0	✓
{1 1 1}	0 0 0	✓
0 {1 1}	-1 0 0	✓
1 0 0	-1 0 0	✓
1 {1 0}	-1 0 0	✓

source **k**:	sink **k**′:	included?
{2 0 0}	0 0 0	✓
{2 1 0}	0 0 0	✓
0 {2 0}	-1 0 0	✓
-1 {2 0}	-1 0 0	✓
-1 {2 1}	-1 0 0	✓
-2 0 0	-1 0 0	
-2 {1 0}	-1 0 0	
-2 {1 1}	-1 0 0	
-2 {2 0}	-1 0 0	
-3 0 0	-1 0 0	
-3 {1 0}	-1 0 0	

Table 5.3: Lattice momenta at which GFFs were calculated. Momentum is related to **k** by $\mathbf{P} \equiv \frac{2\pi}{L}\mathbf{k}$, where L is the spatial extent of the lattice. Curly braces represent all possible rotations and reflections of the enclosed components. Only cases indicated by ✓ were included in the analysis (this is similar to the cut applied in [2, 3]).

The data shown here for the second moment GFFs include the perturbative renor-

---

[6]data set 9
[7]because of large individual momentum components
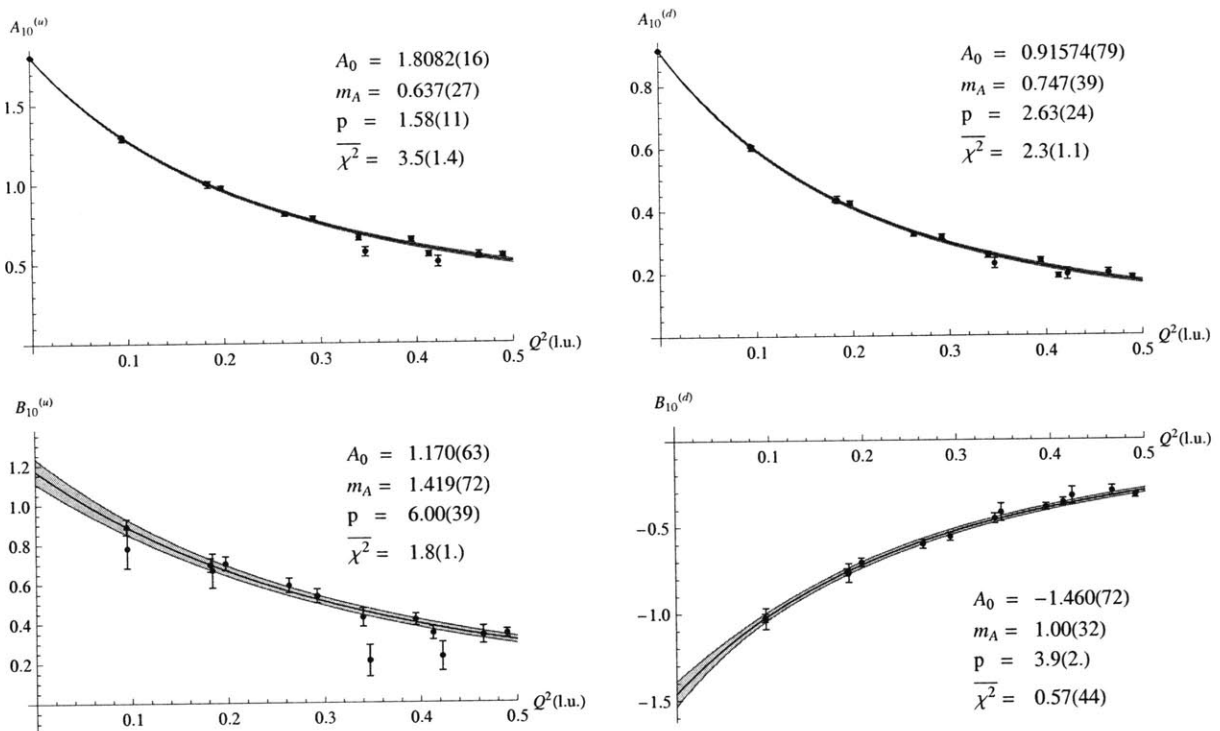
Figure 5-1: Here we show lattice results for the generalized form factors of the zero-derivative vector operators from data set 9. From top to bottom, the GFFs plotted are: $A_{10}^{(f)}$, $B_{10}^{(f)}$. Left hand plots are for flavor u, right hand for flavor d. The lines with error bands are the results of fits with Eq. 5.8; resulting fit parameters and mean χ^2 are shown in inset. All errors are from a jackknife analysis.

malization factors (with non-perturbative improvement) as described above. The first moment results are not shown with any renormalization.

5.2.1 Fits to GFFs

In this section, we discuss the fits we performed to the form factor data. We fit the form factors for two reasons. In cases where lattice data at momentum transfer $Q^2 = -t = 0$ is not available, we need to extrapolate the data to obtain a value for the form factor in the forward limit. Also, to plot the transverse parton distributions discussed in Chapter 4, we need to take fourier transforms of the form factors. For this we need a continuous function that approximates the lattice data.

We emphasize that the form factor fits are motivated by practical considerations, and not by any theoretical functional form. It is common to fit many of these form

$A_{10}^{(u)}$ — axis labels: 1.5, 1.0, 0.5; Q^2(l.u.) 0.0, 0.1, 0.2, 0.3, 0.4, 0.5

$A_0 = 1.8082(16)$
$m_A = 0.639(28)$
$p = 1.60(12)$
$\overline{\chi^2} = 4.7(1.6)$

$A_{10}^{(d)}$ — axis labels: 1.0, 0.8, 0.6, 0.4, 0.2; Q^2(l.u.) 0.0, 0.1, 0.2, 0.3, 0.4, 0.5

$A_0 = 0.91574(79)$
$m_A = 0.744(39)$
$p = 2.63(24)$
$\overline{\chi^2} = 2.8(1.3)$
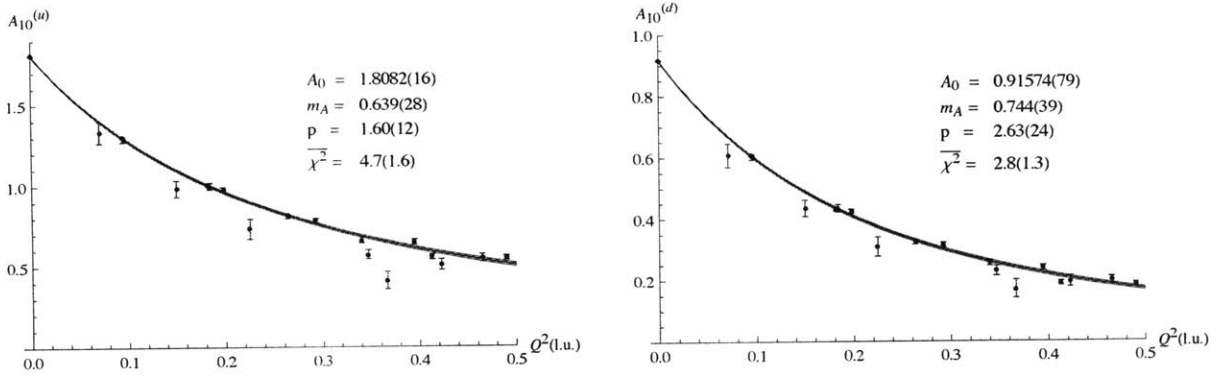
Figure 5-2: Plots of A_{10} for data set 9 showing both the well-behaved momenta that were included in the regular analysis (blue points), as well as the noisy momenta that were excluded (red points). Note that only four out of the six possible bad points appear in these plots. The other two were excluded from the analysis because of negative two-point functions appearing in Eq. 5.5.

$\bar{A}_{10}^{(u)}$

$A_0 = 0.763(14)$
$m_A = 1.16(43)$
$p = 2.2(1.4)$
$\overline{\chi^2} = 1.10(49)$

$\bar{A}_{10}^{(d)}$

$A_0 = -0.2811(85)$
$m_A = 1.29(72)$
$p = 3.7(3.7)$
$\overline{\chi^2} = 0.85(49)$

$\bar{B}_{10}^{(u)}$

$A_0 = 13.4(1.4)$
$m_A = 0.68(17)$
$p = 3.2(1.)$
$\overline{\chi^2} = 1.73(80)$

$\bar{B}_{10}^{(d)}$

$A_0 = -6.0(1.5)$
$m_A = 0.48(17)$
$p = 2.59(94)$
$\overline{\chi^2} = 0.76(46)$
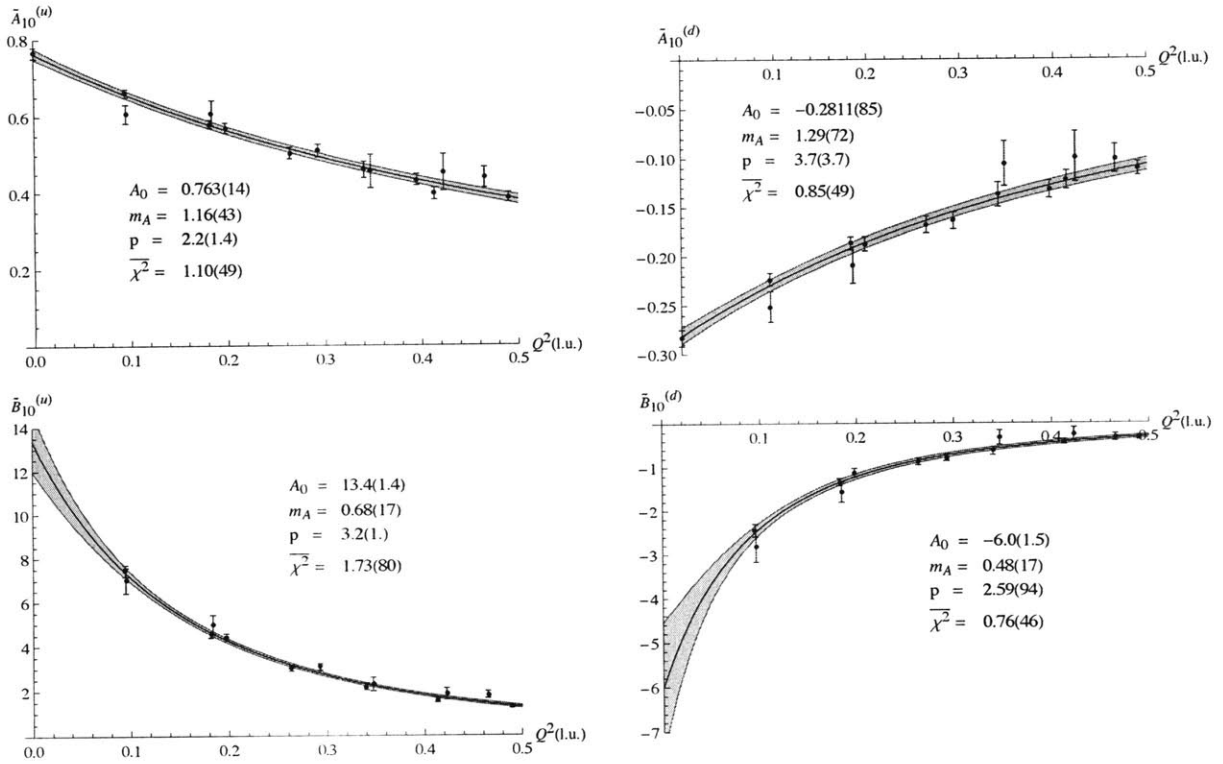
Figure 5-3: Sample results for the generalized form factors of the zero-derivative axial operators. See caption of Fig 5-1 for details.
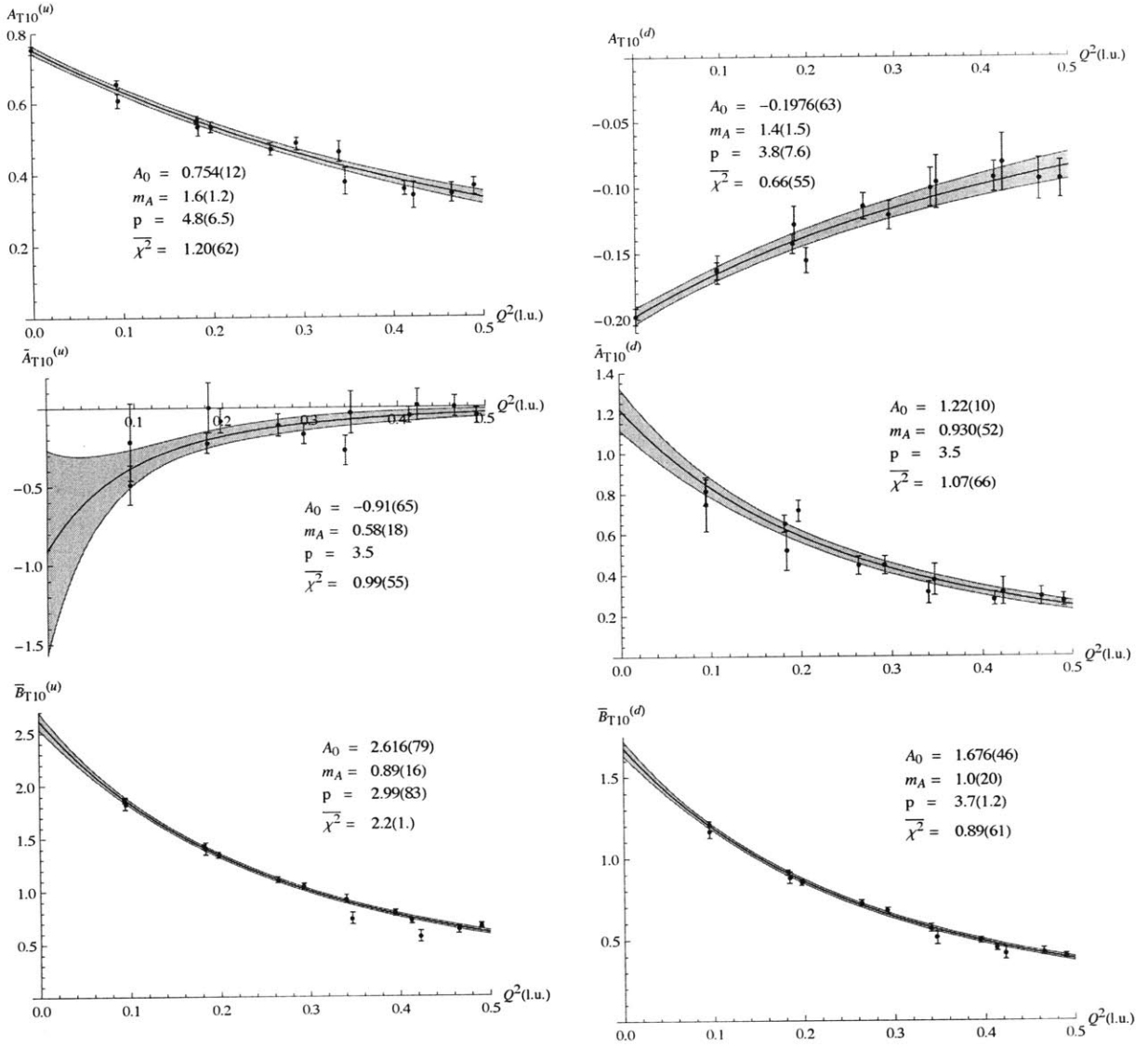
Figure 5-4: Sample results for the generalized form factors of the zero-derivative tensor operators. See caption of Fig 5-1 for details.

factors to a dipole ansatz: $f_2(Q^2) = \frac{A_0}{(1+Q^2/m_A^2)^2}$. In this work, we consider a more general p-pole ansatz [4, 55]:

$$f_p(Q^2) = \frac{A_0}{\left(1 + \frac{Q^2}{m_A^2}\right)^p}. \tag{5.8}$$

There are some practical constraints we must impose on the the value of p, if we are to avoid divergences in the resulting transverse parton distributions [4]. Requiring that the distributions remain finite at $\mathbf{b} = 0$ constrains p to be larger than some

78
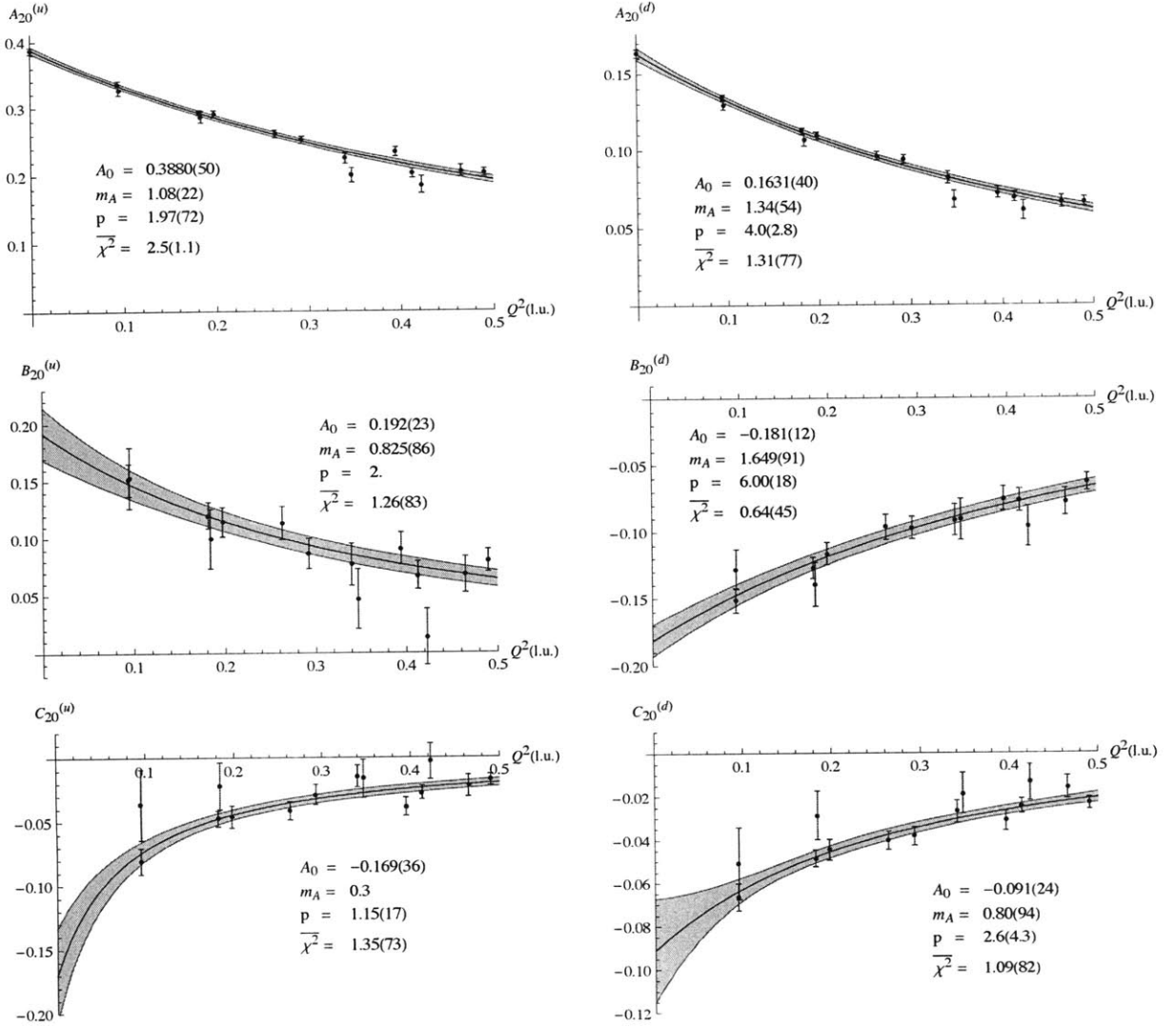
Figure 5-5: Sample results for the generalized form factors of the one-derivative vector operators. See caption of Fig 5-1 for details.

minimum p_{min} (see Tab. 5.4). In most of our fits, we constrain p to be greater than $(p_{min} + 0.5)$ to avoid spurious peaks at the origin. For the GFFs $\tilde{A}_{Tn0}$, which poorly constrained p, we fixed $p = 3.5$. In addition, we require p to be less than 6 in all cases, and keep m_A between 0.3 and 3.3 (in lattice units). These constraints keep poorly determined fits from giving unreasonable values, and in most cases have no impact on the fit results. When fitting GFFs that do not enter into the transverse distributions, we generally allow p to range between 1 and 6. In the particular case of $\tilde{B}_{T21}$, for which the lattice data was consistent with zero, we fixed $p = 1$.

79
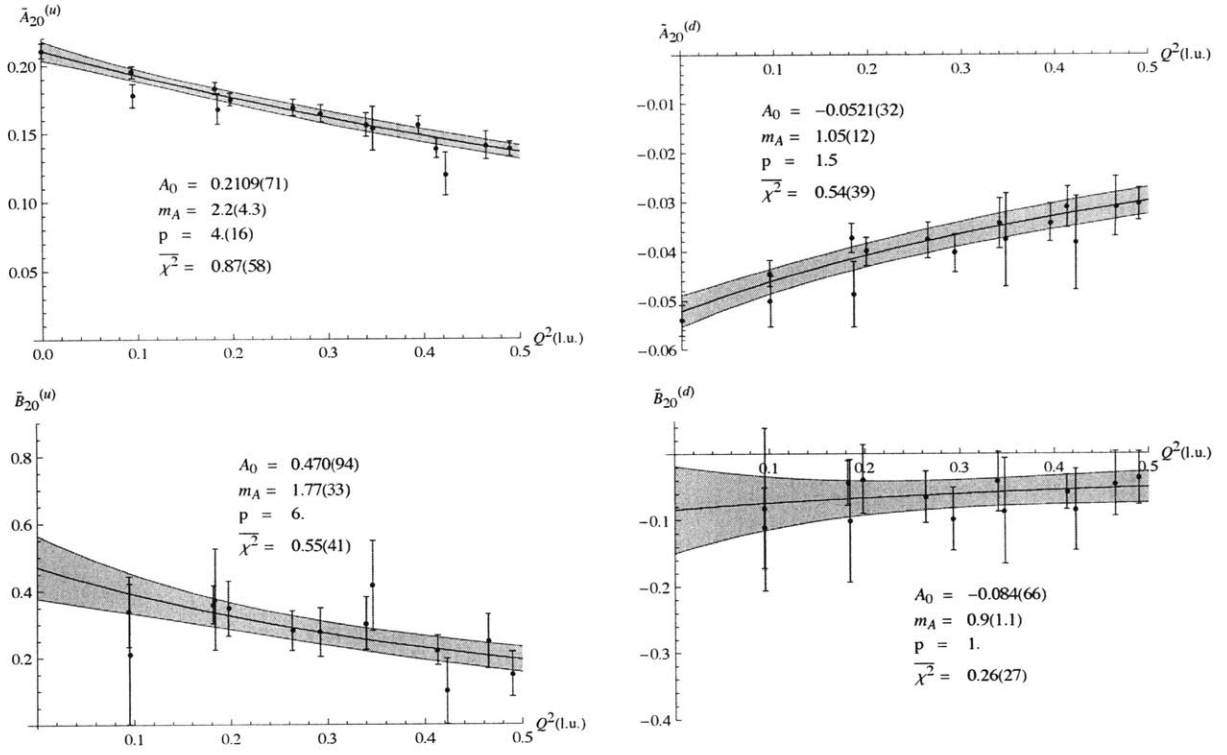
Figure 5-6: Sample results for the generalized form factors of the one-derivative axial operators. See caption of Fig 5-1 for details.

For select cases, we tested the dependence of the fits on the strength of the pole by holding the parameter p fixed at different values and comparing the results. We also checked the dependence on the range of $Q^2 = -t$ included in the fit. These checks are summarized in Appendix E.

GFF:	A_{n0}	B_{n0}	$\tilde{A}_{n0}$	A_{Tn0}	$\tilde{A}_{Tn0}$	$\bar{B}_{Tn0}$
p_{min}:	1	3/2	1	1	2	3/2

Table 5.4: p_{min} for the GFFs in the transverse parton distributions [4]

80
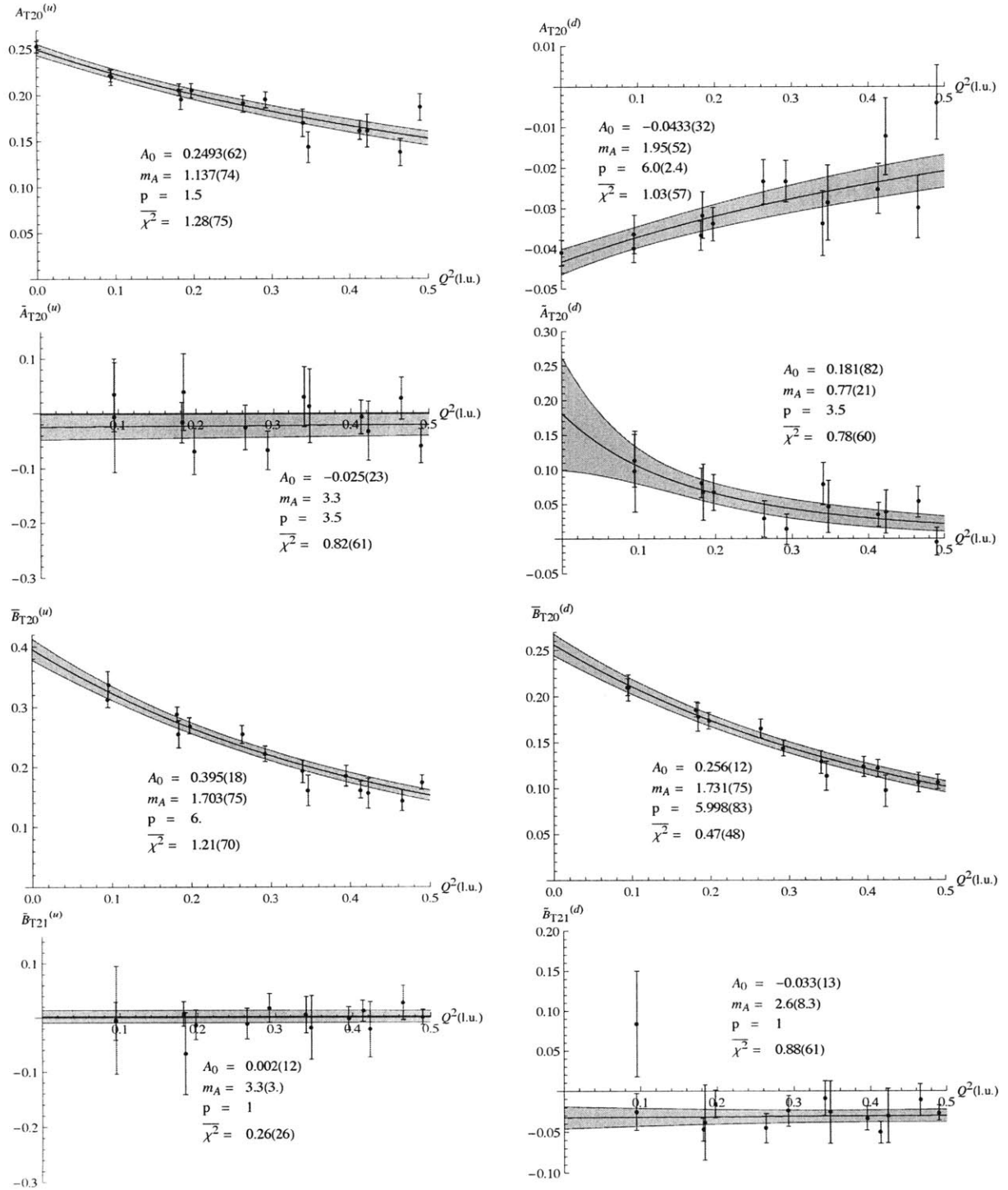
Figure 5-7: Sample results for the generalized form factors of the one-derivative tensor operators. See caption of Fig 5-1 for details.

Chapter 6

Results

In this chapter, we will take a closer look at the results of the calculations discussed in the previous section, with particular emphasis on the physical interpretation of quantities that can be extracted from generalized form factors. We also explore chiral extrapolations of the lattice results.

6.1 Transverse Position PDFs

In this thesis, we have been using the transverse parton distributions in Eqs. 4.19 - 4.23 as a framework for interpreting generalized form factors. In Section 4.4, we looked at many of the usual physical quantities calculated from GFFs, and saw how they arise directly from consideration of the parton distributions. These quantities may in fact be thought of as embodying basic features of the distributions (normalization, mean, variance, etc.). From this perspective, most GFFs have a straightforward interpretation, though their physical significance may be somewhat obscure.

As described in Chapter 5, we can fit the form factor data to smooth functions of $Q^2 = -t$. It is therefore possible to construct (x-moments of) the transverse parton distributions given in Eq. 4.19 and following. We show plots of these distributions in Figs. 6-1 - 6-3. These plots provide a way of bringing together, in a convenient visual summary, all the separate quantities discussed in Section 4.4. In addition, they display information about the more obscure quantities not discussed (e.g. the

Q^2-dependence of $\tilde{A}_{T10}$). Such pictures have an obvious intuitive appeal, though they are more suited to conveying the qualitative features of transverse distributions than quantitative results.

Some additional comments should be made about these pictures. Keep in mind that the lattice data (Figs. 5-1 - 5-7) spans a finite range of Q^2. To make the plots in Figs. 6-1 - 6-3 , we are relying on fits as discussed previously. Since the behavior of the distributions near $|\mathbf{b}| = 0$ is determined by the behavior of the GFFs at $Q^2 \to \infty$, which is strongly influenced by our choice of fitting ansatz, the details of this region (as well as other fine spatial features—or lack thereof) are nearly entirely dependent on the systematics of our fits. Also, we have at present no way to perform a chiral extrapolation of all the GFFs at large values of momentum transfer, so there is no way to extrapolate these pictures to the physical pion mass. [1] Here we show results only for data set 9 (plots for more ensembles are given in Appendix B).

6.2 Chiral Extrapolation Schemes

The quantities presented here have been calculated on lattices with large pion masses. To compare with real world experiments, we need to extrapolate these results to the physical pion mass. For this, we make use of *Chiral Perturbation Theory (χPT)*—an effective field theory of QCD in the limit where the bare light quark masses go to zero. In this limit, chiral symmetry becomes an exact symmetry of the QCD lagrangian, and so the pions (the Goldstone bosons of the *dynamical* breaking of chiral symmetry) become massless. Since the "real world" pion masses are small (relative to the dynamical symmetry-breaking scale $\Lambda_\chi \approx 1.2$ GeV), it is reasonable to perform an expansion in the pion mass, thus organizing corrections to the chiral limit according to a well-defined ordering scheme. In practice, there are several different ways this ordering can be defined, depending on which degrees of freedom are included in the effective field theory and which (mass) scales are considered to be large. Here we briefly summarize the features of the various χPT schemes used in this thesis.

---

[1]For some of the GFFs, though, this may be feasible [33].
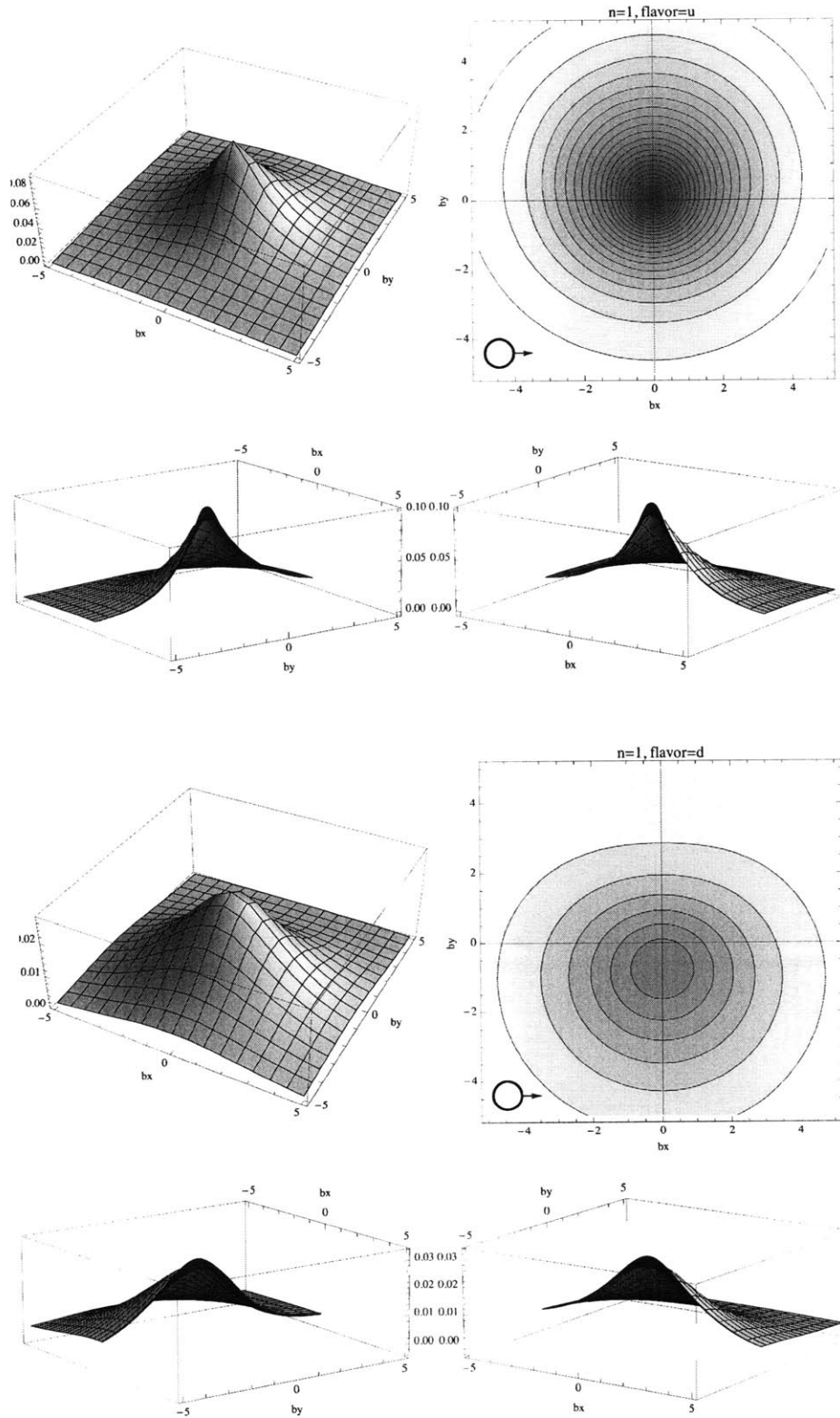
Figure 6-1: First moment transverse distributions of unpolarized quarks in a polarized proton. Each group of plots shows four different views of the same distribution. In particular, the cross sections show slices of the statistical error band for each distribution. The top set is for distribution of up quarks; the bottom set is for down. These results are from data set 9.

85
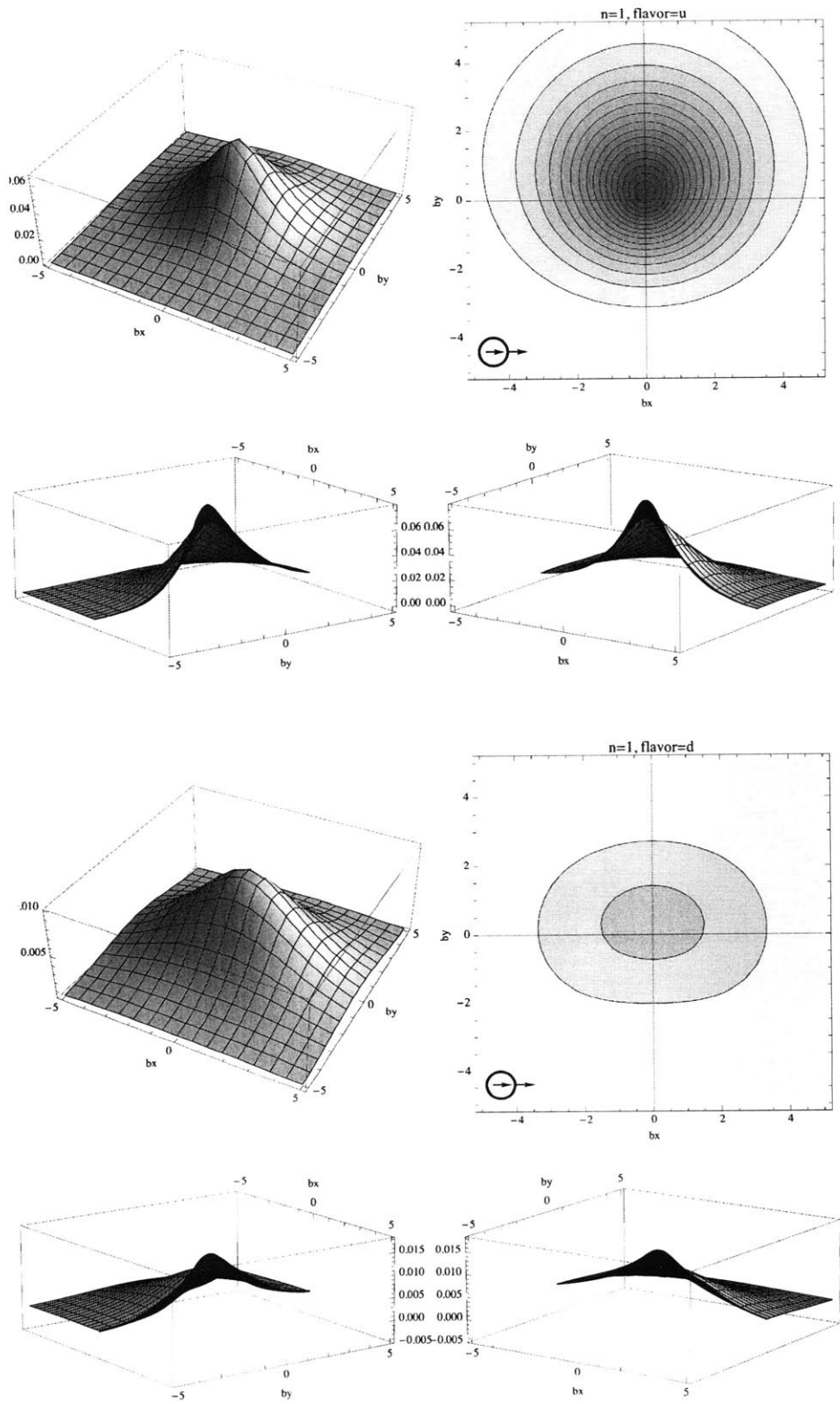
Figure 6-2: First moment transverse distributions of x-polarized quarks in an x-polarized proton. See caption of Fig 6-1 for more details.
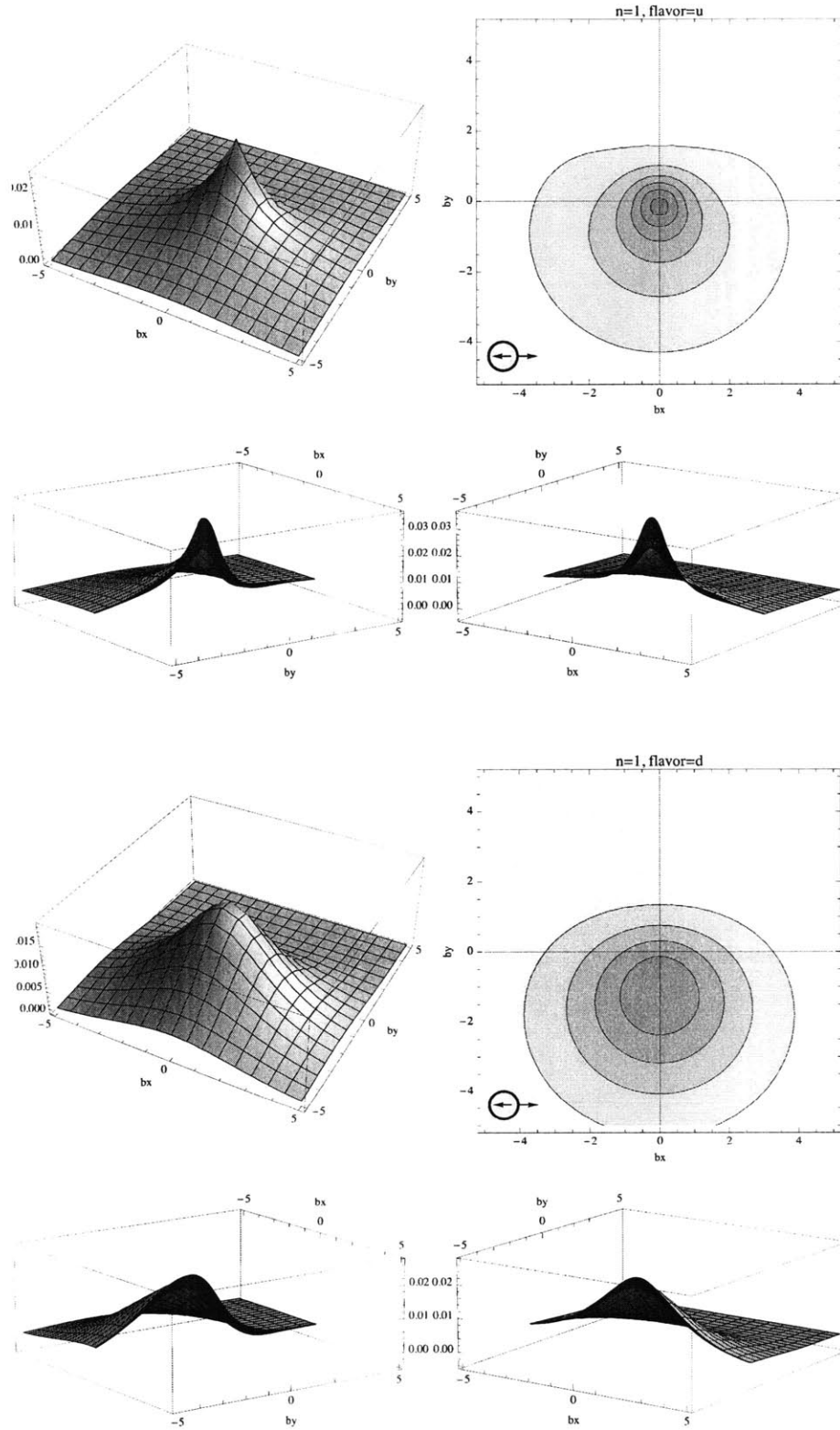
Figure 6-3: First moment transverse distributions of $-x$-polarized quarks in an x-polarized proton. See caption of Fig 6-1 for more details.

6.2.1 Heavy-Baryon χPT

Heavy-baryon chiral perturbation theory (HBχPT) is the most basic flavor of chiral perturbation theory.[2] It takes both Λ_χ and the nucleon mass to be *large* scales, and the pion mass and momentum transfer to be *small* scales. The perturbative expansion is ordered by powers of ϵ, where ϵ is any small scale divided by any large scale. One-loop chiral expressions in the HBχPT scheme for every GFF considered in this thesis can be found in the work by Diehl, Manashov and Schäfer [56, 57]. Because of this availability, we use HBχPT as our primary chiral extrapolation tool.

6.2.2 Covariant Baryon χPT

The covariant baryon chiral perturbation theory (CBχPT) scheme includes corrections due to finite nucleon mass M_N^0 by keeping *all* powers of the factor (m_π/M_0) arising from the calculation of loop diagrams of the effective theory. (In comparison, HBχPT can be thought of as the truncation of this expansion at the power corresponding to the given chiral order.) In our analysis we use the expressions calculated in the I$\overline{\text{R}}$ renormalization scheme of Gail and Hemmert [58, 59]. Unfortunately, CBχPT expressions are not yet available for all quantities we calculate here. In the cases where they are available, it will be interesting to compare the CBχPT extrapolations with the corresponding HBχPT versions.

6.2.3 SSE

The most basic χPT power counting assume that pions and nucleons are the only relevant degrees of freedom. However, this is not always the case—the delta resonance is known to play an important role in the nucleon axial coupling g_A, for example. The SSE (small scale expansion) scheme[58, 60] is one scheme which includes the delta explicitly in its power counting by treating the delta-nucleon mass splitting Δ_M as an additional small mass scale. In the limit where the delta decouples from the theory,

---

[2]There are actually many effective theories that could be labeled as HBχPT. In this thesis, we use the label to refer specifically to the basic χPT power counting as described in this paragraph. This could also be called "nucleon HBχPT."

we recover the standard nucleon HBχPT expressions.[3] As with the covariant case, SSE expressions are available only for a limited set of quantities, so comparison with HBχPT will be useful.

Of course, a perturbative chiral expansion only works for small enough pion masses, and most of our calculations were done at pion masses beyond a credible range of applicability. For this reason, we generally restrict the range of our fits to $m_\pi \lesssim 500$ MeV, when possible.[4] Because of our limited number of data points, we hold fixed some of the low energy constants (LECs) that are relatively well known from phenomenology. Also, some of the CBχPT fits depend explicitly on the nucleon mass at finite m_π; in these cases, we used a simple linear (in m_π) interpolating function to approximate $M_N(m_\pi)$.[5] Table 6.1 gives the nucleon interpolating function, as well as constants that were used as inputs to these fits.

g_A^0	f_π^0	c_A	c_4	Δ_M^0	M_N^0	Interpolating formula for $M_N(m_\pi)$
1.2	86 MeV	1.5	3.5	270 MeV	890 MeV	$0.806\,\mathrm{GeV} + 0.991\,m_\pi$

Table 6.1: inputs to chiral fits.

6.3 Results for Physical Quantities

Here we present results for many of the physical quantities discussed previously in Chapter 4. We show the isovector $(u - d)$ and isoscalar $(u + d)$ flavor combinations.[6] In these plots, the lattice data are shown with the results of various chiral fits. Blue

---

[3]Note that within the broader category of HBχPT, the delta has often been included as an explicit degree of freedom. SSE can be regarded as one particular example of such a scheme.

[4]This is still quite heavy. The fits in this chapter are primarily a test of the plausibility of the chiral extrapolations.

[5]This interpolating function does *not* have the correct behavior in the chiral limit, but it does happen to come surprisingly close to the physical nucleon mass[1].

[6]Note that we define our isoscalar quantities to be normalized according to the lattice $(u + d)$ flavor combination. For example, the isoscalar dirac form factor $F_1^s(0) = A_{10}^{(u+d)}(0) = 3$.

89

circles are data points from $20^3 \times 64$ unchopped lattices (data sets 7-10); yellow diamond is data point from $28^3 \times 64$ unchopped lattice (data set 11); red squares are from chopped lattices (data sets 1 & 2). The experimental or phenomenological point, when applicable, is indicated by a star. The dark part of the error band shows range of m_π values fit (the experimental point is never included in fit). We give the fit χ^2/d.o.f and extrapolated value at physical pion mass (PP) in the inset of each graph. Lowest-moment quantities have been normalized by dividing by $g_V \equiv A_{10}^{(u-d)}(0)$ before fitting. The results from phenomenological analyses of experiments are from [61, 62, 63].

6.3.1 g_A

In Fig. 6-4, we show the results of fitting the (normalized) lattice data for $g_A = \tilde{A}_{10}^{(u-d)}(0)$ with the SSE chiral formula. A fit to the four lightest pion masses (right-hand panel) describes the lattice data reasonably well, but significantly undershoots the experimental value. (Our extrapolated result is consistent with the lattice calculations discussed in [64], but our smaller statistical errors no longer encompass the experimental point.). A fit to just the three lightest masses (the minimum number of points needed to determine all three fit parameters) happens to come quite close to the experimental point, though with a large statistical uncertainty.
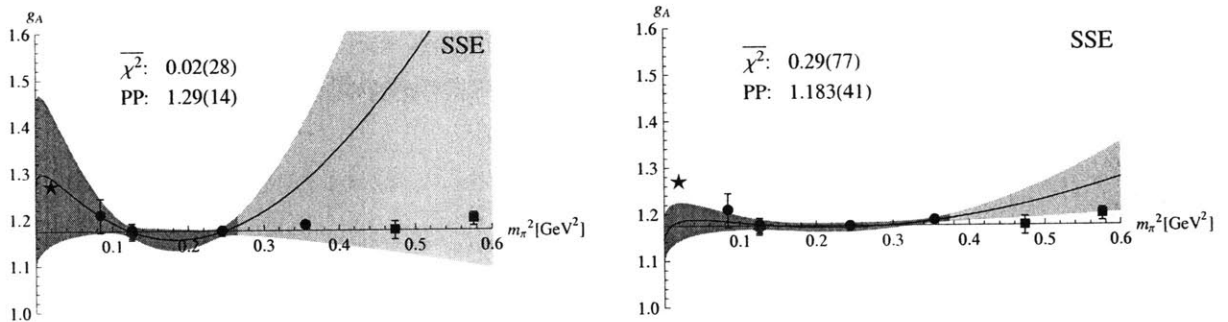
Figure 6-4: SSE fits to g_A. For these fits, we fixed f_π^0, c_A and Δ_M^0 to the values shown in Table 6.1. The three fit parameters were g_A^0, g_1 and a counter-term. Resulting values of g_1 are 4.6(3.1) and 2.4(6) for the left-hand and right-hand fits, respectively.

Figure 6-5 shows the results of HBχPT fits to g_A. It is clear that these fits fail to

describe the lattice data, and miss the experimental point completely. We take this as evidence that inclusion of the delta degrees of freedom (as in the SSE formula) is essential when fitting g_A.
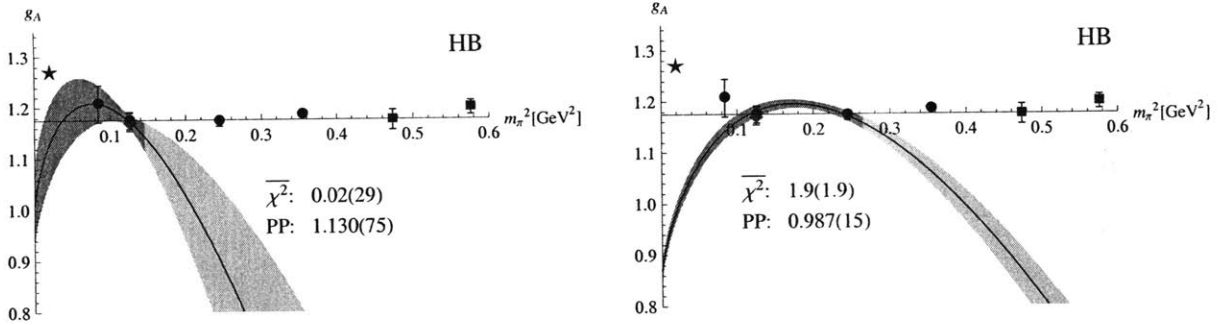
Figure 6-5: HBχPT fits to g_A. Each fit involves two parameters: g_A^0 and a counter-term.

6.3.2 $\Delta\Sigma^{u+d}$

The isoscalar combination $\tilde{A}_{10}^{(u+d)}(0)$ gives the total[7] light quark contribution to $\Delta\Sigma$. HBχPT fits to the lattice data (Fig. 6-6) have poor χ^2 values, but come surprisingly close to the experimental point. The main "feature" of the chiral extrapolations is the precipitous drop at low pion masses. This drop-off provides the connection between the lattice data (which is relatively flat over the fitting range) and experiment. It will be interesting to see whether this behavior shows up in lattice calculations at lighter pion masses. Note that the fits are relatively insensitive to changes in the values of the LECs used.

---

[7]except for disconnected contributions, which we do not calculate in this study
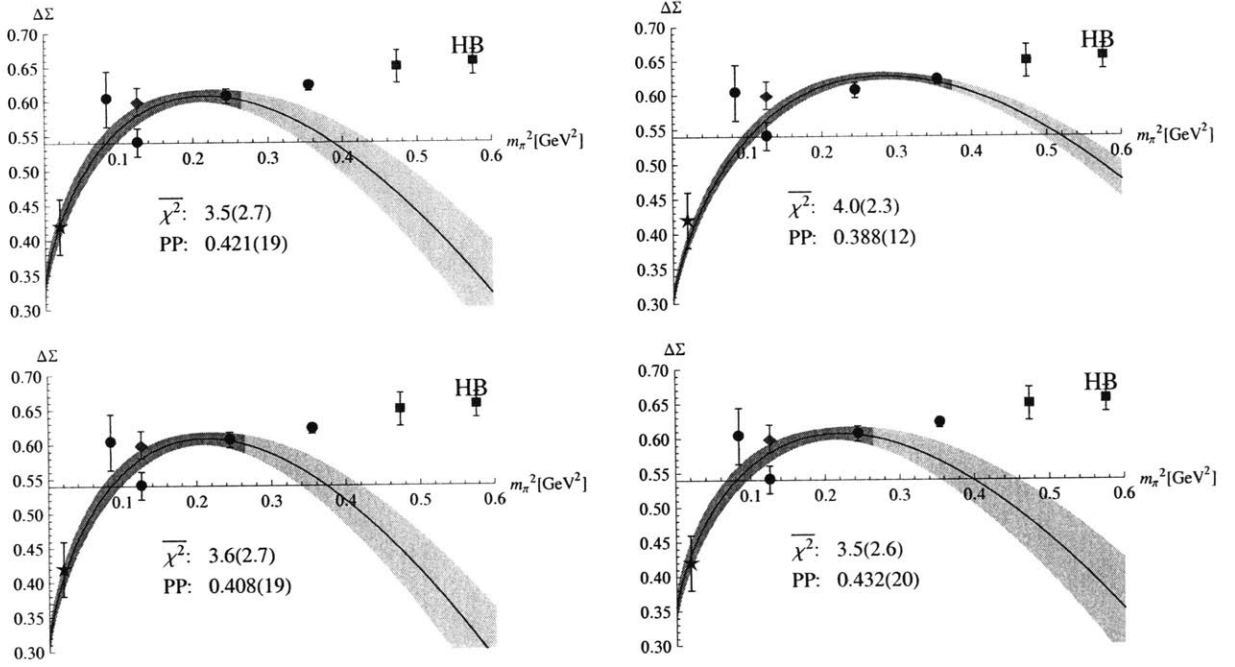
Figure 6-6: HBχPT fits to $\Delta\Sigma^{u+d}$. Upper plots fix $f_\pi^0 = 86$ MeV, $g_A^0 = 1.2$. In the lower left-hand plot we fix $g_A^0 = 1.3$ to illustrate the level of sensitivity to g_A; in the lower right-hand plot we fix $f_\pi^0 = 92$ MeV.

6.3.3 Tensor Charges

Figure 6-7 shows HBχPT fits to the lattice data for the isovector tensor charge ($g_T = A_{T10}^{(u-d)}(0)$). The tensor charge is in many ways the transverse analog of the axial charge g_A, and indeed we note that the HBχPT fits to g_T resemble the HBχPT fits to g_A (Fig. 6-5). By extension, we expect that the inclusion of the delta is necessary for an accurate extrapolation of g_T (also see [65]).
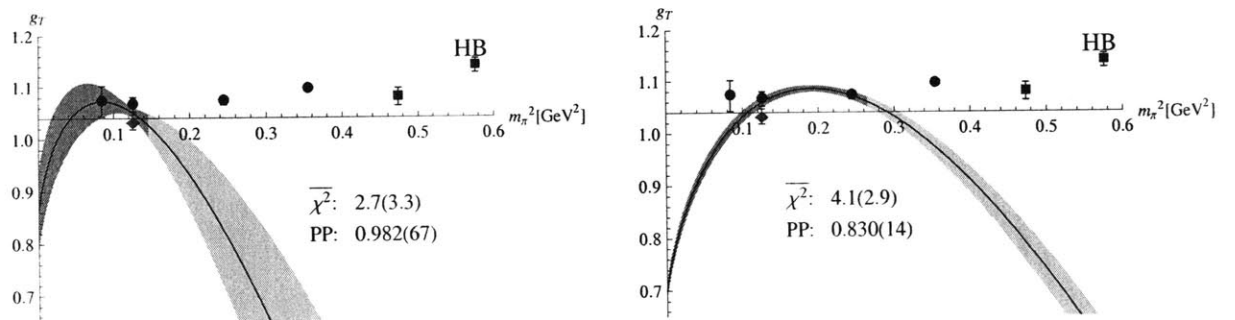
Figure 6-7: HBχPT fits to g_T

Figure 6-8 shows fits to the isoscalar combination $A_{T10}^{(u+d)}(0)$, which we call $\delta\Sigma^{u+d}$ in analogy to the axial $\Delta\Sigma^{u+d}$. Again, note that the resulting extrapolations are almost identical to the axial case shown in Fig. 6-6.
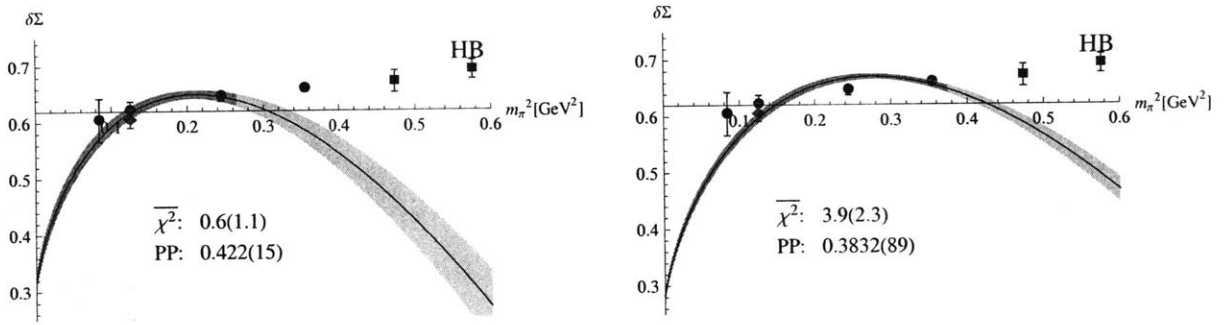
Figure 6-8: HBχPT fits to $\delta\Sigma^{u+d}$

6.3.4 Momentum Fractions

Unpolarized

We perform fits to the unpolarized momentum fraction $\langle x \rangle$ using both the HBχPT and CBχPT formulas (Figs. 6-9, 6-10). In both isovector and isoscalar cases, the covariant fit appears to describe the lattice data over a wider range of pion masses; however, the heavy baryon fit extrapolates closer to the phenomenological point. Note that the HBχPT chiral formula for $\langle x \rangle^{(u+d)}$ at one the one-loop level is simply a linear expression in m_π^2. The corresponding $\mathcal{O}(p^2)$ CBχPT expression has nonanalytic dependence on m_π^2 due to the inclusion of nucleon mass terms.

The CBχPT expression for $\langle x \rangle^{(u-d)}$ depends on the chiral limit value of the polarized momentum fraction $\langle x \rangle_\Delta^{(u-d)}$. For the fit, we set this value to 0.16, based on the HBχPT fit presented in the next section.
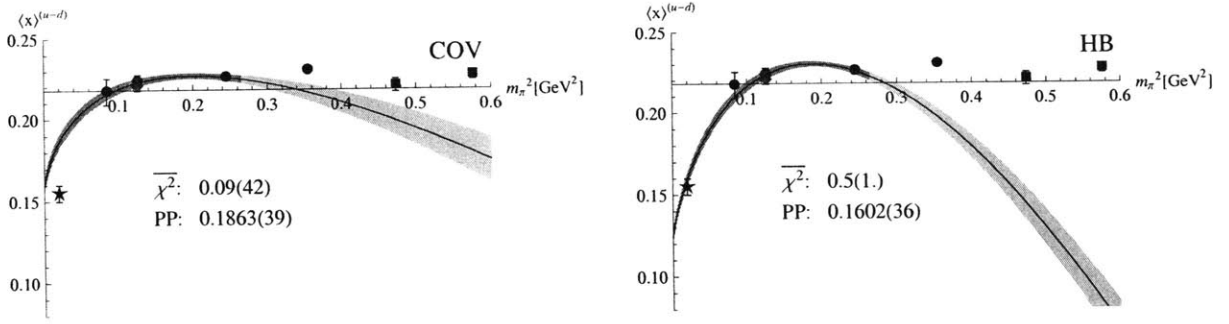
Figure 6-9: Chiral fits to isovector momentum fraction $\langle x \rangle^{(u-d)}$. Left-hand plot: CB$\chi$PT. Right-hand plot: HB$\chi$PT.
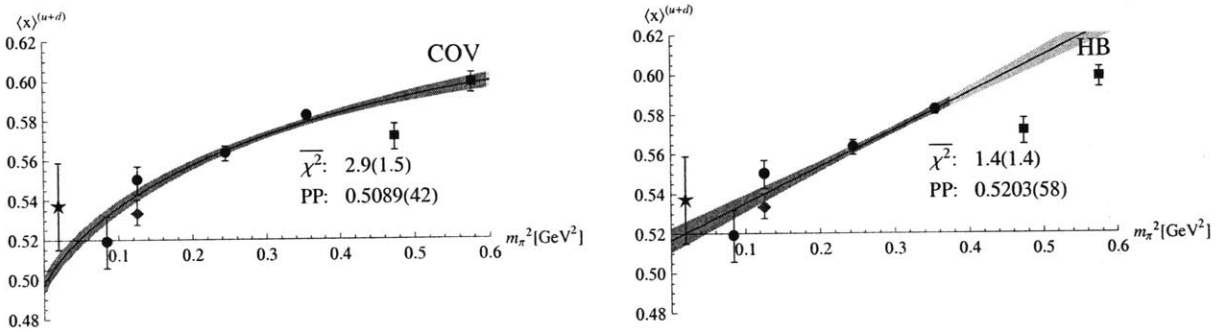
Figure 6-10: Chiral fits to isoscalar momentum fraction $\langle x \rangle^{(u+d)}$. Left-hand plot: CB$\chi$PT. Right-hand plot: HB$\chi$PT.

Polarized

For the polarized momentum fractions $\langle x \rangle_\Delta$ and $\langle x \rangle_\delta$, we fit using HBχPT. The fits for axial polarization (Fig. 6-11) look quite reasonable, and extrapolate well to the physical point. Phenomenological values for tranverse polarization (Fig. 6-12) are not available, but the fits do a noticeably worse job of describing the lattice data.
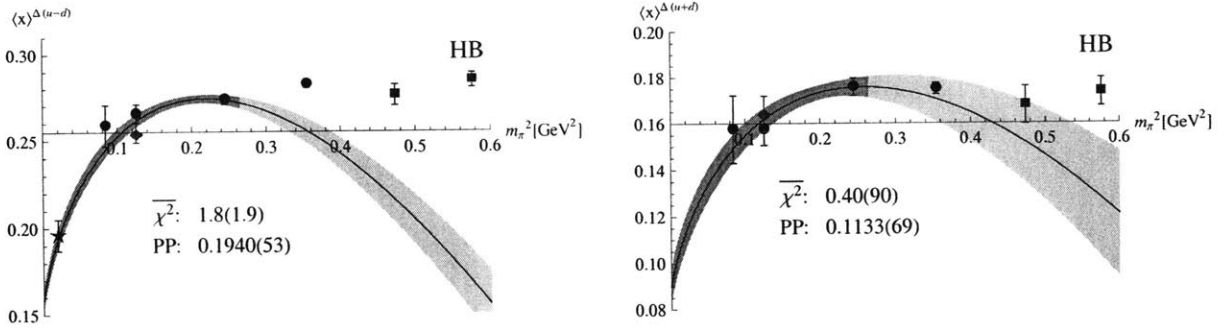
Figure 6-11: HBχPT fits to polarized momentum fraction $\langle x \rangle_\Delta$. Left-hand plot: isovector case $(u - d)$. Right-hand plot: isoscalar case $(u + d)$.
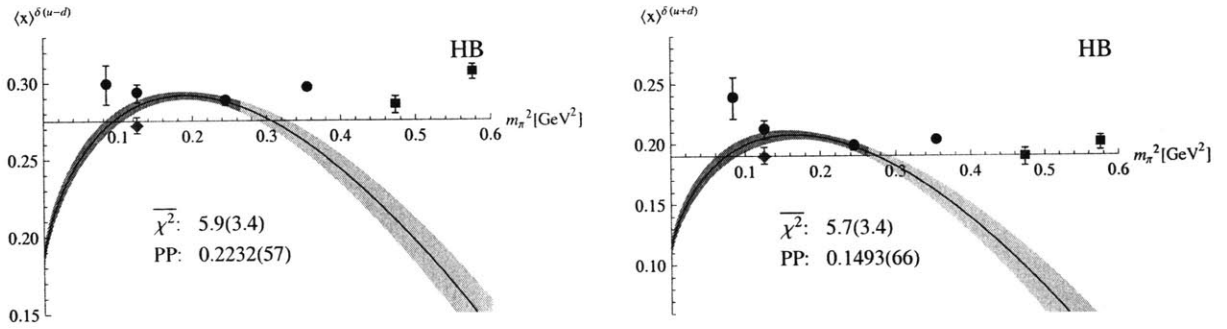
Figure 6-12: HBχPT fits to polarized momentum fraction $\langle x \rangle_\delta$. Left-hand plot: isovector case $(u - d)$. Right-hand plot: isoscalar case $(u + d)$.

6.3.5 Radii

Unpolarized (charge radius)

Figure 6-13 shows data for the slope of $A_{10}^{(u-d)}(t)$ at $t = 0$. As discussed in Section 4.4.3, the three-dimensional charge radius can be expressed in terms of the slope: $\langle r^2 \rangle = 6 \frac{\partial}{\partial t} A_{10}(t)|_{t=0}$. In chiral perturbation theory, this is a divergent quantity, with leading $\log m_\pi$ behavior. At the one-loop level, both the HBχPT and SSE formulas have only one free parameter, which is a constant offset that shifts the whole curve up or down. The shape of the curve in both cases clearly fails to describe the lattice data, but as a plausibility check we constrain the curves to go through the lowest-mass point. (By a fortuitous accident, the curves also pass close to the experimental point.)

95

The $\mathcal{O}(p^4)$ CBχPT formula has a term proportional to the LEC c_6 (which is essentially the chiral limit value of the isovector anomalous magnetic moment, and should have a value of approximately 4.5). Including c_6 as a fit parameter, we get the two-parameter fit shown in the bottom plot of Fig. 6-13. The resulting fit is able to describe the lattice data, but falls short of the experimental point. Also, the value of c_6 from this fit is about 16, which is much too large. Clearly, none of the available formulas are able to describe both the lattice data over the full range of pion mass *and* the experimental point.
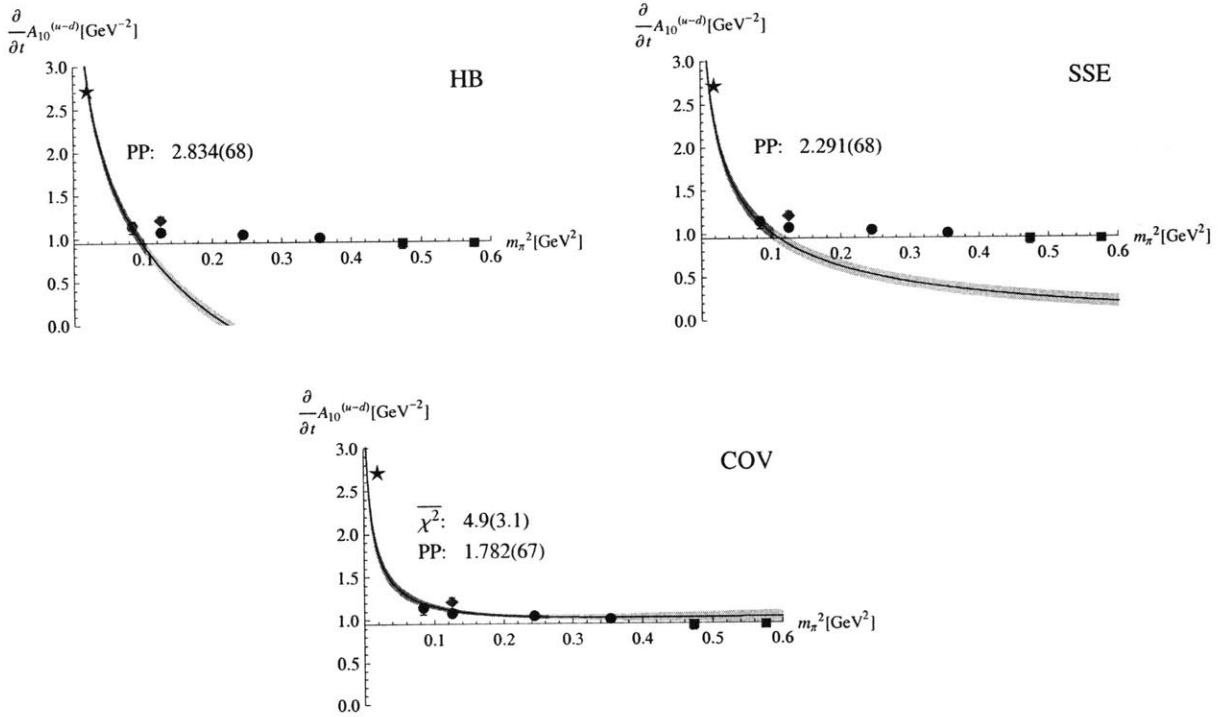
Figure 6-13: Slope of the GFF $A_{10}^{(u-d)}$ with chiral fits. (Note: these slopes were obtained by fitting the form factors to Eq. 5.8 with $p \geq 2$.)

For the isoscalar charge radius (Fig. 6-14), both the HBχPT and CBχPT fits do well at fitting the lattice data, and give very similar extrapolations. However, they completely fail to account for the experimental point. This behavior, while puzzling, is consistent with the results of other lattice studies[3].
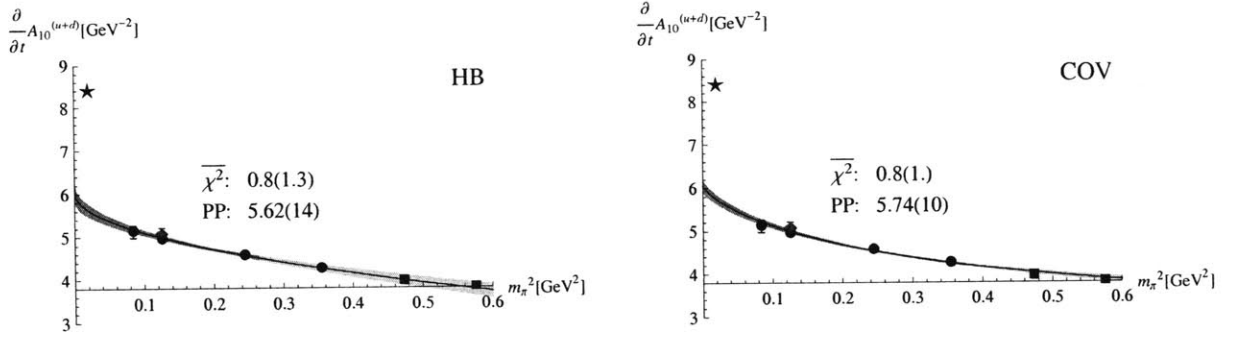
Figure 6-14: Slope of the GFF $A_{10}^{(u+d)}$ with chiral fits. (Note: these slopes were obtained by fitting the form factors to Eq. 5.8 with $p \geq 2$.)

Polarized (spin density radii)

As discussed previously, the slopes of the axial and tensor GFFs $\tilde{A}_{10}$ and A_{T10} can be interpreted respectively as radii of longitudinal and transverse spin densities in appropriately polarized nucleons. At the one-loop order, the HBχPT formula for these quantities is simply a constant plus corrections of $\mathcal{O}(m_\pi)$, so here we fit to the ansatz $C_0 + C_1 m_\pi$.

In Fig. 6-15 we show fits to lattice data for the slope of the axial form factor. Figure 6-16 shows the corresponding fits to the tensor form factor. The fits describe the lattice data reasonably well, although with large uncertainties. In all cases the slopes are significantly less than for the unpolarized form factor.
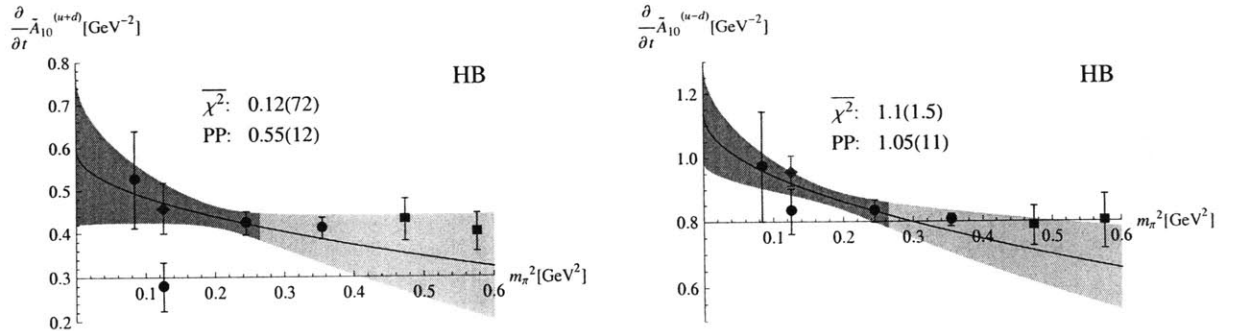
Figure 6-15: Slope of $\tilde{A}_{10}^{(u+d)}$ (left) and $\tilde{A}_{10}^{(u-d)}$ (right) with chiral fits. In the left-hand graph, the outlying point at $m_\pi \approx 350$ MeV was excluded from the fit. (Note: these slopes were obtained by fitting the form factors to Eq. 5.8 with $p \geq 2$.)

97
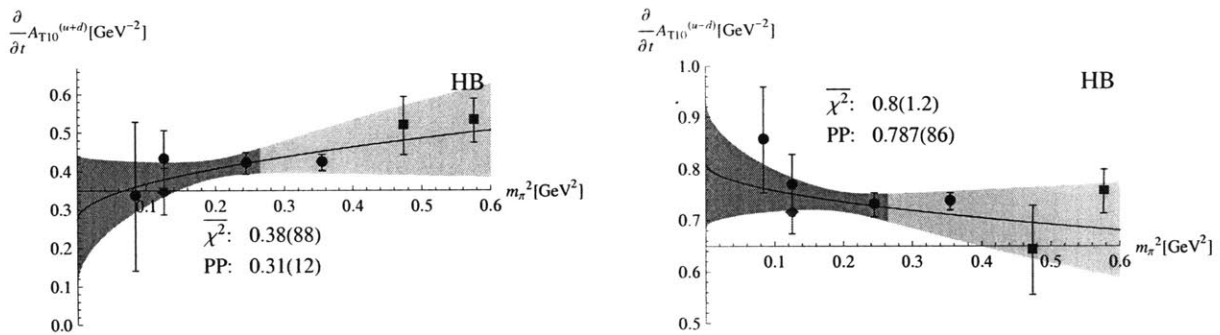
Figure 6-16: Slope of $A_{T10}^{(u+d)}$ (left) and $A_{T10}^{(u-d)}$ (right) with chiral fits. (Note: these slopes were obtained by fitting the form factors to Eq. 5.8 with $p \geq 2$.)

6.3.6 Anomalous Magnetic Moments

Unpolarized

In the case of the anomalous magnetic moment, we have chiral formulas available in all three schemes used in this work: HBχPT, CBχPT and SSE.

Results for the isovector case are shown in Fig. 6-17. All three schemes provide plausible descriptions of the lattice data over the range of the fits, and show the same sharply peaked behavior in the chiral limit. Quantitatively, the SSE and CBχPT extrapolations agree with each other quite well, and are several sigma from the HBχPT extrapolation (though this agreement must be something of a coincidence, because the two schemes involve different corrections to the naïve heavy baryon case).

The SSE formula used in this case contains terms up to *partial* $\mathcal{O}(\epsilon^4)$ [60], and so does not represent a complete or consistent power counting. Nevertheless, the SSE extrapolations come within a few (statistical) sigma of the experimental value, which is relatively good agreement compared with the HBχPT result. Also, the SSE formula contains the LEC c_V, which we include as a free parameter in our fits. From the fit to values of $m_\pi \lesssim 600$ MeV (lower right-hand side of Fig. 6-17), we obtain $c_V = -2.8(6)$ GeV^{-1}, which is consistent with phenomenology.

98
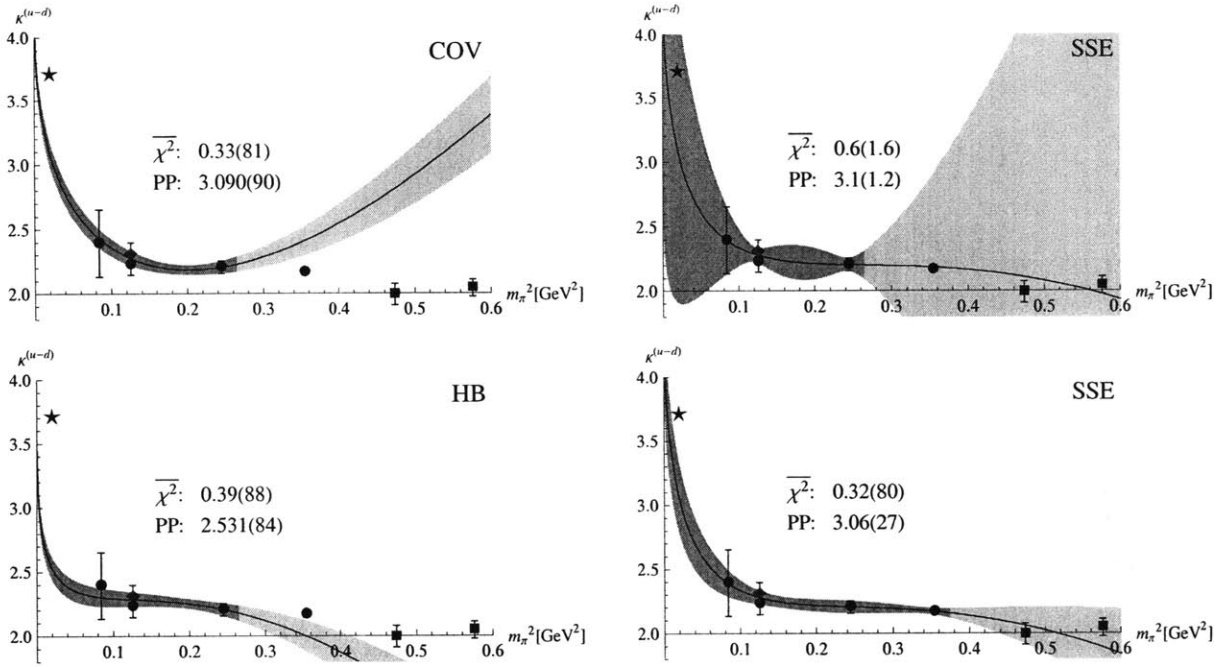
Figure 6-17: Chiral fits to the isovector anomalous magnetic moment κ_v. Upper left-hand plot shows CBχPT fit; lower left-hand plot shows HBχPT fit. Right-hand plots show SSE fits for two different ranges of pion mass.

The isoscalar fits are shown in Fig. 6-18. In this case, the partial $\mathcal{O}(\epsilon^4)$ SSE formula is simply linear in m_π^2 and has *no* dependence on the delta. Thus the "SSE" results in this section can be thought of as simply tree-level HBχPT results. It is interesting to note that the simple linear fits do much better than the one-loop heavy baryon formula, at both fitting the lattice data and extrapolating to the experimental point. The CBχPT formula here is $\mathcal{O}(p^4)$ and agrees well with the linear fit.

99
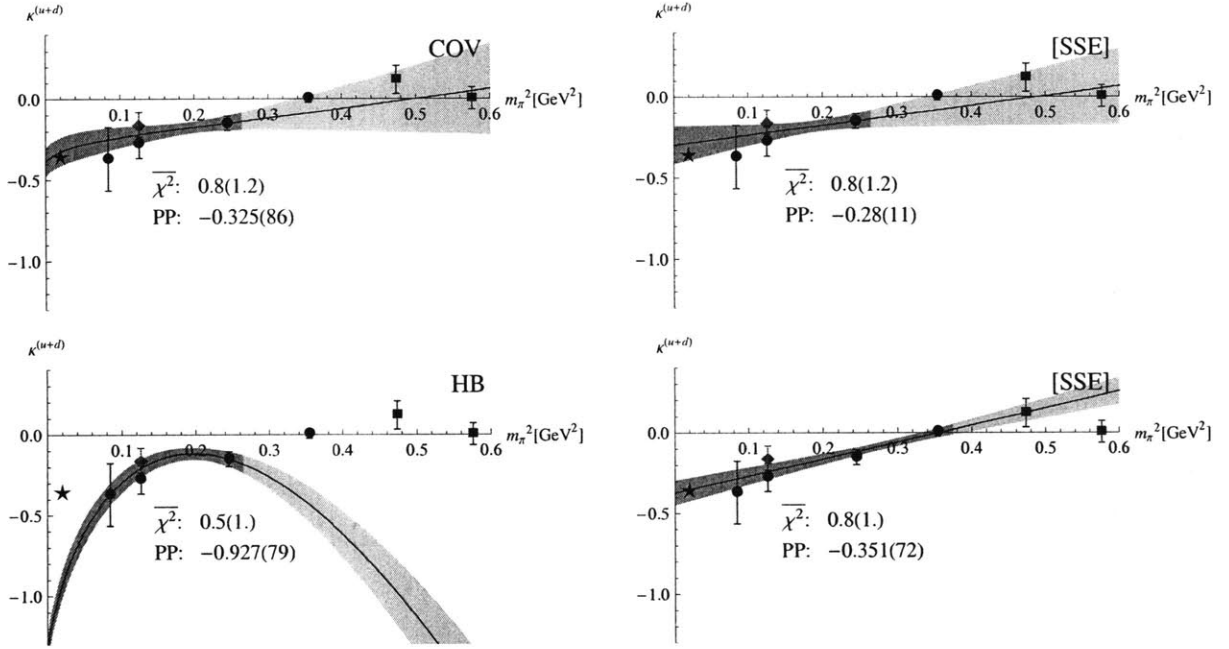
Figure 6-18: Chiral fits to the isoscalar anomalous magnetic moment κ_s. Upper left-hand plot shows CBχPT fit; lower left-hand plot shows HBχPT fit. Right-hand plots show SSE fits for two different ranges of pion mass.

Polarized

As discussed in Chapter 4, one can separate the magnetic moment into contributions from quarks polarized (anti)parallel to the nucleon. The GFF characterizing this separation is $\bar{B}_{T10}(0)$, which we will call κ^δ. For both the isovector (Fig. 6-19) and isoscalar (Fig. 6-20) cases, the heavy baryon fits describe the data reasonably well. (In the isoscalar case, the fit formula depends on the chiral limit value of $A_{T10}^{(u+d)}$. Based on our results for this quantity (see Section 6.3.3), we set this value to be 0.4. The dependence is quite weak: changing this number by a factor of two changes the resulting extrapolation by about one sigma.)

100
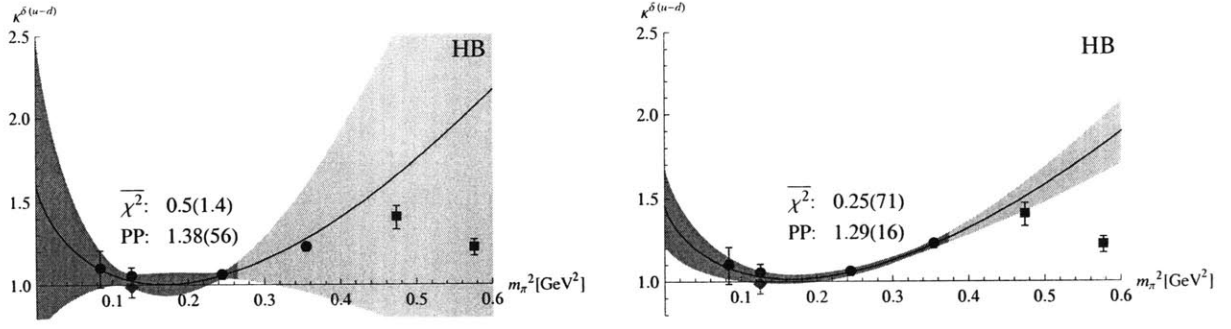
Figure 6-19: HBχPT fits to the isovector "polarized anomalous magnetic moment" κ_v^δ, for two different ranges of included pion mass.
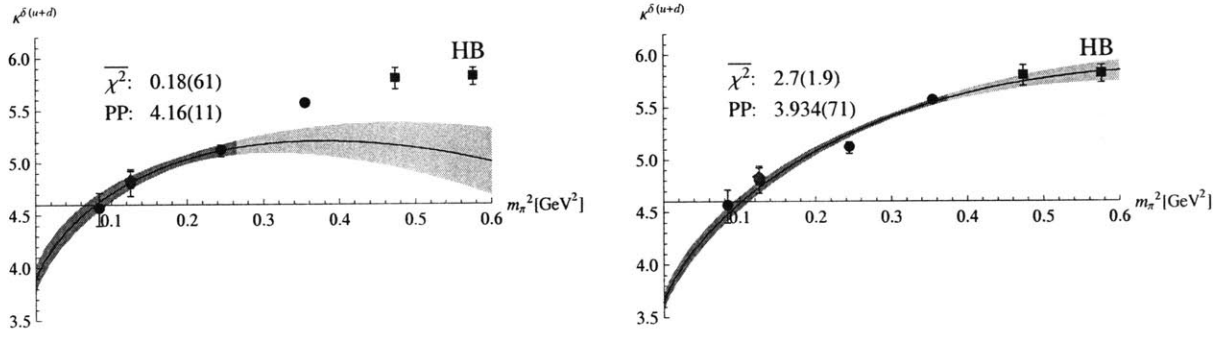
Figure 6-20: HBχPT fits to the isoscalar κ_s^δ, for two different ranges of included pion mass.

6.3.7 Angular Momentum

We saw previously that we can calculate the quark contribution to nucleon angular momentum: $J_q = \frac{1}{2}\left(A_{20}(0) + B_{20}(0)\right)$, as well as the contribution of quark spin to angular momentum: $\frac{1}{2}\Delta\Sigma = \frac{1}{2}\tilde{A}_{10}(0)$. By taking the difference of the two, we obtain the quark *orbital* angular momentum. In addition, we can find the *difference* in contributions to angular momentum from quarks polarized parallel and antiparallel to the nucleon: $\delta J_q = \frac{1}{2}\left(A_{T20}(0) + \bar{B}_{T20}(0)\right)$. Lattice data for these quantities are shown in Fig. 6-21 for up and down flavor quarks individually. (The chiral fits are done with a combination of HBχPT and SSE expressions.)

There are several interesting features of these results. Notice that the total angular momentum contribution of the down quarks is nearly zero (top left panel of Fig. 6-

21). Also, the orbital angular momentum of up quarks is nearly equal and opposite to the orbital angular momentum of down quarks (bottom left panel).[8] For the one case where experimental data is available, lattice results agree well with experiment (top right graph).
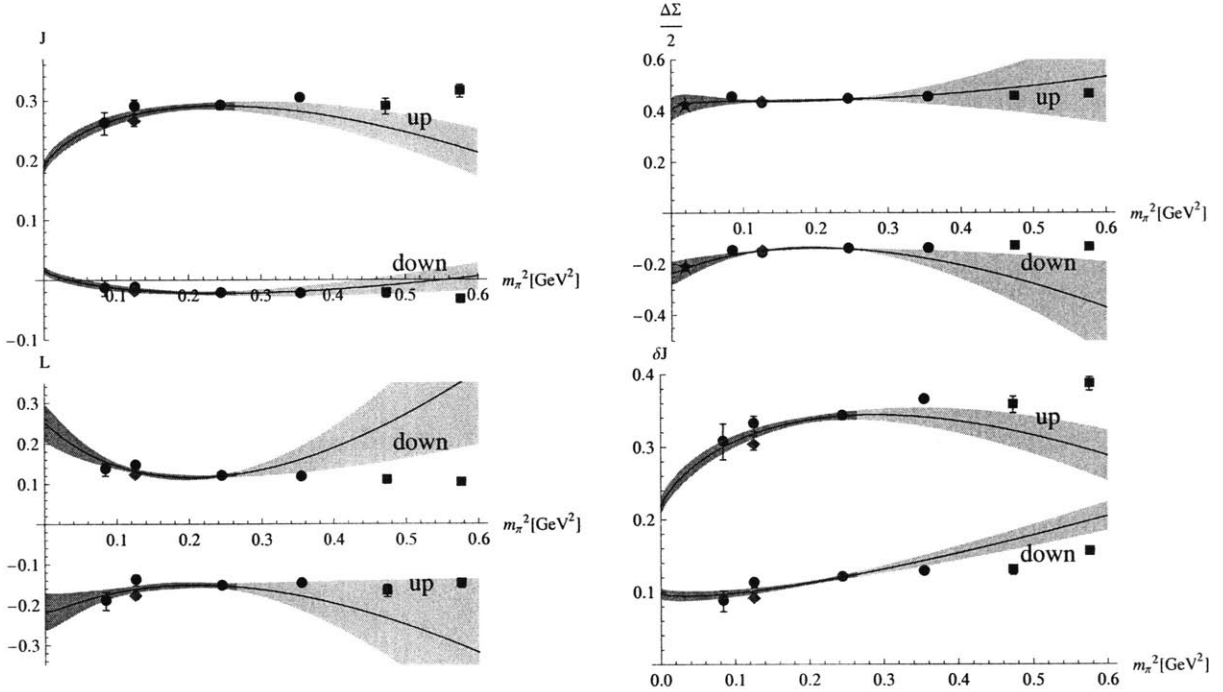
Figure 6-21: Quark angular momentum and various components thereof.

6.4 Comparison between $\langle x^n \rangle_\Delta$ and $\langle x^n \rangle_\delta$

In this section, we look more closely at the difference between the axial and tensor moments $\langle x^n \rangle_\Delta$ and $\langle x^n \rangle_\delta$. As noted in Section 4.4.1, these quantities have similar intuitive interpretations. The main difference between them, if we neglect other relativistic corrections due to the choice of a special longitudinal direction, is the sign of the antiquark contributions. For example, the axial charge[9] is the *sum* of quark,

---

[8]One could say that the quark contribution to nucleon angular momentum is found on the up quarks. Or, one could say that the total quark contribution comes from quark spin. However, it is clearly a logical fallacy to conclude that the quark contribution to nucleon spin can be attributed to the spin of the up quarks!

[9]Here we consider only the isovector flavor combination.

antiquark contributions:

$$g_A = \Delta u + \Delta \bar{u} - (\Delta d + \Delta \bar{d}). \tag{6.1}$$

On the other hand, the tensor charge is the *difference* of quark, antiquark contributions:

$$g_T = \delta u - \delta \bar{u} - (\delta d - \delta \bar{d}). \tag{6.2}$$

Now, Δq and δq (defined here without antiquark contributions) are *not* identical quantities except in the non-relativistic limit [32]. However, for the purposes of this discussion, let us assume that the differences between them are small in relation to the size of the antiquark terms $\Delta \bar{q}$. Then the ratio g_T/g_A can be approximated as:

$$\frac{g_T}{g_A} \approx \frac{\Delta u - \Delta \bar{u} - (\Delta d - \Delta \bar{d})}{\Delta u + \Delta \bar{u} - (\Delta d + \Delta \bar{d})}$$

$$= 1 - 2\frac{\Delta \bar{u} - \Delta \bar{d}}{\Delta u + \Delta \bar{u} - (\Delta d + \Delta \bar{d})}$$

$$= 1 - 2\frac{\Delta \bar{u} - \Delta \bar{d}}{g_A}. \tag{6.3}$$

We can thus estimate the magnitude of the antiquark contributions to g_A by comparing g_A with g_T. In the left-hand plot of Fig. 6-22, we show the lattice data for the ratio g_T/g_A as a function of pion mass, together with a fit to a quadratic in m_π.[10] From this plot, we estimate that the antiquark contributions to g_A are on the order of 5%, and that the quantity $(\Delta \bar{u} - \Delta \bar{d})$ is *positive*. We can compare this with the recent measurements of $\Delta \bar{q}$ in [66], from which we find: $(1 - 2\frac{\Delta \bar{u} - \Delta \bar{d}}{g_A})_{\exp} = 0.76(6)$ at a renormalization scale of 4 GeV^2. This gives antiquark contributions on the order of 10%, and a positive value for $(\Delta \bar{u} - \Delta \bar{d})$. Given the approximations we made in our

---

[10]We saw previously that we don't yet have a reliable chiral formula that can fit g_T, so here we use a polynomial fit ansatz to get some idea of the extrapolation to the physical pion mass.

interpretation of the lattice data, we consider these results to be consistent.

We could also compare the second moments $\langle x \rangle_\Delta$ and $\langle x \rangle_\delta$ (see right-hand plot in Fig. 6-22). The signs of the antiquark contributions in this case are reversed relative to the first moments, and the lattice results reflect this.
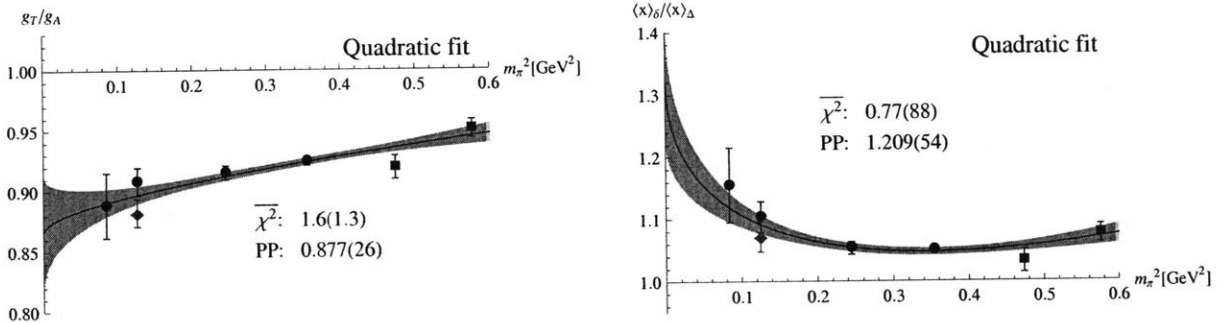
Figure 6-22: Comparison of tensor and axial moments. Left: g_T/g_A. Right: ratio of second moments.

6.5 The Other GFFs

Eight generalized parton distributions (per quark flavor) parameterize the bilocal matrix elements in Eqs. 4.2, 4.3 and 4.4. Only six of these enter into the expressions for transverse quark distributions (Eq. 4.19 and following). As we argued in Chapter 4, the GFFs corresponding to Mellin-moments of these six GPDs (for $\xi = 0$) can be given a straightforward physical interpretation. The other GFFs come into the picture only for $\xi \neq 0$, and so do not have a simple interpretation in terms of transverse parton distributions.

Some of these form factors do have well-established interpretations in other contexts; for example, the GFF $\tilde{B}_{10}(t)$ can be identified as the pseudoscalar form factor $G_P(t)$ [67]. It would be interesting to study these form factors further, and to understand their relationship to the parton distributions discussed here.

6.6 Error Analysis

Error analysis is an essential part of any measurement or numerical calculation. A number without an error bar is nearly useless at best, and deceptive at worst. The uncertainties in a physical measurement generally fall into two categories: statistical (errors resulting from random fluctuations) and systematic (errors resulting from the experimental procedure). The same is true of calculations in lattice QCD (which in some ways can be thought of as a "numerical experiment").

6.6.1 Statistical Uncertainties

Statistical fluctuations are intrinsic to any Monte Carlo procedure. In lattice QCD, these fluctuations are manifest in the random gauge configurations that constitute an ensemble. A great deal of effort has been put into obtaining enough statistics (i.e. large enough ensembles) to bring these uncertainties under control. Indeed, a major feature of the work presented here is the significant reduction of statistical error bars relative to the older calculations presented in [33]. The analysis of statistical error in this calculation was done using the jackknife procedure as described in Appendix D.

6.6.2 Systematic Uncertainties

The nature of systematic uncertainties makes them more difficult to pin down than statistical uncertainties. In some cases, we can only hope to estimate the magnitude of a systematic effect. Such estimates are valuable, however, and we have undertaken several studies in an attempt to understand the potential systematic errors in our results. In the next few sections, we will briefly discuss some of the possible sources of systematic error.

Excited States

As mentioned several times in this thesis, one potential source of systematic error is the contamination of our nucleon measurements with excited states. We studied this possibility by fitting selected operator plateaus with expressions containing excited

state terms (see summary in Appendix F). These terms were negligible on the time slices we use in our analysis, leading us to conclude that excited states are not a significant source of error in our results.

Fits to Form Factors

By arbitrarily selecting a particular ansatz[11] to fit the generalized form factors, we necessarily bias the resulting extrapolations to $t = 0$ (as well as the calculated values of form factor slopes). One way to gauge the severity of this bias is to vary the fit ansatz and observe the resulting change in the fit values. We present the results of such an exploration in Appendix E. We conclude that the choice of fit function may indeed have a significant effect on the extrapolation of form factors, and on the calculation of slopes at $t = 0$. In the worst cases, the systematic error may be several times the statistical uncertainty. It would be desirable to reduce this error by calculating GFFs at more values of t near zero, either by going to larger lattice volumes or through techniques such as partially twisted boundary conditions [68].

Finite Lattice Volume and Lattice Spacing

In this study, most of the calculations were done at a single volume of about $(2.5 \text{ fm})^3$. At one pion mass (~ 350 MeV), calculations were also done at a larger volume of about $(3.5 \text{ fm})^3$ to get an estimate of any finite size effects. With only two data points, it is impossible to do a rigorous analysis, but a survey of the results presented in this chapter suggests that there is not a large systematic effect due to finite volume. In particular, the data for g_A (see Fig. 6-4, for example) shows excellent agreement between the two volumes. Since g_A is known to be particularly sensitive to finite volume effects [69, 70], we conclude that finite volume effects are not significant in this work.[12]

All of our calculations were done at a single lattice spacing, so we have no way to perform any sort of continuum extrapolation with our results. However, comparing

---

[11]in our case, Eq. 5.8

[12]One caveat: calculations at the lowest pion mass are more sensitive to lattice volume.

with other studies (e.g. [3]), we expect the effects of finite lattice spacing to be small.

Chapter 7

Summary and Conclusions

In this work, we have presented results for two different studies of nucleon structure. These studies use lattice QCD to probe the spatial and spin distribution of the quarks in a nucleon, and illustrate the potential of numerical calculations not only to reproduce experimental values, but also to shed light on the behavior of strongly bound systems in QCD.

The first study (Chapter 3) used the calculation of overlaps of trial nucleon sources with the nucleon ground state to perform a variational study of the nucleon wavefunction. By calculating the overlaps for many different trial sources, we were able to determine which trial source most nearly approximates the true nucleon. Not only is this advantageous for future computations, but it also provides insight into nucleon structure. Trial sources with large overlaps give us clues as to where the quarks are inside a nucleon, and what they are doing.

In this study, we achieved overlaps of over 80% with trial sources involving a combination of gauge smearing and quark smearing. The best trial sources were obtained by using only the non-relativistic components of the quark source fields, making all the quark wavefunctions about the same size, and centering all three quarks at the same point.

The second and larger study presented in this thesis used the calculation of generalized form factors to explore nucleon structure through parton distributions. We

obtain expressions for parton distributions in three dimensions: longitudinal (plus-) momentum, and transverse position in the infinite momentum frame. Lattice calculations give us Mellin moments of the longitudinal distributions, leading to two-dimensional (transverse) distributions of charge and energy. We emphasized an intuitive picture of the nucleon as a cloud of point-like constituents, and used this picture as a framework to interpret the physical significance of the form factors we calculate. By taking appropriate linear combinations of the vector, axial and tensor operators, we obtained distributions of quarks with particular spin polarizations. These distributions provide us with a quantitative picture of the quarks inside a nucleon in the infinite momentum frame.

In Chapter 4, we provided an extensive list of specific nucleon observables that can be extracted from these parton distributions. Chapters 5 and 6 presented the results of a major effort to calculate a complete set of generalized form factors for the lowest two Mellin moments, using domain wall fermions on MILC lattices with pion masses as low as 290 MeV. From these form factors, we constructed the transverse distribution functions explicitly. We also performed chiral extrapolations for many selected form factor observables, using three different flavors of chiral perturbation theory.

From these studies, we conclude that lattice QCD has matured as a valuable tool for understanding nucleon structure from first principles.

Appendix A

Tables

A.1 Variational Calculation

R_{quark}		1.1	3.	4.2	4.9	5.3
	1.1	0.01331(61)	0.0474(24)	0.0620(33)	0.0656(36)	0.0660(38)
$R_{diquark}$	3.	0.1508(98)	0.238(17)	0.283(20)	0.296(21)	0.297(21)
	4.2	0.254(19)	0.331(24)	0.360(25)	0.363(26)	0.358(26)
	4.9	0.281(22)	0.340(26)	0.357(27)	0.355(28)	0.348(29)
	5.3	0.280(24)	0.329(28)	0.340(29)	0.335(30)	0.327(31)

Table A.1: Overlap tables for non-APE smeared four-component sources.

R_{quark}		1.1	3.	4.2	4.9	5.3
	1.1	0.01667(81)	0.0834(46)	0.1146(65)	0.1225(72)	0.1236(75)
$R_{diquark}$	3.	0.231(17)	0.364(29)	0.438(33)	0.462(34)	0.468(33)
	4.2	0.380(32)	0.473(38)	0.507(37)	0.508(37)	0.502(37)
	4.9	0.415(37)	0.480(40)	0.491(40)	0.483(40)	0.472(41)
	5.3	0.413(39)	0.462(42)	0.464(42)	0.452(43)	0.439(44)

Table A.2: Overlap tables for non-APE smeared two-component sources.

			R_{quark}		
			3.1	4.3	5.
$R_{diquark}$	3.1	$\ell = 0$	0.397(24)	0.457(24)	0.477(24)
		4	—	0.466(31)	0.473(31)
		8	—	0.426(47)	—
	4.3	$\ell = 0$	0.534(26)	0.570(26)	0.579(26)
		4	0.549(34)	0.561(24)	0.562(24)
		8	0.485(51)	0.518(38)	0.518(50)
	5.	$\ell = 0$	0.566(27)	0.589(27)	0.593(28)
		4	0.570(36)	0.574(26)	0.572(27)
		8	—	0.536(64)	—

Table A.3: Overlap tables for APE smeared four-component sources, at different values of quark-diquark separation ℓ.

			R_{quark}		
			3.1	4.3	5.
$R_{diquark}$	3.1	$\ell = 0$	0.625(40)	0.723(37)	0.754(35)
		4	—	0.737(48)	0.748(46)
		8	—	0.678(76)	—
	4.3	$\ell = 0$	0.767(37)	0.808(35)	0.817(36)
		4	0.784(48)	0.792(34)	0.792(35)
		8	0.678(78)	0.728(58)	0.729(74)
	5.	$\ell = 0$	0.789(37)	0.809(38)	0.810(39)
		4	0.785(50)	0.782(38)	0.777(38)
		8	—	0.723(93)	—

Table A.4: Overlap tables for APE smeared two-component sources, at different values of quark-diquark separation ℓ.

A.2   Generalized Form Factors

Tables A.5 - A.15 give numerical results for the generalized form factors as a function of Q^2 (in lattice units). The top panel of each table gives results for up quarks in a proton, and the bottom panel gives results for down quarks. The last four rows of each panel give the parameters and $\chi^2/\text{d.o.f.}$ resulting from a fit of Eq. 5.8 to the corresponding form factor data. Only Q^2 values indicated with a check mark are included in the fit. Note that while the second moment form factors are renormalized as described in Chapter 5, the first moment results are shown without renormalization. (We choose to display the results this way because we simply use the vector charge $A_{10}^{(u-d)}(0)$ to renormalize the first moment form factors.)

Q^2	$A_{10}^{(u)}$	$B_{10}^{(u)}$	$A_{20}^{(u)}$	$B_{20}^{(u)}$	$C_{20}^{(u)}$	$\tilde{A}_{10}^{(u)}$	$\tilde{B}_{10}^{(u)}$	$\tilde{A}_{20}^{(u)}$	$\tilde{B}_{20}^{(u)}$	$A_{T10}^{(u)}$	$\tilde{A}_{T10}^{(u)}$	$\tilde{B}_{T10}^{(u)}$	$A_{T20}^{(u)}$	$\tilde{A}_{T20}^{(u)}$	$\tilde{B}_{T20}^{(u)}$	$\tilde{B}_{T21}^{(u)}$
✓0.000	1.726(2)	—	0.413(4)	—		0.789(11)		0.229(5)		0.779(11)			0.253(5)			
0.081	1.416(59)	0.741(373)	0.381(21)	0.058(119)	-0.172(144)	0.757(55)		0.225(21)		0.677(47)	0.922(107)	2.290(269)	0.236(21)	0.109(38)	0.268(96)	0.299(332)
✓0.096	1.324(5)	1.164(47)	0.358(3)	0.191(16)	-0.064(12)	0.676(9)	6.786(313)	0.209(4)	0.805(131)	0.659(10)	-0.422(157)	2.302(27)	0.224(4)	0.030(61)	0.429(13)	-0.021(29)
✓0.097	1.313(10)	1.203(99)	0.356(6)	0.148(34)	-0.043(29)	0.672(19)	6.893(706)	0.204(8)	0.686(262)	0.664(17)	-0.361(285)	2.287(49)	0.228(7)	-0.051(106)	0.432(22)	0.034(90)
0.166	1.108(56)	0.720(219)	0.315(19)	0.049(68)	-0.070(42)	0.608(52)	3.184(1.296)	0.199(20)	0.426(421)	0.746(71)	-2.291(738)	2.032(157)	0.235(25)	-0.355(247)	0.352(53)	0.156(117)
✓0.188	1.054(9)	0.889(41)	0.312(4)	0.149(15)	-0.051(7)	0.588(11)	4.725(193)	0.189(4)	0.534(78)	0.568(10)	-0.310(84)	1.828(26)	0.203(5)	—	0.384(12)	0.009(19)
✓0.189	1.036(18)	0.956(90)	0.314(8)	0.141(34)	-0.079(17)	0.564(26)	4.294(540)	0.178(9)	0.395(187)	0.567(20)	-0.303(205)	1.825(54)	0.198(8)	0.114(74)	0.388(22)	0.084(61)
✓0.197	1.049(14)	0.950(51)	0.317(5)	0.167(18)	-0.026(9)	0.593(13)	4.937(261)	0.193(5)	0.595(114)	0.561(16)	-0.193(125)	1.763(34)	0.204(7)	0.039(50)	0.367(13)	-0.019(24)
0.249	0.879(70)	0.598(211)	0.271(23)	0.044(69)	-0.043(36)	0.525(65)	3.141(990)	0.181(26)	0.414(357)	0.584(64)	-0.874(457)	1.598(156)	0.182(23)	0.059(166)	0.336(55)	0.077(112)
✓0.276	0.868(13)	0.697(43)	0.276(5)	0.123(15)	-0.039(7)	0.513(14)	3.318(204)	0.173(5)	0.430(83)	0.501(14)	-0.254(97)	1.479(30)	0.184(6)	0(0.041)	0.338(13)	-0.006(21)
0.286	—		—													
✓0.294	0.850(16)	0.780(49)	0.277(6)	0.148(17)	-0.027(8)	0.508(15)	3.352(221)	0.172(5)	0.484(97)	0.479(17)	-0.109(100)	1.420(33)	0.183(7)	0.038(39)	0.324(13)	0.008(23)
0.360	—		—													
✓0.361	0.736(19)	0.630(54)	0.250(7)	0.128(20)	-0.037(9)	0.477(19)	2.840(237)	0.163(8)	0.461(107)	0.443(22)	-0.052(127)	1.196(39)	0.161(8)	0.043(55)	0.282(17)	-0.012(26)
✓0.364	0.716(31)	0.620(114)	0.237(12)	0.086(34)	-0.037(18)	0.425(39)	2.318(468)	0.145(16)	0.241(206)	0.451(34)	-0.270(212)	1.160(61)	0.167(13)	-0.072(88)	0.278(26)	0.010(51)
✓0.395	0.713(16)	0.592(42)	0.249(6)	0.130(18)	-0.034(8)	0.453(14)	—	0.161(6)	—	0.307(10)	0.462(14)	1.125(34)	0.139(6)	0.115(7)	0.273(16)	-0.042(18)
0.408	—		—													
✓0.443	0.626(20)	0.509(49)	0.225(7)	0.096(16)	-0.036(6)	0.414(18)	2.111(153)	0.146(7)	0.289(71)	0.410(20)	-0.157(73)	1.019(37)	0.156(8)	-0.014(36)	0.255(15)	-0.005(18)
✓0.447	0.591(37)	0.543(100)	0.218(14)	0.087(34)	-0.045(13)	0.360(42)	1.729(351)	0.128(15)	0.153(148)	0.388(34)	-0.210(137)	0.997(66)	0.147(14)	-0.013(62)	0.257(26)	0.023(46)
✓0.475	0.600(21)	0.521(58)	0.216(8)	0.106(20)	-0.020(8)	0.414(23)	2.021(205)	0.148(9)	0.379(102)	0.391(24)	-0.091(94)	0.924(37)	0.151(9)	0.011(40)	0.242(15)	0.008(24)
✓0.491	0.603(15)	0.502(35)	0.221(6)	0.104(13)	-0.027(5)	0.407(14)	2.052(131)	0.149(6)	0.271(78)	0.383(22)	-0.088(74)	0.940(28)	0.149(9)	0.022(32)	0.243(12)	-0.023(12)
A_0	1.726(2)	1.549(74)	0.413(4)	0.217(20)	-0.078(19)	0.789(11)	11.069(1.496)	0.230(5)	1.215(1.043)	0.780(11)	-0.618(261)	2.993(50)	0.253(5)	0.054(77)	0.507(16)	-0.011(12)
m_A	0.770(40)	0.797(34)	1.120(185)	1.029(497)	0.522(122)	0.985(187)	0.603(200)	1.256(1.717)	0.441(1.006)	0.896(67)	0.860(242)	1.143(196)	1.432(943)	0.904(711)	1.931(66)	3.3
p	1.778(169)	2.	1.955(599)	2.013(1.755)	1.	1.657(546)	2.038(783)	1.698(5.418)	1.146(2.68)	1.504(212)	3.5	3.702(1.091)	2.545(3.094)	3.5	6.00000(3)	1
$\overline{\chi^2}$	0.637(658)	0.481(446)	0.586(502)	0.606(604)	1.309(822)	0.526(561)	0.682(633)	0.640(671)	0.479(508)	0.076(106)	0.298(307)	0.238(305)	0.168(199)	0.469(432)	0.202(256)	0.848(718)

Q^2	$A_{10}^{(d)}$	$B_{10}^{(d)}$	$A_{20}^{(d)}$	$B_{20}^{(d)}$	$C_{20}^{(d)}$	$\tilde{A}_{10}^{(d)}$	$\tilde{B}_{10}^{(d)}$	$\tilde{A}_{20}^{(d)}$	$\tilde{B}_{20}^{(d)}$	$A_{T10}^{(d)}$	$\tilde{A}_{T10}^{(d)}$	$\tilde{B}_{T10}^{(d)}$	$A_{T20}^{(d)}$	$\tilde{A}_{T20}^{(d)}$	$\tilde{B}_{T20}^{(d)}$	$\tilde{B}_{T21}^{(d)}$
✓0.000	0.8748(9)		0.186(2)			-0.231(7)		-0.056(3)		-0.190(6)			-0.053(2)			
0.081	0.677(32)	-1.566(255)	0.174(11)	-0.322(70)	-0.070(94)	-0.239(33)	—	-0.063(10)	—	-0.146(23)	0.634(69)	1.587(172)	-0.055(10)	0.094(25)	0.235(61)	-0.052(206)
✓0.096	0.640(3)	-1.103(26)	0.155(2)	-0.212(9)	-0.062(6)	-0.195(6)	-1.885(155)	-0.049(2)	-0.055(66)	-0.162(6)	1.041(79)	1.487(16)	-0.046(2)	0.132(28)	0.296(8)	-0.073(15)
✓0.097	0.634(6)	-1.144(59)	0.155(3)	-0.222(20)	-0.038(17)	-0.210(11)	-2.214(338)	-0.049(4)	0.030(125)	-0.164(9)	0.969(157)	1.531(29)	-0.048(3)	0.123(57)	0.315(12)	-0.022(55)
0.166	0.512(30)	-1.011(153)	0.135(9)	-0.242(44)	0.011(27)	-0.181(29)	-1.240(642)	-0.043(10)	0.167(233)	-0.131(29)	0.897(326)	1.347(93)	-0.050(11)	0.190(125)	0.277(32)	-0.019(69)
✓0.188	0.489(5)	-0.892(24)	0.131(2)	-0.191(9)	-0.042(4)	-0.165(6)	-1.114(98)	-0.044(3)	0.012(47)	-0.145(6)	0.876(50)	1.178(16)	-0.043(2)	0.154(20)	0.258(8)	-0.041(10)
✓0.189	0.483(10)	-0.853(59)	0.132(4)	-0.191(19)	-0.047(11)	-0.172(14)	-1.054(278)	-0.046(5)	-0.061(113)	-0.153(10)	0.943(112)	1.207(33)	-0.048(4)	0.199(42)	0.280(12)	-0.044(36)
✓0.197	0.475(7)	-0.815(34)	0.130(2)	-0.170(11)	-0.039(5)	-0.171(7)	-1.343(139)	-0.044(3)	-0.004(59)	-0.147(7)	0.797(69)	1.118(22)	-0.045(3)	0.164(29)	0.247(8)	-0.049(13)
0.249	0.398(35)	-0.693(143)	0.110(10)	-0.210(43)	-0.006(24)	-0.164(34)	-1.186(545)	-0.036(11)	0.009(219)	-0.133(33)	0.977(272)	1.067(95)	-0.052(12)	0.243(101)	0.261(33)	-0.031(64)
✓0.276	0.386(7)	-0.720(26)	0.112(2)	-0.172(9)	-0.036(4)	-0.146(7)	-0.840(103)	-0.039(3)	-0.008(48)	-0.133(8)	0.728(53)	0.956(19)	-0.040(3)	0.132(22)	0.228(9)	-0.035(11)
0.286	—		—			—		—		—			—			
✓0.294	0.367(8)	-0.648(32)	0.110(2)	-0.151(10)	-0.032(5)	-0.149(8)	-0.876(116)	-0.040(3)	0.013(55)	-0.133(8)	0.649(56)	0.899(22)	-0.042(3)	0.150(22)	0.218(8)	-0.034(13)
0.360	—		—			—		—		—			—			
✓0.361	0.318(10)	-0.586(31)	0.100(3)	-0.166(12)	-0.045(5)	-0.122(10)	-0.594(114)	-0.040(4)	-0.022(59)	-0.115(10)	0.608(59)	0.783(23)	-0.034(4)	0.096(26)	0.196(10)	-0.030(14)
✓0.364	0.303(16)	-0.551(63)	0.096(5)	-0.158(21)	-0.053(11)	-0.117(18)	-0.505(213)	-0.032(7)	0.052(104)	-0.125(15)	0.700(106)	0.790(38)	-0.041(6)	0.144(45)	0.205(15)	-0.031(30)
✓0.395	0.292(9)	-0.506(25)	0.095(3)	-0.125(10)	-0.040(5)	-0.130(8)	—	-0.037(3)	—	-0.071(5)	0.273(9)	0.689(22)	-0.035(3)	0.069(4)	0.176(9)	-0.060(10)
0.408	—		—			—		—		—			—			
✓0.443	0.259(11)	-0.482(30)	0.086(3)	-0.140(11)	-0.033(4)	-0.103(9)	-0.365(83)	-0.033(4)	0.020(43)	-0.112(10)	0.537(46)	0.669(24)	-0.034(4)	0.102(20)	0.181(10)	-0.023(10)
✓0.447	0.246(18)	-0.433(63)	0.084(6)	-0.135(21)	-0.040(9)	-0.099(20)	-0.255(178)	-0.036(7)	-0.045(82)	-0.129(17)	0.625(91)	0.668(44)	-0.043(7)	0.154(35)	0.200(17)	-0.011(25)
✓0.475	0.235(10)	-0.454(34)	0.081(3)	-0.130(12)	-0.035(5)	-0.113(12)	-0.583(107)	-0.031(4)	0.001(57)	-0.107(11)	0.471(55)	0.612(24)	-0.033(5)	0.108(25)	0.171(9)	-0.019(14)
✓0.491	0.236(8)	-0.424(22)	0.083(3)	-0.113(8)	-0.031(3)	-0.115(7)	-0.513(73)	-0.034(3)	0.043(46)	-0.111(11)	0.437(41)	0.573(18)	-0.038(5)	0.096(19)	0.154(7)	-0.045(7)
A_0	0.8748(9)	-1.450(48)	0.186(2)	-0.247(11)	-0.057(7)	-0.232(7)	-4.059(1.44)	-0.055(3)	-0.068(8.521)	-0.188(10)	1.310(94)	1.964(31)	-0.052(2)	0.182(26)	0.354(10)	-0.065(18)
m_A	0.887(52)	1.326(517)	1.186(190)	1.976(86)	0.794(143)	1.357(642)	0.410(221)	1.092(92)	0.303(376)	1.067(2.893)	1.208(61)	1.076(169)	1.261(161)	1.732(276)	1.891(57)	0.751(279)
p	2.726(305)	4.999(3.439)	2.777(836)	6.000(5)	1.	3.220(2.823)	1.627(770)	1.5	6.000(146)	1.587(10.042)	3.5	3.403(904)	1.500(28)	3.5	5.999(78)	1
$\overline{\chi^2}$	0.188(309)	0.464(448)	0.202(247)	1.015(883)	1.430(822)	0.659(504)	1.151(799)	0.193(183)	0.298(363)	0.256(335)	0.497(499)	0.698(597)	0.502(397)	0.708(552)	1.020(849)	1.236(906)

Table A.5: MILC-20^3-m05-chopped — data set 1

Q^2	$A_{10}^{(u)}$	$B_{10}^{(u)}$	$A_{20}^{(u)}$	$B_{20}^{(u)}$	$C_{20}^{(u)}$	$\tilde{A}_{10}^{(u)}$	$\tilde{B}_{10}^{(u)}$	$\tilde{A}_{20}^{(u)}$	$\tilde{B}_{20}^{(u)}$	$A_{T10}^{(u)}$	$\tilde{A}_{T10}^{(u)}$	$\tilde{B}_{T10}^{(u)}$	$A_{T20}^{(u)}$	$\tilde{A}_{T20}^{(u)}$	$\tilde{B}_{T20}^{(u)}$	$\tilde{B}_{T21}^{(u)}$
✓0.000	1.752(2)	—	0.396(5)	—	—	0.788(16)	—	0.222(6)	—	0.756(13)	—	—	0.237(6)	—	—	—
0.079	1.427(59)	1.589(385)	0.335(21)	0.192(134)	0.10(163)	0.750(63)	—	0.175(21)	—	0.641(47)	1.254(110)	3.121(275)	0.206(22)	0.227(42)	0.562(104)	0.076(387)
✓0.096	1.329(7)	1.135(60)	0.346(4)	0.155(21)	-0.058(17)	0.669(13)	6.886(382)	0.204(5)	0.544(170)	0.665(14)	-0.783(195)	2.320(31)	0.219(6)	-0.074(84)	0.425(15)	-0.021(41)
✓0.096	1.328(15)	1.149(123)	0.343(8)	0.141(38)	-0.093(39)	0.697(26)	7.512(801)	0.197(10)	0.365(284)	0.657(22)	-0.455(341)	2.186(61)	0.213(9)	-0.093(118)	0.359(26)	-0.095(129)
✓0.164	1.172(69)	1.172(260)	0.317(22)	0.215(81)	-0.059(48)	0.658(65)	4.372(1.252)	0.175(23)	-0.139(438)	0.678(81)	-0.847(720)	2.131(157)	0.212(27)	-0.174(261)	0.390(59)	-0.01(124)
✓0.188	1.065(12)	0.914(51)	0.305(5)	0.155(18)	-0.041(8)	0.590(14)	4.821(222)	0.187(6)	0.420(99)	0.568(15)	-0.257(101)	1.813(30)	0.196(6)	0.023(42)	0.373(15)	-0.014(23)
✓0.188	1.063(28)	0.906(124)	0.304(11)	0.086(40)	-0.056(22)	0.629(32)	5.356(605)	0.183(11)	0.312(226)	0.562(28)	0.109(235)	1.657(67)	0.194(11)	-0.027(92)	0.281(27)	-0.093(75)
✓0.197	1.023(18)	0.826(62)	0.297(6)	0.111(20)	-0.039(11)	0.577(17)	4.683(310)	0.183(6)	0.337(134)	0.541(18)	-0.261(136)	1.672(40)	0.188(7)	0.046(55)	0.323(16)	0.005(28)
0.246	0.969(103)	1.064(298)	0.291(36)	0.163(83)	-0.022(48)	0.636(98)	3.587(1.153)	0.191(35)	0.318(402)	0.584(98)	0.001(591)	1.674(196)	0.199(34)	-0.150(219)	0.301(65)	-0.075(155)
✓0.275	0.878(19)	0.773(54)	0.273(7)	0.148(20)	-0.034(9)	0.519(19)	3.444(233)	0.172(7)	0.337(99)	0.488(20)	-0.096(109)	1.457(38)	0.181(8)	0.006(49)	0.338(17)	-0.022(26)
0.280	1.507(1.974)	1.575(2.321)	0.379(490)	0.283(563)	0.102(314)	1.004(1.295)	—	0.140(210)	—	0.889(1.164)	1.186(1.476)	2.896(3.602)	0.351(476)	0.334(463)	0.806(1.122)	0.215(718)
✓0.294	0.819(19)	0.669(56)	0.254(6)	0.094(19)	-0.040(10)	0.495(18)	3.310(235)	0.157(7)	0.160(117)	0.445(19)	-0.011(102)	1.243(35)	0.172(7)	0.010(46)	0.246(16)	0.031(28)
0.353																
✓0.359	0.765(28)	0.646(65)	0.245(10)	0.101(24)	-0.023(13)	0.476(26)	2.586(318)	0.160(10)	0.275(160)	0.482(34)	-0.277(179)	1.272(51)	0.173(15)	-0.015(80)	0.319(22)	-0.041(34)
✓0.362	0.760(61)	0.618(167)	0.253(22)	0.089(55)	-0.018(27)	0.498(68)	2.950(760)	0.143(23)	0.134(319)	0.486(66)	-0.414(381)	1.165(107)	0.188(26)	-0.152(146)	0.252(41)	0.027(77)
✓0.395	0.680(22)	0.513(46)	0.234(8)	0.10(19)	-0.034(10)	0.417(20)	—	0.155(8)	—	0.275(13)	0.448(17)	1.088(42)	0.131(8)	0.109(7)	0.259(19)	-0.024(26)
0.403	—	—	—	—	—	—	—	—	—	—	—	—	—	—	—	—
✓0.439	0.632(28)	0.502(54)	0.216(11)	0.101(19)	-0.017(9)	0.398(24)	1.884(214)	0.143(10)	0.186(94)	0.401(28)	-0.152(94)	1.002(48)	0.157(13)	-0.027(47)	0.254(20)	-0.020(22)
✓0.444	0.624(81)	0.377(149)	0.220(31)	0.031(50)	-0.016(26)	0.416(74)	1.707(524)	0.130(24)	0.126(229)	0.400(71)	-0.228(228)	0.828(121)	0.155(29)	-0.094(99)	0.155(42)	0.044(70)
✓0.474	0.607(32)	0.449(73)	0.220(12)	0.099(26)	-0.022(12)	0.405(29)	1.656(250)	0.137(11)	0.047(133)	0.404(31)	-0.167(120)	0.948(56)	0.145(12)	0.038(55)	0.240(22)	-0.002(33)
✓0.491	0.568(19)	0.407(39)	0.208(7)	0.083(14)	-0.025(6)	0.368(18)	1.906(166)	0.140(7)	0.208(91)	0.345(25)	-0.074(81)	0.863(34)	0.139(12)	0.015(40)	0.224(15)	-0.012(15)
A_0	1.752(2)	1.495(88)	0.397(5)	0.178(24)	-0.103(50)	0.789(16)	10.917(1.426)	0.223(7)	0.730(449)	0.762(14)	-2.289(3.095)	3.169(66)	0.238(6)	-0.076(3.741)	0.479(22)	-0.014(45)
m_A	0.780(52)	1.455(56)	1.182(271)	1.953(244)	0.372(146)	1.931(65)	0.881(465)	2.158(1.987)	1.111(2.943)	1.447(677)	0.469(250)	0.741(20)	2.021(2.108)	0.3	1.034(61)	2.172(17.004)
p	1.877(231)	6.	2.147(911)	5.997(423)	1.000(10)	5.988(233)	3.757(2.988)	4.823(8.2)	4.733(19.096)	3.527(3.133)	3.5	2.000(43)	4.408(8.807)	3.5	2.	1
$\overline{\chi}^2$	0.318(368)	0.361(362)	0.327(219)	0.862(665)	0.338(386)	0.450(479)	0.392(323)	0.322(319)	0.312(333)	0.865(652)	0.883(724)	2.758(1.164)	0.281(397)	0.498(571)	3.890(1.474)	0.548(482)

Q^2	$A_{10}^{(d)}$	$B_{10}^{(d)}$	$A_{20}^{(d)}$	$B_{20}^{(d)}$	$C_{20}^{(d)}$	$\tilde{A}_{10}^{(d)}$	$\tilde{B}_{10}^{(d)}$	$\tilde{A}_{20}^{(d)}$	$\tilde{B}_{20}^{(d)}$	$A_{T10}^{(d)}$	$\tilde{A}_{T10}^{(d)}$	$\tilde{B}_{T10}^{(d)}$	$A_{T20}^{(d)}$	$\tilde{A}_{T20}^{(d)}$	$\tilde{B}_{T20}^{(d)}$	$\tilde{B}_{T21}^{(d)}$
✓0.000	0.888(10)	—	0.175(2)	—	—	-0.227(9)	—	-0.054(3)	—	-0.176(7)	—	—	-0.048(3)	—	—	—
0.079	0.641(31)	-1.216(247)	0.144(10)	-0.246(73)	-0.135(90)	-0.190(33)	—	-0.056(10)	—	-0.125(23)	0.678(69)	1.697(173)	-0.034(11)	0.118(24)	0.297(60)	0.086(222)
✓0.096	0.640(4)	-1.083(31)	0.147(2)	-0.192(11)	-0.057(9)	-0.193(7)	-2.133(201)	-0.048(3)	-0.084(87)	-0.156(7)	1.008(95)	1.423(20)	-0.044(3)	0.147(40)	0.262(10)	-0.033(22)
✓0.096	0.632(9)	-1.018(67)	0.145(4)	-0.162(22)	-0.055(21)	-0.183(14)	-2.108(422)	-0.048(6)	-0.111(153)	-0.157(11)	0.924(177)	1.477(39)	-0.046(4)	0.181(62)	0.255(17)	-0.038(75)
0.164	0.481(35)	-0.862(160)	0.121(10)	-0.160(42)	-0.057(27)	-0.155(35)	-2.184(703)	-0.047(11)	-0.142(246)	-0.108(33)	0.642(348)	1.252(90)	-0.040(12)	0.261(135)	0.242(35)	0.048(77)
✓0.188	0.484(7)	-0.854(29)	0.126(2)	-0.158(10)	-0.042(5)	-0.162(8)	-1.144(138)	-0.043(3)	-0.017(52)	-0.149(8)	0.877(58)	1.116(19)	-0.043(3)	0.158(23)	0.223(10)	-0.022(13)
✓0.188	0.472(15)	-0.698(70)	0.124(5)	-0.150(21)	-0.056(13)	-0.131(19)	-0.672(380)	-0.046(7)	-0.053(130)	-0.159(15)	1.057(157)	1.140(46)	-0.047(5)	0.150(54)	0.225(18)	-0.039(49)
✓0.197	0.463(9)	-0.819(35)	0.121(3)	-0.164(11)	-0.033(7)	-0.160(8)	-1.082(176)	-0.041(3)	-0.039(78)	-0.138(9)	0.741(75)	1.076(25)	-0.040(3)	0.115(32)	0.225(10)	-0.046(17)
0.246	0.346(46)	-0.503(169)	0.099(14)	-0.142(44)	-0.036(29)	-0.097(45)	-0.882(641)	-0.049(15)	-0.181(252)	-0.127(43)	1.042(345)	1.004(127)	-0.026(15)	0.075(132)	0.221(44)	0.029(87)
✓0.275	0.377(10)	-0.694(33)	0.109(3)	-0.140(11)	-0.035(6)	-0.140(10)	-0.738(127)	-0.041(4)	-0.040(57)	-0.148(10)	0.800(61)	0.915(25)	-0.042(4)	0.140(26)	0.200(11)	-0.016(15)
0.280	0.496(658)	-0.790(1.129)	0.102(126)	-0.169(255)	0.028(160)	-0.276(375)		-0.088(126)		-0.104(163)	0.668(833)	1.678(2.093)	0.014(67)	0.131(193)	0.326(481)	0.209(488)
✓0.294	0.350(10)	-0.602(32)	0.102(3)	-0.131(11)	-0.031(6)	-0.135(9)	-0.766(146)	-0.042(4)	-0.123(71)	-0.136(11)	0.675(66)	0.834(25)	-0.040(4)	0.122(25)	0.185(10)	-0.022(17)
0.353																
✓0.359	0.326(13)	-0.584(41)	0.093(5)	-0.126(13)	-0.023(7)	-0.141(13)	-0.847(157)	-0.036(5)	0.024(74)	-0.121(15)	0.530(83)	0.753(31)	-0.041(6)	0.128(35)	0.169(14)	-0.026(19)
✓0.362	0.286(28)	-0.598(93)	0.092(10)	-0.131(29)	-0.024(16)	-0.144(32)	-0.969(357)	-0.031(11)	0.008(137)	-0.119(26)	0.389(162)	0.818(73)	-0.040(10)	0.106(63)	0.172(27)	0.029(44)
✓0.395	0.280(10)	-0.527(31)	0.089(4)	-0.113(12)	-0.028(6)	-0.139(10)		-0.034(4)		-0.066(7)	0.267(10)	0.674(25)	-0.029(4)	0.065(4)	0.167(11)	-0.017(14)
0.403																
✓0.439	0.254(14)	-0.477(38)	0.081(5)	-0.104(11)	-0.023(5)	-0.120(13)	-0.625(109)	-0.031(5)	-0.033(49)	-0.122(14)	0.502(61)	0.630(31)	-0.039(6)	0.128(27)	0.152(12)	-0.018(13)
✓0.444	0.224(34)	-0.377(85)	0.072(12)	-0.105(27)	-0.014(14)	-0.090(33)	-0.272(297)	-0.032(11)	0.095(135)	-0.151(39)	0.567(175)	0.657(90)	-0.050(14)	0.148(64)	0.163(31)	0.031(40)
✓0.474	0.225(16)	-0.480(50)	0.075(5)	-0.124(16)	-0.013(7)	-0.101(18)	-0.446(165)	-0.036(7)	-0.032(83)	-0.099(15)	0.392(69)	0.607(37)	-0.037(7)	0.085(33)	0.154(15)	-0.018(21)
✓0.491	0.226(9)	-0.443(27)	0.078(3)	-0.105(10)	-0.025(4)	-0.123(10)	-0.423(98)	-0.030(4)	0.045(59)	-0.110(15)	0.406(52)	0.566(21)	-0.037(7)	0.090(24)	0.149(9)	-0.024(9)
A_0	0.888(10)	-1.436(51)	0.175(3)	-0.221(15)	-0.091(23)	-0.222(9)	-5.244(834)	-0.054(4)	-0.168(763)	-0.175(7)	1.372(114)	1.944(43)	-0.048(3)	0.183(36)	0.308(14)	-0.041(27)
m_A	0.852(60)	0.775(29)	1.373(519)	1.035(82)	0.390(81)	0.925(67)	0.3	1.563(4.189)	0.879(1.952)	2.319(3.27)	1.125(73)	0.771(100)	1.660(509)	1.645(429)	1.043(57)	0.612(455)
p	2.661(351)	2.	3.612(2.431)	2.	1.000(8)	1.5	1.313(151)	3.113(15.806)	5.881(12.127)	5.097(12.302)	3.5	2.027(398)	1.5	3.5	2.	1
$\overline{\chi}^2$	0.497(406)	0.879(609)	0.231(296)	0.380(297)	0.545(425)	0.864(625)	0.760(635)	0.170(161)	0.445(309)	0.487(434)	0.950(752)	0.530(527)	0.203(307)	0.293(409)	0.130(113)	0.427(418)

Table A.6: MILC20³-m04-chopped — data set 2

Q^2	$A_{10}^{(u)}$	$B_{10}^{(u)}$	$A_{20}^{(u)}$	$B_{20}^{(u)}$	$C_{20}^{(u)}$	$\tilde{A}_{10}^{(u)}$	$\tilde{B}_{10}^{(u)}$	$\tilde{A}_{20}^{(u)}$	$\tilde{B}_{20}^{(u)}$	$A_{T10}^{(u)}$	$\tilde{A}_{T10}^{(u)}$	$\tilde{B}_{T10}^{(u)}$	$A_{T20}^{(u)}$	$\tilde{A}_{T20}^{(u)}$	$\tilde{B}_{T20}^{(u)}$	$\tilde{B}_{T21}^{(u)}$
√0.000	1.764(2)	—	0.397(5)	—	—	0.808(17)	—	0.231(7)	—	0.761(13)	—	—	0.247(6)	—	—	—
0.077	1.297(56)	1.106(386)	0.317(20)	0.038(128)	-0.089(165)	0.649(62)	—	0.171(21)	—	0.546(44)	0.749(121)	1.859(302)	0.207(23)	0.076(48)	0.184(119)	0.400(387)
√0.096	1.308(7)	1.059(57)	0.341(5)	0.184(19)	-0.062(14)	0.672(13)	7.255(370)	0.203(5)	0.556(158)	0.662(14)	-0.749(182)	2.184(31)	0.222(6)	-0.066(79)	0.396(15)	0.015(40)
√0.096	1.309(16)	1.069(122)	0.343(9)	0.194(38)	-0.037(38)	0.679(27)	7.727(786)	0.204(10)	0.445(311)	0.660(23)	-0.606(342)	2.237(68)	0.224(9)	-0.121(128)	0.393(28)	-0.058(121)
0.160	1.050(63)	0.863(238)	0.288(22)	0.097(74)	-0.061(52)	0.580(60)	3.945(1.202)	0.162(21)	0.436(397)	0.654(82)	-1.096(760)	1.630(156)	0.217(29)	-0.344(271)	0.268(58)	-0.024(144)
√0.186	1.028(12)	0.830(47)	0.299(5)	0.145(17)	-0.046(8)	0.575(15)	4.612(221)	0.180(6)	0.367(79)	0.571(15)	-0.408(95)	1.701(31)	0.201(6)	-0.045(41)	0.334(15)	0.011(24)
√0.187	1.036(28)	0.784(116)	0.308(11)	0.155(41)	-0.023(23)	0.569(34)	4.377(581)	0.194(13)	0.599(223)	0.589(29)	-0.500(228)	1.728(72)	0.204(11)	0.008(95)	0.339(28)	0.145(82)
√0.197	0.991(16)	0.836(53)	0.291(7)	0.170(19)	-0.020(11)	0.576(17)	4.669(266)	0.184(6)	0.305(116)	0.550(19)	-0.314(123)	1.620(38)	0.199(7)	-0.036(51)	0.328(16)	0.004(28)
0.241	0.798(75)	0.552(213)	0.251(26)	0.121(70)	-0.050(42)	0.419(71)	1.592(908)	0.139(25)	0.482(336)	0.548(78)	-0.628(481)	1.237(149)	0.172(27)	-0.100(181)	0.224(51)	0.043(126)
0.268	0.492(127)	0.137(429)	0.172(52)	-0.151(149)	-0.119(126)	0.349(134)	—	0.044(44)	—	0.235(82)	0.317(148)	0.773(369)	0.140(58)	-0.018(57)	-0.057(143)	0.358(281)
√0.272	0.841(20)	0.653(51)	0.267(7)	0.130(19)	-0.039(10)	0.486(19)	2.978(217)	0.162(7)	0.314(89)	0.501(21)	-0.244(98)	1.386(38)	0.181(8)	-0.005(47)	0.296(18)	0.028(31)
√0.293	0.792(19)	0.621(55)	0.256(7)	0.126(19)	-0.018(10)	0.494(20)	3.235(236)	0.169(8)	0.324(108)	0.487(22)	-0.296(107)	1.278(37)	0.191(8)	-0.085(44)	0.289(15)	0.005(28)
0.339	0.471(126)	0.261(355)	0.120(40)	0.021(108)	-0.024(66)	0.372(127)	1.798(1.354)	0.062(41)	0.160(510)	0.463(242)	-0.991(1.058)	0.607(271)	0.124(78)	-0.229(382)	0.119(101)	0.126(194)
√0.354	0.671(23)	0.434(54)	0.226(9)	0.068(21)	-0.020(12)	0.401(24)	1.853(257)	0.138(9)	0.050(182)	0.474(34)	-0.355(152)	1.075(43)	0.165(14)	-0.041(67)	0.242(21)	-0.008(32)
√0.358	0.697(59)	0.527(128)	0.252(22)	0.062(43)	0.007(26)	0.482(63)	2.170(656)	0.145(22)	-0.189(317)	0.465(80)	-0.218(363)	1.205(123)	0.179(31)	-0.079(145)	0.257(40)	-0.077(77)
0.393																
√0.395	0.645(20)	0.492(42)	0.229(8)	0.112(18)	-0.027(9)	0.394(18)	—	0.143(7)	—	0.267(12)	0.395(15)	0.953(37)	0.128(7)	0.10(7)	0.233(18)	-0.003(22)
√0.433	0.569(28)	0.361(49)	0.205(10)	0.071(17)	-0.016(8)	0.362(25)	1.557(176)	0.133(10)	0.178(81)	0.414(32)	-0.256(99)	0.906(44)	0.167(14)	-0.074(46)	0.222(19)	0.002(22)
0.438																
√0.472	0.551(28)	0.363(61)	0.207(11)	0.062(23)	-0.021(11)	0.385(31)	1.578(230)	0.143(12)	0.209(116)	0.358(33)	-0.125(110)	0.812(52)	0.149(14)	-0.016(52)	0.182(20)	-0.031(32)
√0.491	0.519(18)	0.394(33)	0.196(8)	0.100(14)	-0.023(6)	0.349(16)	1.622(141)	0.130(7)	0.192(84)	0.343(26)	-0.083(77)	0.781(30)	0.151(12)	-0.029(38)	0.205(14)	0.01(15)
A_0	1.764(2)	1.443(92)	0.396(5)	0.249(32)	-0.111(67)	0.807(17)	13.647(2.067)	0.231(7)	0.933(981)	0.765(14)	-1.136(459)	2.905(50)	0.247(6)	-0.055(59)	0.475(20)	0.025(56)
m_A	0.803(51)	1.373(365)	1.554(616)	0.849(666)	0.312(144)	1.644(878)	0.607(192)	1.521(1.193)	0.461(981)	1.933(75)	0.756(177)	1.395(149)	1.240(1.124)	2.152(4.526)	1.776(74)	0.3
p	2.146(250)	5.962(2.695)	3.799(2.838)	2.163(2.674)	1.	5.107(5.106)	2.645(1.011)	3.006(4.422)	1.455(3.063)	5.998(75)	3.5	5.861(1.119)	1.752(2.974)	3.5	6.00000(9)	1
$\overline{\chi^2}$	0.231(205)	0.602(490)	0.377(302)	1.076(772)	0.876(577)	0.505(414)	1.121(823)	0.531(439)	0.610(617)	0.313(382)	0.350(416)	0.415(428)	0.257(218)	0.317(262)	0.236(240)	0.583(459)

Q^2	$A_{10}^{(d)}$	$B_{10}^{(d)}$	$A_{20}^{(d)}$	$B_{20}^{(d)}$	$C_{20}^{(d)}$	$\tilde{A}_{10}^{(d)}$	$\tilde{B}_{10}^{(d)}$	$\tilde{A}_{20}^{(d)}$	$\tilde{B}_{20}^{(d)}$	$A_{T10}^{(d)}$	$\tilde{A}_{T10}^{(d)}$	$\tilde{B}_{T10}^{(d)}$	$A_{T20}^{(d)}$	$\tilde{A}_{T20}^{(d)}$	$\tilde{B}_{T20}^{(d)}$	$\tilde{B}_{T21}^{(d)}$
√0.000	0.8941(9)	—	0.170(3)	—	—	-0.248(10)	—	-0.049(4)	—	-0.194(7)	—	—	-0.048(3)	—	—	—
0.077	0.617(32)	-0.719(245)	0.131(11)	-0.185(73)	-0.012(101)	-0.177(43)	—	-0.038(13)	—	-0.123(25)	0.529(73)	1.325(182)	-0.047(13)	0.081(29)	0.203(72)	-0.267(241)
√0.096	0.631(4)	-1.072(33)	0.141(2)	-0.181(11)	-0.053(8)	-0.206(8)	-1.932(206)	-0.046(3)	-0.113(89)	-0.162(7)	0.932(88)	1.380(22)	-0.043(3)	0.118(37)	0.245(10)	-0.027(21)
√0.096	0.634(9)	-1.048(72)	0.144(4)	-0.177(23)	-0.081(23)	-0.198(17)	-1.321(462)	-0.045(6)	-0.219(171)	-0.166(12)	1.114(168)	1.363(41)	-0.041(4)	0.107(56)	0.248(16)	-0.101(72)
0.160	0.474(34)	-0.792(161)	0.116(10)	-0.158(43)	-0.052(31)	-0.160(41)	-0.735(763)	-0.026(13)	-0.014(242)	-0.139(37)	0.970(362)	1.051(105)	-0.038(13)	0.042(108)	0.217(38)	-0.222(86)
√0.186	0.471(7)	-0.844(31)	0.119(2)	-0.161(11)	-0.047(5)	-0.189(9)	-1.477(117)	-0.042(4)	-0.128(49)	-0.135(8)	0.679(56)	1.072(23)	-0.037(3)	0.055(25)	0.211(10)	-0.046(13)
√0.187	0.488(15)	-0.922(72)	0.124(5)	-0.147(22)	-0.030(14)	-0.228(22)	-2.116(358)	-0.033(7)	0.057(127)	-0.121(15)	0.390(132)	1.118(46)	-0.036(6)	0.079(48)	0.210(16)	-0.054(49)
√0.197	0.464(9)	-0.807(35)	0.119(3)	-0.145(12)	-0.033(6)	-0.168(10)	-1.408(154)	-0.041(3)	-0.199(76)	-0.128(10)	0.619(71)	1.019(26)	-0.035(4)	0.044(31)	0.198(10)	-0.027(17)
0.241	0.328(39)	-0.825(165)	0.089(12)	-0.154(45)	-0.035(23)	-0.172(48)	-1.315(603)	-0.024(15)	-0.030(205)	-0.027(40)	0.003(399)	0.827(105)	-0.033(14)	0.041(102)	0.172(36)	-0.146(76)
0.268	0.182(65)	-0.509(301)	0.063(28)	-0.147(88)	-0.066(70)	0.004(90)	—	-0.007(29)	—	-0.012(42)	0.169(92)	0.423(231)	-0.062(33)	0.016(34)	0.044(85)	-0.249(182)
√0.272	0.365(11)	-0.711(35)	0.102(3)	-0.138(12)	-0.034(6)	-0.178(11)	-1.212(119)	-0.041(4)	-0.122(55)	-0.113(11)	0.507(60)	0.892(28)	-0.037(5)	0.072(29)	0.188(11)	-0.040(16)
√0.293	0.351(10)	-0.654(34)	0.101(3)	-0.133(11)	-0.026(6)	-0.157(11)	-1.083(132)	-0.038(4)	-0.208(65)	-0.10(12)	0.422(61)	0.819(25)	-0.023(5)	-0.014(27)	0.179(10)	-0.034(18)
0.339	0.110(55)	-0.368(235)	0.029(22)	-0.083(72)	-0.009(43)	0.039(84)	0.726(873)	0.030(29)	0.142(306)	-0.016(127)	0.205(602)	0.172(168)	0.013(42)	-0.217(217)	0.096(63)	-0.159(110)
√0.354	0.288(12)	-0.532(41)	0.090(4)	-0.120(13)	-0.036(7)	-0.126(13)	-0.613(133)	-0.037(4)	-0.152(65)	-0.088(15)	0.378(70)	0.689(29)	-0.024(6)	0.017(33)	0.170(13)	-0.050(18)
√0.358	0.319(28)	-0.571(84)	0.10(10)	-0.131(28)	-0.024(16)	-0.151(31)	-0.602(321)	-0.036(10)	-0.159(133)	-0.115(29)	0.446(140)	0.741(69)	-0.038(12)	0.094(58)	0.154(24)	-0.060(42)
0.393																
√0.395	0.275(11)	-0.508(32)	0.088(4)	-0.120(12)	-0.024(6)	-0.129(11)	—	-0.036(4)	—	-0.069(7)	0.254(10)	0.643(26)	-0.031(4)	0.058(5)	0.149(12)	-0.033(14)
√0.433	0.229(14)	-0.478(39)	0.080(5)	-0.108(13)	-0.028(5)	-0.136(14)	-0.618(98)	-0.034(5)	-0.099(48)	-0.095(16)	0.371(55)	0.587(32)	-0.025(6)	0.030(23)	0.153(13)	-0.045(13)
0.438																
√0.472	0.233(14)	-0.436(43)	0.077(5)	-0.087(14)	-0.019(7)	-0.118(18)	-0.577(139)	-0.028(7)	-0.117(69)	-0.065(16)	0.215(58)	0.503(30)	-0.022(7)	0.026(27)	0.130(12)	-0.018(20)
√0.491	0.214(10)	-0.427(27)	0.073(4)	-0.106(9)	-0.019(4)	-0.120(10)	-0.594(82)	-0.024(4)	-0.114(58)	-0.078(16)	0.279(47)	0.518(22)	-0.025(7)	0.036(24)	0.128(9)	-0.024(9)
A_0	0.8941(9)	-1.388(62)	0.170(3)	-0.211(20)	-0.083(42)	-0.244(10)	-2.844(272)	-0.049(4)	-0.154(66)	-0.196(13)	1.379(152)	1.797(36)	-0.049(4)	0.195(142)	0.287(12)	-0.049(18)
m_A	0.824(59)	1.259(631)	1.208(327)	1.214(1.879)	0.557(841)	1.782(1.425)	1.256(64)	1.732(4.181)	3.286(933)	1.618(1.182)	0.894(68)	1.437(321)	1.807(1.618)	0.700(321)	1.871(209)	0.922(490)
p	2.624(353)	4.444(3.9)	2.856(1.429)	2.567(7.179)	1.462(2.463)	5.047(7.464)	6.	2.681(13.074)	5.631(9.277)	5.725(7.212)	3.5	5.915(2.377)	5.541(8.777)	3.5	5.971(1.158)	1
$\overline{\chi^2}$	0.514(407)	0.286(251)	0.284(372)	0.279(311)	0.808(617)	1.110(551)	1.205(894)	0.248(270)	0.581(528)	0.357(264)	0.899(519)	0.503(355)	0.590(335)	0.755(428)	0.261(324)	0.481(510)

Table A.7: MILC-20^3-m03-chopped — data set 3

Q^2	$A_{10}^{(u)}$	$B_{10}^{(u)}$	$A_{20}^{(u)}$	$B_{20}^{(u)}$	$C_{20}^{(u)}$	$\tilde{A}_{10}^{(u)}$	$\tilde{B}_{10}^{(u)}$	$\tilde{A}_{20}^{(u)}$	$\tilde{B}_{20}^{(u)}$	$A_{T10}^{(u)}$	$\tilde{A}_{T10}^{(u)}$	$\tilde{B}_{T10}^{(u)}$	$A_{T20}^{(u)}$	$\tilde{A}_{T20}^{(u)}$	$\tilde{B}_{T20}^{(u)}$	$\tilde{B}_{T21}^{(u)}$
✓0.000	1.787(2)		0.375(9)		---	0.809(29)	—	0.214(11)	..	0.742(23)			0.237(10)			
0.074	1.109(88)	0.302(657)	0.295(38)	0.203(189)	-0.081(251)	0.520(112)		0.184(37)		0.603(83)	0.702(205)	1.737(512)	0.187(39)	0.113(71)	0.276(177)	-0.064(608)
✓0.095	1.295(13)	0.915(85)	0.325(7)	0.132(30)	-0.083(22)	0.654(23)	6.310(592)	0.189(9)	0.279(242)	0.655(24)	-1.004(282)	2.056(55)	0.218(10)	-0.209(130)	0.382(25)	-0.024(63)
✓0.096	1.302(29)	1.117(215)	0.319(13)	0.187(59)	0.013(59)	0.648(49)	7.377(1.313)	0.186(17)	0.092(428)	0.648(39)	-0.739(513)	2.219(107)	0.237(17)	-0.473(197)	0.379(41)	0.036(192)
0.156	0.956(91)	0.623(414)	0.268(30)	0.110(104)	-0.009(70)	0.513(111)	4.327(1.868)	0.161(34)	0.140(566)	0.535(111)	0.320(1.037)	1.458(252)	0.230(42)	-0.513(370)	0.254(79)	-0.123(225)
✓0.184	1.003(20)	0.705(73)	0.288(8)	0.128(27)	-0.055(13)	0.575(25)	4.363(334)	0.177(9)	0.278(139)	0.539(24)	-0.202(146)	1.503(48)	0.202(11)	-0.031(65)	0.266(23)	0.103(40)
✓0.186	1.023(49)	0.930(189)	0.281(17)	0.192(54)	-0.067(35)	0.611(62)	4.795(922)	0.185(22)	0.487(323)	0.593(50)	-0.667(332)	1.538(101)	0.204(19)	-0.168(134)	0.263(41)	0.054(123)
✓0.197	0.962(27)	0.729(89)	0.284(11)	0.162(30)	-0.057(16)	0.549(29)	4.289(417)	0.163(10)	0.331(207)	0.507(29)	-0.213(184)	1.512(63)	0.183(13)	-0.012(85)	0.336(27)	0.035(43)
0.234	—	—	—	—	—	—		—								
0.255	0.386(185)	0.391(683)	0.120(83)	0.379(275)	0.107(205)	0.137(237)	—	0.068(77)	—	0.103(131)	0.184(247)	0.451(619)	0.078(104)	-0.054(95)	-0.141(242)	-0.170(502)
✓0.269	0.814(31)	0.492(79)	0.253(11)	0.079(30)	-0.041(15)	0.525(34)	3.008(345)	0.169(12)	0.130(146)	0.498(34)	-0.296(152)	1.149(52)	0.195(15)	-0.075(69)	0.213(26)	0.111(48)
✓0.293	0.784(32)	0.579(88)	0.245(11)	0.129(29)	-0.019(16)	0.533(36)	3.431(357)	0.163(12)	0.435(170)	0.428(34)	-0.135(145)	1.113(60)	0.170(15)	-0.066(66)	0.251(24)	-0.024(44)
0.323	—	—	—	—	—	—		—								
✓0.349	0.672(47)	0.534(114)	0.213(17)	0.087(41)	-0.013(20)	0.407(45)	1.614(460)	0.136(17)	-0.231(249)	0.549(87)	-0.728(332)	0.953(84)	0.217(38)	-0.282(146)	0.243(36)	-0.003(58)
✓0.353	0.724(112)	0.894(433)	0.248(37)	0.149(113)	-0.103(44)	0.688(192)	4.198(1.468)	0.228(71)	0.626(580)	0.405(80)	-0.081(451)	0.895(160)	0.186(37)	-0.079(236)	0.163(62)	0.160(165)
0.382		—		—		—		—								
✓0.395	0.610(30)	0.456(68)	0.204(12)	0.045(28)	-0.041(15)	0.399(30)	—	0.143(12)	—	0.218(19)	0.347(24)	0.835(59)	0.108(12)	0.093(11)	0.217(27)	-0.022(34)
✓0.425	0.564(42)	0.419(90)	0.186(15)	0.048(31)	-0.022(13)	0.386(43)	1.350(273)	0.131(16)	0.034(122)	0.354(49)	-0.101(137)	0.684(67)	0.159(23)	-0.096(67)	0.134(29)	-0.005(38)
0.432		—		—												
✓0.469	0.661(77)	0.391(131)	0.217(25)	0.117(45)	-0.032(20)	0.356(65)	1.224(375)	0.118(25)	-0.150(206)	0.424(73)	-0.277(194)	0.751(95)	0.191(35)	-0.164(94)	0.175(41)	-0.011(59)
✓0.490	0.531(29)	0.325(55)	0.192(11)	0.074(23)	-0.014(10)	0.346(27)	1.477(220)	0.122(12)	0.151(136)	0.328(46)	-0.081(117)	0.702(44)	0.111(24)	0.052(63)	0.180(21)	0.019(25)
A_0	1.787(2)	1.263(236)	0.375(8)	0.204(41)	-0.112(33)	0.794(29)	10.575(950)	0.212(10)	0.565(324)	0.749(23)	-2.420(3.188)	3.145(120)	0.241(9)	-0.726(3.204)	0.485(41)	0.089(98)
m_A	0.657(58)	0.992(1.371)	1.869(1.101)	1.546(226)	1.188(532)	1.635(1.869)	1.087(54)	2.302(534)	1.143(360)	1.836(538)	0.513(283)	0.650(35)	2.409(684)	0.503(939)	0.821(70)	0.325(232)
p	1.617(245)	3.191(7.248)	5.369(5.89)	6.	5.980(3.738)	4.840(10.214)	6.0000(4)	5.856(2.36)	6.	5.857(3.276)	3.5	2.001(123)	5.983(2.555)	3.5	2.	1
$\overline{\chi^2}$	0.347(314)	0.517(495)	0.398(269)	0.963(743)	0.926(452)	0.604(445)	1.120(724)	0.418(300)	0.972(722)	0.745(516)	0.810(562)	0.605(534)	0.899(658)	1.179(800)	1.368(871)	1.062(608)

Q^2	$A_{10}^{(d)}$	$B_{10}^{(d)}$	$A_{20}^{(d)}$	$B_{20}^{(d)}$	$C_{20}^{(d)}$	$\tilde{A}_{10}^{(d)}$	$\tilde{B}_{10}^{(d)}$	$\tilde{A}_{20}^{(d)}$	$\tilde{B}_{20}^{(d)}$	$A_{T10}^{(d)}$	$\tilde{A}_{T10}^{(d)}$	$\tilde{B}_{T10}^{(d)}$	$A_{T20}^{(d)}$	$\tilde{A}_{T20}^{(d)}$	$\tilde{B}_{T20}^{(d)}$	$\tilde{B}_{T21}^{(d)}$
✓0.000	0.906(1)		0.159(5)			-0.259(16)	—	-0.050(6)		-0.202(12)			-0.046(5)			
0.074	0.604(56)	-2.074(476)	0.114(19)	-0.261(122)	-0.097(157)	-0.247(70)		-0.026(21)		-0.075(44)	0.481(130)	1.204(326)	-0.066(26)	0.097(48)	0.243(121)	-0.704(402)
✓0.095	0.623(7)	-1.064(55)	0.134(4)	-0.165(17)	-0.077(13)	-0.215(12)	-2.356(323)	-0.043(5)	-0.075(126)	-0.178(12)	1.005(143)	1.308(36)	-0.047(6)	0.175(71)	0.228(16)	-0.115(39)
✓0.096	0.619(16)	-0.972(118)	0.133(6)	-0.123(34)	-0.054(33)	-0.202(29)	-1.422(733)	-0.047(9)	-0.177(262)	-0.182(21)	1.008(275)	1.255(67)	-0.039(7)	-0.001(109)	0.201(27)	-0.045(111)
0.156	0.430(52)	-1.277(274)	0.094(14)	-0.137(66)	-0.031(43)	-0.103(66)	0.033(1.106)	-0.014(21)	0.062(337)	-0.144(62)	1.095(565)	1.006(169)	-0.019(22)	-0.097(192)	0.152(55)	-0.117(146)
✓0.184	0.472(11)	-0.791(50)	0.114(4)	-0.143(17)	-0.033(8)	-0.180(14)	-1.601(190)	-0.040(5)	-0.177(81)	-0.130(13)	0.556(81)	0.986(32)	-0.035(6)	0.041(36)	0.173(15)	-0.074(25)
✓0.186	0.459(26)	-0.903(110)	0.116(8)	-0.129(33)	-0.056(24)	-0.214(32)	-1.894(482)	-0.038(11)	-0.038(204)	-0.126(26)	0.183(217)	0.921(67)	-0.032(9)	-0.107(80)	0.142(24)	0.040(85)
✓0.197	0.430(14)	-0.715(54)	0.110(4)	-0.109(17)	-0.044(10)	-0.185(15)	-1.452(229)	-0.037(5)	0.034(115)	-0.164(17)	0.734(109)	0.938(38)	-0.044(7)	0.167(49)	0.204(15)	-0.041(31)
0.234																
0.255	0.214(117)	-1.088(621)	0.039(50)	0.003(154)	0.037(131)	-0.126(147)		-0.040(49)		-0.109(84)	0.152(166)	0.391(418)	-0.088(68)	0.002(58)	0.013(146)	-0.322(327)
✓0.269	0.369(16)	-0.655(55)	0.096(5)	-0.127(18)	-0.022(9)	-0.149(18)	-1.141(182)	-0.041(7)	-0.337(94)	-0.101(18)	0.414(95)	0.750(34)	-0.026(9)	-0.004(44)	0.132(16)	-0.035(29)
✓0.293	0.338(17)	-0.539(57)	0.097(5)	-0.089(18)	-0.039(9)	-0.123(18)	-0.663(188)	-0.036(6)	-0.171(105)	-0.136(18)	0.479(92)	0.707(38)	-0.037(8)	0.069(42)	0.159(15)	-0.053(33)
0.323																
✓0.349	0.306(24)	-0.477(65)	0.087(8)	-0.10(24)	-0.033(12)	-0.121(22)	-0.685(198)	-0.026(9)	-0.114(117)	-0.102(33)	0.396(126)	0.578(54)	-0.012(15)	0.004(63)	0.129(23)	-0.083(35)
✓0.353	0.248(42)	-0.522(188)	0.100(16)	-0.043(53)	-0.047(25)	-0.194(86)	-0.855(672)	-0.031(25)	-0.001(234)	-0.086(39)	0.125(230)	0.657(109)	-0.012(14)	-0.103(112)	0.134(42)	-0.066(99)
0.382	—															
✓0.395	0.255(16)	-0.434(41)	0.082(6)	-0.112(18)	-0.051(9)	-0.123(15)	—	-0.033(6)	—	-0.059(11)	0.207(14)	0.527(35)	-0.031(7)	0.052(7)	0.134(18)	-0.050(22)
✓0.425	0.244(21)	-0.358(55)	0.070(7)	-0.095(20)	-0.022(9)	-0.095(22)	-0.495(147)	-0.023(8)	-0.074(76)	-0.066(25)	0.240(79)	0.482(45)	-0.025(12)	0.035(38)	0.097(19)	-0.059(26)
0.432																
✓0.469	0.229(33)	-0.393(78)	0.078(11)	-0.057(26)	-0.029(13)	-0.143(33)	-0.738(238)	-0.021(12)	-0.026(126)	-0.070(32)	0.153(102)	0.483(62)	-0.022(14)	0.033(48)	0.132(27)	-0.037(42)
✓0.490	0.213(15)	-0.341(36)	0.069(5)	-0.093(14)	-0.022(6)	-0.104(15)	-0.397(123)	-0.037(6)	0.028(91)	-0.079(26)	0.238(69)	0.445(28)	-0.044(13)	0.091(36)	0.123(14)	-0.029(15)
A_0	0.906(1)	-1.469(134)	0.160(5)	-0.182(24)	-0.106(53)	-0.261(16)	-3.855(589)	-0.050(6)	-0.205(119)	-0.209(12)	1.569(328)	1.870(98)	-0.048(5)	0.077(105)	0.264(25)	-0.144(118)
m_A	0.689(66)	1.004(634)	1.383(932)	1.016(154)	0.375(155)	1.677(288)	1.046(79)	1.085(231)	1.631(588)	1.659(178)	0.785(98)	0.763(208)	1.829(2.778)	1.641(3.315)	0.949(99)	0.406(280)
p	2.050(347)	3.719(3.812)	3.675(4.548)	2.	1.	5.909(1.849)	6.	1.5	6.	5.997(144)	3.5	2.392(973)	4.869(13.523)	3.5	2.	1
$\overline{\chi^2}$	0.323(298)	0.406(258)	0.243(263)	0.867(745)	1.291(753)	0.580(356)	0.714(433)	0.461(382)	1.187(660)	0.814(541)	0.928(585)	0.265(254)	0.871(657)	1.838(972)	1.284(807)	0.484(489)

Table A.8: MILC-20^3-m02-chopped — data set 4

Q^2	$A_{10}^{(u)}$	$B_{10}^{(u)}$	$A_{20}^{(u)}$	$B_{20}^{(u)}$	$C_{20}^{(u)}$	$\tilde{A}_{10}^{(u)}$	$\tilde{B}_{10}^{(u)}$	$\tilde{A}_{20}^{(u)}$	$\tilde{B}_{20}^{(u)}$	$A_{T10}^{(u)}$	$\tilde{A}_{T10}^{(u)}$	$\tilde{B}_{T10}^{(u)}$	$A_{T20}^{(u)}$	$\tilde{A}_{T20}^{(u)}$	$\tilde{B}_{T20}^{(u)}$	$\tilde{B}_{T21}^{(u)}$
✓0.000	1.810(4)	—	0.384(20)	—	—	0.815(51)	...	0.195(21)	—	0.780(43)	—	—	0.248(23)	—	—	—
0.070	1.590(1.518)	0.837(3.365)	0.471(491)	0.134(1.019)	-0.275(1.308)	0.587(772)	...	0.005(191)	...	1.118(1.242)	0.171(1.079)	0.390(2.703)	0.151(270)	0.214(492)	0.529(1.23)	-0.777(3.873)
✓0.094	1.287(26)	0.881(155)	0.310(14)	0.136(49)	-0.116(41)	0.687(41)	9.309(1.05)	0.178(15)	-0.048(432)	0.607(42)	-0.212(503)	1.783(102)	0.217(22)	-0.147(254)	0.257(48)	0.204(139)
✓0.095	1.195(54)	0.409(376)	0.279(24)	0.181(101)	-0.108(101)	0.843(116)	11.554(2.685)	0.177(35)	0.442(842)	0.645(74)	-0.063(959)	1.871(654)	0.212(33)	-0.440(396)	0.304(90)	-0.318(467)
0.150	0.625(213)	0.159(1.097)	0.111(71)	0.070(300)	0.080(228)	0.514(319)	8.780(4.821)	0.061(96)	-1.014(1.458)	0.313(283)	0.360(2.489)	1.134(657)	0.122(116)	0.856(1.298)	-0.055(278)	0.718(883)
✓0.182	0.966(35)	0.690(125)	0.263(13)	0.119(44)	-0.047(23)	0.517(38)	4.141(506)	0.160(16)	0.281(227)	0.546(44)	-0.531(265)	1.354(91)	0.184(21)	0.001(132)	0.227(43)	0.079(88)
✓0.184	0.884(90)	0.028(356)	0.269(34)	0.255(100)	-0.036(73)	0.775(129)	5.111(1.571)	0.171(46)	0.434(600)	0.536(97)	-0.475(607)	1.441(254)	0.189(41)	-0.285(277)	0.385(104)	-0.364(293)
✓0.197	0.913(51)	0.615(146)	0.258(19)	0.069(46)	-0.050(33)	0.547(52)	4.362(694)	0.161(20)	0.314(330)	0.505(60)	0.050(335)	1.258(112)	0.189(28)	0.028(147)	0.266(45)	0.038(105)
0.225	0.400(235)	-0.027(920)	0.143(88)	0.313(315)	-0.170(202)	0.097(347)	-2.004(3.474)	0.030(122)	0.139(1.307)	0.135(384)	0.929(2.526)	0.718(760)	0.150(139)	0.201(745)	0.075(260)	0.294(667)
0.236	0.114(370)	0.966(1.942)	-0.009(195)	-0.113(559)	-0.145(458)	0.120(650)	—	-0.025(185)	—	0.109(336)	0.531(690)	1.314(1.724)	0.770(664)	-0.406(416)	-1.102(1.098)	4.254(3.521)
✓0.263	0.709(56)	0.603(145)	0.213(21)	0.149(55)	-0.057(29)	0.364(54)	2.338(521)	0.149(23)	0.311(245)	0.563(68)	-0.750(262)	0.885(117)	0.169(32)	-0.004(154)	0.146(57)	0.124(103)
✓0.292	0.710(60)	0.568(155)	0.237(22)	0.163(53)	0.037(34)	0.398(67)	1.674(611)	0.145(26)	-0.063(337)	0.540(76)	-0.305(281)	1.031(125)	0.196(32)	-0.142(130)	0.231(53)	-0.181(111)
0.301	—	—	—	—	—	—	—	—	—	—	—	—	—	—	—	—
✓0.340	0.610(78)	0.204(179)	0.191(30)	0.101(77)	-0.030(36)	0.389(89)	1.972(662)	0.085(32)	-0.132(317)	0.440(122)	-0.475(424)	0.581(145)	0.161(58)	-0.109(214)	0.160(77)	0.014(129)
✓0.347	0.499(171)	0.200(505)	0.212(63)	0.019(148)	-0.009(80)	0.260(250)	1.506(1.624)	0.156(99)	0.119(777)	0.670(248)	-0.643(960)	0.727(313)	0.295(108)	-0.419(412)	0.094(124)	-0.328(387)
0.367	—	—	—	—	—	—	—	—	—	—	—	—	—	—	—	—
✓0.395	0.555(58)	0.194(112)	0.224(27)	0.069(48)	-0.046(27)	0.331(55)	—	0.108(24)	—	0.171(40)	0.270(40)	0.643(99)	0.076(28)	0.083(22)	0.194(56)	-0.087(77)
0.413	—	—	—	—	—	—	—	—	—	—	—	—	—	—	—	—
0.422	—	—	—	—	—	—	—	—	—	—	—	—	—	—	—	—
✓0.465	0.523(86)	0.209(172)	0.188(32)	-0.001(60)	-0.054(32)	0.473(103)	2.148(613)	0.163(40)	0.611(305)	0.691(164)	-0.684(376)	0.455(130)	0.214(67)	-0.118(175)	0.049(61)	0.124(117)
✓0.490	0.451(51)	0.342(90)	0.172(21)	0.011(34)	-0.034(17)	0.301(46)	0.774(339)	0.107(19)	-0.171(240)	0.398(97)	-0.261(215)	0.546(80)	0.199(54)	-0.089(120)	0.160(43)	0.024(48)
A_0	1.810(4)	1.153(321)	0.372(18)	0.229(71)	-0.199(196)	0.842(50)	40.859(9.36)	0.200(19)	0.363(450)	0.745(44)	-0.446(163)	2.642(284)	0.235(24)	-0.091(86)	0.345(66)	0.101(164)
m_A	0.693(119)	1.219(2.152)	0.847(64)	1.265(248)	0.3	1.047(685)	0.3	2.142(392)	1.418(1.283)	0.958(141)	3.300(209)	1.086(910)	1.260(436)	3.300(289)	1.703(306)	0.3
p	1.994(586)	5.276(15.603)	1.5	6.	1.114(807)	2.879(3.344)	2.026(220)	5.948(1.406)	6.	1.5	3.5	4.862(6.946)	1.5	3.5	6.	1
$\overline{\chi^2}$	0.452(436)	1.045(670)	0.501(344)	0.950(632)	0.843(599)	1.297(731)	0.774(623)	0.435(369)	0.807(545)	0.818(525)	0.595(534)	0.567(501)	0.453(444)	0.402(423)	0.891(647)	1.186(691)

Q^2	$A_{10}^{(d)}$	$B_{10}^{(d)}$	$A_{20}^{(d)}$	$B_{20}^{(d)}$	$C_{20}^{(d)}$	$\tilde{A}_{10}^{(d)}$	$\tilde{B}_{10}^{(d)}$	$\tilde{A}_{20}^{(d)}$	$\tilde{B}_{20}^{(d)}$	$A_{T10}^{(d)}$	$\tilde{A}_{T10}^{(d)}$	$\tilde{B}_{T10}^{(d)}$	$A_{T20}^{(d)}$	$\tilde{A}_{T20}^{(d)}$	$\tilde{B}_{T20}^{(d)}$	$\tilde{B}_{T21}^{(d)}$
✓0.000	0.917(2)	—	0.164(9)	—	—	-0.332(36)	—	-0.065(12)	—	-0.190(24)	—	—	-0.035(11)	—	—	—
0.070	0.635(549)	-3.822(4.274)	0.215(239)	-1.122(1.368)	-0.516(1.032)	-0.576(696)	—	-0.325(363)	—	0.078(252)	0.847(969)	2.115(2.421)	-0.001(163)	0.304(407)	0.760(1.019)	-0.141(2.443)
✓0.094	0.619(16)	-0.951(97)	0.132(7)	-0.153(32)	-0.083(24)	-0.240(26)	-2.601(609)	-0.052(10)	-0.019(250)	-0.179(25)	0.842(270)	1.188(65)	-0.025(12)	0.034(148)	0.202(33)	-0.028(80)
✓0.095	0.596(35)	-1.047(248)	0.132(14)	-0.123(62)	-0.018(70)	-0.243(68)	-3.026(1.471)	-0.079(24)	-0.214(556)	-0.146(42)	0.857(550)	1.187(142)	-0.039(20)	0.230(224)	0.168(57)	0.024(266)
0.150	0.300(130)	-0.681(788)	0.052(39)	-0.059(180)	-0.004(142)	-0.338(218)	-2.422(3.117)	-0.173(80)	-1.092(1.014)	-0.380(203)	2.536(1.604)	0.775(436)	-0.016(69)	-0.060(612)	0.088(170)	0.064(532)
✓0.182	0.424(20)	-0.705(79)	0.107(8)	-0.102(30)	-0.052(15)	-0.225(27)	-1.920(337)	-0.045(11)	-0.148(146)	-0.158(29)	0.623(157)	0.876(62)	-0.020(14)	0.048(81)	0.178(30)	-0.015(56)
✓0.184	0.428(54)	-1.043(255)	0.133(18)	-0.124(68)	-0.084(48)	-0.221(85)	-2.422(1.063)	-0.059(31)	-0.230(409)	-0.138(57)	0.108(409)	0.964(153)	-0.017(23)	-0.101(192)	0.190(65)	-0.188(205)
✓0.197	0.444(29)	-0.582(104)	0.115(11)	-0.112(32)	-0.047(22)	-0.201(33)	-1.815(416)	-0.062(12)	-0.215(225)	-0.149(37)	0.610(225)	0.912(81)	-0.028(18)	0.057(101)	0.185(32)	0.004(67)
0.225	0.251(145)	-0.599(742)	0.081(53)	-0.049(169)	-0.161(133)	-0.247(250)	-3.479(2.786)	-0.084(84)	-0.249(776)	-0.009(196)	-0.269(1.127)	0.602(444)	-0.020(85)	0.013(551)	0.038(168)	0.206(444)
0.236	0.044(242)	-0.824(1.326)	0.105(157)	-0.192(375)	-0.328(400)	0.187(415)	—	-0.103(160)	—	0.269(312)	-0.126(427)	-0.346(1.079)	0.061(229)	0.146(196)	0.358(495)	-0.700(1.206)
✓0.263	0.320(29)	-0.494(94)	0.087(12)	-0.067(34)	-0.020(18)	-0.209(34)	-1.274(338)	-0.058(15)	-0.139(159)	-0.040(43)	-0.045(178)	0.644(72)	-0.016(21)	0.027(99)	0.093(36)	0.032(64)
✓0.292	0.378(37)	-0.454(101)	0.106(13)	-0.067(34)	-0.040(19)	-0.247(45)	-2.026(418)	-0.082(16)	-0.585(211)	-0.078(45)	0.152(182)	0.783(86)	-0.036(22)	0.009(91)	0.169(37)	-0.040(75)
0.301	—	—	—	—	—	—	—	—	—	—	—	—	—	—	—	—
✓0.340	0.252(38)	-0.287(117)	0.069(17)	-0.122(47)	-0.045(23)	-0.168(54)	-1.101(395)	-0.038(22)	0.002(189)	-0.004(64)	-0.010(223)	0.515(96)	0.012(30)	0.027(126)	0.158(54)	0.078(76)
✓0.347	0.186(90)	-0.442(373)	0.063(30)	-0.132(97)	-0.024(51)	-0.124(184)	-0.403(1.236)	-0.035(58)	0.270(447)	-0.031(88)	0.307(374)	0.562(234)	-0.024(41)	-0.077(190)	0.139(93)	-0.247(238)
0.367	—	—	—	—	—	—	—	—	—	—	—	—	—	—	—	—
✓0.395	0.223(31)	-0.353(76)	0.090(14)	-0.104(34)	-0.039(18)	-0.117(32)	—	-0.049(14)	—	-0.074(26)	0.164(26)	0.424(66)	-0.01(18)	0.040(14)	0.102(37)	-0.039(48)
0.413	—	—	—	—	—	—	—	—	—	—	—	—	—	—	—	—
0.422	—	—	—	—	—	—	—	—	—	—	—	—	—	—	—	—
✓0.465	0.235(49)	-0.210(117)	0.044(15)	-0.051(37)	0.003(23)	-0.094(64)	-0.405(384)	-0.043(24)	0.176(221)	0.003(66)	0.255(176)	0.403(91)	-0.073(36)	0.153(95)	0.104(45)	0.042(74)
✓0.490	0.163(29)	-0.249(60)	0.070(12)	-0.077(26)	-0.016(12)	-0.123(30)	-0.796(215)	-0.047(13)	-0.246(170)	-0.050(56)	0.089(129)	0.377(55)	0.048(35)	-0.113(79)	0.077(28)	-0.006(33)
A_0	0.917(2)	-1.483(316)	0.163(9)	-0.166(52)	-0.115(68)	-0.317(34)	-3.853(927)	-0.061(12)	-0.190(198)	-0.207(22)	2.511(1.446)	1.645(106)	-0.035(11)	0.410(1.991)	0.254(45)	-0.029(113)
m_A	0.771(180)	0.961(1.155)	1.361(1.956)	0.928(317)	1.111(1.993)	1.676(341)	1.237(160)	3.054(6.356)	2.574(4.165)	1.417(240)	0.535(138)	1.312(67)	1.540(1.471)	0.429(660)	1.624(252)	0.305(3.03)
p	2.734(1.122)	4.310(8.411)	4.019(10.74)	2.	5.776(14.901)	5.922(1.922)	6.	4.452(16.782)	5.990(3.27)	6.0000(1)	3.5	6.000(7)	5.788(8.559)	3.5	6.	1
$\overline{\chi^2}$	0.790(556)	0.416(419)	0.881(590)	0.418(400)	0.509(463)	0.499(355)	0.597(521)	0.643(453)	1.076(853)	0.918(507)	0.838(532)	0.560(495)	0.880(583)	0.665(510)	0.510(423)	0.456(375)

Table A.9: MILC-20^3-m01-chopped — data set 5

Q^2	$A_{10}^{(u)}$	$B_{10}^{(u)}$	$A_{20}^{(u)}$	$B_{20}^{(u)}$	$C_{20}^{(u)}$	$\tilde{A}_{10}^{(u)}$	$\tilde{B}_{10}^{(u)}$	$\tilde{A}_{20}^{(u)}$	$\tilde{B}_{20}^{(u)}$	$A_{T10}^{(u)}$	$\tilde{A}_{T10}^{(u)}$	$\bar{B}_{T10}^{(u)}$	$A_{T20}^{(u)}$	$\tilde{A}_{T20}^{(u)}$	$\bar{B}_{T20}^{(u)}$	$\bar{B}_{T21}^{(u)}$
✓0.000	1.808(4)	—	0.371(17)	—	—	0.765(52)	—	0.207(20)	—	0.700(46)	—	—	0.243(24)	—	—	—
0.042	1.782(100)	2.821(981)	0.364(42)	-0.134(288)	-0.412(409)	0.909(145)	—	0.238(47)	—	0.621(94)	1.345(305)	3.350(763)	0.197(56)	0.080(140)	0.195(350)	-0.139(1.267)
✓0.049	1.500(18)	1.033(191)	0.348(16)	0.118(62)	-0.214(52)	0.721(42)	12.124(1.245)	0.199(16)	0.706(508)	0.644(44)	-0.300(575)	2.262(117)	0.236(22)	-0.155(284)	0.392(52)	0.237(198)
✓0.049	1.479(25)	0.642(294)	0.325(19)	0.137(95)	-0.048(109)	0.813(68)	13.369(2.165)	0.203(22)	0.945(755)	0.654(59)	-0.398(889)	1.940(163)	0.234(26)	-0.433(402)	0.418(81)	0.160(509)
0.086	1.361(80)	1.431(525)	0.306(32)	0.088(160)	-0.241(117)	0.901(119)	10.718(2.969)	0.229(41)	1.018(891)	0.680(118)	-0.232(1.496)	2.393(328)	0.186(46)	0.470(551)	0.330(146)	0.327(367)
✓0.096	1.295(27)	0.866(160)	0.309(16)	0.106(49)	-0.071(29)	0.708(45)	8.772(808)	0.196(16)	0.899(271)	0.612(41)	-0.438(349)	1.929(98)	0.206(20)	0.047(168)	0.353(46)	0.091(96)
✓0.097	1.227(38)	0.526(267)	0.286(19)	-0.006(86)	-0.167(65)	0.692(74)	7.933(1.576)	0.210(22)	1.611(482)	0.600(58)	-0.761(583)	1.771(144)	0.221(24)	-0.315(278)	0.348(70)	-0.062(289)
✓0.101	1.199(42)	0.625(201)	0.304(18)	0.089(63)	-0.029(44)	0.675(54)	8.550(1.124)	0.180(19)	0.877(442)	0.523(56)	0.374(502)	1.667(129)	0.205(28)	0.103(209)	0.341(59)	0.081(140)
0.128	1.172(90)	1.358(433)	0.262(32)	0.006(143)	-0.208(104)	0.766(114)	6.957(1.985)	0.231(42)	0.699(706)	0.583(110)	-0.151(923)	1.824(284)	0.195(51)	0.291(468)	0.320(117)	0.565(317)
0.142	1.128(36)	0.676(147)	0.278(15)	0.076(50)	-0.061(32)	0.648(47)	6.375(712)	0.192(17)	0.864(252)	0.594(45)	-0.572(292)	1.650(95)	0.191(23)	0.068(175)	0.263(45)	0.140(98)
0.149	—	—	—	—	—	—	—	—	—	—	—	—	—	—	—	—
✓0.150	1.015(42)	0.459(172)	0.269(18)	0.071(53)	-0.031(36)	0.600(54)	5.599(818)	0.179(20)	1.403(360)	0.505(54)	-0.125(363)	1.511(109)	0.177(25)	0.109(167)	0.278(54)	-0.015(118)
0.185	0.999(43)	0.543(160)	0.274(19)	0.026(56)	-0.059(35)	0.571(58)	4.436(758)	0.182(21)	0.864(351)	0.486(66)	0.167(411)	1.475(108)	0.194(32)	0.167(219)	0.293(53)	0.221(129)
✓0.186	0.924(57)	0.653(252)	0.239(20)	0.056(81)	-0.052(46)	0.528(90)	3.911(1.11)	0.160(31)	0.555(457)	0.441(74)	0.683(522)	1.223(152)	0.161(33)	0.211(248)	0.272(75)	0.088(198)
0.187	—	—	—	—	—	—	—	—	—	—	—	—	—	—	—	—
0.201	0.929(56)	0.577(155)	0.287(26)	0.048(60)	-0.065(44)	0.583(59)	—	0.164(25)	—	0.376(42)	0.540(64)	1.314(160)	0.151(27)	0.111(29)	0.263(72)	-0.004(138)
0.210	—	—	—	—	—	—	—	—	—	—	—	—	—	—	—	—
✓0.227	0.860(43)	0.523(127)	0.252(19)	0.060(45)	-0.070(21)	0.558(56)	3.703(535)	0.173(20)	0.692(209)	0.489(51)	-0.055(240)	1.281(94)	0.167(26)	0.089(128)	0.268(47)	0.067(74)
✓0.229	0.777(62)	0.358(220)	0.204(22)	-0.037(73)	-0.092(36)	0.448(90)	3.031(843)	0.152(30)	0.566(289)	0.414(73)	0.070(333)	0.942(143)	0.167(31)	-0.085(163)	0.235(68)	0.006(165)
✓0.243	0.806(49)	0.381(170)	0.223(19)	0.018(50)	-0.073(32)	0.512(68)	3.297(656)	0.133(25)	0.535(333)	0.391(66)	0.309(310)	1.001(101)	0.168(33)	0.074(176)	0.267(55)	-0.073(119)
✓0.251	0.814(51)	0.452(121)	0.262(22)	0.050(44)	-0.052(25)	0.564(53)	4.135(575)	0.165(22)	0.636(320)	0.336(69)	0.546(285)	1.082(105)	0.118(43)	0.181(167)	0.227(47)	-0.016(84)
A_0	1.808(4)	1.131(275)	0.374(17)	0.187(143)	-0.198(66)	0.798(50)	21.962(6.945)	0.214(19)	1.297(419)	0.720(47)	0(-13\n6. 10)	2.624(152)	0.253(24)	0.001(144)	0.459(70)	0.128(176)
m_A	0.707(148)	0.630(120)	0.798(53)	0.535(1.869)	0.302(80)	1.878(211)	0.367(237)	2.189(414)	1.429(386)	1.593(159)	0.3	1.235(57)	1.697(268)	0.344(5.944)	0.807(130)	0.3
p	2.056(756)	2.	1.5	2.715(15.446)	1.	5.998(53)	1.781(1.178)	6.000(4)	6.	5.997(70)	3.5	6.00000(3)	5.991(512)	3.5	2.	1
$\overline{\chi^2}$	0.705(551)	0.537(482)	0.890(704)	0.365(470)	1.324(708)	0.521(311)	0.477(486)	0.349(283)	0.690(582)	0.519(443)	1.217(768)	1.253(848)	0.211(226)	0.705(604)	0.096(154)	0.296(327)

Q^2	$A_{10}^{(d)}$	$B_{10}^{(d)}$	$A_{20}^{(d)}$	$B_{20}^{(d)}$	$C_{20}^{(d)}$	$\tilde{A}_{10}^{(d)}$	$\tilde{B}_{10}^{(d)}$	$\tilde{A}_{20}^{(d)}$	$\tilde{B}_{20}^{(d)}$	$A_{T10}^{(d)}$	$\tilde{A}_{T10}^{(d)}$	$\bar{B}_{T10}^{(d)}$	$A_{T20}^{(d)}$	$\tilde{A}_{T20}^{(d)}$	$\bar{B}_{T20}^{(d)}$	$\bar{B}_{T21}^{(d)}$
✓0.000	0.917(2)	—	0.155(10)	—	—	-0.315(36)	—	-0.056(14)	—	-0.178(26)	—	—	-0.033(11)	—	—	—
0.042	0.841(60)	0.084(639)	0.152(24)	-0.252(177)	-0.189(293)	-0.215(83)	—	-0.036(27)	—	-0.171(60)	0.906(180)	2.269(451)	-0.026(33)	0.055(98)	0.137(246)	-0.308(796)
✓0.049	0.729(10)	-1.233(115)	0.139(8)	-0.202(44)	-0.104(32)	-0.269(27)	-2.468(781)	-0.052(12)	0.087(324)	-0.201(24)	1.688(350)	1.464(86)	-0.049(12)	0.356(175)	0.215(38)	-0.113(105)
✓0.049	0.735(15)	-1.027(186)	0.132(10)	-0.089(62)	-0.043(73)	-0.193(37)	-1.334(1.173)	-0.050(17)	-0.532(472)	-0.181(32)	1.390(500)	1.428(106)	-0.029(12)	0.286(236)	0.149(53)	0.026(323)
0.086	0.677(56)	-0.613(354)	0.153(20)	-0.068(102)	-0.234(68)	-0.188(70)	-2.984(1.477)	-0.027(24)	-0.746(565)	-0.167(62)	1.392(768)	1.498(195)	-0.035(24)	0.395(308)	0.127(95)	0.247(235)
✓0.096	0.602(16)	-1.063(98)	0.121(8)	-0.180(37)	-0.058(17)	-0.250(26)	-2.274(424)	-0.049(11)	0.065(176)	-0.190(24)	1.218(192)	1.250(74)	-0.050(11)	0.252(96)	0.204(35)	0.023(58)
✓0.097	0.612(24)	-0.919(171)	0.119(10)	-0.096(55)	-0.042(45)	-0.230(44)	-2.905(927)	-0.041(17)	-0.093(332)	-0.154(34)	0.695(376)	1.250(97)	-0.028(13)	0.245(170)	0.158(45)	0.087(187)
✓0.101	0.595(21)	-1.073(136)	0.116(8)	-0.161(44)	-0.028(26)	-0.224(29)	-1.714(588)	-0.051(12)	0.039(292)	-0.216(30)	1.255(275)	1.099(91)	-0.037(13)	0.114(133)	0.189(39)	-0.031(93)
0.128	0.547(62)	-0.555(310)	0.133(20)	-0.059(96)	-0.181(67)	-0.117(76)	-0.753(1.222)	-0.015(25)	-0.328(448)	-0.107(64)	0.670(632)	1.047(177)	-0.008(27)	0.147(277)	0.153(81)	0.240(205)
0.142	0.498(21)	-0.961(94)	0.107(8)	-0.161(36)	-0.047(19)	-0.212(28)	-1.373(397)	-0.040(11)	0.185(184)	-0.168(28)	0.887(204)	1.069(72)	-0.048(14)	0.149(101)	0.186(36)	0.007(62)
0.149	—	—	—	—	—	—	—	—	—	—	—	—	—	—	—	—
✓0.150	0.499(22)	-1.020(120)	0.105(8)	-0.146(38)	-0.029(23)	-0.225(31)	-1.744(491)	-0.047(12)	0.361(249)	-0.183(31)	0.759(229)	1.081(81)	-0.048(13)	0.164(102)	0.170(34)	-0.010(80)
0.185	0.409(24)	-0.798(106)	0.099(10)	-0.146(41)	-0.048(21)	-0.210(33)	-1.502(413)	-0.051(14)	-0.001(222)	-0.142(37)	0.613(228)	0.923(79)	-0.059(19)	0.139(128)	0.174(32)	-0.110(84)
✓0.186	0.421(40)	-0.550(164)	0.095(12)	-0.030(53)	-0.041(31)	-0.142(55)	-0.871(688)	-0.046(22)	-0.306(301)	-0.165(42)	0.673(292)	0.819(105)	-0.055(17)	0.218(150)	0.094(49)	-0.073(122)
0.187	—	—	—	—	—	—	—	—	—	—	—	—	—	—	—	—
0.201	0.388(30)	-0.680(105)	0.092(10)	-0.166(45)	-0.043(28)	-0.172(32)	—	-0.050(13)	—	-0.060(23)	0.298(40)	0.751(101)	-0.034(16)	0.069(19)	0.177(47)	0.010(87)
0.210	—	—	—	—	—	—	—	—	—	—	—	—	—	—	—	—
✓0.227	0.349(26)	-0.730(99)	0.089(10)	-0.134(35)	-0.042(15)	-0.191(32)	-1.175(291)	-0.046(13)	-0.01(149)	-0.130(32)	0.514(146)	0.831(75)	-0.058(16)	0.132(81)	0.183(31)	-0.048(53)
✓0.229	0.372(46)	-0.511(158)	0.087(12)	-0.044(48)	-0.040(27)	-0.203(58)	-1.339(591)	-0.046(22)	-0.177(224)	-0.135(45)	0.458(249)	0.851(105)	-0.043(17)	0.183(115)	0.136(42)	0.009(96)
✓0.243	0.361(29)	-0.728(123)	0.082(9)	-0.10(36)	-0.021(20)	-0.195(38)	-1.244(402)	-0.049(17)	-0.034(226)	-0.177(38)	0.507(201)	0.682(76)	-0.052(18)	0.054(97)	0.150(34)	-0.084(81)
✓0.251	0.345(26)	-0.620(80)	0.077(9)	-0.137(34)	-0.010(16)	-0.167(27)	-0.366(295)	-0.044(12)	0.275(207)	-0.161(42)	0.687(179)	0.644(73)	-0.037(22)	0.072(95)	0.169(33)	-0.006(53)
A_0	0.917(2)	-1.423(142)	0.155(10)	-0.194(53)	-0.152(59)	-0.291(36)	-3.571(854)	-0.053(14)	-0.034(4.107)	-0.197(25)	2.193(422)	1.760(103)	-0.043(10)	0.433(205)	0.204(44)	-0.024(39)
m_A	0.767(155)	1.328(97)	1.431(590)	0.833(226)	0.3	0.795(154)	0.984(125)	1.416(1.167)	0.525(12.898)	2.543(1.)	0.691(93)	1.238(60)	3.3	0.698(243)	1.298(480)	3.3
p	2.775(1.033)	6.	5.646(4.079)	2.	1.404(545)	1.5	6.	1.5	5.641(21.007)	5.999(70)	3.5	6.	1.5	3.5	2.	1
$\overline{\chi^2}$	0.175(258)	0.866(795)	0.084(135)	1.286(1.039)	0.518(556)	0.655(401)	0.980(687)	0.044(88)	0.891(832)	0.538(404)	0.396(458)	0.684(383)	0.694(563)	0.215(316)	0.618(701)	0.331(336)

Table A.10: MILC-28³-m01-chopped — data set 6

Q^2	$A_{10}^{(u)}$	$B_{10}^{(u)}$	$A_{20}^{(u)}$	$B_{20}^{(u)}$	$C_{20}^{(u)}$	$\tilde{A}_{10}^{(u)}$	$\tilde{B}_{10}^{(u)}$	$\tilde{A}_{20}^{(u)}$	$\tilde{B}_{20}^{(u)}$	$A_{T10}^{(u)}$	$\tilde{A}_{T10}^{(u)}$	$\bar{B}_{T10}^{(u)}$	$A_{T20}^{(u)}$	$\tilde{A}_{T20}^{(u)}$	$\bar{B}_{T20}^{(u)}$	$\bar{B}_{T21}^{(u)}$
✓0.000	1.7678(6)	—	0.406(2)	—	—	0.788(4)	—	0.229(2)	—	0.765(4)	—	—	0.249(2)	—	—	—
0.077	1.387(17)	1.354(117)	0.358(6)	0.198(36)	-0.091(47)	0.703(19)	—	0.205(7)	—	0.621(15)	1.049(34)	2.607(84)	0.223(7)	0.182(14)	0.449(36)	0.211(106)
✓0.096	1.321(2)	1.102(17)	0.350(1)	0.172(6)	-0.063(4)	0.672(4)	7.251(104)	0.206(2)	0.465(47)	0.657(4)	-0.538(47)	2.197(9)	0.227(2)	-0.033(21)	0.407(5)	0.037(11)
✓0.096	1.313(4)	1.107(35)	0.344(2)	0.158(10)	-0.049(10)	0.669(7)	7.102(210)	0.202(3)	0.452(77)	0.651(6)	-0.532(83)	2.159(17)	0.220(3)	-0.058(30)	0.392(7)	-0.027(33)
0.160	1.110(18)	1.040(71)	0.321(6)	0.183(21)	-0.077(13)	0.615(18)	5.112(346)	0.188(6)	0.631(110)	0.599(20)	-0.284(173)	1.868(42)	0.201(7)	0.028(66)	0.354(17)	0.012(39)
✓0.186	1.041(3)	0.862(14)	0.307(1)	0.155(5)	-0.048(2)	0.582(4)	4.618(58)	0.188(2)	0.424(24)	0.571(4)	-0.359(24)	1.701(9)	0.205(2)	-0.016(11)	0.346(4)	0.016(7)
✓0.187	1.033(7)	0.842(32)	0.301(3)	0.146(10)	-0.029(6)	0.578(9)	4.518(153)	0.184(3)	0.424(54)	0.564(7)	-0.373(57)	1.651(16)	0.198(3)	-0.039(23)	0.334(7)	-0.023(22)
✓0.197	1.012(5)	0.836(16)	0.298(2)	0.146(5)	-0.027(3)	0.576(5)	4.580(77)	0.184(2)	0.362(36)	0.556(5)	-0.318(35)	1.623(11)	0.200(2)	-0.024(15)	0.333(4)	-0.014(8)
0.241	0.909(23)	0.788(66)	0.282(8)	0.160(20)	-0.051(12)	0.530(21)	3.440(271)	0.168(7)	0.483(89)	0.523(21)	-0.253(120)	1.441(43)	0.180(8)	-0.018(47)	0.317(16)	-0.008(35)
0.268	0.997(186)	0.924(264)	0.307(57)	0.107(75)	-0.032(66)	0.585(119)	⋯	0.163(39)	—	0.467(94)	0.795(147)	1.947(361)	0.207(46)	0.127(39)	0.299(96)	0.065(143)
✓0.272	0.849(5)	0.697(15)	0.272(2)	0.139(6)	-0.039(3)	0.514(5)	3.287(60)	0.173(2)	0.389(25)	0.496(5)	-0.216(26)	1.362(10)	0.184(2)	-0.002(12)	0.304(5)	0.014(7)
✓0.293	0.813(5)	0.660(14)	0.262(2)	0.126(5)	-0.022(3)	0.504(5)	3.201(60)	0.168(2)	0.368(32)	0.483(6)	-0.236(26)	1.268(10)	0.182(2)	-0.023(12)	0.282(4)	-0.013(8)
0.339	0.741(128)	0.746(207)	0.260(45)	0.135(63)	-0.053(32)	0.419(87)	2.622(693)	0.133(30)	0.559(223)	0.478(106)	-0.226(364)	1.130(194)	0.168(40)	0.009(152)	0.266(64)	-0.034(92)
✓0.354	0.723(7)	0.579(18)	0.246(2)	0.124(6)	-0.030(3)	0.454(7)	2.449(70)	0.158(3)	0.273(36)	0.445(8)	-0.129(37)	1.146(13)	0.172(4)	-0.007(19)	0.279(6)	0.001(10)
✓0.358	0.731(13)	0.579(36)	0.245(5)	0.111(12)	-0.024(6)	0.457(15)	2.345(148)	0.149(6)	0.210(65)	0.450(14)	-0.178(63)	1.107(24)	0.172(6)	-0.034(28)	0.272(10)	-0.006(19)
0.393	0.703(43)	0.730(86)	0.239(15)	0.126(26)	-0.026(14)	0.450(38)	2.130(288)	0.139(13)	0.276(113)	0.470(50)	-0.316(193)	1.042(70)	0.171(20)	-0.122(81)	0.253(24)	-0.068(38)
✓0.395	0.667(6)	0.502(12)	0.234(2)	0.109(5)	-0.023(3)	0.429(5)	—	0.153(2)	—	0.276(4)	0.422(4)	1.020(11)	0.137(2)	0.109(2)	0.255(5)	-0.005(6)
✓0.433	0.622(7)	0.480(14)	0.225(3)	0.111(5)	-0.027(2)	0.412(7)	1.907(48)	0.148(3)	0.271(22)	0.409(7)	-0.139(22)	0.956(12)	0.159(3)	-0.004(11)	0.241(5)	0(0.006)
✓0.438	0.613(14)	0.455(32)	0.217(5)	0.112(10)	-0.014(5)	0.400(15)	1.749(106)	0.140(5)	0.256(41)	0.401(12)	-0.193(40)	0.912(23)	0.153(5)	-0.026(18)	0.236(9)	-0.019(16)
✓0.472	0.576(8)	0.451(19)	0.211(3)	0.104(7)	-0.020(3)	0.391(8)	1.737(64)	0.139(3)	0.207(32)	0.374(8)	-0.104(27)	0.849(13)	0.153(4)	-0.010(14)	0.221(6)	-0.002(9)
✓0.491	0.557(5)	0.422(10)	0.206(2)	0.096(4)	-0.019(2)	0.380(5)	1.757(41)	0.140(2)	0.248(26)	0.361(7)	-0.073(22)	0.825(9)	0.149(4)	0.004(11)	0.216(4)	-0.004(4)
A_0	1.7678(6)	1.464(34)	0.406(2)	0.197(7)	-0.115(17)	0.787(5)	12.972(647)	0.228(2)	0.591(41)	0.765(4)	-0.968(110)	2.975(22)	0.250(2)	-0.084(75)	0.480(7)	0.01(65)
m_A	0.717(12)	1.025(179)	1.033(57)	2.019(68)	0.321(36)	1.271(142)	0.544(55)	1.516(394)	1.741(105)	1.408(233)	0.739(48)	0.834(40)	1.493(676)	0.637(304)	1.016(108)	0.3
p	1.718(51)	3.253(929)	1.772(176)	6.000(3)	1.	2.743(552)	2.090(231)	2.546(1.217)	6.	3.310(1.028)	3.5	2.386(174)	2.593(2.13)	3.5	2.009(348)	1
$\overline{\chi^2}$	0.480(297)	0.337(281)	1.137(604)	0.672(522)	5.174(1.547)	0.263(225)	1.981(1.002)	0.770(611)	0.988(797)	0.539(401)	0.773(522)	2.421(1.019)	0.945(517)	0.560(533)	1.663(778)	2.426(1.18)

Q^2	$A_{10}^{(d)}$	$B_{10}^{(d)}$	$A_{20}^{(d)}$	$B_{20}^{(d)}$	$C_{20}^{(d)}$	$\tilde{A}_{10}^{(d)}$	$\tilde{B}_{10}^{(d)}$	$\tilde{A}_{20}^{(d)}$	$\tilde{B}_{20}^{(d)}$	$A_{T10}^{(d)}$	$\tilde{A}_{T10}^{(d)}$	$\bar{B}_{T10}^{(d)}$	$A_{T20}^{(d)}$	$\tilde{A}_{T20}^{(d)}$	$\bar{B}_{T20}^{(d)}$	$\bar{B}_{T21}^{(d)}$
✓0.000	0.8958(3)	—	0.1760(8)	—	—	-0.245(3)	—	-0.054(11)	—	-0.190(2)	—	—	-0.0468(9)	—	—	—
0.077	0.653(10)	-1.049(72)	0.149(3)	-0.212(22)	-0.084(28)	-0.201(11)	—	-0.046(4)	—	-0.135(7)	0.653(22)	1.636(54)	-0.038(4)	0.115(9)	0.289(22)	0.012(75)
✓0.096	0.631(1)	-1.094(9)	0.1462(7)	-0.191(3)	-0.061(2)	-0.207(2)	-2.125(55)	-0.0494(9)	-0.159(24)	-0.160(2)	0.917(24)	1.399(6)	-0.0414(9)	0.111(11)	0.259(3)	-0.043(6)
✓0.096	0.630(2)	-1.079(19)	0.145(1)	-0.182(6)	-0.049(6)	-0.210(4)	-2.182(113)	-0.049(2)	-0.095(42)	-0.162(3)	0.918(44)	1.368(11)	-0.042(1)	0.107(16)	0.241(5)	-0.043(21)
0.160	0.496(9)	-0.866(45)	0.129(3)	-0.169(13)	-0.051(8)	-0.181(11)	-1.304(200)	-0.046(4)	-0.045(64)	-0.146(10)	0.792(93)	1.181(28)	-0.041(4)	0.125(36)	0.219(11)	-0.029(24)
✓0.186	0.469(2)	-0.846(8)	0.1231(7)	-0.160(3)	-0.044(1)	-0.180(2)	-1.395(34)	-0.0452(9)	-0.117(13)	-0.140(2)	0.721(15)	1.074(6)	-0.0373(9)	0.099(7)	0.220(3)	-0.034(4)
✓0.187	0.469(4)	-0.820(19)	0.123(1)	-0.150(5)	-0.040(4)	-0.183(5)	-1.480(89)	-0.046(2)	-0.108(32)	-0.137(4)	0.649(34)	1.053(11)	-0.039(1)	0.094(13)	0.209(5)	-0.039(13)
✓0.197	0.459(2)	-0.806(11)	0.1206(9)	-0.153(4)	-0.037(2)	-0.177(3)	-1.340(44)	-0.045(10)	-0.096(21)	-0.135(3)	0.662(20)	1.032(7)	-0.037(1)	0.093(9)	0.212(3)	-0.031(5)
0.241	0.389(11)	-0.686(42)	0.113(4)	-0.141(12)	-0.044(7)	-0.164(12)	-1.120(163)	-0.044(4)	-0.066(55)	-0.128(10)	0.593(72)	0.926(28)	-0.039(4)	0.096(28)	0.199(10)	-0.030(23)
0.268	0.415(79)	-0.339(153)	0.120(23)	-0.179(55)	-0.072(38)	-0.067(42)	—	-0.022(14)	—	-0.060(23)	0.445(84)	1.117(210)	-0.015(16)	0.092(24)	0.232(61)	0.017(91)
✓0.272	0.363(2)	-0.673(9)	0.1055(9)	-0.140(3)	-0.037(1)	-0.160(3)	-1.023(35)	-0.043(10)	-0.111(14)	-0.123(3)	0.569(17)	0.859(7)	-0.034(1)	0.081(8)	0.193(3)	-0.034(4)
✓0.293	0.347(3)	-0.627(10)	0.1028(10)	-0.130(3)	-0.032(2)	-0.153(3)	-0.932(37)	-0.041(1)	-0.072(18)	-0.118(3)	0.507(17)	0.809(7)	-0.033(1)	0.076(8)	0.182(3)	-0.025(5)
0.339	0.270(49)	-0.312(122)	0.091(16)	-0.106(35)	-0.037(19)	-0.091(36)	-0.300(337)	-0.025(13)	0.041(126)	-0.079(43)	0.339(208)	0.646(119)	-0.022(17)	0.093(88)	0.139(39)	0.022(54)
✓0.354	0.295(3)	-0.545(11)	0.093(1)	-0.128(4)	-0.033(2)	-0.144(4)	-0.730(38)	-0.039(1)	-0.10(19)	-0.109(4)	0.458(19)	0.715(8)	-0.032(2)	0.077(9)	0.176(4)	-0.029(6)
✓0.358	0.307(7)	-0.555(22)	0.096(2)	-0.129(7)	-0.028(4)	-0.144(8)	-0.726(78)	-0.038(3)	-0.052(34)	-0.114(6)	0.466(34)	0.707(15)	-0.035(3)	0.091(14)	0.165(6)	-0.015(12)
0.393	0.279(19)	-0.500(51)	0.091(6)	-0.123(15)	-0.025(8)	-0.122(18)	-0.489(151)	-0.033(6)	0.042(64)	-0.117(19)	0.491(88)	0.649(39)	-0.034(7)	0.073(34)	0.142(13)	-0.037(24)
✓0.395	0.271(3)	-0.501(9)	0.087(1)	-0.118(3)	-0.028(2)	-0.134(3)	—	-0.038(1)	—	-0.064(2)	0.256(3)	0.648(7)	-0.028(1)	0.063(1)	0.161(3)	-0.028(4)
✓0.433	0.241(4)	-0.467(10)	0.083(1)	-0.113(3)	-0.027(1)	-0.131(4)	-0.584(27)	-0.037(1)	-0.074(13)	-0.100(4)	0.387(14)	0.602(8)	-0.030(2)	0.066(7)	0.154(4)	-0.027(4)
✓0.438	0.248(7)	-0.434(20)	0.084(2)	-0.105(6)	-0.022(3)	-0.122(8)	-0.541(60)	-0.037(3)	-0.074(24)	-0.103(6)	0.378(24)	0.581(15)	-0.032(2)	0.072(11)	0.146(5)	-0.018(10)
✓0.472	0.227(4)	-0.423(12)	0.079(1)	-0.099(4)	-0.023(2)	-0.123(5)	-0.546(37)	-0.035(2)	-0.083(20)	-0.089(4)	0.312(17)	0.543(8)	-0.027(2)	0.052(8)	0.142(4)	-0.025(6)
✓0.491	0.214(3)	-0.405(8)	0.075(10)	-0.100(3)	-0.024(1)	-0.117(3)	-0.500(23)	-0.034(1)	-0.057(16)	-0.091(4)	0.328(13)	0.523(6)	-0.026(2)	0.056(6)	0.137(3)	-0.020(3)
A_0	0.8958(3)	-1.492(19)	0.1762(8)	-0.224(4)	-0.088(5)	-0.245(3)	-3.634(277)	-0.054(1)	-0.182(99)	-0.190(2)	1.242(32)	1.905(13)	-0.0468(10)	0.134(10)	0.299(5)	-0.052(7)
m_A	0.792(14)	0.845(69)	1.071(60)	1.004(20)	0.423(22)	1.082(173)	0.637(120)	1.634(3.531)	0.722(2.098)	0.980(182)	1.027(20)	0.795(37)	1.185(680)	1.355(96)	1.240(288)	0.615(98)
p	2.474(82)	2.485(314)	2.372(243)	2.	1.	2.066(576)	2.509(589)	2.653(11.21)	1.515(6.045)	1.759(588)	3.5	2.233(160)	1.762(1.845)	3.5	2.767(1.111)	1
$\overline{\chi^2}$	1.276(605)	0.448(389)	0.627(495)	1.264(763)	1.872(993)	0.234(273)	0.272(253)	0.118(161)	0.710(488)	0.319(282)	0.989(585)	1.221(655)	0.595(567)	0.453(380)	2.077(965)	0.456(369)

Table A.11: MILC-20³-m03-unchopped — data set 7

Q^2	$A_{10}^{(u)}$	$B_{10}^{(u)}$	$A_{20}^{(u)}$	$B_{20}^{(u)}$	$C_{20}^{(u)}$	$\tilde{A}_{10}^{(u)}$	$\tilde{B}_{10}^{(u)}$	$\tilde{A}_{20}^{(u)}$	$\tilde{B}_{20}^{(u)}$	$A_{T10}^{(u)}$	$\tilde{A}_{T10}^{(u)}$	$\tilde{B}_{T10}^{(u)}$	$A_{T20}^{(u)}$	$\tilde{A}_{T20}^{(u)}$	$\tilde{B}_{T20}^{(u)}$	$\tilde{B}_{T21}^{(u)}$
✓0.000	1.785(11)	—	0.395(3)	—	—	0.784(8)	—	0.225(3)	—	0.757(6)	—	—	0.243(3)	—	—	—
0.074	1.382(33)	0.938(188)	0.365(12)	0.077(58)	-0.131(77)	0.680(34)	—	0.194(12)	—	0.619(25)	0.927(54)	2.301(134)	0.229(14)	0.147(23)	0.361(58)	0.217(191)
✓0.095	1.309(3)	1.018(26)	0.340(2)	0.161(8)	-0.071(6)	0.663(6)	7.117(147)	0.203(2)	0.407(63)	0.648(6)	-0.534(70)	2.025(14)	0.223(3)	-0.075(32)	0.378(7)	0.006(18)
✓0.096	1.294(7)	0.937(50)	0.330(4)	0.141(15)	-0.036(15)	0.661(12)	7.056(332)	0.197(4)	0.330(108)	0.646(10)	-0.550(125)	1.947(27)	0.220(4)	-0.126(49)	0.355(11)	-0.102(51)
0.156	1.084(32)	0.692(111)	0.307(10)	0.101(31)	-0.031(23)	0.562(30)	4.207(522)	0.176(11)	0.085(173)	0.628(36)	-0.657(277)	1.647(66)	0.223(15)	-0.237(111)	0.337(26)	-0.079(68)
✓0.184	1.019(5)	0.775(21)	0.298(2)	0.136(7)	-0.048(4)	0.576(6)	4.476(82)	0.184(2)	0.336(35)	0.561(6)	-0.320(38)	1.565(12)	0.202(3)	-0.016(18)	0.324(7)	0.008(11)
✓0.186	1.002(10)	0.748(45)	0.285(4)	0.119(15)	-0.037(9)	0.558(13)	4.031(209)	0.177(5)	0.291(76)	0.550(11)	-0.298(80)	1.486(26)	0.193(5)	0.004(35)	0.298(11)	0.026(33)
✓0.197	0.994(7)	0.781(23)	0.290(3)	0.137(8)	-0.037(5)	0.568(7)	4.456(105)	0.181(3)	0.290(51)	0.551(8)	-0.328(46)	1.474(16)	0.199(4)	-0.038(22)	0.308(7)	0.011(17)
0.234	0.895(39)	0.600(106)	0.278(12)	0.116(30)	-0.020(20)	0.477(35)	2.534(401)	0.172(13)	0.221(134)	0.523(33)	-0.282(177)	1.387(69)	0.180(14)	0.028(79)	0.276(25)	-0.083(63)
0.255	0.739(162)	0.535(322)	0.222(56)	0.085(104)	0.094(89)	0.390(114)	—	0.131(40)	—	0.354(84)	0.282(98)	0.671(241)	0.192(60)	0.076(42)	0.171(104)	0.180(225)
✓0.269	0.827(7)	0.633(22)	0.263(3)	0.122(8)	-0.033(4)	0.510(8)	3.048(81)	0.170(3)	0.301(37)	0.498(9)	-0.250(39)	1.260(15)	0.182(4)	0.004(21)	0.284(8)	-0.001(13)
✓0.293	0.796(8)	0.620(22)	0.254(3)	0.117(8)	-0.031(4)	0.489(9)	2.872(85)	0.165(3)	0.241(46)	0.481(9)	-0.239(37)	1.160(16)	0.180(4)	-0.020(18)	0.258(7)	0.013(13)
0.323	0.620(157)	0.284(221)	0.232(58)	0.044(75)	-0.068(52)	0.335(105)	1.954(1.151)	0.111(35)	0.096(372)	0.648(340)	-1.109(1.187)	0.718(227)	0.217(116)	-0.262(406)	0.162(77)	0.102(135)
✓0.349	0.717(12)	0.512(28)	0.239(4)	0.093(10)	-0.025(5)	0.446(11)	2.124(96)	0.157(4)	0.166(50)	0.467(15)	-0.203(58)	1.018(20)	0.185(7)	-0.056(31)	0.259(10)	-0.021(15)
✓0.353	0.701(20)	0.486(58)	0.231(7)	0.085(18)	-0.026(9)	0.445(26)	2.169(221)	0.158(10)	0.179(93)	0.459(22)	-0.229(93)	0.967(35)	0.183(9)	-0.132(41)	0.250(15)	-0.081(32)
0.382	0.636(68)	0.234(123)	0.214(24)	0.051(42)	-0.037(24)	0.365(62)	1.900(464)	0.135(22)	0.057(198)	0.436(92)	-0.244(321)	0.794(108)	0.226(49)	-0.341(161)	0.224(41)	-0.043(70)
✓0.395	0.647(8)	0.498(17)	0.228(4)	0.109(8)	-0.025(4)	0.430(8)	—	0.156(3)	—	0.260(6)	0.374(6)	0.896(16)	0.133(4)	0.103(3)	0.236(8)	-0.017(10)
✓0.425	0.612(11)	0.434(21)	0.217(4)	0.087(8)	-0.024(3)	0.401(10)	1.688(67)	0.145(4)	0.192(30)	0.411(12)	-0.125(32)	0.865(18)	0.166(6)	-0.020(17)	0.230(9)	-0.008(10)
✓0.432	0.578(22)	0.396(47)	0.199(8)	0.063(15)	-0.028(7)	0.362(23)	1.411(145)	0.139(9)	0.142(58)	0.374(20)	-0.099(54)	0.750(32)	0.149(8)	-0.025(27)	0.192(14)	-0.008(25)
✓0.469	0.572(14)	0.410(28)	0.204(5)	0.073(10)	-0.014(5)	0.390(14)	1.579(91)	0.140(6)	0.176(47)	0.404(15)	-0.161(42)	0.771(22)	0.162(7)	-0.040(19)	0.204(10)	-0.037(15)
✓0.490	0.541(8)	0.408(14)	0.203(3)	0.094(6)	-0.022(3)	0.378(8)	1.652(59)	0.142(3)	0.278(40)	0.383(12)	-0.150(29)	0.731(12)	0.148(6)	0.003(16)	0.203(6)	0.003(7)
A_0	1.785(11)	1.345(64)	0.395(3)	0.186(14)	-0.136(18)	0.783(8)	13.911(988)	0.223(3)	0.534(107)	0.757(6)	-0.772(124)	2.715(35)	0.244(3)	-0.10(243)	0.442(10)	-0.004(6)
m_A	0.653(16)	0.807(203)	0.930(11)	1.128(1.03)	0.3000(8)	1.071(166)	0.503(62)	1.156(30)	0.518(105)	0.917(17)	0.843(81)	0.972(96)	1.163(39)	0.755(977)	1.014(25)	3.3
p	1.556(65)	2.161(793)	1.5	2.382(3.624)	1.013(100)	2.067(555)	2.075(269)	1.5	1.	1.5	3.5	3.145(503)	1.5	3.5	2.	1
$\overline{\chi^2}$	0.948(585)	0.783(728)	1.550(904)	1.560(1.103)	1.006(610)	0.591(519)	3.106(1.371)	0.599(552)	1.054(720)	0.612(502)	0.384(397)	2.339(1.08)	1.158(709)	1.718(1.124)	1.555(906)	1.948(875)

Q^2	$A_{10}^{(d)}$	$B_{10}^{(d)}$	$A_{20}^{(d)}$	$B_{20}^{(d)}$	$C_{20}^{(d)}$	$\tilde{A}_{10}^{(d)}$	$\tilde{B}_{10}^{(d)}$	$\tilde{A}_{20}^{(d)}$	$\tilde{B}_{20}^{(d)}$	$A_{T10}^{(d)}$	$\tilde{A}_{T10}^{(d)}$	$\tilde{B}_{T10}^{(d)}$	$A_{T20}^{(d)}$	$\tilde{A}_{T20}^{(d)}$	$\tilde{B}_{T20}^{(d)}$	$\tilde{B}_{T21}^{(d)}$
✓0.000	0.9045(5)	—	0.169(1)	—	—	-0.250(4)	—	-0.049(2)	—	-0.188(3)	—	—	-0.045(1)	—	—	—
0.074	0.673(17)	-1.205(119)	0.149(6)	-0.201(33)	-0.060(49)	-0.184(21)	—	-0.038(6)	—	-0.135(13)	0.634(32)	1.589(80)	-0.036(7)	0.103(15)	0.259(37)	-0.007(119)
✓0.095	0.620(2)	-1.056(14)	0.139(1)	-0.179(5)	-0.063(3)	-0.209(3)	-2.234(85)	-0.045(1)	-0.085(34)	-0.157(3)	0.864(35)	1.305(10)	-0.040(2)	0.117(17)	0.241(5)	-0.063(9)
✓0.096	0.615(4)	-1.040(28)	0.136(2)	-0.168(8)	-0.056(9)	-0.203(7)	-2.225(177)	-0.042(2)	-0.094(58)	-0.149(4)	0.757(62)	1.263(16)	-0.039(2)	0.111(25)	0.225(7)	-0.077(31)
0.156	0.502(17)	-0.945(75)	0.127(5)	-0.148(18)	-0.051(13)	-0.171(19)	-1.123(316)	-0.043(6)	-0.179(105)	-0.150(18)	0.776(150)	1.126(43)	-0.038(7)	0.049(60)	0.229(17)	-0.065(40)
✓0.184	0.452(3)	-0.799(12)	0.117(1)	-0.151(4)	-0.046(2)	-0.180(4)	-1.356(51)	-0.042(2)	-0.088(20)	-0.134(3)	0.640(22)	0.989(9)	-0.037(2)	0.104(10)	0.203(4)	-0.040(6)
✓0.186	0.448(6)	-0.758(27)	0.112(2)	-0.140(8)	-0.041(6)	-0.187(9)	-1.557(127)	-0.040(3)	-0.099(48)	-0.131(6)	0.597(47)	0.953(15)	-0.037(2)	0.096(21)	0.183(7)	-0.053(20)
✓0.197	0.439(3)	-0.745(15)	0.113(1)	-0.142(5)	-0.039(3)	-0.173(4)	-1.244(61)	-0.040(2)	-0.057(29)	-0.135(4)	0.651(26)	0.941(9)	-0.035(2)	0.112(13)	0.197(4)	-0.023(8)
0.234	0.388(20)	-0.723(74)	0.111(6)	-0.139(17)	-0.046(12)	-0.172(22)	-1.199(249)	-0.041(7)	-0.136(85)	-0.125(19)	0.502(116)	0.916(47)	-0.047(7)	0.110(49)	0.180(16)	-0.063(39)
0.255	0.323(75)	-0.568(223)	0.052(22)	-0.055(58)	0.060(53)	-0.131(64)	—	-0.013(20)	—	-0.072(34)	0.339(78)	0.853(197)	-0.002(27)	0.054(28)	0.134(70)	0.100(145)
✓0.269	0.345(4)	-0.632(13)	0.10(1)	-0.132(5)	-0.036(2)	-0.160(4)	-0.944(47)	-0.040(2)	-0.088(23)	-0.118(4)	0.485(22)	0.786(10)	-0.034(2)	0.091(12)	0.178(5)	-0.029(8)
✓0.293	0.332(4)	-0.564(14)	0.094(1)	-0.114(5)	-0.032(2)	-0.156(5)	-0.915(48)	-0.037(2)	-0.062(27)	-0.117(5)	0.468(22)	0.729(9)	-0.033(2)	0.090(11)	0.163(4)	-0.015(8)
0.323	0.239(66)	-0.556(201)	0.074(23)	-0.070(49)	-0.029(31)	-0.112(58)	-0.655(611)	-0.038(20)	-0.207(254)	-0.102(128)	0.409(522)	0.715(188)	-0.028(46)	0.023(191)	0.164(60)	-0.046(83)
✓0.349	0.287(6)	-0.521(17)	0.087(2)	-0.117(6)	-0.028(3)	-0.141(6)	-0.657(55)	-0.034(2)	-0.055(26)	-0.111(7)	0.441(28)	0.655(13)	-0.027(3)	0.056(14)	0.164(6)	-0.043(9)
✓0.353	0.280(10)	-0.476(34)	0.086(3)	-0.113(10)	-0.038(5)	-0.130(13)	-0.596(107)	-0.034(5)	-0.072(44)	-0.093(9)	0.370(42)	0.604(21)	-0.027(4)	0.058(21)	0.142(9)	-0.035(19)
0.382	0.266(34)	-0.538(92)	0.087(11)	-0.135(24)	-0.048(15)	-0.128(33)	-0.474(253)	-0.033(12)	-0.052(103)	-0.122(38)	0.395(143)	0.593(78)	-0.021(13)	-0.003(57)	0.147(26)	-0.050(44)
✓0.395	0.251(4)	-0.432(12)	0.082(2)	-0.106(5)	-0.031(2)	-0.128(5)	—	-0.034(2)	—	-0.056(3)	0.225(4)	0.571(10)	-0.023(2)	0.058(2)	0.148(5)	-0.024(6)
✓0.425	0.233(6)	-0.439(15)	0.078(2)	-0.108(5)	-0.027(2)	-0.129(6)	-0.522(38)	-0.035(2)	-0.055(18)	-0.098(6)	0.358(20)	0.554(12)	-0.027(3)	0.060(10)	0.145(6)	-0.031(6)
✓0.432	0.221(10)	-0.377(30)	0.074(3)	-0.086(9)	-0.029(4)	-0.122(13)	-0.488(86)	-0.030(5)	-0.017(34)	-0.099(9)	0.331(33)	0.501(21)	-0.035(4)	0.094(16)	0.110(8)	-0.028(15)
✓0.469	0.215(7)	-0.359(18)	0.072(2)	-0.088(6)	-0.025(3)	-0.113(8)	-0.429(55)	-0.030(3)	-0.039(28)	-0.089(7)	0.314(22)	0.479(12)	-0.028(3)	0.066(11)	0.125(6)	-0.027(10)
✓0.490	0.200(4)	-0.349(10)	0.070(1)	-0.090(4)	-0.023(2)	-0.111(4)	-0.428(33)	-0.033(2)	-0.024(22)	-0.089(6)	0.300(17)	0.456(7)	-0.029(4)	0.068(10)	0.124(4)	-0.019(4)
A_0	0.9045(5)	-1.477(35)	0.169(1)	-0.214(6)	-0.098(10)	-0.248(5)	-4.157(527)	-0.049(2)	-0.129(34)	-0.186(3)	1.124(50)	1.798(23)	-0.045(1)	0.144(17)	0.284(8)	-0.100(39)
m_A	0.725(19)	0.879(128)	0.964(81)	0.954(29)	0.394(33)	1.341(478)	0.600(157)	1.245(510)	1.520(291)	0.875(35)	1.030(32)	0.809(58)	1.100(99)	1.352(151)	1.015(335)	0.354(116)
p	2.286(107)	2.921(662)	2.089(307)	2.	1.	3.257(2.097)	2.664(839)	1.545(1.154)	6.	1.5	3.5	2.430(261)	1.5	3.5	2.122(1.137)	1
$\overline{\chi^2}$	0.672(470)	1.110(728)	0.668(548)	1.150(795)	1.074(604)	0.447(328)	0.597(466)	0.428(373)	0.361(391)	0.628(401)	0.755(543)	1.588(806)	0.590(381)	0.739(538)	2.617(1.191)	1.138(808)

Table A.12: MILC-20³-m02-unchopped — data set 8

Q^2	$A_{10}^{(u)}$	$B_{10}^{(u)}$	$A_{20}^{(u)}$	$B_{20}^{(u)}$	$C_{20}^{(u)}$	$\tilde{A}_{10}^{(u)}$	$\tilde{B}_{10}^{(u)}$	$\tilde{A}_{20}^{(u)}$	$\tilde{B}_{20}^{(u)}$	$A_{T10}^{(u)}$	$\tilde{A}_{T10}^{(u)}$	$\tilde{B}_{T10}^{(u)}$	$A_{T20}^{(u)}$	$\tilde{A}_{T20}^{(u)}$	$\tilde{B}_{T20}^{(u)}$	$\tilde{B}_{T21}^{(u)}$
✓0.000	1.808(2)	—	0.387(5)	—	—	0.765(14)	—	0.211(5)	—	0.753(12)	—	—	0.252(6)	—	—	—
0.070	1.331(66)	0.232(392)	0.328(27)	0.008(119)	-0.009(169)	0.580(76)	—	0.150(23)	—	0.530(51)	0.784(127)	1.942(317)	0.249(34)	0.121(54)	0.295(134)	0.509(451)
✓0.094	1.301(7)	0.889(40)	0.336(4)	0.151(14)	-0.081(10)	0.661(10)	7.436(259)	0.195(4)	0.337(105)	0.654(12)	-0.489(127)	1.868(28)	0.221(7)	0.034(66)	0.313(13)	-0.007(35)
✓0.095	1.284(13)	0.780(98)	0.325(7)	0.153(27)	-0.037(28)	0.607(24)	6.995(583)	0.178(9)	0.211(209)	0.606(20)	-0.217(247)	1.830(56)	0.219(9)	-0.007(100)	0.336(23)	-0.005(100)
0.150	0.984(51)	0.425(194)	0.272(18)	0.109(54)	-0.043(43)	0.496(56)	3.956(820)	0.176(19)	0.147(266)	0.520(63)	-0.344(464)	1.500(123)	0.185(26)	0.154(221)	0.296(53)	0.195(156)
✓0.182	1.008(8)	0.694(34)	0.292(4)	0.120(12)	-0.048(6)	0.580(11)	4.517(133)	0.183(5)	0.358(57)	0.551(12)	-0.224(64)	1.422(23)	0.206(6)	-0.017(37)	0.288(12)	0.007(23)
✓0.184	1.00(21)	0.667(86)	0.286(9)	0.099(26)	-0.022(18)	0.609(32)	4.979(423)	0.168(11)	0.373(151)	0.533(25)	0(0.160)	1.402(57)	0.195(11)	0.039(70)	0.255(23)	-0.066(76)
✓0.197	0.978(13)	0.701(35)	0.290(5)	0.114(13)	-0.046(9)	0.570(13)	4.406(168)	0.175(5)	0.346(82)	0.532(15)	-0.082(78)	1.343(27)	0.205(8)	-0.069(42)	0.269(13)	-0.013(28)
0.225	0.732(62)	0.523(180)	0.238(22)	0.043(49)	-0.020(34)	0.419(72)	2.440(710)	0.135(25)	0.031(214)	0.412(68)	-0.019(344)	1.167(125)	0.145(27)	0.097(152)	0.247(52)	0.019(138)
0.236																
✓0.263	0.811(14)	0.591(37)	0.260(6)	0.113(14)	-0.042(7)	0.504(15)	3.018(130)	0.168(6)	0.279(60)	0.470(18)	-0.112(71)	1.107(28)	0.190(9)	-0.026(41)	0.255(15)	-0.011(28)
✓0.292	0.782(15)	0.537(35)	0.251(5)	0.086(13)	-0.029(8)	0.510(16)	3.069(145)	0.164(6)	0.275(73)	0.484(18)	-0.167(67)	1.045(28)	0.195(9)	-0.068(35)	0.222(13)	0.018(27)
0.301																
✓0.340	0.662(18)	0.427(47)	0.225(8)	0.077(18)	-0.015(9)	0.459(22)	2.185(155)	0.156(9)	0.301(80)	0.462(29)	-0.275(94)	0.925(37)	0.169(15)	0.030(55)	0.193(19)	0.005(34)
✓0.347	0.572(28)	0.209(79)	0.200(10)	0.047(26)	-0.016(15)	0.456(44)	2.291(306)	0.153(16)	0.413(134)	0.378(37)	-0.034(136)	0.742(55)	0.143(17)	0.014(67)	0.161(26)	-0.019(59)
0.367	0.409(54)	0.294(188)	0.134(20)	0.056(59)	-0.026(28)	0.251(86)	0.801(485)	0.095(31)	0.262(174)	0.235(55)	0.196(239)	0.589(106)	0.076(25)	0.153(134)	0.116(52)	0.053(123)
✓0.395	0.649(15)	0.415(30)	0.233(7)	0.091(14)	-0.038(7)	0.433(15)	—	0.155(7)	—	0.242(11)	0.334(11)	0.790(29)	0.136(9)	0.084(7)	0.185(17)	-0.002(22)
✓0.413	0.555(16)	0.346(33)	0.202(6)	0.067(12)	-0.027(5)	0.397(16)	1.577(94)	0.138(7)	0.220(45)	0.358(19)	-0.052(50)	0.715(26)	0.161(10)	-0.007(31)	0.161(14)	0.012(20)
✓0.422	0.508(33)	0.230(71)	0.185(12)	0.014(24)	-0.003(14)	0.452(48)	1.847(261)	0.120(16)	0.098(98)	0.339(37)	0.013(100)	0.571(53)	0.161(18)	-0.032(54)	0.156(25)	-0.022(51)
✓0.465	0.548(22)	0.336(45)	0.205(8)	0.068(16)	-0.022(8)	0.439(27)	1.807(151)	0.141(10)	0.247(81)	0.345(27)	0.003(67)	0.631(35)	0.137(15)	0.027(38)	0.144(18)	0.027(32)
✓0.490	0.547(13)	0.344(23)	0.203(6)	0.080(10)	-0.018(4)	0.386(13)	1.286(86)	0.138(5)	0.149(67)	0.363(24)	-0.058(51)	0.667(22)	0.186(14)	-0.060(31)	0.174(12)	0(0.014)
A_0	1.808(2)	1.170(63)	0.388(5)	0.192(23)	-0.169(36)	0.763(14)	13.355(1.388)	0.211(7)	0.470(94)	0.754(12)	-0.912(647)	2.616(79)	0.249(6)	-0.025(23)	0.395(18)	0.002(12)
m_A	0.637(27)	1.419(72)	1.079(224)	0.825(86)	0.3	1.164(432)	0.680(166)	2.186(4.336)	1.768(332)	1.634(1.168)	0.583(182)	0.890(159)	1.137(74)	3.3	1.703(75)	3.295(2.995)
p	1.583(113)	5.997(390)	1.971(721)	2.	1.149(172)	2.211(1.43)	3.205(1.025)	4.439(15.889)	6.	4.785(6.486)	3.5	2.994(832)	1.5	3.5	6.0000(2)	1
$\overline{\chi}^2$	3.496(1.399)	1.806(1.006)	2.462(1.066)	1.261(830)	1.351(735)	1.098(485)	1.729(799)	0.869(575)	0.553(406)	1.201(624)	0.993(553)	2.171(1.037)	1.276(751)	0.816(612)	1.213(700)	0.259(265)

Q^2	$A_{10}^{(d)}$	$B_{10}^{(d)}$	$A_{20}^{(d)}$	$B_{20}^{(d)}$	$C_{20}^{(d)}$	$\tilde{A}_{10}^{(d)}$	$\tilde{B}_{10}^{(d)}$	$\tilde{A}_{20}^{(d)}$	$\tilde{B}_{20}^{(d)}$	$A_{T10}^{(d)}$	$\tilde{A}_{T10}^{(d)}$	$\tilde{B}_{T10}^{(d)}$	$A_{T20}^{(d)}$	$\tilde{A}_{T20}^{(d)}$	$\tilde{B}_{T20}^{(d)}$	$\tilde{B}_{T21}^{(d)}$
✓0.000	0.9157(8)	—	0.163(3)	—	—	-0.283(8)	—	-0.054(3)	—	-0.198(6)	—	—	-0.041(3)	—	—	—
0.070	0.607(38)	-1.289(268)	0.125(15)	-0.245(79)	-0.061(103)	-0.262(51)	—	-0.077(15)	—	-0.167(31)	0.500(84)	1.255(210)	-0.056(20)	0.075(33)	0.190(83)	-0.378(290)
✓0.094	0.607(4)	-1.025(24)	0.134(2)	-0.152(9)	-0.067(6)	-0.223(6)	-2.448(145)	-0.044(3)	-0.112(61)	-0.164(7)	0.812(69)	1.211(17)	-0.040(3)	0.113(38)	0.210(9)	-0.025(22)
✓0.095	0.600(8)	-1.030(61)	0.129(3)	-0.128(15)	-0.051(17)	-0.251(16)	-2.802(367)	-0.050(5)	-0.083(122)	-0.162(11)	0.744(130)	1.161(37)	-0.036(5)	0.097(58)	0.209(14)	0.084(66)
0.150	0.435(27)	-0.776(130)	0.108(9)	-0.168(36)	-0.069(27)	-0.208(37)	-1.471(533)	-0.061(12)	-0.357(164)	-0.180(37)	0.936(294)	0.895(85)	-0.042(15)	0.126(122)	0.167(34)	-0.035(94)
✓0.182	0.432(5)	-0.762(21)	0.112(2)	-0.127(8)	-0.049(4)	-0.187(7)	-1.342(85)	-0.037(3)	-0.044(34)	-0.143(7)	0.651(42)	0.912(16)	-0.037(4)	0.081(21)	0.186(8)	-0.047(14)
✓0.184	0.435(12)	-0.767(54)	0.106(4)	-0.140(16)	-0.029(11)	-0.209(19)	-1.570(234)	-0.049(7)	-0.101(92)	-0.128(13)	0.517(95)	0.880(35)	-0.032(6)	0.067(41)	0.177(15)	-0.039(46)
✓0.197	0.424(7)	-0.706(24)	0.109(2)	-0.117(8)	-0.045(5)	-0.187(7)	-1.126(98)	-0.040(3)	-0.038(52)	-0.156(9)	0.714(53)	0.851(18)	-0.034(4)	0.067(26)	0.174(9)	-0.016(17)
0.225	0.309(32)	-0.623(123)	0.082(11)	-0.121(33)	-0.010(22)	-0.177(42)	-1.096(401)	-0.046(14)	-0.160(136)	-0.102(39)	0.322(216)	0.634(84)	-0.043(16)	0.104(99)	0.107(33)	-0.035(82)
0.236	—															
✓0.263	0.323(7)	-0.603(25)	0.096(3)	-0.097(9)	-0.040(4)	-0.168(8)	-0.880(79)	-0.038(4)	-0.066(39)	-0.114(10)	0.443(45)	0.723(19)	-0.023(5)	0.028(26)	0.165(10)	-0.046(18)
✓0.292	0.314(8)	-0.561(24)	0.093(3)	-0.097(8)	-0.038(4)	-0.164(9)	-0.785(79)	-0.040(4)	-0.098(48)	-0.122(11)	0.446(45)	0.675(18)	-0.023(5)	0.013(22)	0.144(9)	-0.025(19)
0.301																
✓0.340	0.256(9)	-0.456(29)	0.082(4)	-0.091(12)	-0.027(5)	-0.138(12)	-0.636(92)	-0.034(5)	-0.042(45)	-0.100(15)	0.310(54)	0.568(23)	-0.034(8)	0.080(31)	0.129(13)	-0.009(21)
✓0.347	0.229(16)	-0.420(52)	0.068(5)	-0.091(15)	-0.019(9)	-0.106(23)	-0.326(167)	-0.038(9)	-0.086(80)	-0.096(20)	0.374(76)	0.507(38)	-0.029(9)	0.046(38)	0.113(16)	-0.026(38)
0.367	0.170(30)	-0.310(123)	0.043(10)	-0.052(36)	0.007(17)	-0.088(55)	-0.427(311)	-0.047(19)	-0.231(107)	-0.062(34)	0.247(142)	0.356(70)	-0.021(15)	-0.002(76)	0.101(32)	-0.104(86)
✓0.395	0.239(8)	-0.391(20)	0.072(4)	-0.075(9)	-0.031(5)	-0.133(9)	—	-0.034(4)	—	-0.059(7)	0.193(7)	0.492(18)	-0.023(5)	0.048(4)	0.124(11)	-0.033(15)
✓0.413	0.189(8)	-0.364(23)	0.069(3)	-0.077(9)	-0.025(3)	-0.123(9)	-0.428(57)	-0.031(4)	-0.058(26)	-0.092(11)	0.280(33)	0.447(19)	-0.025(6)	0.035(17)	0.122(10)	-0.051(13)
✓0.422	0.195(18)	-0.327(49)	0.060(6)	-0.096(15)	-0.014(8)	-0.099(26)	-0.243(145)	-0.038(9)	-0.084(62)	-0.082(22)	0.316(66)	0.415(38)	-0.012(10)	0.039(31)	0.097(17)	-0.030(33)
✓0.465	0.198(12)	-0.299(29)	0.066(4)	-0.078(10)	-0.016(5)	-0.101(14)	-0.322(86)	-0.031(6)	-0.045(49)	-0.094(16)	0.291(44)	0.423(23)	-0.030(8)	0.053(22)	0.106(11)	-0.011(20)
✓0.490	0.184(7)	-0.326(16)	0.066(4)	-0.063(6)	-0.023(3)	-0.111(7)	-0.338(53)	-0.030(3)	-0.037(40)	-0.094(14)	0.273(31)	0.395(14)	-0.004(9)	-0.005(20)	0.107(8)	-0.027(9)
A_0	0.9157(8)	-1.460(72)	0.163(4)	-0.181(12)	-0.091(24)	-0.281(8)	-6.008(1.459)	-0.052(3)	-0.084(66)	-0.198(6)	1.218(103)	1.676(46)	-0.043(3)	0.181(82)	0.256(12)	-0.033(13)
m_A	0.747(39)	1.001(325)	1.343(537)	1.649(91)	0.803(944)	1.293(724)	0.483(166)	1.054(118)	0.878(1.128)	1.396(1.513)	0.930(52)	0.996(198)	0.770(212)		1.731(75)	2.620(8.329)
p	2.632(243)	3.911(2.046)	3.999(2.816)	5.996(182)	2.579(4.341)	3.689(3.726)	2.590(943)	1.5	1.	3.753(7.617)	3.5	3.653(1.181)	5.952(2.379)	3.5	5.998(83)	1
$\overline{\chi}^2$	2.320(1.125)	0.568(435)	1.308(769)	0.638(447)	1.092(821)	0.854(493)	0.758(458)	0.540(389)	0.260(275)	0.664(548)	1.066(657)	0.885(615)	1.033(567)	0.781(604)	0.468(480)	0.884(608)

Table A.13: MILC-20^3-m01-unchopped — data set 9

Q^2	$A_{10}^{(u)}$	$B_{10}^{(u)}$	$A_{20}^{(u)}$	$B_{20}^{(u)}$	$C_{20}^{(u)}$	$\tilde{A}_{10}^{(u)}$	$\tilde{B}_{10}^{(u)}$	$\tilde{A}_{20}^{(u)}$	$\tilde{B}_{20}^{(u)}$	$A_{T10}^{(u)}$	$\tilde{A}_{T10}^{(u)}$	$\bar{B}_{T10}^{(u)}$	$A_{T20}^{(u)}$	$\tilde{A}_{T20}^{(u)}$	$\bar{B}_{T20}^{(u)}$	$\bar{B}_{T21}^{(u)}$
✓0.000	1.811(7)	—	0.368(10)	—	—	0.810(29)	—	0.208(12)	—	0.749(26)	—	—	0.268(13)	—	—	—
0.068	1.194(118)	0.553(740)	0.288(48)	0.060(218)	-0.448(291)	0.761(141)	—	0.248(46)	—	0.558(100)	0.701(268)	1.733(670)	0.205(76)	0.038(125)	0.087(314)	0.393(1.004)
✓0.094	1.282(15)	0.867(85)	0.322(8)	0.159(30)	-0.073(24)	0.650(20)	7.357(495)	0.197(8)	0.171(227)	0.649(28)	-0.408(290)	1.884(59)	0.244(15)	-0.109(156)	0.305(33)	0.072(80)
✓0.095	1.252(30)	0.563(189)	0.310(12)	0.136(54)	-0.036(56)	0.758(57)	8.794(1.212)	0.194(19)	0.417(456)	0.591(42)	0.424(533)	1.694(119)	0.219(18)	0.089(241)	0.214(52)	-0.281(267)
0.146	0.999(96)	0.439(379)	0.216(29)	0.014(101)	-0.013(86)	0.703(131)	3.389(1.746)	0.197(40)	0.258(541)	0.375(137)	0.989(1.021)	1.673(281)	0.246(64)	-0.271(473)	0.213(118)	0.524(325)
✓0.180	1.001(19)	0.618(65)	0.294(8)	0.111(25)	-0.060(14)	0.576(22)	4.205(277)	0.182(9)	0.297(116)	0.534(26)	-0.118(128)	1.446(54)	0.221(16)	-0.143(91)	0.269(31)	-0.033(58)
✓0.183	1.002(45)	0.283(182)	0.294(17)	0.020(55)	-0.059(41)	0.595(70)	3.457(872)	0.189(27)	0.085(336)	0.588(57)	-0.621(359)	1.457(127)	0.226(26)	-0.038(166)	0.114(52)	0.078(188)
✓0.197	0.932(24)	0.544(73)	0.276(10)	0.142(26)	-0.039(18)	0.520(26)	3.675(321)	0.178(10)	0.223(168)	0.523(34)	-0.207(174)	1.249(58)	0.213(17)	-0.006(95)	0.260(31)	0.074(61)
0.220																
0.227	0.686(255)	1.292(886)	0.160(108)	-0.149(231)	-0.189(220)	-0.013(270)		0.037(88)		0.140(176)	0.394(333)	0.969(831)	0.282(200)	-0.052(147)	-0.164(376)	0.616(794)
✓0.261	0.850(31)	0.504(80)	0.276(13)	0.088(34)	-0.045(17)	0.527(33)	2.909(300)	0.186(14)	0.350(146)	0.483(42)	-0.049(158)	1.201(71)	0.193(24)	0.098(104)	0.199(43)	0.031(73)
0.290																
✓0.292	0.735(28)	0.461(76)	0.261(12)	0.099(27)	-0.039(16)	0.498(34)	2.758(287)	0.184(13)	0.301(148)	0.497(40)	-0.320(140)	0.990(63)	0.216(22)	-0.114(87)	0.205(33)	-0.047(70)
✓0.336	0.633(43)	0.399(104)	0.235(19)	0.098(43)	-0.024(21)	0.352(47)	1.122(351)	0.145(18)	0.291(186)	0.540(90)	-0.357(268)	0.911(96)	0.131(42)	0.108(142)	0.181(54)	0.125(81)
✓0.344	0.812(130)	0.733(320)	0.257(43)	0.203(98)	-0.058(42)	0.459(156)	1.376(942)	0.077(52)	-0.005(383)	0.414(111)	0.209(458)	0.924(215)	0.186(54)	0.047(223)	0.153(86)	-0.115(226)
0.359						—			—							
✓0.395	0.594(31)	0.251(64)	0.200(12)	0.115(27)	-0.017(13)	0.375(30)	—	0.141(13)	—	0.191(23)	0.298(22)	0.705(56)	0.088(20)	0.078(15)	0.176(39)	-0.047(46)
✓0.407	0.546(34)	0.259(66)	0.203(15)	0.088(28)	-0.027(13)	0.367(38)	1.249(229)	0.126(14)	0.147(105)	0.465(64)	-0.265(145)	0.712(67)	0.162(36)	-0.004(92)	0.178(40)	0.032(52)
✓0.418	0.590(111)	0.220(219)	0.205(41)	0.015(70)	-0.073(40)	0.314(143)	0.835(744)	0.123(53)	0.336(296)	0.376(119)	-0.351(317)	0.878(200)	0.131(52)	0.170(161)	0.103(90)	0.218(200)
✓0.463	0.624(70)	0.490(136)	0.235(26)	0.078(46)	-0.019(23)	0.504(80)	1.616(385)	0.145(28)	0.314(191)	0.355(80)	0.159(190)	0.705(115)	0.196(45)	0.004(113)	0.157(56)	0.059(96)
✓0.490	0.485(24)	0.332(43)	0.202(11)	0.094(19)	-0.031(9)	0.350(30)	1.317(187)	0.132(10)	0.269(125)	0.306(55)	-0.021(114)	0.577(42)	0.117(39)	0.049(80)	0.133(27)	-0.016(33)
A_0	1.811(7)	1.122(166)	0.365(9)	0.156(35)	-0.117(104)	0.809(29)	20.949(8.515)	0.216(10)	0.283(162)	0.747(26)	-0.331(270)	2.529(99)	0.267(12)	-0.333(706)	0.336(43)	0.043(98)
m_A	0.630(55)	0.698(75)	2.046(825)	1.187(360)	0.408(764)	0.933(450)	0.357(165)	2.424(207)	3.295(1.718)	0.929(783)	1.093(609)	1.327(38)	2.236(366)	0.455(330)	1.785(241)	0.3
p	1.617(231)	2.	5.579(4.177)	2.	1.109(1.84)	1.912(1.528)	1.837(665)	5.996(136)	3.965(16.812)	1.615(2.407)	3.5	6.000(9)	5.976(1.328)	3.5	6.	1
$\overline{\chi^2}$	0.820(450)	1.262(567)	0.851(463)	0.781(589)	0.414(341)	1.207(614)	1.395(741)	0.840(518)	0.292(272)	0.578(380)	0.990(544)	0.815(536)	0.599(377)	0.637(423)	0.964(654)	0.835(488)

Q^2	$A_{10}^{(d)}$	$B_{10}^{(d)}$	$A_{20}^{(d)}$	$B_{20}^{(d)}$	$C_{20}^{(d)}$	$\tilde{A}_{10}^{(d)}$	$\tilde{B}_{10}^{(d)}$	$\tilde{A}_{20}^{(d)}$	$\tilde{B}_{20}^{(d)}$	$A_{T10}^{(d)}$	$\tilde{A}_{T10}^{(d)}$	$\bar{B}_{T10}^{(d)}$	$A_{T20}^{(d)}$	$\tilde{A}_{T20}^{(d)}$	$\bar{B}_{T20}^{(d)}$	$\bar{B}_{T21}^{(d)}$
✓0.000	0.915(3)		0.150(5)			-0.269(17)		-0.051(7)		-0.206(16)			-0.031(8)			
0.068	0.515(63)	-1.562(495)	0.105(27)	-0.228(157)	-0.106(195)	-0.232(87)	—	-0.062(27)	—	0.029(58)	0.341(168)	0.852(420)	-0.017(50)	0.019(82)	0.049(205)	0.227(697)
✓0.094	0.602(7)	-0.980(48)	0.128(4)	-0.122(18)	-0.062(14)	-0.230(12)	-2.405(301)	-0.035(5)	-0.074(134)	-0.184(17)	1.019(167)	1.194(41)	-0.030(9)	0.046(93)	0.190(20)	-0.111(59)
✓0.095	0.585(16)	-1.074(127)	0.124(7)	-0.145(33)	-0.079(37)	-0.196(32)	-3.088(703)	-0.052(12)	-0.624(283)	-0.116(22)	0.508(281)	1.015(81)	-0.023(10)	0.067(135)	0.165(36)	0.253(191)
0.146	0.403(51)	-0.899(244)	0.079(16)	-0.130(62)	-0.036(50)	-0.066(73)	-0.712(946)	-0.015(23)	0.061(311)	-0.154(82)	1.626(630)	0.867(180)	-0.029(36)	0.128(277)	0.108(73)	0.115(205)
✓0.180	0.435(10)	-0.734(41)	0.111(4)	-0.126(16)	-0.051(8)	-0.181(14)	-1.262(160)	-0.034(5)	-0.120(70)	-0.148(17)	0.620(86)	0.868(34)	-0.022(10)	0.077(55)	0.139(17)	-0.019(36)
✓0.183	0.422(26)	-0.927(122)	0.112(9)	-0.099(35)	-0.068(25)	-0.206(40)	-1.895(511)	-0.026(15)	-0.333(199)	-0.089(35)	0.314(228)	0.899(86)	-0.022(14)	0.130(107)	0.099(40)	0.040(127)
✓0.197	0.411(12)	-0.729(50)	0.103(4)	-0.118(16)	-0.031(11)	-0.208(17)	-1.575(213)	-0.030(6)	0.106(108)	-0.136(21)	0.659(112)	0.851(41)	-0.038(11)	0.086(61)	0.167(21)	-0.024(43)
0.220																
0.227	0.246(124)	0.783(593)	0.008(61)	-0.155(173)	0.112(146)	-0.057(170)	—	0.016(54)	—	-0.073(108)	0.424(205)	1.068(513)	-0.036(120)	0.044(101)	0.113(258)	-0.190(530)
✓0.261	0.346(15)	-0.658(56)	0.093(7)	-0.113(21)	-0.043(10)	-0.164(21)	-0.908(180)	-0.021(8)	0.088(83)	-0.105(25)	0.362(103)	0.770(45)	-0.029(16)	0.103(68)	0.099(25)	-0.013(46)
0.290																
✓0.292	0.284(15)	-0.531(48)	0.087(6)	-0.085(17)	-0.033(11)	-0.181(21)	-0.802(181)	-0.027(8)	-0.004(99)	-0.097(24)	0.368(95)	0.643(43)	-0.01(13)	-0.024(57)	0.135(23)	-0.079(43)
✓0.336	0.232(21)	-0.510(70)	0.085(10)	-0.072(26)	-0.019(13)	-0.172(27)	-0.703(203)	-0.029(10)	0.066(113)	-0.162(41)	0.590(130)	0.618(64)	-0.033(25)	0.102(90)	0.155(36)	-0.018(56)
✓0.344	0.284(53)	-0.457(168)	0.087(18)	-0.170(53)	-0.032(26)	-0.138(73)	-1.00(458)	-0.048(29)	-0.120(203)	-0.046(60)	-0.011(234)	0.498(124)	-0.048(28)	0.095(119)	0.150(61)	-0.006(132)
0.359																
✓0.395	0.220(17)	-0.378(37)	0.080(7)	-0.050(17)	-0.039(9)	-0.122(17)	—	-0.029(8)	—	-0.047(15)	0.173(14)	0.441(36)	-0.035(12)	0.045(10)	0.119(26)	-0.118(32)
✓0.407	0.192(17)	-0.408(45)	0.064(7)	-0.080(18)	-0.012(8)	-0.128(21)	-0.531(130)	-0.030(8)	-0.059(66)	-0.062(35)	0.258(84)	0.482(46)	-0.026(19)	0.072(53)	0.102(24)	-0.014(33)
✓0.418	0.179(49)	-0.659(173)	0.057(18)	-0.092(49)	-0.021(23)	-0.164(91)	-0.969(476)	-0.002(31)	0.082(184)	-0.053(75)	-0.019(214)	0.520(131)	-0.049(33)	0.140(109)	0.091(61)	0.166(124)
✓0.463	0.198(33)	-0.481(86)	0.067(12)	-0.144(31)	-0.043(15)	-0.125(45)	-0.524(234)	-0.035(17)	0.037(122)	-0.102(48)	0.500(120)	0.593(80)	-0.027(25)	0.073(67)	0.146(36)	-0.069(63)
✓0.490	0.178(14)	-0.275(28)	0.066(6)	-0.048(12)	-0.026(6)	-0.114(14)	-0.383(112)	-0.033(6)	0.015(80)	-0.059(35)	0.172(73)	0.384(28)	-0.034(23)	0.054(47)	0.093(19)	-0.041(23)
A_0	0.915(3)	-1.380(75)	0.151(5)	-0.171(23)	-0.115(54)	-0.269(15)	-5.983(3.588)	-0.044(7)	-1.236(2.018)	-0.204(15)	1.341(294)	1.554(105)	-0.028(7)	0.075(45)	0.205(29)	-0.046(18)
m_A	0.740(84)	1.315(47)	1.743(564)	1.620(189)	0.349(123)	1.786(386)	0.403(311)	1.024(339)	0.510(237)	1.502(1.648)	0.844(115)	1.221(866)	3.123(5.925)	3.134(4.963)	1.051(192)	3.3
p	2.641(523)	6.	5.804(3.432)	6.	1.	5.877(2.186)	1.913(1.289)	1.5	6.	5.554(10.616)	3.5	4.873(5.969)	1.5	3.5	2.	1
$\overline{\chi^2}$	0.607(412)	1.119(726)	0.386(287)	1.416(795)	1.018(562)	0.503(354)	0.615(542)	0.760(442)	1.143(654)	1.166(673)	1.678(827)	1.285(626)	0.416(337)	0.370(310)	0.808(560)	1.306(709)

Table A.14: MILC-20^3-m007-unchopped — data set 10

Q^2	$A_{10}^{(u)}$	$B_{10}^{(u)}$	$A_{20}^{(u)}$	$B_{20}^{(u)}$	$C_{20}^{(u)}$	$\tilde{A}_{10}^{(u)}$	$\tilde{B}_{10}^{(u)}$	$\tilde{A}_{20}^{(u)}$	$\tilde{B}_{20}^{(u)}$	$A_{T10}^{(u)}$	$\tilde{A}_{T10}^{(u)}$	$\bar{B}_{T10}^{(u)}$	$A_{T20}^{(u)}$	$\tilde{A}_{T20}^{(u)}$	$\bar{B}_{T20}^{(u)}$	$\tilde{B}_{T21}^{(u)}$
✓0.000	1.812(2)	—	0.378(5)	—	—	0.791(14)	—	0.209(6)	—	0.733(12)	—	—	0.231(5)	—	—	—
0.042	1.560(22)	1.436(219)	0.353(11)	0.165(77)	-0.231(109)	0.782(32)	—	0.197(11)	—	0.639(22)	0.994(65)	2.471(162)	0.218(15)	0.141(34)	0.348(85)	0.090(323)
✓0.049	1.505(4)	1.039(51)	0.350(4)	0.135(16)	-0.091(14)	0.714(12)	10.966(351)	0.196(5)	-0.013(140)	0.693(11)	-0.885(155)	2.171(32)	0.221(6)	-0.020(81)	0.348(17)	-0.056(47)
✓0.049	1.498(6)	1.067(88)	0.334(5)	0.153(26)	-0.008(28)	0.730(17)	11.338(548)	0.190(7)	-0.218(195)	0.679(14)	-0.793(210)	2.163(44)	0.216(6)	-0.079(95)	0.366(22)	-0.196(141)
0.086	1.341(21)	1.237(146)	0.321(9)	0.199(42)	-0.089(27)	0.703(28)	7.075(666)	0.193(10)	0.246(209)	0.648(27)	-0.194(297)	2.047(74)	0.211(13)	-0.108(136)	0.333(36)	-0.097(95)
✓0.096	1.285(6)	0.916(44)	0.324(4)	0.119(15)	-0.076(7)	0.660(12)	7.205(203)	0.190(5)	0.328(68)	0.642(10)	-0.553(71)	1.848(26)	0.211(5)	-0.070(41)	0.319(15)	-0.005(26)
✓0.097	1.269(9)	0.913(73)	0.310(5)	0.124(23)	-0.054(16)	0.650(19)	6.847(391)	0.189(8)	0.289(144)	0.638(14)	-0.720(141)	1.855(41)	0.207(6)	-0.096(69)	0.333(20)	-0.068(79)
✓0.101	1.250(9)	0.839(53)	0.314(4)	0.128(18)	-0.042(11)	0.640(13)	7.340(260)	0.186(5)	0.391(111)	0.610(14)	-0.464(116)	1.758(34)	0.208(6)	-0.021(64)	0.309(17)	-0.079(40)
0.128	1.172(23)	1.094(120)	0.299(9)	0.157(38)	-0.065(23)	0.647(29)	5.425(467)	0.185(11)	0.135(167)	0.624(28)	-0.452(224)	1.761(63)	0.224(13)	-0.246(109)	0.315(29)	-0.037(83)
0.142	1.117(8)	0.814(41)	0.300(4)	0.106(15)	-0.059(8)	0.609(13)	5.271(173)	0.182(5)	0.309(67)	0.592(12)	-0.388(78)	1.583(25)	0.204(6)	-0.059(44)	0.295(14)	0.004(27)
✓0.149	1.124(75)	1.146(241)	0.305(28)	0.129(77)	-0.133(75)	0.646(70)	—	0.196(25)	—	0.482(46)	0.728(76)	1.786(189)	0.203(31)	0.104(39)	0.245(99)	0.174(197)
✓0.150	1.077(10)	0.706(45)	0.288(4)	0.112(15)	-0.031(9)	0.586(14)	5.160(203)	0.178(5)	0.377(91)	0.565(13)	-0.367(92)	1.495(30)	0.194(6)	-0.025(50)	0.279(15)	-0.042(32)
0.185	0.985(11)	0.654(40)	0.286(5)	0.095(14)	-0.063(8)	0.559(13)	3.909(179)	0.167(5)	0.068(85)	0.575(16)	-0.431(93)	1.391(26)	0.203(8)	-0.120(53)	0.276(15)	-0.017(31)
✓0.186	0.970(16)	0.690(70)	0.271(6)	0.118(22)	-0.036(13)	0.557(22)	3.946(279)	0.155(8)	-0.096(120)	0.566(18)	-0.397(119)	1.383(41)	0.204(8)	-0.185(61)	0.305(20)	-0.130(51)
✓0.187	0.998(67)	1.107(189)	0.280(22)	0.165(58)	-0.070(38)	0.610(61)	3.253(695)	0.183(23)	0.360(240)	0.524(79)	0.070(430)	1.546(132)	0.209(36)	-0.175(212)	0.258(63)	-0.018(112)
0.201	0.938(13)	0.586(42)	0.277(6)	0.104(18)	-0.043(12)	0.543(13)	—	0.163(6)	—	0.367(10)	0.515(14)	1.252(34)	0.156(7)	0.108(8)	0.255(20)	-0.058(35)
✓0.210	0.931(31)	0.855(119)	0.258(11)	0.166(36)	-0.027(19)	0.590(39)	3.591(398)	0.165(14)	0.032(160)	0.531(33)	-0.241(188)	1.320(72)	0.197(16)	-0.158(93)	0.313(32)	-0.112(74)
✓0.227	0.881(11)	0.605(34)	0.267(4)	0.089(12)	-0.049(5)	0.528(13)	3.156(111)	0.163(5)	0.119(51)	0.539(13)	-0.338(52)	1.234(23)	0.191(7)	-0.068(32)	0.264(13)	-0.006(20)
✓0.229	0.861(17)	0.558(59)	0.253(6)	0.104(20)	-0.024(9)	0.501(24)	2.955(209)	0.155(8)	-0.020(79)	0.531(18)	-0.349(83)	1.224(40)	0.194(8)	-0.112(41)	0.272(18)	-0.049(40)
✓0.243	0.828(13)	0.535(41)	0.253(5)	0.080(14)	-0.039(8)	0.506(17)	2.987(153)	0.154(6)	0.114(84)	0.508(16)	-0.265(75)	1.129(29)	0.186(8)	-0.070(43)	0.268(15)	-0.033(32)
✓0.251	0.827(12)	0.522(33)	0.257(5)	0.091(13)	-0.036(7)	0.505(12)	3.291(143)	0.160(5)	0.425(90)	0.493(19)	-0.255(72)	1.103(25)	0.184(10)	-0.054(44)	0.241(14)	-0.032(21)
A_0	1.812(2)	1.247(65)	0.375(5)	0.156(19)	-0.106(20)	0.792(14)	20.345(2.384)	0.209(6)	0.297(101)	0.738(12)	-1.051(192)	2.612(59)	0.228(6)	-0.080(31)	0.380(19)	-0.058(51)
m_A	0.643(26)	1.299(41)	0.908(484)	1.627(181)	0.364(63)	0.844(26)	0.327(68)	2.209(436)	1.432(413)	1.104(626)	0.727(88)	0.830(205)	1.317(579)	3.3	1.070(70)	0.494(515)
p	1.665(123)	6.0000(3)	1.507(1.776)	5.982(314)	1.	1.5	1.603(303)	5.726(2.085)	6.	2.000(2.107)	3.5	2.709(1.1)	1.509(1.435)	3.5	2.	1
$\overline{\chi^2}$	0.503(418)	1.406(1.095)	1.615(840)	0.617(569)	2.528(1.155)	0.490(472)	1.434(827)	0.601(423)	4.020(1.768)	0.796(524)	0.495(395)	1.076(886)	0.372(336)	0.719(621)	0.751(674)	0.998(698)

Q^2	$A_{10}^{(d)}$	$B_{10}^{(d)}$	$A_{20}^{(d)}$	$B_{20}^{(d)}$	$C_{20}^{(d)}$	$\tilde{A}_{10}^{(d)}$	$\tilde{B}_{10}^{(d)}$	$\tilde{A}_{20}^{(d)}$	$\tilde{B}_{20}^{(d)}$	$A_{T10}^{(d)}$	$\tilde{A}_{T10}^{(d)}$	$\bar{B}_{T10}^{(d)}$	$A_{T20}^{(d)}$	$\tilde{A}_{T20}^{(d)}$	$\bar{B}_{T20}^{(d)}$	$\tilde{B}_{T21}^{(d)}$
✓0.000	0.918(10)	—	0.156(3)	—	—	-0.255(9)	—	-0.045(3)	—	-0.191(7)	—	—	-0.041(3)	—	—	—
0.042	0.751(13)	-1.181(138)	0.148(6)	-0.106(46)	-0.188(66)	-0.224(19)	—	-0.044(6)	—	-0.157(11)	0.592(43)	1.482(108)	-0.024(8)	0.088(24)	0.221(61)	0.139(188)
✓0.049	0.735(2)	-1.207(26)	0.142(2)	-0.175(10)	-0.079(8)	-0.233(7)	-3.617(183)	-0.046(3)	-0.242(69)	-0.169(7)	0.809(76)	1.428(19)	-0.039(3)	0.104(42)	0.217(10)	-0.047(27)
✓0.049	0.735(4)	-1.141(43)	0.136(3)	-0.157(14)	-0.077(18)	-0.220(10)	-3.511(292)	-0.043(4)	-0.213(102)	-0.158(8)	0.713(115)	1.414(28)	-0.034(3)	0.061(55)	0.200(13)	-0.150(86)
0.086	0.626(12)	-0.953(85)	0.132(4)	-0.115(25)	-0.083(15)	-0.188(17)	-2.117(368)	-0.037(6)	-0.088(125)	-0.143(15)	0.808(170)	1.284(50)	-0.024(7)	0.005(85)	0.186(24)	-0.065(60)
✓0.096	0.603(3)	-1.003(23)	0.129(2)	-0.153(9)	-0.068(4)	-0.209(7)	-2.224(99)	-0.042(3)	-0.088(39)	-0.158(6)	0.829(44)	1.206(17)	-0.037(3)	0.080(23)	0.203(9)	-0.048(16)
✓0.097	0.602(5)	-0.975(40)	0.124(3)	-0.146(13)	-0.064(10)	-0.199(11)	-2.220(210)	-0.037(4)	-0.072(77)	-0.146(8)	0.746(84)	1.186(26)	-0.032(3)	0.054(40)	0.181(13)	-0.103(49)
✓0.101	0.594(5)	-0.981(30)	0.125(2)	-0.147(12)	-0.048(6)	-0.209(7)	-2.249(154)	-0.043(3)	-0.107(72)	-0.156(7)	0.781(66)	1.176(23)	-0.034(4)	0.098(35)	0.192(12)	-0.041(23)
0.128	0.531(14)	-0.839(73)	0.120(5)	-0.132(22)	-0.069(12)	-0.164(17)	-1.270(264)	-0.029(6)	-0.034(101)	-0.133(15)	0.702(127)	1.112(46)	-0.019(7)	-0.039(63)	0.177(21)	-0.089(57)
0.142	0.504(4)	-0.849(23)	0.118(2)	-0.142(9)	-0.055(4)	-0.188(7)	-1.518(96)	-0.038(3)	-0.051(42)	-0.154(7)	0.780(44)	1.037(16)	-0.036(4)	0.077(28)	0.189(9)	-0.043(18)
✓0.149	0.509(39)	-0.824(145)	0.143(15)	-0.090(48)	-0.115(45)	-0.182(39)	—	-0.042(13)	—	-0.092(24)	0.449(55)	1.130(139)	-0.003(18)	0.070(24)	0.175(61)	0.140(130)
✓0.150	0.492(5)	-0.834(25)	0.113(2)	-0.127(10)	-0.042(5)	-0.189(8)	-1.608(116)	-0.039(3)	-0.073(61)	-0.143(7)	0.691(53)	0.993(19)	-0.031(4)	0.074(29)	0.169(10)	-0.020(20)
0.185	0.432(6)	-0.733(24)	0.111(3)	-0.123(10)	-0.056(5)	-0.182(8)	-1.348(101)	-0.040(4)	-0.136(45)	-0.123(9)	0.508(48)	0.904(17)	-0.030(4)	0.081(30)	0.175(9)	-0.016(18)
✓0.186	0.433(9)	-0.657(40)	0.104(3)	-0.117(13)	-0.055(8)	-0.168(13)	-1.261(163)	-0.039(5)	-0.160(67)	-0.115(11)	0.491(70)	0.877(27)	-0.024(5)	0.029(37)	0.175(13)	-0.101(33)
✓0.187	0.441(35)	-0.692(115)	0.126(12)	-0.069(37)	-0.072(24)	-0.133(35)	-0.868(400)	-0.033(11)	-0.049(145)	-0.116(43)	0.701(265)	1.011(98)	-0.011(22)	0.076(130)	0.165(41)	0.058(71)
0.201	0.422(8)	-0.695(23)	0.103(3)	-0.130(11)	-0.040(7)	-0.174(8)	—	-0.039(3)	—	-0.096(6)	0.335(9)	0.846(22)	-0.029(4)	0.062(5)	0.157(13)	-0.041(21)
✓0.210	0.397(17)	-0.554(75)	0.101(6)	-0.104(21)	-0.051(12)	-0.137(22)	-1.057(225)	-0.030(8)	-0.125(89)	-0.102(19)	0.431(118)	0.854(48)	-0.018(9)	-0.010(58)	0.176(22)	-0.117(50)
✓0.227	0.374(6)	-0.645(22)	0.103(2)	-0.112(9)	-0.048(3)	-0.163(7)	-0.999(63)	-0.036(3)	-0.091(28)	-0.122(8)	0.502(33)	0.802(16)	-0.030(4)	0.069(19)	0.166(9)	-0.034(13)
✓0.229	0.370(9)	-0.626(38)	0.098(3)	-0.108(12)	-0.049(6)	-0.162(13)	-1.029(123)	-0.035(5)	-0.125(50)	-0.109(10)	0.461(51)	0.773(27)	-0.026(5)	0.047(28)	0.155(12)	-0.085(28)
✓0.243	0.357(6)	-0.630(25)	0.096(3)	-0.107(9)	-0.042(5)	-0.164(10)	-1.029(101)	-0.040(4)	-0.104(46)	-0.112(9)	0.445(44)	0.751(19)	-0.026(4)	0.058(25)	0.159(10)	-0.037(19)
✓0.251	0.357(7)	-0.603(18)	0.095(3)	-0.113(8)	-0.035(4)	-0.156(7)	-0.813(83)	-0.038(3)	-0.009(51)	-0.135(11)	0.520(45)	0.727(18)	-0.026(7)	0.055(28)	0.149(9)	-0.022(14)
A_0	0.918(10)	-1.473(35)	0.156(3)	-0.191(12)	-0.095(9)	-0.256(9)	-6.982(617)	-0.046(3)	-0.257(195)	-0.188(7)	1.059(74)	1.729(32)	-0.041(3)	0.101(34)	0.227(12)	-0.063(24)
m_A	0.702(33)	0.664(14)	0.810(21)	0.852(52)	0.437(41)	0.803(69)	0.301(29)	1.233(197)	0.320(233)	0.801(58)	0.982(56)	0.749(121)	1.162(2.818)	1.122(356)	1.087(74)	0.561(256)
p	2.344(207)	2.	1.5	2.	1.	1.503(198)	1.545(138)	1.5	1.	1.5	3.5	2.311(599)	2.906(13.385)	3.5	2.	1
$\overline{\chi^2}$	0.170(229)	0.814(798)	1.113(725)	0.508(579)	1.778(1.123)	0.509(523)	0.390(389)	0.384(395)	0.770(662)	1.107(762)	1.087(754)	0.445(522)	0.620(534)	0.366(437)	0.521(386)	1.500(1.183)

Table A.15: MILC-28³-m01-unchopped — data set 11

Appendix B

Plots of Transverse Parton Distributions

B.1 Contour Plots

Figures B-1 through B-4 show contour plots of transverse quark distributions for some of the data sets studied in this thesis. Each page of plots contains results for the first and second moments of the distributions for up and down flavor quarks. The legend in the corner of each plot indicates the polarization state shown: the outer arrow shows the direction of the proton spin, and the inner arrow shows the direction of the quark spin. A missing arrow denotes the unpolarized case. The contour spacing is 0.004 for the $n = 1$ plots, and 0.002 for the $n = 2$ plots.

B.2 Three-dimensional Plots

In Figs. B-5 and B-6 we show three-dimensional views for selected cases of the contour plots in Figs. B-1 through B-4 , in order to make the statistical error bands visible. As noted elsewhere, the apparent structure on small distance scales in some of the plots is due to poorly determined fits to GFFs that are nearly zero, and is generally not statistically significant.
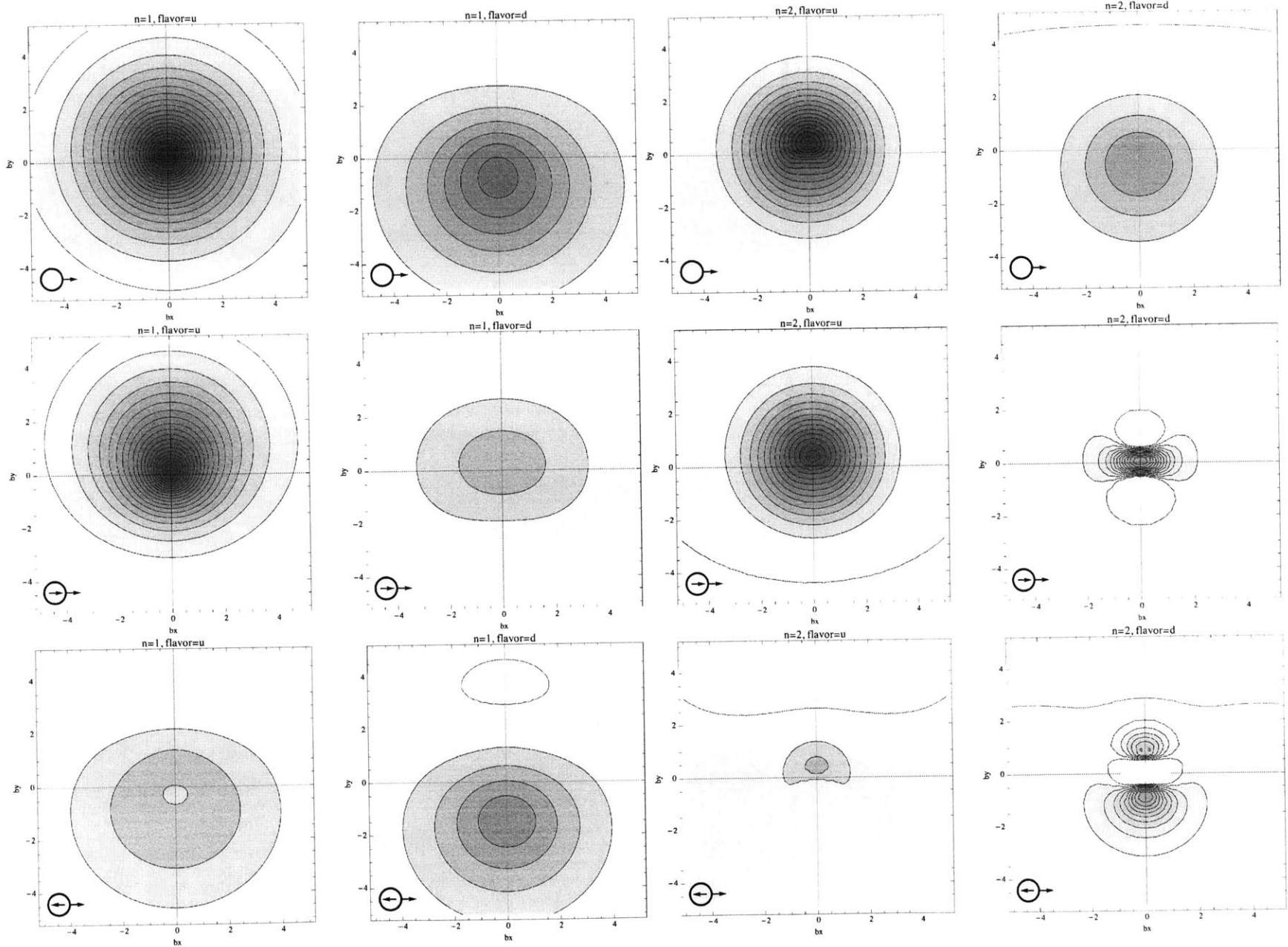
Figure B-1: Contour plots of transverse parton distributions for data set 10.

126
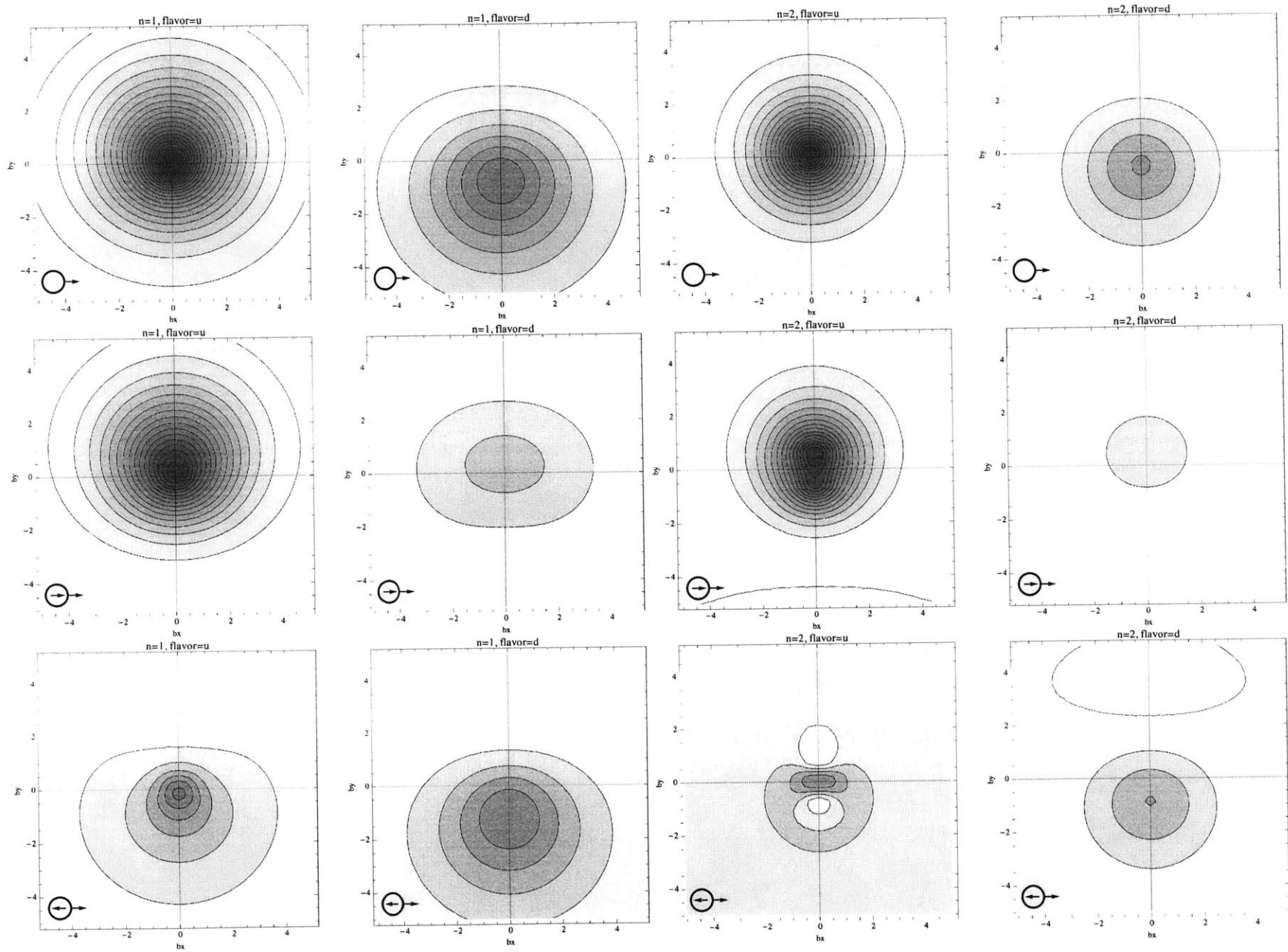
Figure B-2: Contour plots of transverse parton distributions for data set 9.
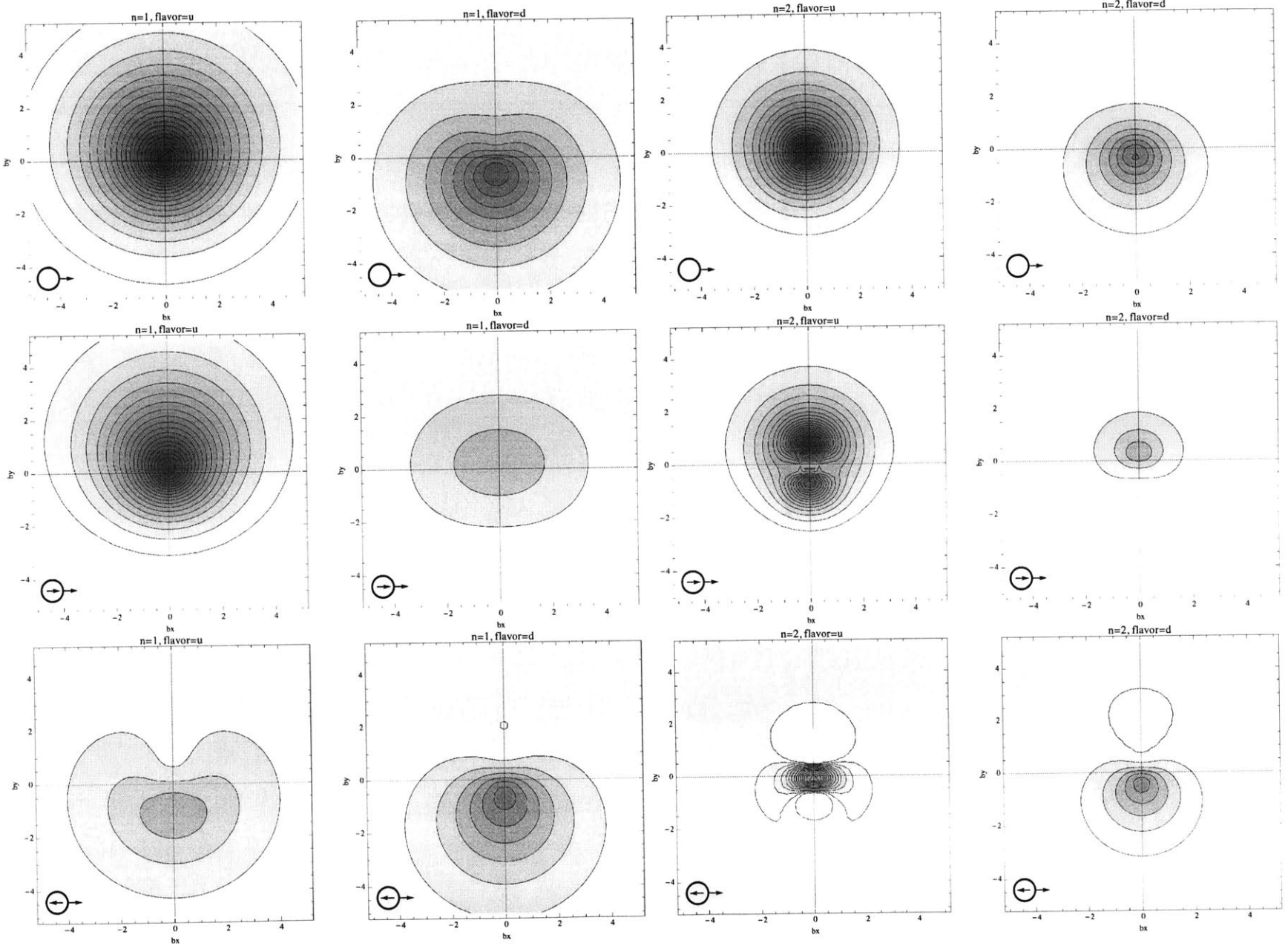
Figure B-3: Contour plots of transverse parton distributions for data set 11.

128
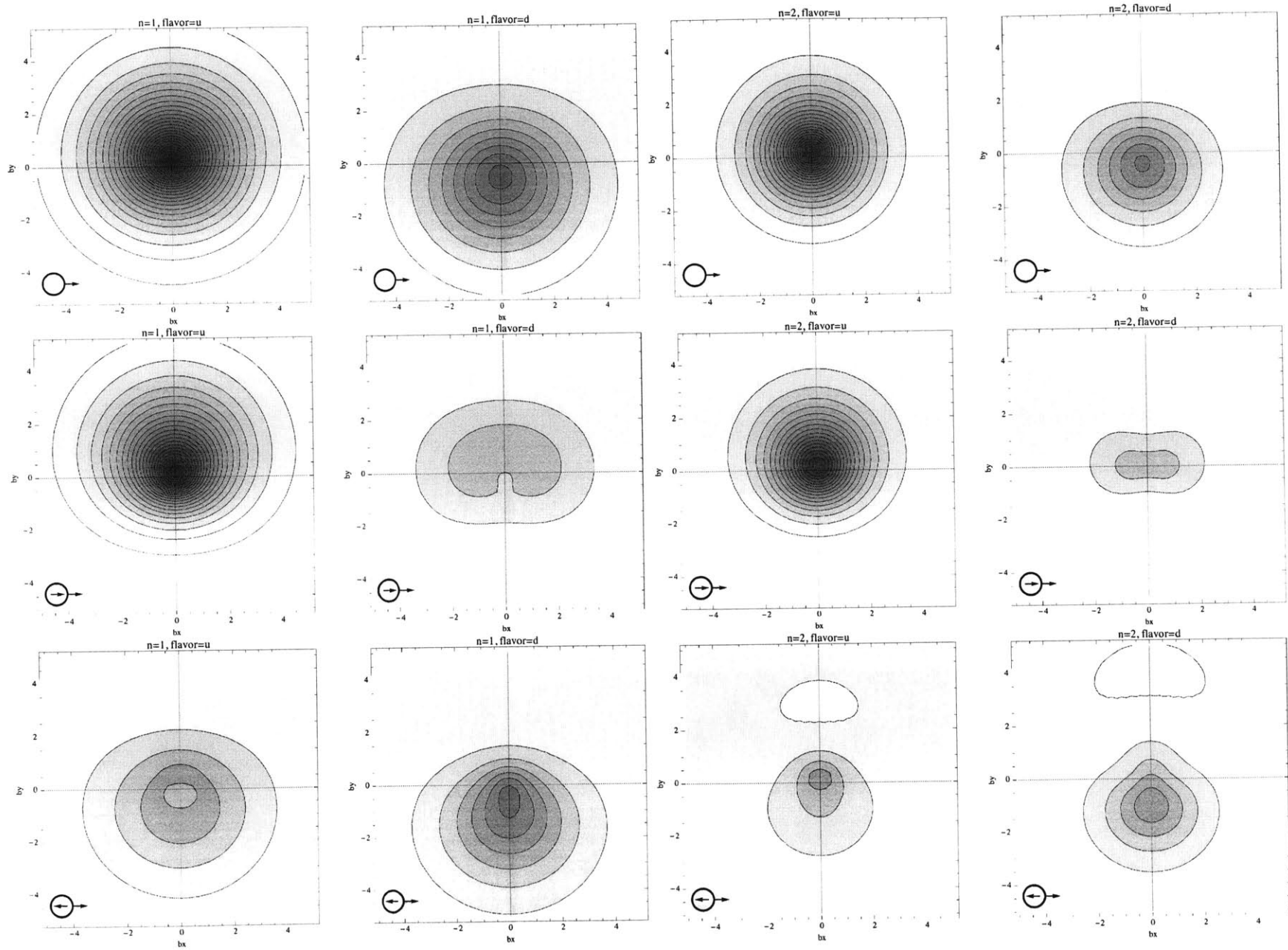
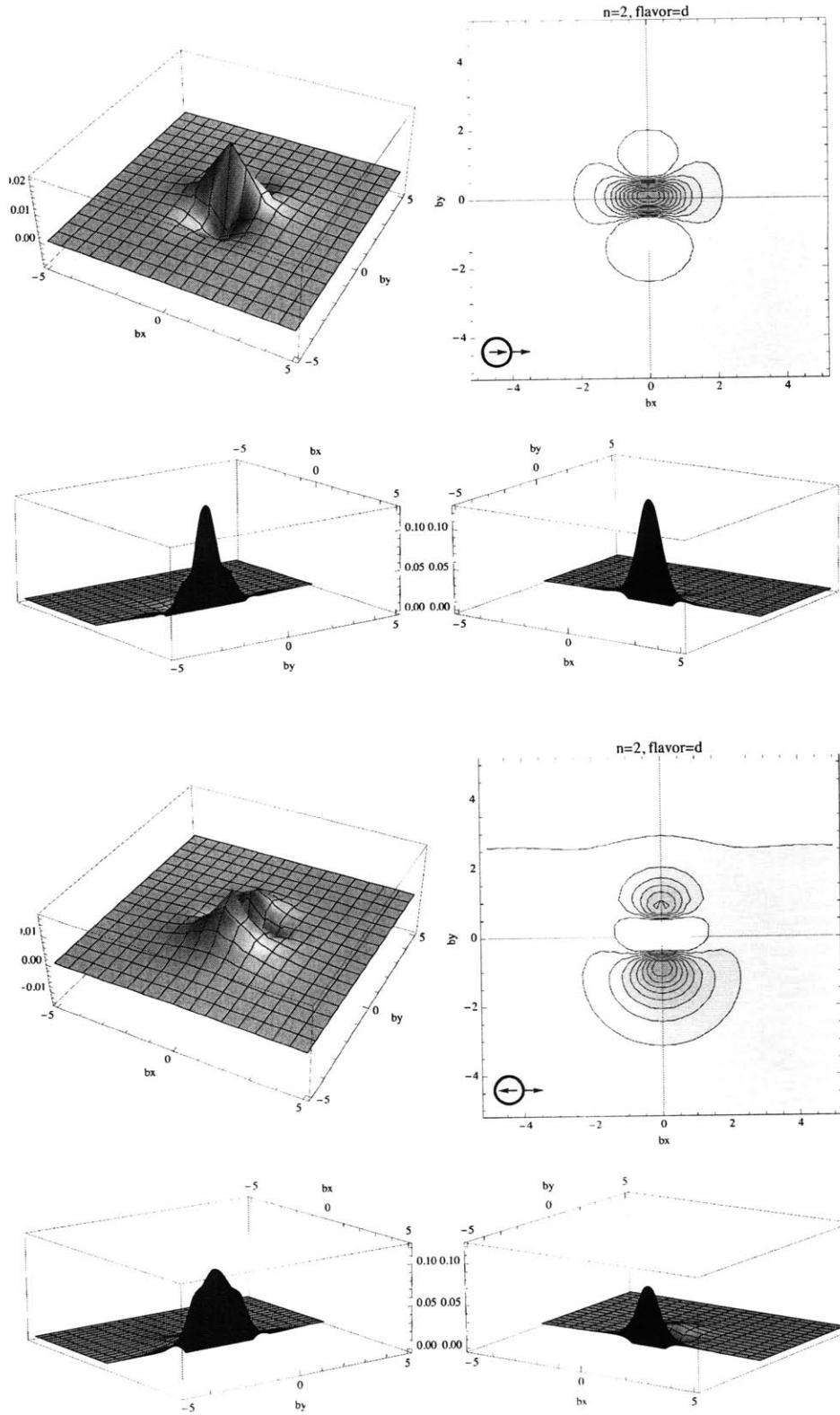Figure B-4: Contour plots of transverse parton distributions for data set 1.

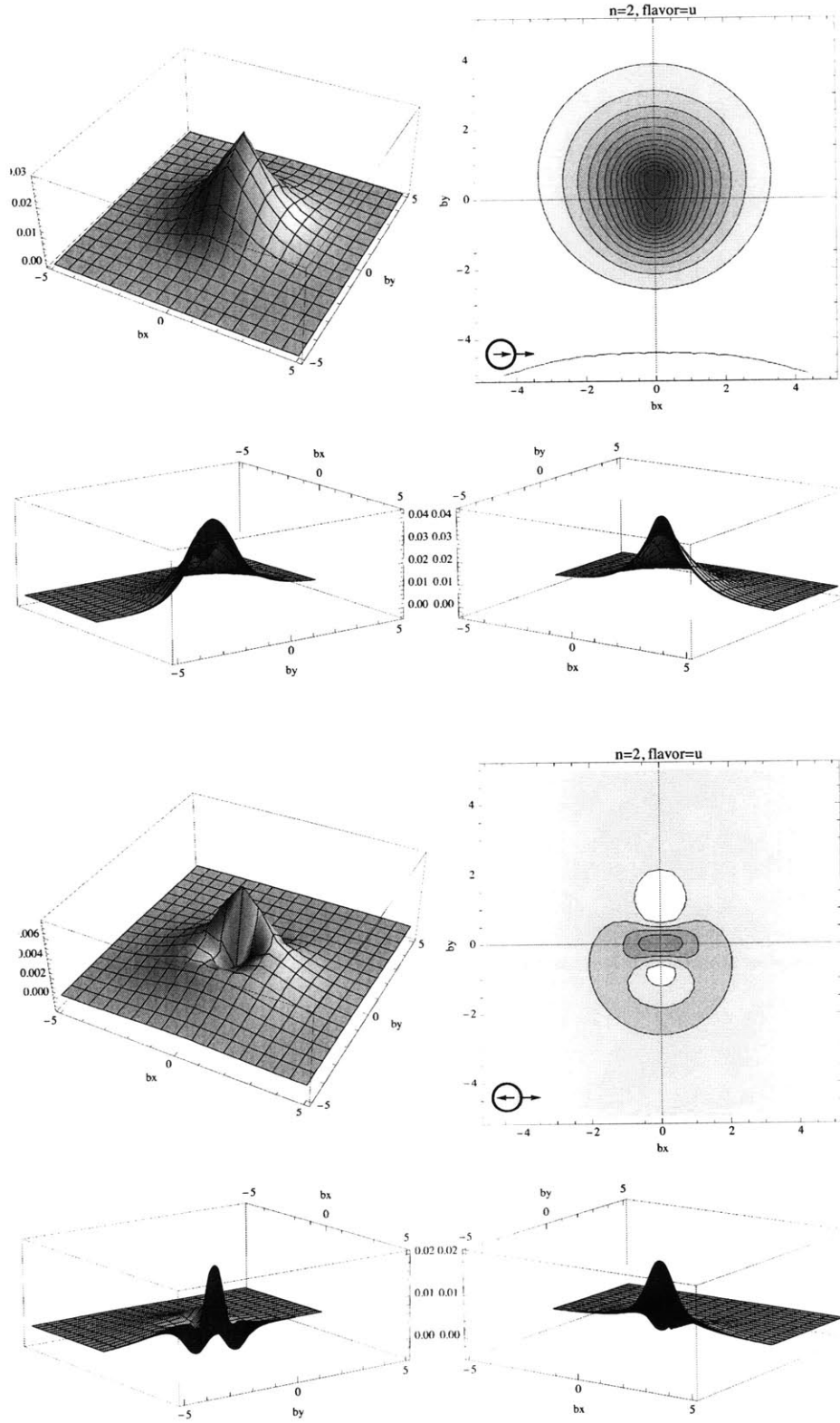Figure B-5: Detail for the $n = 2$, flavor d case of selected transverse distributions for data set 10.

Figure B-6: Detail for the $n = 2$, flavor u case of selected transverse distributions for data set 9.

Appendix C

Spin States

Here we give an explicit representation of the spin states used in this thesis. We use the dirac basis, where:

$$\gamma^0 = \begin{pmatrix} \mathbb{I} & 0 \\ 0 & -\mathbb{I} \end{pmatrix}, \qquad \gamma^i = \begin{pmatrix} 0 & \sigma^i \\ -\sigma^i & 0 \end{pmatrix}, \qquad \gamma^5 = \begin{pmatrix} 0 & \mathbb{I} \\ \mathbb{I} & 0 \end{pmatrix}. \qquad (\text{C.1})$$

C.1   Spin States in the Lab Frame

For a spin-1/2 particle at rest, we have:

$$u_+(0) \propto \begin{pmatrix} 1 \\ 0 \\ 0 \\ 0 \end{pmatrix}, \qquad u_-(0) \propto \begin{pmatrix} 0 \\ 1 \\ 0 \\ 0 \end{pmatrix} \qquad (\text{C.2})$$

for spin up and spin down, respectively.[1]

If we boost the spinors in (C.2) to a finite momentum $\mathbf{p}$, we obtain:

---

[1]The antiparticle spinors $v_\pm$ will not be considered in this discussion.

$$u_+(\mathbf{p}) = N \begin{pmatrix} 1 \\ 0 \\ \frac{p^z}{E+M} \\ \frac{p^x+ip^y}{E+M} \end{pmatrix}, \qquad u_-(\mathbf{p}) = N \begin{pmatrix} 0 \\ 1 \\ \frac{p^x-ip^y}{E+M} \\ \frac{-p^z}{E+M} \end{pmatrix}, \qquad \text{(C.3)}$$

where the standard normalization is $N = \sqrt{E+M}$. Note that the spinors in (C.3) are no longer eigenstates of the spin operator. The $+$ and $-$ labels on $u_\pm(\mathbf{p})$ should be understood as "reminders" of the spin of the original unboosted state, not as an actual spin label. For convenience, we may refer to such states as "spin up [down] states with momentum $\mathbf{p}$"; more precisely, they should be understood as "spin up [down] states, *boosted* to momentum $\mathbf{p}$."

C.2   Light Cone Helicity States

For the distributions in Eqs. 4.19 - 4.23, it is useful to define states of definite *light cone helicity* $u_\pm^{LC}(\mathbf{p})$ [30, 31]. These are states, with momentum $\mathbf{p}$ in the lab frame, that have a definite helicity when viewed from a frame moving at (nearly) light speed in the negative z-direction. In other words, $u_\pm^{LC}(\mathbf{p})$ are eigenstates of the helicity operator taken in a reference frame with $v^z \to -c$ [30]. These spinors are (written in the lab frame) [31]:

$$u_+^{LC}(\mathbf{p}) = N \begin{pmatrix} E+M+p^z \\ p^x+ip^y \\ E-M+p^z \\ p^x+ip^y \end{pmatrix}, \qquad u_-^{LC}(\mathbf{p}) = N \begin{pmatrix} -p^x+ip^y \\ E+M+p^z \\ p^x-ip^y \\ -E+M-p^z \end{pmatrix}, \qquad \text{(C.4)}$$

where we use the normalization $N = \frac{1}{\sqrt{2(E+p^z)}}$, giving $\bar{u}_s^{LC} u_s^{LC} = 2m$. Note that for $\mathbf{p} = p^z \hat{z}$ (i.e. the lab frame momentum only in the z-direction) the spinors in (C.4) coincide[2] with the ordinary lab frame helicity eigenstates $u_\pm^H(\mathbf{p})$, where:

---

[2]up to a possible phase

$$u_+^H(\mathbf{p}) = N' \begin{pmatrix} p^z + |\mathbf{p}| \\ p^x + ip^y \\ \frac{|\mathbf{p}|(p^z+|\mathbf{p}|)}{E+M} \\ \frac{|\mathbf{p}|(p^x+ip^y)}{E+M} \end{pmatrix}, \qquad u_-^H(\mathbf{p}) = N' \begin{pmatrix} -\sqrt{p^2 - p^{z2}} \\ e^{i\theta}(p^z + |\mathbf{p}|) \\ \frac{|\mathbf{p}|\sqrt{p^2-p^{z2}}}{E+M} \\ -e^{i\theta}\frac{|\mathbf{p}|(p^z+|\mathbf{p}|)}{E+M} \end{pmatrix}. \qquad (C.5)$$

The normalization here is $N' = \sqrt{\frac{E+M}{2|\mathbf{p}|(p^z+|\mathbf{p}|)}}$. (The phase $\theta \equiv \arctan(p^y/p^x)$ is not uniquely defined for $p^x, p^y \to 0$, but can be ignored in the limit where $\mathbf{p} = p^z\hat{z}$.)

C.3   Spin Projectors

The spinors in (C.4) represent the spin states selected by the "projectors" in Eq. 4.5. This can be verified explicitly by checking Eq. 4.7. For ease of notation let us define:

$$G^\pm \equiv \gamma^+ \frac{1 \pm \gamma_5}{2}. \qquad (C.6)$$

By straightforward manipulations:

$$G^+ u_+^{LC} = \sqrt{(E + p^z)} \begin{pmatrix} 1 \\ 0 \\ -1 \\ 0 \end{pmatrix} = \gamma^+ u_+^{LC} \qquad (C.7)$$

$$G^- u_-^{LC} = \sqrt{(E + p^z)} \begin{pmatrix} 0 \\ 1 \\ 0 \\ 1 \end{pmatrix} = \gamma^+ u_-^{LC} \qquad (C.8)$$

$$G^\pm u_\mp^{LC} = 0. \qquad (C.9)$$

From the above equations, it is easy to prove Eq. 4.7.

135

In the same way, it is straightforward to check Eq. 4.8. Thus we see that by using the projectors in Eqs. 4.5 and 4.6, we have *selected* the light-cone helicity eigenstates to be our basis states for quark spin.

C.4   Melosh Rotation

In this section, I discuss the kinematical transformation between lab frame spin states and light cone helicity states. I will closely follow the discussion found in [41]. Other useful references are [71, 72].

It was demonstrated in the previous section that the quark spin states used in Eqs. 4.19 - 4.23 are eigenstates of light-cone helicity. In writing down these equations, we have chosen to use light-cone helicity states for the *proton* spin states as well (see Appendix H). However, we will often want to calculate quantities in the lab frame. In particular, we will be interested in proton wave packets in transverse position space, which involve integrals over transverse momentum. For $p^z = 0$ but $\mathbf{p} \neq 0$, the light-cone spinors (C.4) are *not* the same as the "lab frame spin states" (C.3). Rather, we find:

$$u_+^{LC}(\mathbf{p}) = N_p \left(u_+(\mathbf{p}) + \frac{p^x + ip^y}{E + M} u_-(\mathbf{p}) \right)$$

(C.10)

$$u_-^{LC}(\mathbf{p}) = N_p \left(u_-(\mathbf{p}) - \frac{p^x - ip^y}{E + M} u_+(\mathbf{p}) \right)$$

where $N_p \equiv \sqrt{\frac{E+M}{2E}}$. If we keep the transverse momentum small[3], p^x, $p^y \ll M$, then we have:

$$u_+^{LC}(\mathbf{p}) \approx u_+(\mathbf{p}) + \frac{p^x + ip^y}{2M} u_-(\mathbf{p})$$

(C.11)

$$u_-^{LC}(\mathbf{p}) \approx u_-(\mathbf{p}) - \frac{p^x - ip^y}{2M} u_+(\mathbf{p}).$$

---

[3]In other words, if we build *large* transverse nucleon wave packets.

This transformation (C.11) is known as the *Melosh rotation*. In position space, it results in a non-trivial perpendicular shift of the wave packet for transversely polarized states. To see this, consider a particle polarized in the $\hat{x}$-direction in its rest frame, with small transverse momentum $\mathbf{p}_\perp$ in the lab frame. Then in the lab frame we have the spin state:

$$u_{+\hat{x}}(\mathbf{p}_\perp) = \frac{1}{\sqrt{2}}\big(u_+(\mathbf{p}_\perp) + u_-(\mathbf{p}_\perp)\big).$$

Let us now consider a transverse momentum space wave packet $\psi_{+\hat{x}}(\mathbf{p}_\perp)$, where $\psi_{+\hat{x}}(\mathbf{p}_\perp)$ is a symmetric function that is non-zero only for small values of $\mathbf{p}_\perp$. The corresponding position space wave packet:

$$\phi_{+\hat{x}}(\mathbf{r}_\perp) = \int d^2\mathbf{p}_\perp e^{i\mathbf{r}_\perp \cdot \mathbf{p}_\perp}\psi_{+\hat{x}}(\mathbf{p}_\perp) \tag{C.12}$$

is centered at the origin and has a large spatial extent ($RM \gg 1$). The complete state can then be written:

$$|\psi, +\hat{x}\rangle = \int d^2\mathbf{p}_\perp \psi_{+\hat{x}}(\mathbf{p}_\perp)\, u_{+\hat{x}}(\mathbf{p}_\perp) \tag{C.13}$$

$$= \int d^2\mathbf{p}_\perp \psi_{+\hat{x}}(\mathbf{p}_\perp) \left(\left(1 - \frac{ip^y}{2M}\right) u_{+\hat{x}}^{LC}(\mathbf{p}_\perp) + \frac{p^x}{2M}u_{-\hat{x}}^{LC}(\mathbf{p}_\perp) \right) \tag{C.14}$$

$$\equiv \int d^2\mathbf{p}_\perp \left(\psi_{+\hat{x}}^{LC}(\mathbf{p}_\perp)\, u_{+\hat{x}}^{LC}(\mathbf{p}_\perp) + \psi_{-\hat{x}}^{LC}(\mathbf{p}_\perp)\, u_{-\hat{x}}^{LC}(\mathbf{p}_\perp) \right), \tag{C.15}$$

where we used the Melosh rotation (C.11) in the second step. The transversely polarized light cone states are given by:

$$u_{\pm\hat{x}}^{LC}(\mathbf{p}_\perp) = \frac{1}{\sqrt{2}}\big(u_+^{LC}(\mathbf{p}_\perp) \pm u_-^{LC}(\mathbf{p}_\perp)\big).$$

We see that the "light cone wave packets" in momentum space are:

$$\psi_{+\hat{x}}^{LC}(\mathbf{p}_\perp) = \left(1 - \frac{ip^y}{2M}\right)\psi_{+\hat{x}}(\mathbf{p}_\perp) \tag{C.16}$$

$$\psi_{-\hat{x}}^{LC}(\mathbf{p}_\perp) = \frac{ip^x}{2M}\psi_{+\hat{x}}(\mathbf{p}_\perp). \tag{C.17}$$

The corresponding position space wave packets are (for $\mathbf{p}_\perp \ll M$):

$$\phi_{+\hat{x}}^{LC}(\mathbf{r}_\perp) = \phi_{+\hat{x}}\left(\mathbf{r}_\perp - \frac{\hat{y}}{2M}\right) \tag{C.18}$$

$$\phi_{-\hat{x}}^{LC}(\mathbf{r}_\perp) = \frac{-i}{2M}\frac{\partial}{\partial r_x}\phi_{+\hat{x}}(\mathbf{r}_\perp). \tag{C.19}$$

In the limit where $\phi_{+\hat{x}}(\mathbf{r}_\perp)$ describes a delocalized state (for example, a broad gaussian in position space), $\phi_{-\hat{x}}^{LC}(\mathbf{r}_\perp)$ can be ignored. Then the position space wave packet for a light cone polarized state is the same as the wave packet for the corresponding lab frame polarized state, but shifted by $\frac{1}{2M}$ in the perpendicular direction. This remarkable result is important when interpreting the results of our calculations (which were done using light cone helicity states) in the lab frame. Effectively, we will take the coordinate origin[4] of the transverse parton distributions for a nucleon polarized in the $\hat{x}$-direction (using light cone spin states) to be shifted by $-\frac{1}{2M}$ in the $\hat{y}$ direction. Burkardt explores this effect in [41]. In this thesis, we take the "Melosh shift" for granted when dealing with polarized nucleon states, and refer the reader to Burkardt's paper for a more thorough analysis.

---

[4]which we intend to correspond to the *lab frame* center of mass

Appendix D

Jackknife Error Analysis

In this Appendix we summarize key features of the jackknife method for estimating statistical errors. Here we will focus on a practical, intuitive description of the techniques used in this thesis. A more thorough treatment can be found in the excellent work by B. Efron [73].

Consider a data set consisting of N independent measurements of some quantity Q: $\{Q_1, Q_2, \cdots, Q_N\}$. For example, Q might be the value of the nucleon two-point function (for some particular source) at Euclidean time $t = 0$, calculated for an ensemble of N gauge configurations. We take the average of the N measurements

$$\bar{Q} = \frac{1}{N} \sum_i Q_i \qquad (D.1)$$

as our estimate of the "true value" of Q, and the standard error

$$\sigma = \left(\frac{1}{N(N-1)} \sum_i (Q_i - \bar{Q})^2 \right)^{1/2} \qquad (D.2)$$

as a measure of the uncertainty in our estimate $\bar{Q}$.

However, there are some quantities of interest that *cannot* be expressed as a simple average over a data set as in (D.1). For example, the overlap of a trial nucleon source with the ground state (as in Chapter 3) is extracted from a fit to the nucleon two-point function. To properly weight the data points in the fit, we must already have

a good idea of the uncertainty in each data point. The overlap resulting from such a procedure depends upon the individual configurations in an intrinsically non-linear way. In other words, the overlap is calculated for an *ensemble* of configurations, but is not well-defined on an *individual* configuration. Formula (D.2) clearly cannot be used to estimate the uncertainty in such quantities.

The jackknife is a simple, yet powerful, extension of (D.2) to "non-linear" quantities such as the overlap. Instead of treating our data set as a single ensemble of N configurations, we consider it to be a collection of N (overlapping) *sub*-ensembles of $N-1$ configurations each. The ith sub-ensemble $E_{(i)}$ is composed of all configurations *except* the ith one.[1] Now we define $Q_{(i)}$ as the quantity Q calculated for sub-ensemble $E_{(i)}$. Our estimate of the true value is given by the jackknife average:

$$Q_{(.)} = \frac{1}{N} \sum_i Q_{(i)}, \qquad (D.3)$$

and the uncertainty in $Q_{(.)}$ is estimated by the jackknife error:

$$\sigma_{JK} = \left(\frac{N-1}{N} \sum_i (Q_{(i)} - Q_{(.)})^2 \right)^{1/2}. \qquad (D.4)$$

Note that for the special case of a "linear" quantity,[2] (D.3) is identical to (D.1), and (D.4) reduces to (D.2). We take the jackknife as a *prescription* for estimating statistical errors for any quantity we calculate on an ensemble of lattices.

A big advantage of using jackknife error analysis is that correlations between quantities are dealt with in a reasonable way. For example, we expect that there exists a positive correlation between lattice three-point functions and two-point functions calculated on a particular region of a gauge configuration. When calculating the ratios of three-point functions to two-point functions as defined in Eq. 5.5, this positive correlation will tend to cancel out. In a jackknife analysis, this cancellation happens for every sub-ensemble, reducing the overall statistical fluctuation.

---

[1] Any two sub-ensembles will thus be very similar, differing only in a single configuration.
[2] That is, one for which $Q_{(i)} = \frac{1}{N-1} \sum_{j \neq i} Q_j$.

The jackknife procedure can be further extended to quantities that depend on multiple independent ensembles.[3] This is particularly useful for chiral extrapolations, which involve fits to data points from calculations at many different pion masses. Here we will describe the "super jackknife" technique invented by C. Dawson [74].

Suppose we have a collection C of M different ensembles: $C = \{E^1, E^2, \cdots, E^M\}$, with N_m configurations in ensemble E^m. Let $N_C \equiv \sum_m N_m$. Define N_C "sub-collections" in the following way:

- For ensemble E^1, construct the N_1 regular jackknife sub-ensembles in the usual way.

- For each sub-ensemble $E^1_{(i)}$, construct the sub-collection $C^1_{(i)}$ by associating $E^1_{(i)}$ with the *full* ensembles $E^{(2)}$, $E^{(3)}$, etc: $C^1_{(i)} = \{E^1_{(i)}, E^2, \cdots, E^M\}$. This defines N_1 sub-collections.

- In the same way, construct N_2 sub-collections from the sub-ensembles for E^2: $C^2_{(i)} = \{E^1, E^2_{(i)}, E^3, \cdots, E^M\}$.

- Proceed in the same manner for the rest of the ensembles, constructing in total $N_1 + N_2 + \cdots + N_M$ distinct sub-collections.

It is now completely straightforward to generalize (D.3) and (D.4) to quantities that depend on collections of ensembles: simply replace the sum over sub-ensembles with a sum over sub-collections. It is easy to check that this prescription is equivalent[4] to the original jackknife prescription for quantities defined on individual ensembles. Moreover, this prescription appropriately takes into account the correlations within a particular ensemble, while forcing correlations between different ensembles to be zero (as they should be).

The jackknife (and super jackknife) prescription is essentially a resampling scheme, where the resampled data sets are defined in a precise, deterministic way. Another common resampling scheme is the bootstrap (see [73]), which involves the generation

---

[3]Let us refer to a set of multiple ensembles as a "collection."
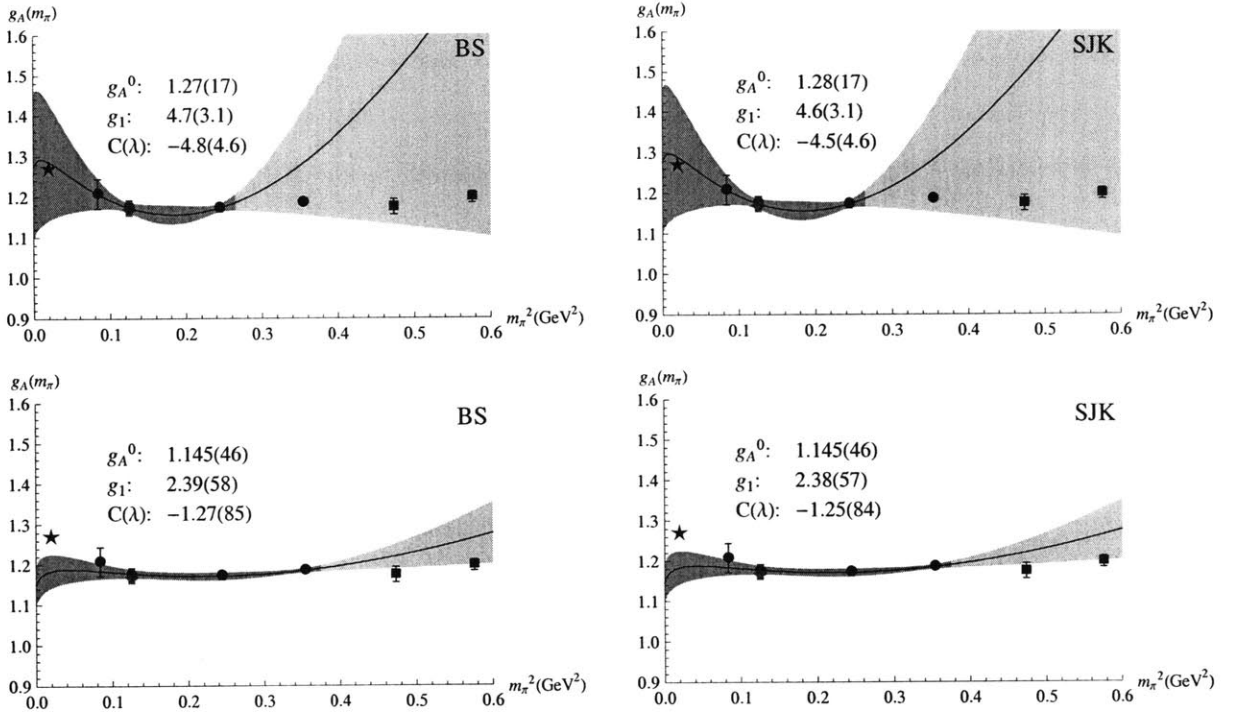[4]In the limit of large ensembles.

141

Figure D-1: Results of a comparison of a super jackknife analysis (right hand plots) with a bootstrap error analysis (left hand plots). The bootstrap analysis was done using 5000 resampled ensembles. The difference between the upper and lower plots is the range of m_π values included in the fit.

of a very large number of sample data sets drawn randomly (with replacement) from the original data set. It is interesting to compare the (super) jackknife prescription with a bootstrap analysis, to see how different they might be. Figure D-1 compares super jackknife with a bootstrap analysis of SSE chiral fits to lattice data for g_A. It is clear that the two schemes give almost identical results in these cases. Since the super jackknife procedure is computationally less demanding than bootstrap, we use super jackknife to calculate statistical uncertainties for all chiral fits presented in this thesis.

Appendix E

Studies of Fits to Form Factors

In this appendix we explore some variations of the fits discussed in Chapter 5. To test the sensitivity of the fits to the "pole ansatz," we hold p fixed rather than making it a fit parameter. In addition, we change the range of Q^2 included in the fit.

Figure E-1 shows four such fits to the GFF $A_{10}^{(u)}$ (all data from data set 9: the MILC $20^3 \times 64$, $m_q = 0.01$ unchopped ensemble). In Figs. E-2 and E-3, we show exploratory fits to $B_{10}^{(u)}$ and $\bar{B}_{T20}^{(u)}$, respectively. We are particularly interested in the variation of the extrapolation to $Q^2 = 0$ and of the slope at $Q^2 = 0$, since these are quantities that often enter into calculations of observables.

In the case of $A_{10}^{(u)}$, there is a data point at Q^2 which strongly constrains the fit— the parameter A_0 hardly changes as we vary the value of p and the range of Q^2 values fit. The systematic variation in A_0 from changing the fit ansatz is about one-third of the statistical uncertainty. However, the slope of the form factor at $Q^2 = 0$ shows much more significant variation; in particular, the slope is strongly affected by the value of p used in the fit. Changing from $p = 1.5$ to $p = 2$ caused the slope of the resulting fit at zero momentum transfer to change from 7.15(12) to 6.70(11), when fitting over the full range[1] of Q^2. This is a change of about four times the statistical uncertainty, and suggests that the systematic errors in the form factor slopes—and derived quantities such as $\langle r^2 \rangle$—are significant.

For the form factor $B_{10}^{(u)}$, lattice data is not available at $Q^2 = 0$, so the fit parameter

---

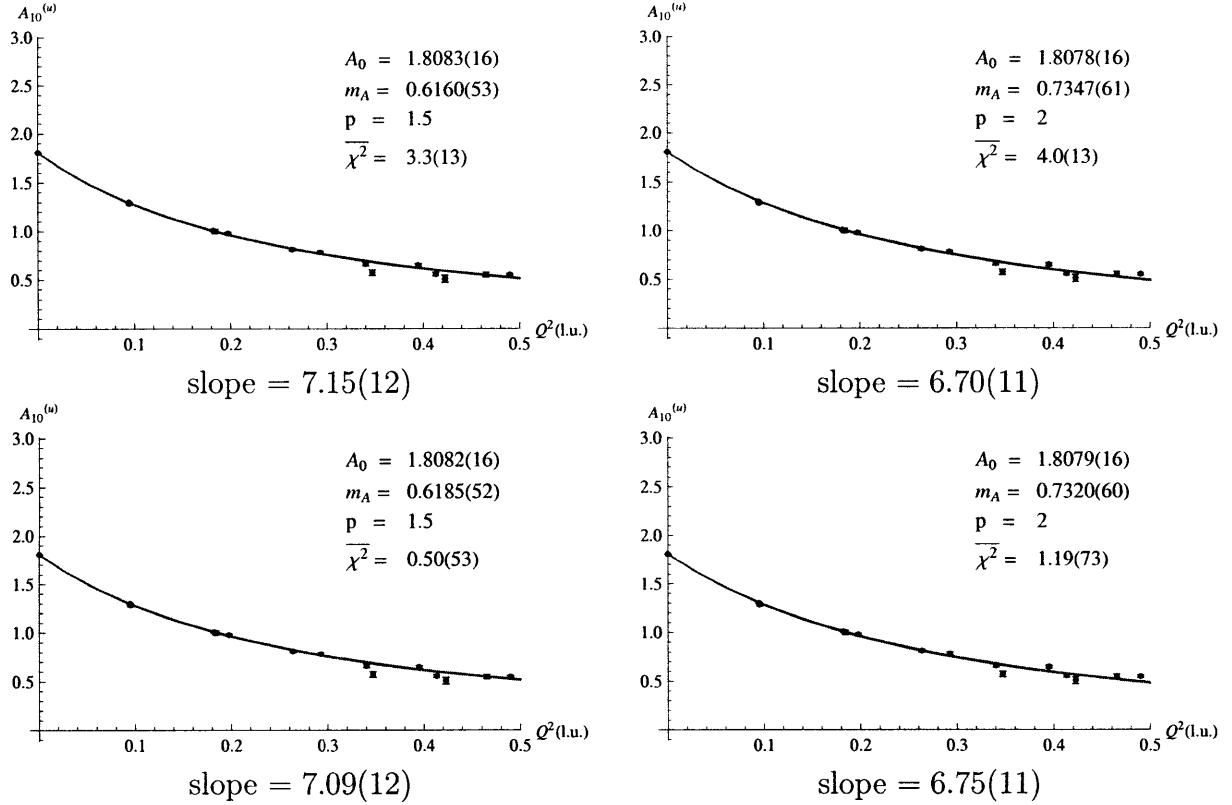[1]Note that changing the fit range has little impact on the result.

Figure E-1: Explorations of p-pole fits to the A_{10} GFFs. The dark part of the error band shows the range of m_π included in the fit.

A_0 (which represents the extrapolation to $Q^2 = 0$) is much more sensitive to changes in p and fit range than in the case of $A_{10}^{(u)}$. Restricting the fit to $Q^2 < 0.3$ (in lattice units) shifted the extrapolated value by about twice the statistical uncertainty. We also observe a potentially significant dependence on the value of p chosen. Similarly, the form factor slopes vary by up to three (statistical) sigma as the fit technology changes.

The second-moment form factor $\bar{B}_{T20}^{(u)}$ has similar behavior. Both the value and the slope of the form factor at zero momentum transfer show systematic variation comparable to the statistical fluctuations.

We conclude from this exploration that systematic effects from choice of fit ansatz and fitting range can be significant (i.e. several times the statistical errors), especially when extracting slopes of form factors at $Q^2 = 0$. It would be good to reduce this uncertainty by performing lattice calculations at smaller non-zero values of momentum
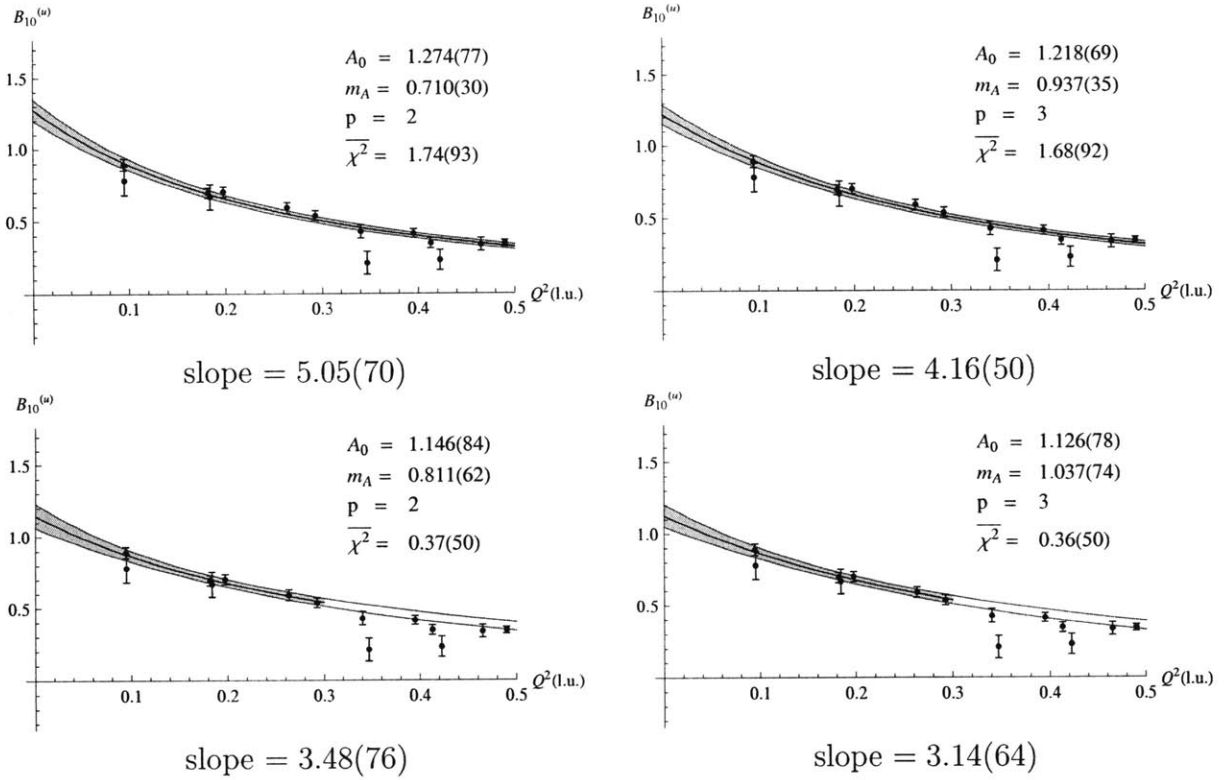
Top-left plot:

$B_{10}^{(u)}$

$A_0 = 1.274(77)$
$m_A = 0.710(30)$
$p = 2$
$\overline{\chi^2} = 1.74(93)$

Q^2(l.u.)

slope $= 5.05(70)$

Top-right plot:

$B_{10}^{(u)}$

$A_0 = 1.218(69)$
$m_A = 0.937(35)$
$p = 3$
$\overline{\chi^2} = 1.68(92)$

Q^2(l.u.)

slope $= 4.16(50)$

Bottom-left plot:

$B_{10}^{(u)}$

$A_0 = 1.146(84)$
$m_A = 0.811(62)$
$p = 2$
$\overline{\chi^2} = 0.37(50)$

Q^2(l.u.)

slope $= 3.48(76)$

Bottom-right plot:

$B_{10}^{(u)}$

$A_0 = 1.126(78)$
$m_A = 1.037(74)$
$p = 3$
$\overline{\chi^2} = 0.36(50)$

Q^2(l.u.)

slope $= 3.14(64)$

Figure E-2: Explorations of p-pole fits to the B_{10} GFFs. The dark part of the error band shows the range of m_π included in the fit.

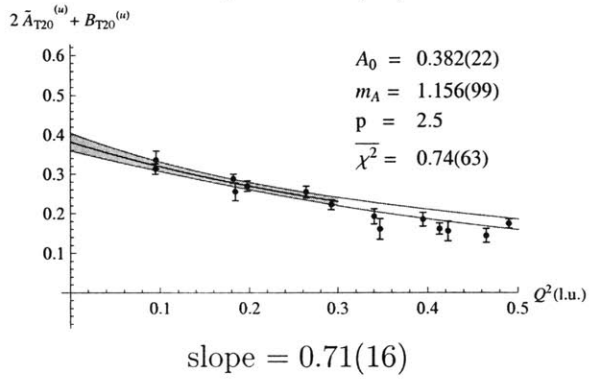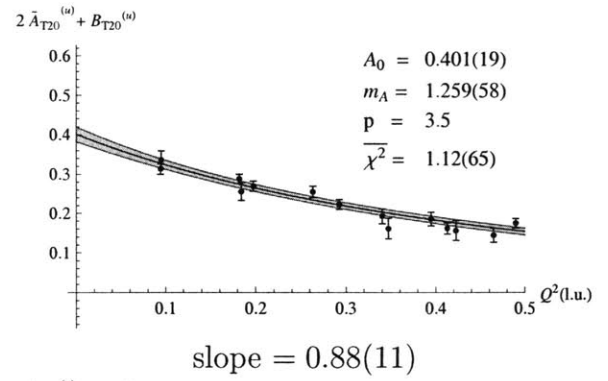transfer (either by taking larger lattice volumes, or using techniques such as twisted boundary conditions [68]).
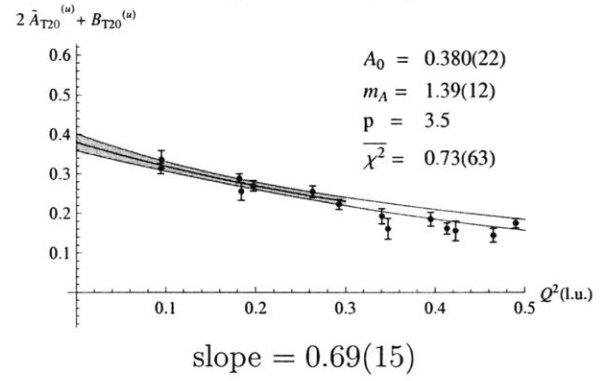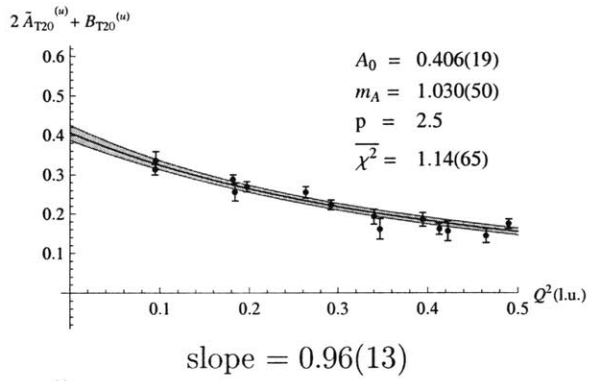
Figure E-3: Explorations of p-pole fits to the $\bar{B}_{T20}$ GFFs. The dark part of the error band shows the range of m_π included in the fit.

Appendix F

Operator Plateaus and Excited States

Even the best nucleon source we can construct on the lattice has contamination from excited states. Far away (in Euclidean time) from the source or sink, these contaminations become negligible, and the ground state dominates. However, statistical noise also increases as we move away from the source, so we would like to find an optimal distance—far enough from the source that excited states are negligible, but not so far that noise swamps the signal—at which to measure nucleon operators. It is therefore important to check whether excited states can indeed be ignored at our chosen source-sink separation. One way to do this is by fitting the lattice data to extract the excited state contributions.

In Chapter 3, we show that the nucleon two-point function can be written as a sum of exponentials:

$$C(t, P) = \sum_n A_n e^{-E_n(P)t}. \tag{F.1}$$

In addition, for the calculations performed in Chapter 5, we observe that the lattice data appears to "oscillate" due to negative eigenvalues of the transfer matrix [75].
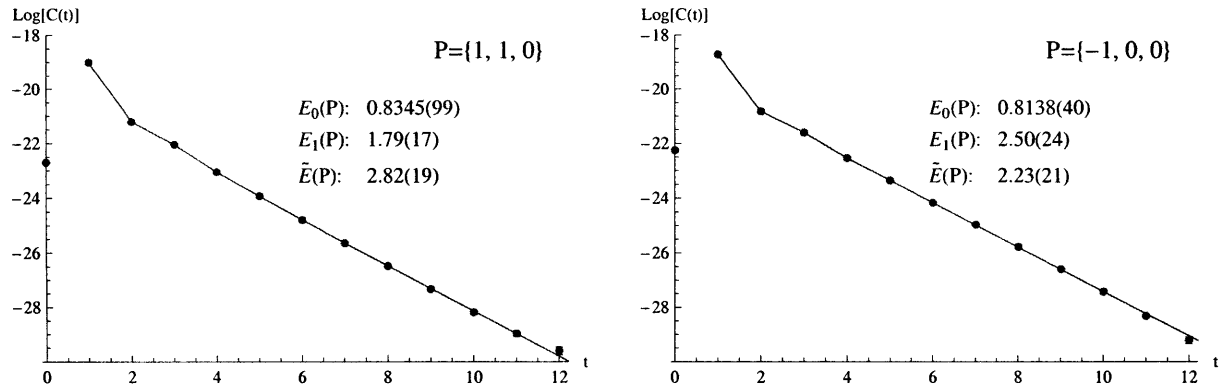
Figure F-1: Fits to lattice two-point data using (F.2). Extracted energies (in lattice units) are given in inset. Lattice data is from data set 9.

We account for this by including a term proportional to $(-1)^t$ in our fit ansatz:

$$C_{fit}^2(t) = A_0 e^{-E_0 t} + A_1 e^{-E_1 t} + (-1)^t \tilde{A} e^{-\tilde{E} t}. \tag{F.2}$$

(In practice, we use an analytic expression like $\cos(\pi t)$ in place of $(-1)^t$ when we do the fit.) For a given value of momentum P, we can estimate the effective excited and oscillating state "masses" from a fit to (F.2). Figure F-1 shows examples of such fits to two-point functions.

The excited state contaminations for the lattice operators (nucleon "three-point" functions) are similar, but now we have contaminations coming from both the source and the sink. For the ratio defined in Eq. 5.5, we can write the leading terms:

$$R_{\mathcal{O}}(P, P', t) = \langle 0, P' | \mathcal{O} | 0, P \rangle$$
$$+ C_{10} \, e^{(E_1(P') - E_0(P'))(t - t_{snk})} \langle 1, P' | \mathcal{O} | 0, P \rangle$$
$$+ C_{01} \, e^{-(E_1(P) - E_0(P))(t - t_{src})} \langle 0, P' | \mathcal{O} | 1, P \rangle$$
$$+ \cdots \tag{F.3}$$

where $|n, P\rangle$ represents the nth energy eigenstate with momentum P (so the nucleon ground state would be $|0, P\rangle$). Including oscillating contaminations coming from the

148

P=1,1,0 ; P'=−1,0,0 ; vector1 op4 U (unchopped)
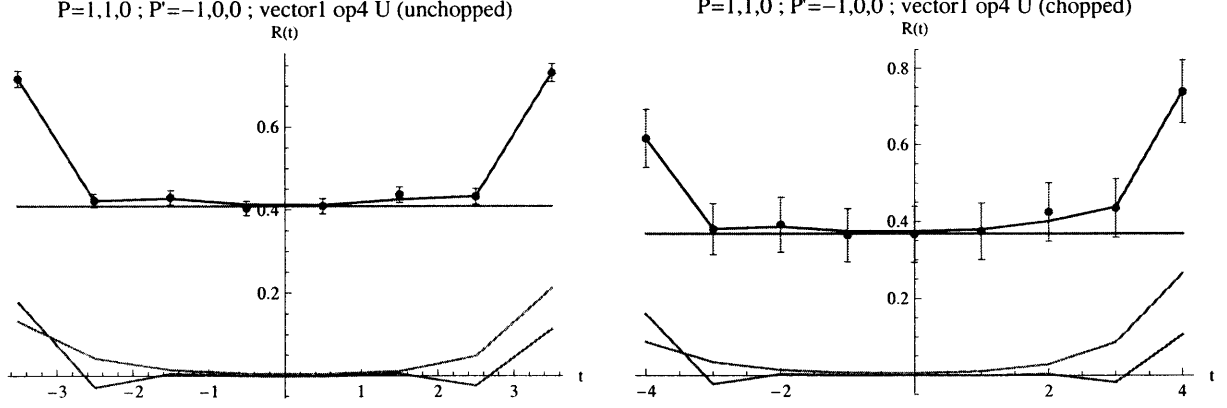
P=1,1,0 ; P'=−1,0,0 ; vector1 op4 U (chopped)

Figure F-2: Fits to sample lattice operator plateaus using ansatz (F.4). Left-hand plot is for the unchopped data set 9; right-hand plot is for the corresponding chopped data set 5. In each case, the blue line shows the fit result, the straight purple line shows the constant piece (A_{00}), the brown line shows the excited state contributions, and the green line shows the oscillating terms.

source and the sink, we obtain the following fit ansatz for $R_{\mathcal{O}}(P, P', t)$:

$$
\begin{aligned}
R_{fit}(t) = A_{00} \\
+ A_{10}\, e^{\Delta E'(t - t_{snk})} + A_{01}\, e^{-\Delta E(t - t_{src})} \\
+ (-1)^{(t - t_{snk})}\, \tilde{A}_{10}\, e^{\Delta \tilde{E}'(t - t_{snk})} + (-1)^{(t - t_{src})}\, \tilde{A}_{01}\, e^{-\Delta \tilde{E}(t - t_{src})}
\end{aligned}
\tag{F.4}
$$

where we define $\Delta E' \equiv E_1(P') - E_0(P')$, $\Delta \tilde{E}' \equiv \tilde{E}(P') - E_0(P')$, etc. If we include as inputs the masses obtained from fitting the two-point function, then (F.4) is, in general, a fit with five free parameters: the ground state operator A_{00}, the excited state terms A_{10} and A_{01}, and the oscillating terms $\tilde{A}_{10}$ and $\tilde{A}_{01}$. Figure F-2 shows examples of fits to data for lattice operators. We conclude that the excited states are indeed negligible near the center of the plateau.

Appendix G

Nucleon Operators on the Lattice

G.1 Calculating Operators

The ratio in Eq. 5.5 can be written (neglecting excited state contributions):

$$R_{\mathcal{O}}^{cont}(P', P) = (E(P')E(P))^{-1/2} \times \left(\frac{1}{2}\text{Tr}[\Gamma^{\text{unpol}}(\not{P}' + m)] \frac{1}{2}\text{Tr}[\Gamma^{\text{unpol}}(\not{P} + m)] \right)^{-1/2}$$

$$\times \frac{1}{4}\text{Tr}[\Gamma^{\text{pol}}(\not{P}' + m)\mathcal{K}_{\mathcal{O}}(P', P)(\not{P} + m)]. \qquad (G.1)$$

Note that the above expression is written in Minkowski space. The left-hand side of (G.1) is constructed from three-point and two-point functions, as described in Chapter 5. In our calculations, we use $\Gamma^{\text{unpol}} = \frac{1}{4}(1 + \gamma_0)$ and $\Gamma^{\text{pol}} = \frac{1}{4}(1 + \gamma_0)(1 - \gamma_5\gamma_3)$.

Following the notation of [52], the kernel $\mathcal{K}_{\mathcal{O}}(P', P)$ is defined for an operator $\mathcal{O}$ by:

$$\langle P'|\mathcal{O}|P \rangle = \bar{U}(P')\mathcal{K}_{\mathcal{O}}(P', P)U(P)$$

For example, in the case of the zero-derivative vector operator $\mathcal{O}^\mu = \bar{\psi}(0)\gamma^\mu\psi(0)$, we have:

$$\langle P'|\mathcal{O}^\mu|P \rangle = \bar{U}(P')\left\{ \gamma^\mu A_{10}(t) + \frac{i}{2m}\sigma^{\mu\alpha}\Delta_\alpha B_{10}(t) \right\}U(P)$$

$$\implies \mathcal{K}_{\mathcal{O}^\mu}(P', P) = \gamma^\mu A_{10}(t) + \frac{i}{2m}\sigma^{\mu\alpha}\Delta_\alpha B_{10}(t).$$

G.1.1 GFF parameterization of lattice operators

The expression used for the kernel depends on the conventions for the form factor decomposition of the corresponding operator. Table G.1 gives an explicit listing of the kernels for the operators we use.

operator	kernel
$\bar{\psi}(0)\gamma^{\mu}\psi(0)$	$\gamma^{\mu}A_{10} + \frac{i}{2m}\sigma^{\mu\alpha}\Delta_{\alpha}B_{10}$
$\bar{\psi}(0)\gamma^{\{\mu_1}\overleftrightarrow{D}^{\mu_2\}}\psi(0)$	$(-i)\left(\bar{P}^{\{\mu_1}\gamma^{\mu_2\}}A_{20} + \frac{i}{2m}\bar{P}^{\{\mu_1}\sigma^{\mu_2\}\alpha}\Delta_{\alpha}B_{20} + \frac{1}{m}\Delta^{\{\mu_1}\Delta^{\mu_2\}}C_{20} \right)$
$\bar{\psi}(0)\gamma^{\mu}\gamma_5\psi(0)$	$\gamma_{\mu}\gamma_5\widetilde{A}_{10} + \frac{1}{2m}\Delta^{\mu}\gamma_5\widetilde{B}_{10}$
$\bar{\psi}(0)\gamma^{\{\mu_1}\gamma_5\overleftrightarrow{D}^{\mu_2\}}\psi(0)$	$(-i)\left(\bar{P}^{\{\mu_1}\gamma^{\mu_2\}}\gamma_5\widetilde{A}_{20} + \frac{1}{2m}\Delta^{\{\mu_1}\bar{P}^{\mu_2\}}\gamma_5\widetilde{B}_{20} \right)$
$\bar{\psi}(0)i\sigma^{\mu\nu}\psi(0)$	$i\sigma^{\mu\nu}A_{T10} + \frac{1}{m^2}(\bar{P}^{\mu}\Delta^{\nu} - \bar{P}^{\nu}\Delta^{\mu})\widetilde{A}_{T10} + \frac{1}{2m}(\gamma^{\mu}\Delta^{\nu} - \gamma^{\nu}\Delta^{\mu})B_{T10}$
$\bar{\psi}(0)i\sigma^{\mu\{\nu}\overleftrightarrow{D}^{\mu_1\}}\psi(0)$	$(-i)\Big(i\sigma^{\mu\{\nu}\bar{P}^{\mu_1\}}A_{T20} + \frac{1}{m^2}(\bar{P}^{\mu}\Delta^{\{\nu}\bar{P}^{\mu_1\}} - \Delta^{\mu}\bar{P}^{\{\nu}\bar{P}^{\mu_1\}})\widetilde{A}_{T20}$ $+\frac{1}{2m}(\gamma^{\mu}\Delta^{\{\nu}\bar{P}^{\mu_1\}} - \Delta^{\mu}\gamma^{\{\nu}\bar{P}^{\mu_1\}})B_{T20}$ $+\frac{1}{m}(\gamma^{\mu}\bar{P}^{\{\nu}\Delta^{\mu_1\}} - \bar{P}^{\mu}\gamma^{\{\nu}\Delta^{\mu_1\}})\widetilde{B}_{T21} \Big)$

Table G.1: Minkowski space operators and kernels. Curly braces denote symmetrization of indices.

G.1.2 Euclidean space

So far, all expressions given have been for Minkowski space. However, our lattice calculations are done in Euclidean space. To extract GFFs from a lattice calculation, we must find Euclidean versions for these expressions.

For convenience, we collect some useful identities. Our Minkowski metric is: $\text{diag}(-1, -1, -1, 1)$, where the time component is written last. A four-vector V transforms:

$$V_{Euc}^{j} = V_{Mink}^{j}$$

$$V_{Euc}^{4} = iV_{Mink}^{4}$$

But the gamma matrices:

$$\gamma^j_{Euc} = -i\gamma^j_{Mink}$$

$$\gamma^4_{Euc} = \gamma^4_{Mink}$$

So, for example, $(\not{P} + m)_{Mink} = (-i\not{P} + m)_{Euc}$. Applying these rules carefully, we obtain Euclidean expressions for the kernels of the Euclidean operators corresponding to the (Minkowski) operators in Table G.1. These are listed in Table G.2.

Euclidean operator	Euclidean kernel
$\bar{q}(0)\gamma^\mu q(0)$	$\gamma^\mu A_{10} + \frac{1}{2m}\sigma^{\mu\alpha}\Delta_\alpha B_{10}$
$\bar{q}(0)\gamma^{\{\mu_1}\overleftrightarrow{D}^{\mu_2\}}q(0)$	$(i)\left(\bar{P}^{\{\mu_1}\gamma^{\mu_2\}}A_{20} + \frac{1}{2m}\bar{P}^{\{\mu_1}\sigma^{\mu_2\}\alpha}\Delta_\alpha B_{20} - \frac{i}{m}\Delta^{\{\mu_1}\Delta^{\mu_2\}}C_{20}\right)$
$\bar{q}(0)\gamma^\mu\gamma_5 q(0)$	$\gamma_\mu\gamma_5\widetilde{A}_{10} - \frac{i}{2m}\Delta^\mu\gamma_5\widetilde{B}_{10}$
$\bar{q}(0)\gamma^{\{\mu_1}\gamma_5\overleftrightarrow{D}^{\mu_2\}}q(0)$	$(i)\left(\bar{P}^{\{\mu_1}\gamma^{\mu_2\}}\gamma_5\widetilde{A}_{20} - \frac{i}{2m}\Delta^{\{\mu_1}\bar{P}^{\mu_2\}}\gamma_5\widetilde{B}_{20}\right)$
$\bar{q}(0)i\sigma^{\mu\nu}q(0)$	$i\sigma^{\mu\nu}A_{T10} - \frac{1}{m^2}(\bar{P}^\mu\Delta^\nu - \bar{P}^\nu\Delta^\mu)\widetilde{A}_{T10} - \frac{i}{2m}(\gamma^\mu\Delta^\nu - \gamma^\nu\Delta^\mu)B_{T10}$
$\bar{q}(0)i\sigma^{\mu\{\nu}\overleftrightarrow{D}^{\mu_1\}}q(0)$	$(i)\left(i\sigma^{\mu\{\nu}\bar{P}^{\mu_1\}}A_{T20} - \frac{1}{m^2}(\bar{P}^\mu\Delta^{\{\nu}\bar{P}^{\mu_1\}} - \Delta^\mu\bar{P}^{\{\nu}\bar{P}^{\mu_1\}})\widetilde{A}_{T20}\right.$ $-\frac{i}{2m}(\gamma^\mu\Delta^{\{\nu}\bar{P}^{\mu_1\}} - \Delta^\mu\gamma^{\{\nu}\bar{P}^{\mu_1\}})B_{T20}$ $\left.-\frac{i}{m}(\gamma^\mu\bar{P}^{\{\nu}\Delta^{\mu_1\}} - \bar{P}^\mu\gamma^{\{\nu}\Delta^{\mu_1\}})\widetilde{B}_{T21}\right)$

Table G.2: Euclidean space operators and kernels (all dirac matrices and four-vectors in this table are the Euclidean versions).

G.2 Moments of Continuum Operators

In this section we show explicitly how the local lattice operators arise from Mellin moments of the bilocal continuum operators. To be concrete, we will write out the expressions for the vector operator in Eq. 4.2 (the same procedure applies for axial

and tensor operators). The matrix element can be written:

$$F \equiv \int \frac{dz^-}{4\pi} e^{ix\bar{P}^+ z^-} \left\langle P', S' \left| \bar{\psi}\left(-\frac{z}{2}\right) \gamma^+ e^{-ig \int_{-.5z^-}^{.5z^-} dz' A^+(z')} \psi\left(\frac{z}{2}\right) \right| P, S \right\rangle \Bigg|_{z^i=z^+=0} , \quad (G.2)$$

where we write out the Wilson line explicitly. The lowest moment gives:

$$\int_{-1}^{1} dx\, F = \int_{-1}^{1} dx \int \frac{dz^-}{4\pi} e^{ix\bar{P}^+ z^-} \left\langle P', S' \left| \bar{\psi}\left(-\frac{z}{2}\right) \gamma^+ e^{-ig \int_{-.5z^-}^{.5z^-} dz' A^+(z')} \psi\left(\frac{z}{2}\right) \right| P, S \right\rangle \Bigg|_{z^i=z^+=0}$$

$$= \int_{-\infty}^{\infty} dx \int \frac{dz^-}{4\pi} e^{ix\bar{P}^+ z^-} \left\langle P', S' \left| \bar{\psi}\left(-\frac{z}{2}\right) \gamma^+ e^{-ig \int_{-.5z^-}^{.5z^-} dz' A^+(z')} \psi\left(\frac{z}{2}\right) \right| P, S \right\rangle \Bigg|_{z^i=z^+=0}$$

$$= \int \frac{dz^-}{4\pi}\, 2\pi\, \delta(\bar{P}^+ z^-) \left\langle P', S' \left| \bar{\psi}\left(-\frac{z}{2}\right) \gamma^+ e^{-ig \int_{-.5z^-}^{.5z^-} dz' A^+(z')} \psi\left(\frac{z}{2}\right) \right| P, S \right\rangle \Bigg|_{z^i=z^+=0}$$

$$= \frac{1}{2\bar{P}^+} \left\langle P', S' \left| \bar{\psi}(0)\, \gamma^+ \psi(0) \right| P, S \right\rangle. \quad (G.3)$$

(In the second step we made use of the fact that F must vanish for $|x| > 1$.) Comparing this with Eqs. 4.11 and 4.26, we see immediately that:

$$\int_{-1}^{1} dx\, H(x, \xi, t) = A_{10}(t) \qquad \int_{-1}^{1} dx\, E(x, \xi, t) = B_{10}(t).$$

154

The second moment is similar:

$$\int_{-1}^{1} x\, dx\, F = \int_{-\infty}^{\infty} dx \int \frac{dz^-}{4\pi} \frac{1}{i\bar{P}^+} \left(\frac{\partial}{\partial z^-} e^{ix\bar{P}^+ z^-} \right)$$

$$\times \langle P', S' | \bar{\psi}\left(-\frac{z}{2}\right) \gamma^+ e^{-ig\int_{-.5z^-}^{.5z^-} dz' A^+(z')} \psi\left(\frac{z}{2}\right) | P, S \rangle \Bigg|_{z^i = z^+ = 0}$$

$$= \int \frac{dz^-}{4\pi} \frac{i}{\bar{P}^+} 2\pi \delta(\bar{P}^+ z^-)$$

$$\times \frac{\partial}{\partial z^-} \langle P', S' | \bar{\psi}\left(-\frac{z}{2}\right) \gamma^+ e^{-ig\int_{-.5z^-}^{.5z^-} dz' A^+(z')} \psi\left(\frac{z}{2}\right) | P, S \rangle \Bigg|_{z^i = z^+ = 0}$$

$$= \frac{i}{2(\bar{P}^+)^2} \langle P', S' | \bar{\psi}(0)\, \gamma^+ \left(\frac{1}{2}\overrightarrow{\partial}^+ - \frac{1}{2}\overleftarrow{\partial}^+ - igA^+(0) \right) \psi(0) | P, S \rangle$$

$$= \frac{i}{2(\bar{P}^+)^2} \langle P', S' | \bar{\psi}(0)\, \gamma^+ \overleftrightarrow{D}^+ \psi(0) | P, S \rangle. \tag{G.4}$$

Note that the Wilson line in the definition of the bilocal operator leads directly to the covariant derivative in the local operator. Using the generalized form factor decomposition shown in the second entry of Table G.1, we find:

$$\int_{-1}^{1} x\, dx\, H(x, \xi, t) = A_{20}(t) + 4\xi^2 C_{20}(t) \qquad \int_{-1}^{1} x\, dx\, E(x, \xi, t) = B_{20}(t) - 4\xi^2 C_{20}(t).$$

In this way, relations can be found connecting all the form factors to GPDs.

G.3   Explicit List of Lattice Operators

As discussed previously (Eq. 4.25), the lattice operators we calculate have the general form:

$$\mathcal{O}_\Gamma^{\{\mu_1 \cdots \mu_n\}} = \bar{\psi}(0)\, \Gamma^{\{\mu_1} \overleftrightarrow{D}^{\mu_2} \cdots \overleftrightarrow{D}^{\mu_n\}} \psi(0)$$

Specific index combinations of these operators are taken in order to obtain twist-two operators that belong to irreducible representations of H(4) (see [76] and references

155

therein). The choice of these index combinations is not unique, so in the next section we give an explicit listing of the conventions used (also see [52, 34]).

G.3.1   Vector and axial operators

First let us consider the vector and axial operators, which can be written:

$$\mathcal{O}_{[5]}^{\{\mu_1 \cdots \mu_n\}} = \bar{\psi}(0) \, \gamma^{\{\mu_1} \, [\gamma_5] \, \overleftrightarrow{D}^{\mu_2} \cdots \overleftrightarrow{D}^{\mu_n\}} \, \psi(0),$$

where the [5] indicates the possible inclusion of γ_5. For the zero-derivative ($n = 1$) case, there are just the four operators:

$$\mathcal{O}_{lat,[5]}^{x} = \mathcal{O}_{[5]}^{1} \qquad\qquad \mathcal{O}_{lat,[5]}^{y} = \mathcal{O}_{[5]}^{2}$$

$$\mathcal{O}_{lat,[5]}^{z} = \mathcal{O}_{[5]}^{3} \qquad\qquad \mathcal{O}_{lat,[5]}^{t} = \mathcal{O}_{[5]}^{4}$$

For the one-derivative ($n = 2$) operators, there are two irreducible representations of H(4) we can use. There are three "diagonal" operators (belonging to the $\tau_1^{(3)}$ representation):

$$\mathcal{O}_{lat,[5]}^{1,n=2} = \frac{1}{2} \left(\mathcal{O}_{[5]}^{11} + \mathcal{O}_{[5]}^{22} - \mathcal{O}_{[5]}^{33} - \mathcal{O}_{[5]}^{44} \right)$$

$$\mathcal{O}_{lat,[5]}^{2,n=2} = \frac{1}{\sqrt{2}} \left(\mathcal{O}_{[5]}^{33} - \mathcal{O}_{[5]}^{44} \right)$$

$$\mathcal{O}_{lat,[5]}^{3,n=2} = \frac{1}{\sqrt{2}} \left(\mathcal{O}_{[5]}^{11} - \mathcal{O}_{[5]}^{22} \right)$$

There are also six non-diagonal operators (belonging to the $\tau_1^{(6)}$ representation):

$$\mathcal{O}_{lat,[5]}^{xy} = \mathcal{O}_{[5]}^{12} \qquad\qquad \mathcal{O}_{lat,[5]}^{xz} = \mathcal{O}_{[5]}^{13}$$

$$\mathcal{O}_{lat,[5]}^{xt} = \mathcal{O}_{[5]}^{14} \qquad\qquad \mathcal{O}_{lat,[5]}^{yz} = \mathcal{O}_{[5]}^{23}$$

$$\mathcal{O}_{lat,[5]}^{yt} = \mathcal{O}_{[5]}^{24} \qquad\qquad \mathcal{O}_{lat,[5]}^{zt} = \mathcal{O}_{[5]}^{34}$$

Note that the operators above have already been symmetrized in their two indices:
$\mathcal{O}_{[5]}^{\mu\nu} = \frac{1}{2} \left(\mathcal{O}_{[5]}^{\mu\nu} + \mathcal{O}_{[5]}^{\nu\mu} \right)$

156

G.3.2 Tensor operators

We can write the tensor operators as:

$$\mathcal{O}_T^{\nu\{\mu_1\cdots\mu_n\}} = \bar{\psi}(0)\, i\sigma^{\nu\{\mu_1}\overleftrightarrow{D}^{\mu_2}\cdots\overleftrightarrow{D}^{\mu_n\}}\psi(0).$$

For $n = 1$ (zero derivatives), the operators are simple:

$$\mathcal{O}_{lat,T}^{xy} = \mathcal{O}_T^{12} \qquad \mathcal{O}_{lat,T}^{xz} = \mathcal{O}_T^{13}$$

$$\mathcal{O}_{lat,T}^{xt} = \mathcal{O}_T^{14} \qquad \mathcal{O}_{lat,T}^{yz} = \mathcal{O}_T^{23}$$

$$\mathcal{O}_{lat,T}^{yt} = \mathcal{O}_T^{24} \qquad \mathcal{O}_{lat,T}^{zt} = \mathcal{O}_T^{34}$$

Note that these operators are automatically *antisymmetric* in their two indices.

The case $n = 2$ (one derivative) is a bit more complicated. There are two inequivalent 8-dimensional representations ($\tau_1^{(8)}$ and $\tau_2^{(8)}$) that we use, for a total of 16 operators. Explicitly:

For $\tau_1^{(8)}$:

$$\mathcal{O}_{lat,T}^1 = \mathcal{O}_T^{122} - \mathcal{O}_T^{133}$$

$$\mathcal{O}_{lat,T}^2 = \mathcal{O}_T^{211} - \mathcal{O}_T^{233}$$

$$\mathcal{O}_{lat,T}^3 = \mathcal{O}_T^{311} - \mathcal{O}_T^{322}$$

$$\mathcal{O}_{lat,T}^4 = \mathcal{O}_T^{411} - \mathcal{O}_T^{422}$$

$$\mathcal{O}_{lat,T}^5 = (\mathcal{O}_T^{122} + \mathcal{O}_T^{133} - 2\times\mathcal{O}_T^{144})\frac{1}{\sqrt{3}}$$

$$\mathcal{O}_{lat,T}^6 = (\mathcal{O}_T^{211} + \mathcal{O}_T^{233} - 2\times\mathcal{O}_T^{244})\frac{1}{\sqrt{3}}$$

$$\mathcal{O}_{lat,T}^7 = (\mathcal{O}_T^{311} + \mathcal{O}_T^{322} - 2\times\mathcal{O}_T^{344})\frac{1}{\sqrt{3}}$$

$$\mathcal{O}_{lat,T}^8 = (\mathcal{O}_T^{411} + \mathcal{O}_T^{422} - 2\times\mathcal{O}_T^{433})\frac{1}{\sqrt{3}}$$

For $\tau_2^{(8)}$:

$$\mathcal{O}_{lat,T}^9 = 2 \times \mathcal{O}_T^{123}$$

$$\mathcal{O}_{lat,T}^{10} = 2 \times \mathcal{O}_T^{124}$$

$$\mathcal{O}_{lat,T}^{11} = 2 \times \mathcal{O}_T^{134}$$

$$\mathcal{O}_{lat,T}^{12} = 2 \times \mathcal{O}_T^{234}$$

$$\mathcal{O}_{lat,T}^{13} = (\mathcal{O}_T^{213} - \mathcal{O}_T^{321})\frac{2}{\sqrt{3}}$$

$$\mathcal{O}_{lat,T}^{14} = (\mathcal{O}_T^{214} - \mathcal{O}_T^{421})\frac{2}{\sqrt{3}}$$

$$\mathcal{O}_{lat,T}^{15} = (\mathcal{O}_T^{314} - \mathcal{O}_T^{431})\frac{2}{\sqrt{3}}$$

$$\mathcal{O}_{lat,T}^{16} = (\mathcal{O}_T^{324} - \mathcal{O}_T^{432})\frac{2}{\sqrt{3}}$$

For completeness, we include our normalization conventions. Note that final indices have already been symmetrized: $\mathcal{O}_T^{123} = \frac{1}{2}\left(\mathcal{O}_T^{123} + \mathcal{O}_T^{132}\right)$.

Appendix H

Fourier Transform of F

In this Appendix, we discuss how we go from Eq. 4.11 to the transverse parton distributions in Eq. 4.19. (Similar manipulations can be performed on the axial and tensor matrix elements.)

H.1   Spinor Products

The first step is to evaluate the proton bilinears that appear in Eqs. 4.11 - 4.13. The four-momenta P and P' are generally not the same, but we consider the case where their plus components are equal: $P^+ = (P^+)'$. Using the light cone helicity spinors in Appendix C, we find:

$$\bar{u}_{\pm}^{LC}(P')\,\gamma^+\,u_{\pm}^{LC}(P) = 2P^+$$

$$\bar{u}_{\pm}^{LC}(P')\,\gamma^+\,u_{\mp}^{LC}(P) = 0$$

$$\bar{u}_{\pm}^{LC}(P')\,\gamma^+\,\gamma_5\,u_{\pm}^{LC}(P) = \pm 2P^+$$

$$\bar{u}_{\pm}^{LC}(P')\,\gamma^+\,\gamma_5\,u_{\mp}^{LC}(P) = 0 \tag{H.1}$$

$$\bar{u}_{\pm}^{LC}(P')\,i\sigma^{+1}\,u_{\mp}^{LC}(P) = \pm 2P^+$$

$$\bar{u}_{\pm}^{LC}(P')\,i\sigma^{+i}\,u_{\pm}^{LC}(P) = 0$$

$$\bar{u}_{\pm}^{LC}(P')\,i\sigma^{+2}\,u_{\mp}^{LC}(P) = 2iP^+$$

and so on. Note that the light cone spinors result in particularly simple products when $P^+ = (P^+)'$. This would generally not be the case for an arbitrary spinor basis (such as the "lab frame" spin states in Eq. C.3).

Now we can write out the matrix element F (Eq. 4.11) for a particular proton spin state. For $\xi = 0$, $S = S' = \perp$ (so that $u = u_\perp^{LC}$), we find:

$$F = H(x, 0, -\boldsymbol{\Delta}^2) + \frac{i\Delta_y}{2m} E(x, 0, -\boldsymbol{\Delta}^2). \tag{H.2}$$

H.2 Fourier Transform of GFFs

The next step is to take the Fourier transform of (H.2):

$$\mathcal{F} = \int \frac{d^2\boldsymbol{\Delta}}{(2\pi)^2} e^{-i\mathbf{b}\cdot\boldsymbol{\Delta}} F \tag{H.3}$$

$$= \int \frac{d^2\boldsymbol{\Delta}}{(2\pi)^2} e^{-i\mathbf{b}\cdot\boldsymbol{\Delta}} \left\{ H(x, 0, -\boldsymbol{\Delta}^2) + \frac{i\Delta_y}{2m} E(x, 0, -\boldsymbol{\Delta}^2) \right\} \tag{H.4}$$

$$= \mathcal{H}(x, b^2) - \frac{1}{2m} \frac{\partial}{\partial b^y} \int \frac{d^2\boldsymbol{\Delta}}{(2\pi)^2} e^{-i\mathbf{b}\cdot\boldsymbol{\Delta}} E(x, 0, -\boldsymbol{\Delta}^2) \tag{H.5}$$

$$= \mathcal{H}(x, \mathbf{b}) - \frac{1}{2m} \frac{\partial}{\partial b^y} \mathcal{E}(x, \mathbf{b}), \tag{H.6}$$

which gives us Eq. 4.20. Mellin moments of $\mathcal{H}(x, \mathbf{b})$ correspond to Fourier transforms of the generalized form factors $A_{n0}(t)$:

$$\int_{-1}^{1} dx\, x^n\, \mathcal{H}(x, \mathbf{b}) = \int \frac{d^2\boldsymbol{\Delta}}{(2\pi)^2} e^{-i\mathbf{b}\cdot\boldsymbol{\Delta}}\, A_{n0}(-\boldsymbol{\Delta}^2) \equiv \mathcal{A}_{n0}(\mathbf{b}^2), \tag{H.7}$$

and similarly for the other GPDs. To proceed further, we need to know more about the functional form of the GFFs. Let us assume that the form factors can be approximated by our p-pole fit ansatz $A(Q^2) = \frac{A_0}{(1+Q^2/m_A^2)^p}$ (see Eq. 5.8). Then we can perform the Fourier transform analytically. It is straightforward but tedious to verify the results

given in [4], which we reproduce here for reference:

$$\mathcal{A}(b^2) = C(m_A\,b)^{p-1}K_{p-1}(m_A\,b)$$

$$\frac{\partial}{\partial b^2}\mathcal{A}(b^2) = -\frac{1}{2}Cm_A^2\,(m_A\,b)^{p-2}K_{p-2}(m_A\,b)$$

$$\left(\frac{\partial}{\partial b^2}\right)^2\mathcal{A}(b^2) = \frac{1}{4}m_A^4\,C(m_A\,b)^{p-3}K_{p-3}(m_A\,b)$$

$$\frac{\partial}{\partial b^i}\frac{\partial}{\partial b^i}\mathcal{A}(b^2) = -Cm_A^2\,(m_A\,b)^{p-2}\left\{2K_{p-2}(m_A\,b) - m_A\,b\,K_{p-3}(m_A\,b)\right\},$$

(H.8)

where $C \equiv \frac{m_A^2\,A_0}{2^p\pi\Gamma(p)}$, and K is a modified Bessel function of the second kind.

Bibliography

[1] A. Walker-Loud *et al.* Phys.Rev.D **79**, 054502 (2009).

[2] W. Schroers *et al.* (2009). To be published.

[3] S. N. Syritsyn *et al.* (2009). [arXiv:hep-lat/0907.4194].

[4] M. Diehl and Ph. Hagler. Eur. Phys. J. C **44** pp. 87–101 (2005). [arXiv:hep-ph/0504175v1].

[5] M. Creutz. *Quarks, Gluons, and Lattices.* Cambridge University Press (1983).

[6] M.Peskin and D.Schroeder. *An Introduction to Quantum Field Theory.* Westview Press (1995).

[7] J. Smit. *Introduction to Quantum Fields on a Lattice.* Cambridge University Press (2002).

[8] D. Sigaev. Ph.D. thesis, MIT (2008).

[9] D. B. Kaplan. Phys. Lett. B **288** pp. 342–347 (1992). [arXiv:hep-lat/9206013v1].

[10] Y. Shamir. Nucl.Phys. B **406** pp. 90–106 (1993). [arXiv:hep-lat/9303005v1].

[11] S. Aoki *et al.* (2008). [arXiv:hep-lat/0807.1661v1].

[12] D. Renner. Ph.D. thesis, MIT (2004).

[13] J. Foley *et al.* Comput. Phys. Commun **172** pp. 145–162 (2005). [arXiv:hep-lat/0505023v1].

[14] K.-F. Liu. Phys.Rev.D **59**, 112001 (1999). [arXiv:hep-ph/9806491v1].

[15] V. Gadiyak, X. Ji and Ch. Jung. Phys. Rev. D **65**, 094510 (2002). [arXiv:hep-lat/0112040v1].

[16] R. L. Jaffe and F. Wilczek. Phys. Rev. Lett. **91**, 232003 (2003).

[17] R. L. Jaffe. "Exotica." (2005).

[18] F. Wilczek. "Diquarks as inspiration and as objects." (2004).

[19] M. Ida and R. Kobayashi. Prog. Theor. Phys. **36**, 846 (1966).

[20] B.L. Ioffe. Nucl. Phys. B **188**, 317 (1981).

[21] C. Alexandrou, Ph. de Focrand and B. Lucini. Phys. Rev. Lett. **97**, 222002 (2006).

[22] D. Dolgov *et al.* Phys. Rev. D **66**, 034506 (2002).

[23] C. Michael. Nucl. Phys. B **259**, 58 (1985).

[24] M. Lüscher. Commun. Math. Phys. **54** pp. 283–292 (1977).

[25] M. Göckeler *et al.* Nucl. Phys. Proc. Suppl. **42** pp. 337–345 (1995).

[26] M. Albanese *et al.* Phys. Lett. B **192**, 163 (1987).

[27] M. Diehl. Phys.Rept. **388** pp. 41–277 (2003). [arXiv:hep-ph/0307382v2].

[28] D. E. Soper. Phys. Rev. D **15** pp. 1141 – 1149 (1977).

[29] R. L. Jaffe (1996). [arXiv:hep-ph/9602236v1].

[30] J. Kogut and D. Soper. Phys.Rev. D **1**, 10 (1970).

[31] M. Diehl. Eur.Phys.J.C **19** pp. 485–492 (2001).

[32] R.Jaffe and X. Ji. Phys Rev Lett **67**, 5 (1991).

[33] Ph. Hägler *et al.* Phys.Rev.D **77**, 094502 (2008).

[34] M. Gockeler *et al.* Phys. Lett. B **627** pp. 113–123 (2005). [arXiv:hep-lat/0507001v1].

[35] M. Burkardt. Int. J. Mod. Phys. A **18** pp. 173–208 (2003). [arXiv:hep-ph/0207047v3].

[36] M. Burkardt (2005). [arXiv:hep-ph/0510408v1].

[37] M. Diehl. Eur. Phys. J. C **25** pp. 223–232 (2002). [arXiv:hep-ph/0205208v2].

[38] M. Burkardt (2007). [arXiv:hep-ph/0711.1881v2].

[39] J. A. Rinehimer and G. A. Miller (2009). [arXiv:nucl-th/0902.4286v1].

[40] J. D. Jackson. *Classical Electrodynamics*. John Wiley & Sons, Inc., third ed. (1999).

[41] M. Burkardt. Phys.Rev. D **72**, 094020 (2005). [arXiv:hep-ph/0505189v4].

[42] X. Ji. Phys.Rev.Lett. **78** pp. 610–613 (1997).

[43] H. Ohanian. Am. J. Phys. **54**, 500 (1986).

[44] C. Bernard *et al.* Phys.Rev.D **64**, 054506 (2001). [arXiv:hep-lat/0104002v2].

[45] M. Golterman (2008). [arXiv:hep-ph/0812.3110v1].

[46] K. Orginos and D. Toussaint. Phys. Rev. D **60**, 054503 (1999).

[47] C. Aubin *et al.* Phys.Rev.D **70**, 094505 (2004). [arXiv:hep-lat/0402030v1].

[48] A. Hasenfratz and F. Knechtli. Phys. Rev. D **64**, 034504 (2001). [arXiv:hep-lat/0103029v2].

[49] M. F. Lin *et al.* (2008). [arXiv:hep-lat/0810.1933v1].

[50] R. G. Edwards and B. Joo (2004). [arXiv:hep-lat/0409003v1].

[51] P.A. Boyle. [http://www.ph.ed.ac.uk/~paboyle/bagel/Bagel.html].

[52] Ph. Hägler *et al.* Phys.Rev.D **68**, 034505 (2003).

[53] B. Bistrović. Ph.D. thesis, MIT (2005).

[54] W. H. Press, S. A. Teukolsky, W. T. Vetterling and B. P. Flannery. *Numerical Recipes in C.* Cambridge University Press (1997).

[55] M. Göckeler *et al.* Phys. Rev. Lett. **98**, 222001 (2007). [arXiv:hep-lat/0612032v1].

[56] M. Diehl, A. Manashov and A. Schafer. Eur.Phys.J.A **29** pp. 315–326 (2006).

[57] M. Diehl, A. Manashov and A. Schafer. Eur.Phys.J.A **31** pp. 335–355 (2007).

[58] T. A. Gail. Ph.D. thesis, Technische Universität München (2007).

[59] M. Dorati, T. A. Gail and T. R. Hemmert. Nucl.Phys.A **798** pp. 96–131 (2008).

[60] M.Procura. Unpublished notes.

[61] HERMES Collaboration. Phys. Rev. D **75**, 012007 (2007).

[62] D. Dolgov *et al.* Phys. Rev. D **66**, 034506 (2002). [arXiv:hep-lat/0201021v3].

[63] C. Amsler *et al.* (Particle Data Group). Physics Letters B **667**, 1 (2008).

[64] D. Renner *et al.* J. Phys. Conf. Ser. **46** pp. 152–156 (2006). [arXiv:hep-lat/0607008v2].

[65] A.W. Thomas W. Detmold, W. Melnitchouk. Phys.Rev.D **66**, 054501 (2002).

[66] D. de Florian, R. Sassot, M. Stratmann and W. Vogelsang (2009). [arXiv:hep-ph/0904.3821v1].

[67] M. R. Schindler, T. Fuchs, J. Gegelia and S. Scherer. Phys.Rev.C **75**, 025202 (2007). [arXiv:nucl-th/0611083v1].

[68] P.A. Boyle, A. Juttner J.M. Flynn, C.T. Sachrajda and J.M. Zanotti (2007). [arXiv:hep-lat/0703005v1].

[69] S. Sasaki, T. Blum, S. Ohta and K. Orginos. Nucl.Phys.Proc.Suppl. **106** pp. 302–304 (2002). [arXiv:hep-lat/0110053v1].

[70] A. A. Khan *et al.* Nucl.Phys.Proc.Suppl. **140** pp. 408–410 (2005). [arXiv:hep-lat/0409161v3].

[71] H.J. Melosh. Phys.Rev. D **9**, 4 (1974).

[72] B.-Q. Ma. J.Phys.G **17** pp. 53–58 (1991). [arxiv:hep-ph/0711.2335v1].

[73] B. Efron. *The Jackknife, the Bootstrap, and Other Resampling Plans.* Society for Industrial and Applied Mathematics (1982).

[74] T. Blum, C. Dawson and T. Izubuchi. Private Communication.

[75] S. Syritsyn and J. W. Negele (2007). [arXiv:hep-lat/0710.0425v1].

[76] A. Pochinsky. Ph.D. thesis, MIT (1997).